POLYPUBLIE
Polytechnique Montréal

POLYTECHNIQUE MONTRÉAL
UNIVERSITÉ D'INGÉNIERIE

Titre: Title:	Parallel finite element modeling of the hydrodynamics in agitated tanks
Auteur: Author:	Christian Alberto Rivera Aparicio
Date:	2009
Type:	Mémoire ou thèse / Dissertation or Thesis
Référence: Citation:	Rivera Aparicio, C. A. (2009). Parallel finite element modeling of the hydrodynamics in agitated tanks [Thèse de doctorat, École Polytechnique de Montréal]. PolyPublie. https://publications.polymtl.ca/8463/

Document en libre accès dans PolyPublie
Open Access document in PolyPublie

URL de PolyPublie: PolyPublie URL:	https://publications.polymtl.ca/8463/
Directeurs de recherche: Advisors:	Philippe A. Tanguy, & Mourad Heniche
Programme: Program:	Non spécifié

UNIVERSITÉ DE MONTRÉAL

PARALLEL FINITE ELEMENT MODELING OF THE HYDRODYNAMICS IN
AGITATED TANKS

CHRISTIAN ALBERTO RIVERA APARICIO
DÉPARTEMENT DE GÉNIE CHIMIQUE
ÉCOLE POLYTECHNIQUE DE MONTRÉAL

THÈSE PRÉSENTÉE EN VUE DE L'OBTENTION
DU DIPLÔME DE PHILOSOPHIAE DOCTOR (Ph. D.)
(GÉNIE CHIMIQUE)
MAI 2009

Canada

UNIVERSITÉ DE MONTRÉAL

ÉCOLE POLYTECHNIQUE DE MONTRÉAL

Cette thèse intitulée:

PARALLEL FINITE ELEMENT MODELING OF THE HYDRODYNAMICS IN
AGITATED TANKS

présentée par: RIVERA APARICIO Christian Alberto
en vue de l'obtention du diplôme de: Philosophiae Doctor
a été dûment acceptée par le jury d'examen constitué de:

M. LEGROS Robert, Ph. D., président
M. TANGUY Philippe, Ph. D., membre et directeur de recherche
M. HENICHE Mourad, Doct., membre et codirecteur de recherche
M., DUFOUR Steven, Ph. D., membre
M., ROBERT Jean-Loup, Ph. D., membre

To my mother and my father

Acknowledgements

Résumé

Des cuves agitées opérant en régime de transition sont souvent rencontrées dans les procédés industriels. Une bonne connaissance de l'écoulement généré dans les cuves de mélange est utile pour pouvoir déterminer les conditions d'opérations optimales ou pour pouvoir proposer des directives de conception. Les modèles de simulation en dynamique des fluides numériques (CFD) permettent de livrer ce type d'information. Le principal handicap des modèles de CFD est le coût informatique élevé en mémoire et en temps de calcul demandé, pour pouvoir prédire avec une bonne précision les écoulements dans la cuve agitée en particulier ceux en régime de transition. Afin d'éviter cette limitation, l'objectif de cette thèse est de développer une stratégie numérique permettant de modéliser le régime de transition dans les cuves agitées en utilisant le calcul parallèle.

Pour compléter l'objectif principal, la première phase du projet est consacrée au développement d'un algorithme élément fini parallèle qui soit capable de prédire l'hydrodynamique de problèmes d'écoulements tridimensionnels incompressibles sur des maillages non structurés. La parallélisation se base sur une méthode de décomposition de domaine sans chevauchement. Des multiplicateurs de Lagrange sont utilisés pour assurer la continuité aux frontières entre les sous-domaines. L'originalité du travail réside dans la résolution couplée du système d'équations en vitesse-pression-

multiplicateurs de Lagrange découlant de la discrétisation des équations de Navier-Stokes avec un solveur parallèle à mémoire distribuée de type Krylov et un préconditionnement par factorisation incomplète (ILU). Une technique de pénalisation est introduite aux interfaces entre sous-domaines pour éviter le blocage de l'algorithme de factorisation ILU. Pour s'assurer de la portabilité du code, le protocole de communication Message Passing Interface (MPI) est employé. La méthode est vérifiée sur différents cas de référence, tels que l'écoulement dans une conduite et dans une cavité, avec des maillages tétraédriques non-structurés. On montre ainsi que l'algorithme de partitionnement et la numérotation des variables physiques sont essentiels pour la performance du solveur parallèle. Une accélération des temps de calcul variant entre 5 et 13 est obtenue avec 16 processeurs.

La seconde phase est consacrée au développement d'un algorithme parallèle prenant en compte la technique du maillage glissant (sliding mesh) pour s'assurer de la rotation des agitateurs. Les multiplicateurs de Lagrange sont utilisés aux interfaces de glissement pour garantir la continuité entre les deux partitions stationnaire et fixe. Pour stabiliser le solveur lorsque la convection devient dominante, deux méthodes sont utilisées, le schéma de Newton-Raphson et la linéarisation semi-implicite. Cette méthode de stabilisation est validée pour des écoulements entre deux cylindres concentriques et dans des cuves agitées. Une accélération des temps de calcul de presque 8 est obtenue avec 16 processeurs.

Finalement, pour présenter l'utilité des algorithmes parallèles développés, la dernière partie de cette thèse sera consacrée à la caractérisation de l'hydrodynamique d'un mélangeur coaxial en régime de transition. Le mélangeur coaxial est composé d'une grande palette (Maxblend) et d'un agitateur à double ruban hélicoïdal montés sur deux arbres coaxiaux indépendants et tournants à des vitesses différentes. Les maillages en tétraèdres utilisés comptent 1.4 à 3.8 millions de nœuds, produisant un système d'équations respectivement de 4.4 à 14.5 millions d'inconnues. Les simulations sont basées sur la résolution des équations de Navier-Stokes avec l'aide du solveur parallèle développé. Pour modéliser la rotation des agitateurs, une approche hybride est utilisée. Elle est basée sur l'appariement des méthodes de maillage glissant et de domaine fictif. La consommation de puissance ainsi que les temps de mélanges obtenus des simulations montrent une bonne concordance avec les résultats expérimentaux. Les simulations permettent d'observer l'écoulement à partir du régime laminaire profond jusqu'au régime de transition.

Abstract

Agitated tanks operating in the transition flow regime are often encountered in industrial processes. Knowledge of the flow generated within the mixing tanks is useful to determine optimal operating conditions or to propose design guidelines. Computational fluid dynamics (CFD) models are able to give such insight. The main problem of the CFD models is the high computational cost required to accurately predict the transition flow regime in stirred tanks. In order to circumvent this limitation, the general scope of the thesis is to develop a numerical strategy to model the transition flow regime of agitated tanks employing parallel computing.

To accomplish the main objective, the first stage of the project focuses on the development of a parallel finite element algorithm capable to predict the hydrodynamics of three-dimensional incompressible fluid flow problems on unstructured grids. The parallelization is based on non-overlapping domain decomposition methods. Lagrange multipliers are used to enforce continuity at the boundaries between subdomains. The novelty of the work is the coupled resolution of the velocity-pressure-Lagrange multiplier system of the discrete Navier-Stokes equations by a distributed memory parallel ILU preconditioned Krylov method. A penalty function on the interface constraints equations is introduced to avoid the locking of the ILU factorization algorithm. To ensure portability of the code, a message

based memory distributed model with MPI is employed. The method has been tested over different benchmark cases such as the lid-driven cavity and pipe flow with unstructured tetrahedral grids. It is shown that the partition algorithm and the order of the physical variables are central to parallelization performance. A speed-up in the range of 5 to 13 is obtained with 16 processors.

The second step involves the design of a parallel sliding mesh technique in view of the necessity to take into account the unsteady motions of the agitators. Lagrange multipliers are used at the sliding interfaces to enforce the continuity between the fixed and moving subdomains. To handle the convective term, both the Newton-Raphson scheme and the semi-implicit linearization are utilized. The method is validated for concentric cylinders and stirred tank flows. Running on 16 processors, the obtained speed-up is close to 8.

Finally, to show the utility of the constructed parallel algorithms the last part of this thesis consists in the characterization of the hydrodynamics of a coaxial mixer in the transition regime. The coaxial mixer is composed of a large paddle (Maxblend) impeller and a double helical ribbon agitator mounted on two independent coaxial shafts rotating at different speeds. The used tetrahedral grids consisted on 1.4 to 3.8M of nodes producing 4.4 and 13.5M equations to solve. The simulations are based on the resolution of the Navier-Stokes equations with help of the developed parallel three-dimensional finite element solver. To model the rotation of agitators, which rotates at

different speeds, a hybrid approach based on the novel finite element sliding mesh and the fictitious domain method is used. The power consumption and mixing times obtained from the simulations show good agreement with the ones acquired from a laboratory pilot rig. The simulations allow observing the flow as it evolves from deep laminar to transition regime.

Condensé en français

Le mélange de fluides dans une cuve agitée peut se faire en régime laminaire, de transition ou turbulent, tout dépendant des conditions d'opération telles que la nature du produit ou bien des contraintes du procédé. Il est étonnant que le régime d'écoulement de transition n'ait pas reçu le même intérêt scientifique que le mélange en régime laminaire et turbulent (TATTERSON, 1991; HARNBY et al. 1997 et PAUL et al. 2003). Ainsi, les opérations de mélange en régime de transition sont typiquement conçues sur la base de mesures expérimentales ou de modèles validés pour le régime laminaire ou pour le régime turbulent se rapprochant le plus des conditions d'opération souhaitées. Pourtant, la compréhension du mécanisme de mélange dans le régime d'écoulement de transition est essentielle pour maximiser la sécurité et l'efficacité du procédé. La technologie standard utilisée pour mélanger en régime de transition consiste à reprendre l'équipement employé pour le régime laminaire (agitateurs de proximité: ancre ou rubans hélicoïdaux) ou pour le régime turbulent (turbines, palettes, hydrofoils). Une façon d'aborder le problème de façon plus efficace consiste à combiner les agitateurs «laminaires» et «turbulents» pour concevoir une configuration hybride plus versatile. Toutefois, l'optimisation est plus complexe étant donné que cela demande une compréhension accrue de la nouvelle hydrodynamique résultant de

l'interaction entre les deux agitateurs. Dans cette perspective, les modèles numériques permettent d'apporter des éléments de réponse.

La modélisation numérique de l'écoulement dans une cuve agitée est gouvernée par les équations de Navier-Stokes. Lorsque ces dernières sont discrétisées avec un schéma numérique, comme les éléments finis ou les volumes finis, on obtient un système d'équations algébrique. L'obstacle principal pour modéliser le régime de transition dans les cuves agitées est que la maille de la grille de calcul a besoin d'être raffinée suffisamment pour bien évaluer le terme d'inertie, composante clé du momentum dans ces conditions d'écoulement Il en résulte une augmentation considérable de la taille du système d'équations. Bien évidemment, cela entraîne des exigences importantes en ressources informatiques aussi bien en mémoire qu'en temps de calcul. À cet égard, l'option de recourir au calcul distribué paraît difficile à écarter. La disponibilité d'ordinateurs multiprocesseurs à prix abordables est un argument de taille qui plaide en faveur de cette option. Par conséquent, l'objectif principal de cette thèse est de développer une stratégie numérique pour modéliser le régime de transition dans des cuves agitées en ayant recours au calcul distribué.

Pour atteindre l'objectif principal, le premier objectif spécifique du travail est consacré au développement d'un algorithme élément fini parallèle capable de prédire l'hydrodynamique d'un problème d'écoulement tridimensionnel de fluide incompressible sur des maillages non structurées. Le deuxième objectif spécifique

quant à lui, implique la conception d'une technique de maillage glissant parallèle afin de tenir compte de la rotation des agitateurs. Finalement, pour démontrer l'efficacité des algorithmes parallèles développés, le dernier objectif est consacré à la caractérisation de l'hydrodynamique d'un agitateur multiple dans une cuve de mélange opérant en régime de transition.

La mise en œuvre informatique consiste à adapter le logiciel POLY3D (Rheosoft, Inc.) pour y intégrer les nouveaux algorithmes parallèles. Développé à l'origine au début des années 80 en Fortran, POLY3D est un solveur d'élément fini tridimensionnel séquentiel dédié à la résolution de problèmes thermo-fluides avec des éléments finis tétraèdres à pression discontinue conservant la masse localement. Les nouveaux algorithmes sont développés et testés sur des ordinateurs IBM-P690 à 16 processeurs avec une mémoire partagée de 64GB. Pour s'assurer de la portabilité du code, notre choix s'est porté vers le protocole de communication Message Passing Interface (MPI). Les maillages tétraédriques tridimensionnels utilisés pour effectuer les tests sont générés avec l'aide des logiciels commerciaux I-DEAS (Siemens) et GAMBIT (ANSYS). Enfin, le post-traitement des résultats est effectué avec le logiciel ENSIGHT (CEI).

La stratégie de parallélisation se base sur les méthodes de décomposition de domaine sans chevauchement. Les multiplicateurs de Lagrange sont utilisés pour assurer la continuité aux frontières entre les sous-domaines. L'espace des multiplicateurs de

Lagrange est discrétisé en utilisant des fonctions de Dirac. Cela se fait avec l'idée de simplifier la discrétisation de la contrainte d'interface ce qui permet son imposition ponctuelle. Par conséquent, on élimine le besoin de calculer des intégrales de surface à la frontière entre les sous-domaines. L'originalité de ce travail réside dans la résolution couplée du système d'équations en variables de vitesse-pression-multiplicateurs de Lagrange résultant de la discrétisation des équations de Navier-stokes par une méthode de Krylov parallèle et un préconditionnement par factorisation incomplète ILU (0) avec mémoire distribuée. Une technique de pénalisation est introduite à l'interface pour éviter le blocage de l'algorithme de factorisation ILU.

La méthode est vérifiée sur deux cas de référence (écoulement dans une conduite et dans une cavité) en utilisant des approximations par éléments finis discontinues en pression ($P1^+$-P0/$P2^+$-P1) sur des maillages, en tétraèdres, non structurés. Puisque le terme convectif n'est pas encore considéré pour le moment, les écoulements de Stokes (problèmes linéaires) sont résolus avec le solveur parallèle de Krylov du type gradient conjugué (GC) et multiplicateurs de Lagrange. On constate que l'accélération des temps de calcul n'est pas linéaire en raison de deux facteurs: i) le temps système généré dans chacune des opérations de préconditionnement matrice-vecteur; ii) l'augmentation du nombre d'itérations du GC nécessaires pour converger par rapport au nombre de partitions. Pour l'écoulement dans une conduite, l'accélération globale des temps de calcul pour le nombre maximum de partitions utilisées (16) varie dans une plage de 8 à 14, ce qui donne une efficacité de parallélisation variant entre 50 et 88%. Pour

l'écoulement dans une cavité, le nombre d'itérations montre une augmentation plus drastique par rapport au nombre de partitions. En conséquence, l'accélération globale des temps de calcul par rapport à la série séquentielle est de 5 à 5.8 fois plus rapide en calculant sur 16 processeurs. Afin d'améliorer cette performance, l'ordre des variables physiques ainsi que la stratégie de partitionnement sont étudiés. Dans ce travail, il est démontré que la performance en parallèle peut être améliorée en utilisant une stratégie adéquate dans le cas des maillages non structurées, où l'homogénéité de l'interface et la connectivité de la partition sont des paramètres clés dans l'obtention d'une bonne performance, même au prix d'une plus grande aire interfaciale. Avec cette stratégie, une accélération globale de 11 est obtenue, ce qui signifie une efficacité parallèle de 68%.

Afin de considérer les frontières mobiles de l'agitateur, un algorithme parallèle de maillage glissant a été développé pour la simulation par éléments finis des écoulements tridimensionnels incompressibles et visqueux sur des maillages non structurés. Comme pour le solveur parallèle, la technique des multiplicateurs de Lagrange est utilisée aux interfaces de glissement pour assurer la continuité entre les partitions stationnaires et fixes. La méthode est validée dans deux cas d'écoulement : i) entre deux cylindres concentriques; ii) dans une cuve agitée, démontrant une excellente précision. Pour stabiliser le solveur lorsque la convection domine, deux méthodes sont utilisées, à savoir, le schéma de Newton-Raphson et la linéarisation semi-implicite. Il est prouvé que la technique de maillage glissant en combinaison avec le schéma de Newton-

Raphson apporte une précision légèrement supérieure à celle obtenue avec le schéma semi-implicite, surtout quand de grands pas de temps sont employés. Cependant, le schéma semi-implicite économise une quantité considérable de temps CPU. Il est établi que la technique de maillage glissant est très stable pour converger en utilisant des grands pas de temps que le schéma implicites de type Gear autorise. Comme on pouvait s'y attendre, la technique montre une réduction quadratique de l'erreur en fonction de la taille du pas de temps. L'approche est parallélisée pour simuler l'écoulement non permanent dans une cuve agitée avec des chicanes. La consommation de puissance calculée présente une différence de 2% par rapport aux données expérimentales. Une accélération de 7.4 est obtenue avec 16 processeurs. Il est confirmé que la technique permet de partitionner encore plus, autant la partition de glissement que celle fixe, pour avoir un nombre souhaité de partitions, permettant ainsi une parallélisation encore plus agressive.

Finalement, l'hydrodynamique et le mécanisme de mélange à l'échelle macroscopique du mélangeur coaxial composé d'une large palette (Maxblend®) et d'un double ruban hélicoïdal montés sur deux arbres coaxiaux indépendants sont étudiés par simulation numérique. Les simulations sont basées sur la résolution des équations de Navier-Stokes avec l'aide du solveur parallèle développé. Pour modéliser la rotation des agitateurs qui tournent à des vitesses différentes, une approche hybride est utilisée basée sur l'appariement des techniques de maillage glissant et de domaine fictif. Le

maillage tétraédrique utilisé contient de 1.4 à 3.8 millions de nœuds, correspondant respectivement à un nombre d'inconnues variant de 4.4 à 14.5 millions d'inconnues.

Les simulations permettent d'observer les patrons d'écoulements produits par le mélangeur coaxial Superblend alors que l'hydrodynamique évolue du régime laminaire profond jusqu'au régime de transition. L'écoulement se caractérise par la formation de plusieurs zones de recirculation au-dessus et en dessous du milieu de la cuve. Pour le mode contre-rotatif, plusieurs tourbillons, dont le nombre augmente en fonction du nombre de Reynolds, ont été observés sur une section transversale horizontale au milieu de la cuve. Ce phénomène n'est pas observé en mode co-rotatif. De plus, le patron d'écoulement en mode co-rotatif montre un écoulement vers le haut à la paroi de la cuve et vers le bas près de l'arbre de rotation. Le patron s'inverse en mode contre-rotatif, à savoir que le fluide se déplace vers le bas près de la paroi et vers le haut à proximité de l'arbre.

À partir des profils de pompage et de cisaillement le long de la hauteur du mélangeur, on observe que le pompage moyen et les valeurs de cisaillement sont supérieurs en mode contre-rotatif comparativement au mode co-rotatif. Cependant, quand le mélangeur fonctionne en mode contre-rotatif, ces variables montrent une distribution hétérogène le long de la hauteur de la cuve, ce qui contraste avec les patrons plus homogènes observés en mode co-rotatif. Les valeurs du cisaillement ainsi que ceux du pompage sont constants en régime laminaire, par contre en régime de transition, ils

augmentent considérablement. En plus, il est prouvé que l'effet principal du mode de rotation sur le pompage axial est que dans le mode co-rotatif la zone d'écoulement axial principale est localisée dans la partie supérieure de la cuve, tandis qu'en mode contre-rotatif, elle se trouve dans la région inférieure.

En terme de consommation d'énergie, le mode co-rotatif consomme moins de puissance et les temps de mélange sont égaux ou plus petits que ceux qu'on obtient en mode contre-rotatif. La consommation de puissance plus élevée demandée par le mode contre-rotatif est causée par la présence de tourbillons à haut cisaillement, lesquels sont générés entre les deux mélangeurs coaxiaux. Les temps de mélange plus longs obtenus avec le mode contre-rotatif sont causés par les difficultés rencontrées par le traceur pour atteindre la zone d'écoulement axial la plus importante dans le mélangeur, se situant dans la zone centrale inférieure de la cuve. Finalement, basé sur le concept d'énergie de mélange, on observe que le mode co-rotatif est plus efficace que le mode contre-rotatif. Le coût de consommation d'énergie pour pomper et pour cisailler diminue quand les mélangeurs fonctionnent en co-rotation.

À la lumière des résultats obtenus dans le cadre de cette thèse, de nouvelles perspectives de recherche apparaissent. Par rapport à la méthodologie, il serait intéressant de combiner le développement du solveur parallèle avec des techniques multi-grilles pour pouvoir contrôler l'augmentation du nombre d'itérations par rapport au nombre de sous-domaines. Afin de résoudre des problèmes sur des maillages

beaucoup plus fins que ceux utilisés dans le présent travail, une avenue de recherche possible est l'extension de la méthode de parallélisation aux éléments finis moins riches; nous pensons notamment à l'élément MINI. Par rapport à l'analyse du mélange, la caractérisation du mélangeur Superblend demeure un champ d'investigation ouvert. Il serait, en effet approprié d'analyser les effets du rapport des vitesses des agitateurs intérieur et extérieur ainsi que ceux de la rhéologie non-Newtonienne sur l'hydrodynamique.

Table of contents

List of tables

List of figures

List of algorithms

Nomenclature

Symbol	Description	Units
a	empirical constant in Forschner model	dimensionless
c	concentration	mol/m^3
$\bar{c}$	average concentration	mol
C_s	empirical constant in Wassmer-Hungenberg model	dimensionless
c_{geom}	geometrical constant in Wassmer-Hungenberg model	dimensionless
d_e	internal diameter of the inner cylinder in the Couette flow	m
D	diameter of the agitator	m
D_i	diameter of inner agitator in coaxial mixers	m
D_o	diameter of outer agitator in coaxial mixers	m
E_{mix}	mixing energy	dimensionless
$E(n)$	parallel efficiency	%
H	tank height	m
Kp	power number constant	dimensionless
Ks	shear constant from Metzner-Otto model	dimensionless
K_2	empirical constant in Forschner model	dimensionless
$K_{transition}$	empirical parameter in Forschner model	dimensionless
m	consistency index in power-law model	$Pa\ s^n$
n	flow behaviour index in power law model	dimensionless
np	number of processors	
N_c	characteristic rotational speed	rev/s
N_o	rotational speed of inner agitator	rev/s
N_i	rotational speed of outer agitator	rev/s

Np	power number	dimensionless
Nq	pumping number	dimensionless
Ns	shear number	dimensionless
$\overline{Nq}$	average pumping number	dimensionless
$\overline{Ns}$	average shear number	dimensionless
Q	pumping rate	m^3/s
P	power consumption of the mixer	W
p	pressure field	Pa
Re	Reynolds number	dimensionless
Re_{MO}	Reynolds number Metzner-Otto modified	dimensionless
Re_m	Reynolds number modified	dimensionless
s	standard deviation of the concentration	mol
$S(n)$	parallel speed-up	dimensionless
Tm	mixing time	s
t	time	s
t_s	sequential run time	s
t_n	parallel run time	s
$\mathbf{v}$	velocity field	m/s
$\dot{\mathbf{v}}$	velocity time derivative	m/s^2
$\mathbf{v}_m$	sliding partition velocity	m/s
v_z'	estimation of the axial velocity in the Cheng-Carreau model	m/s
V	volume of the mixing tank	m^3
z	distance from the bottom of the tank	m

Greek symbols:

Symbol	Description	Units
μ	viscosity	Pa s
ρ	density	kg/m^3
φ	shape function for the velocity space	dimensionless
ψ	shape function for the pressure space	dimensionless
ξ	shape function for the Lagrange multiplier space	dimensionless
$\dot{\gamma}$	rate-of-strain tensor	s^{-1}
$\dot{\gamma}_a$	apparent (effective) deformation rate	s^{-1}
τ	stress tensor	Pa
λ	Lagrange multiplier	N
Ω	computational domain	-
Γ	subdomain interface	-
η_e	effective viscosity	Pa s
ω'	angular velocity estimation in Cheng-Carreau model	rev/s

Sub- and superscripts:

$*$	related with the virtual finite element method
θ	tangential component
r	radial component
SM	related with the sliding mesh method

t time step iteration

T transpose

z axial component

Abbreviations:

LBB	Babuska-Brezzi-Ladyzhenskaya condition
BiCGSTAB	Bi-conjugate gradient stabilized method
CEBE	clustered-element-by-element preconditioner
CFD	computational fluid dynamics
CG	conjugate gradient method
CMC	carboximethyl cellulose
COV	coefficient of variation
CPU	computer processor unit
DHR	double helical ribbon
EBE	element-by-element preconditioner
FETI	finite element tearing and interconnecting method
GMRES	generalized minimal residual method
ILU	incomplete lower upper factorization
ILU (0)	incomplete lower upper factorization with zero fill-in
LDA	laser Doppler anemometry
LIF	particle laser induced fluorescence

MFR	multiple frame of reference
MPI	message passing interface
PBT	pitched blade turbine
PIV	particle image velocimetry
QMR	quasi-minimal residual method
SM	sliding mesh
VFEM	virtual finite element method

Chapter 1.   Introduction

1.1 Mixing in the transition flow regime

Mixing is defined as the combination of two or more dissimilar portions of materials, resulting in the attainment of a desired level of uniformity, either physical or chemical, in the final product. In the processing of industrial fluids, it is necessary to introduce mechanical energy to promote good homogeneity (HOLLAND and CHAPMAN, 1966). The standard equipment consists in a tank provided with an agitator mounted on a rotating shaft located at the center of the vessel. The motion of the impeller produces high velocity streams that transfer momentum to stagnant zones, resulting in a fully developed flow.
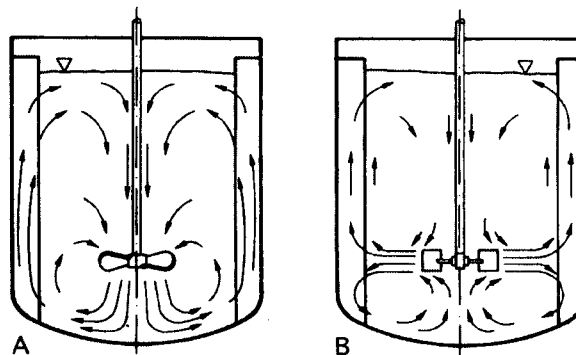
Figure 1-1: Schematic representation of the flow inside agitated tanks (HOLLAND and CHAPMAN, 1966).

The flow intensity depends on the relationship between the fluid movement induced by the agitator and the resistance presented by the viscous forces of the fluid, which defines the mixing Reynolds number (Re). The mixing flow regime can be classified in laminar, transitional and turbulent based on the relation between the dimensionless power consumption (Np) and the Reynolds numbers.

Fluid mixing occurs in any of the flow regimes describe above, depending on the product characteristic and the process constraints. It can be remarked that the transition flow regime has not received the same scientific interest as laminar and turbulent mixing (TATTERSON; 1991; NIENOW et al.; 1997; PAUL et al., 2003). Equipment that operates in the transition regime is typically designed based on experimental measurements or models valid in the laminar or the turbulent regime, whichever is closer to the transitional operating conditions. However, the transitional flows show more complex patterns than the laminar ones but without developing as much hydrodynamic fluctuations as in fully turbulent conditions. In the initial stage of the transition regime instabilities appear but they vanish due the still high molecular viscosity. As the flow becomes less dependent on the viscosity, these instabilities grow until secondary flows are formed. In its final stage, the flow is very unstable fluctuating until it becomes fully turbulent. Some examples where the transition regime is encountered are given next.

A common case is found in the scaling-up of agitated tanks. If the power input per volume or the tip velocity speed rules are chosen to keep the same viscous dissipation distribution, the flow evolves from the laminar to the transition regime as shown in Figure 1-2 and Figure 1-3, respectively.
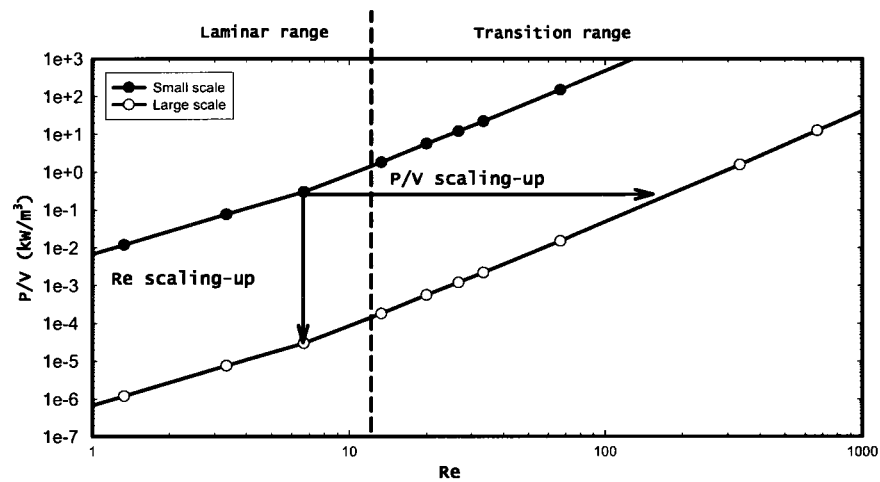
Figure 1-2: Variation of specific power for different Re at different scales.
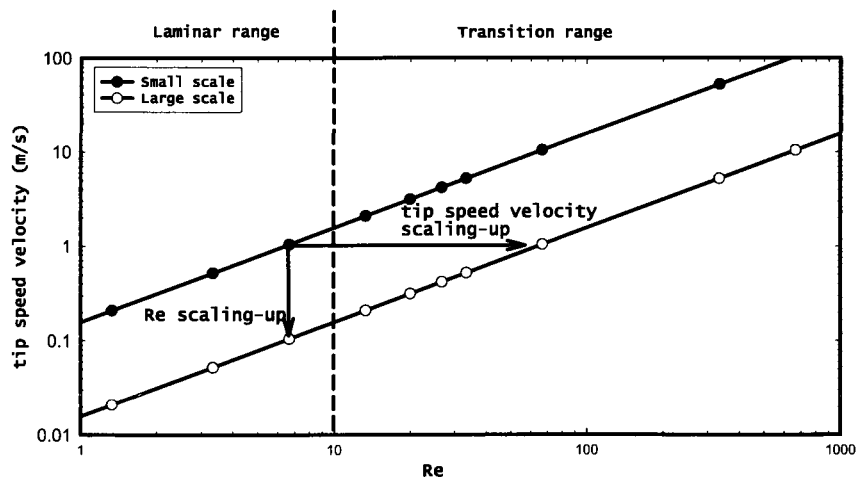
Figure 1-3: Variation of tip speed velocity for different Re at different scales.

The transition flow regime is also present in the mixing of moderate viscosity materials that are sensitive to shear or heat such as cell culture broths, crystals and colorant suspensions. With these fluids, attempting to reach the turbulent regime by increasing the rotational speed of the impeller becomes inefficient since the energy introduced to the system is converted mostly in heat due to viscous dissipation. On the other hand, keeping the flow in deep laminar regime may require longer processing times ($N\theta$) in most mixing configurations as shown in Figure 1-4. In these conditions, the transitional regime may be the best option for a successful mixing.
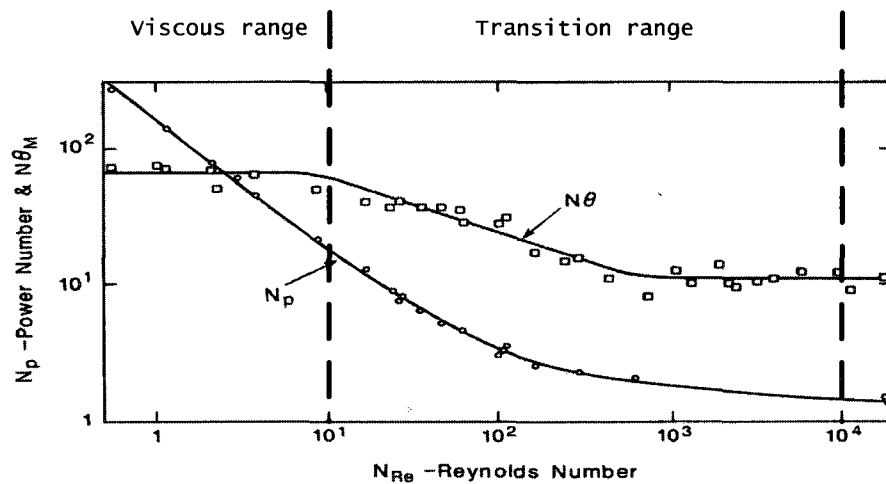
Figure 1-4: Variation of dimensionless mixing time ($N\theta$) and power consumption (Np) in laminar and transition regime (NOVAK and RIEGER, 1969).

Transition regime is becoming potentially important for the industries that utilize solvents in their products. Environment regulations seeking to minimize discharge of volatile organic compounds (VOCs) have encouraged companies to reduce or eliminate

solvents from many products which translate in the processing of materials with higher viscosities (COHEN and LANGHORN, 2004). As a consequence these industries might be forced at some point to mix at lower Reynolds number; i.e., from the turbulent regime to the transition or laminar ones.

Finally the transition regime is found in the mixing of materials that experience changes in viscosity during processing such as in fermentations, cosmetics or bulk polymerization operations. These processes start out with watery liquids where turbulent mixing is possible. However, as the viscosity starts to build-up due to the addition of ingredients or to physico-chemical changes, the process needs to be carried out in the best scenario in the transition flow regime. Turbulent conditions become no longer feasible due to the large increases in the fluid viscosity. Lack of knowledge of the hydrodynamics in this regime may lead to complications in the control of the process reducing the quality, yield of the product and sometimes the safety of the process.

1.2 Technology to mix in transition flow regime

The standard technology used to mix in the transition flow regime consists of the equipment utilized in the laminar (proximity agitators: anchors or helical ribbons) or the turbulent (turbines, paddles, hydrofoils) regimes as can be deduced from Figure 1-5. Baffles need to be included in the design to avoid central vortex formation when

turbulent agitators are used. The efficiency of these agitators in transition regime is usually lower than in any other regime, i.e., proximity impellers are more efficient in laminar conditions and turbines, paddles and hydrofoils are more efficient in turbulent regime.
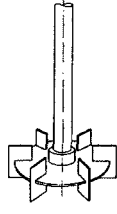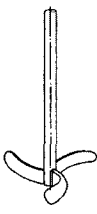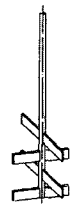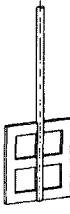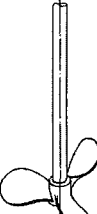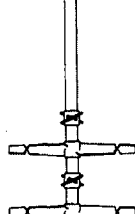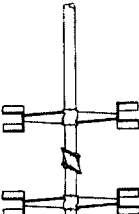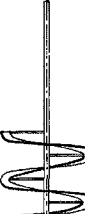
Figure 1-5: Agitators for different viscosity ranges (ZLOKARNIK, 2001)

An efficient mixer for the transition region should provide enough shear action to disperse the materials. Furthermore, the pumping capacity produced by such impeller should generate good circulation through the tank to avoid hot spots or segregated zones. One option is the fusion of different agitators as in the case of the Maxblend™ agitator (Sumitomo Heavy Industries), where a grid and a wide paddle were blended as

shown in Figure 1-6. The grid helps to enhance dispersion while the paddle produces

pumping. Maxblend™ has been shown to be very efficient in the transition region

(IRANSHAHI et al., 2007).

Grid part

Maxblend agitator

Paddle part
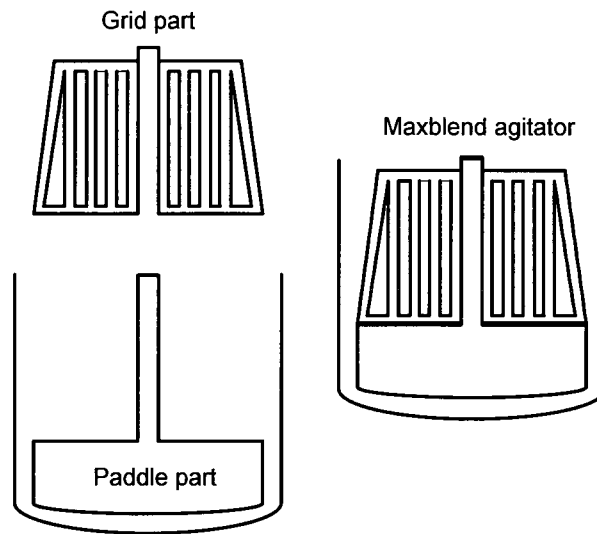
Figure 1-6: Maxblend™ Agitator (Sumitomo Heavy Industries, Japan)

Another approach is to combine laminar and turbulent impellers to build hybrid

configurations with higher versatility. This concept has been employed to design novel

configurations composed of multiple agitators rotating at different speeds. ESPINOSA-

SOLARES et al. (2002) proposed a helical ribbon with a turbine at the bottom of the

tank to disperse gas in viscous fluids (Figure 1-7a). THIBAULT and TANGUY (2002)

presented the performance of a coaxial mixer composed of an anchor and a series of

rods and a pitched-blade turbine for the production of pigment suspensions used in the

paper coating industry (Figure 1-7b). FOUCAULT et al. (2006) used an anchor and a

set of different turbines to mix fluids with non-Newtonian viscosities. BARAR POUR et al. (2007) utilized an angled anchor (Paravisc™) in combination with an eccentric positioned rotor-stator to disperse solids in liquids phases (Figure 1-7c). KHOPKAR et al. (2007) employed the same design to prepare emulsions. As can be noted from the wide diversity of applications, combination of impellers generally gives good results. However its optimization is more complex since it requires a deeper understanding of the new hydrodynamics obtained from the interaction between agitators.
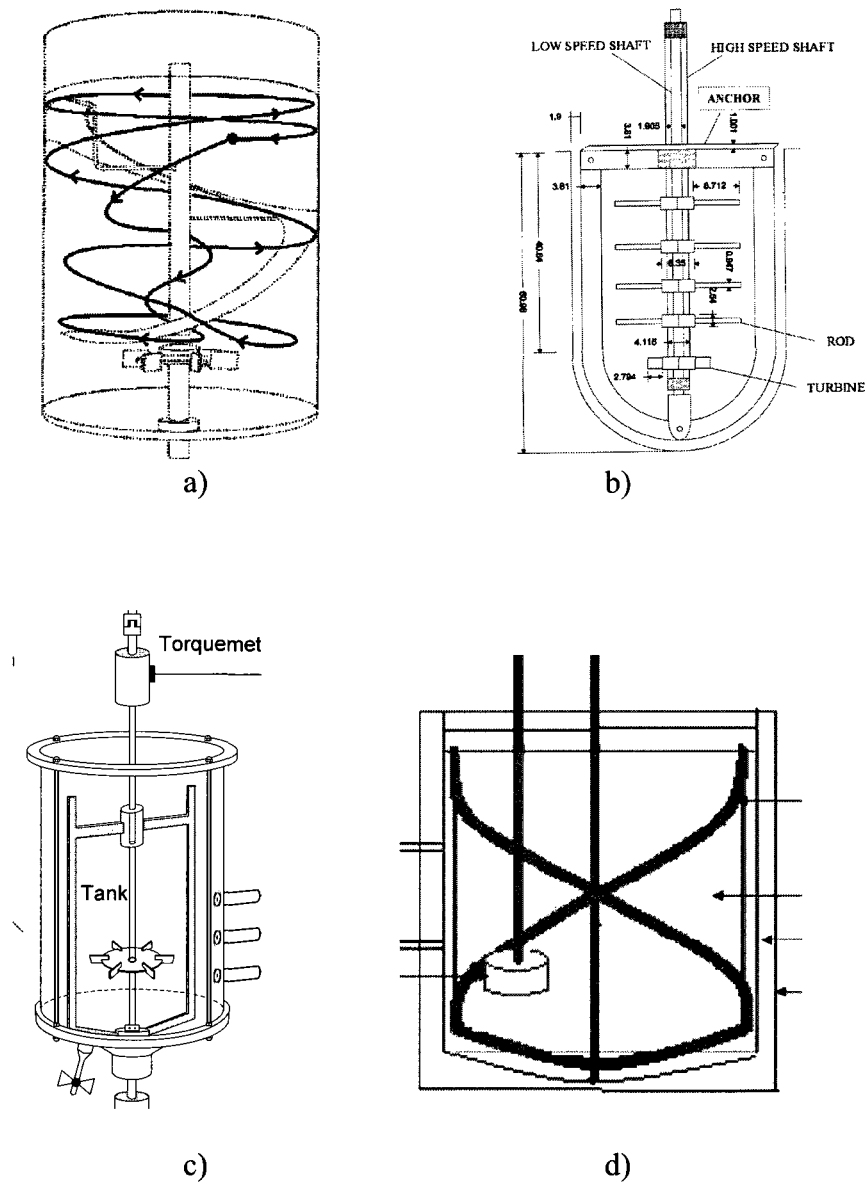
Figure 1-7: Novel mixing technologies suitable for transition regime. a) Helical ribbon

and turbine (ESPINOSA-SOLARES et al., 2002); b) Anchor and series of rods

(THIBAULT and TANGUY, 2002); c) Anchor and turbine (FOUCAULT et al., 2006);

d) Angled anchor (Paravisc™) and rotor-stator (BARAR POUR et al., 2007).

1.3 Methods to characterize mixing hydrodynamics

An understanding of the fluid mixing mechanism in the transition flow regime is a critical step to maximize safety and efficiency. The mixing operation can be characterized utilizing experimental and numerical models. Experimental works are usually carried out on small pilot rigs where power consumption and mixing times can be determined by several techniques developed through the years (ASCANIO et al., 2004; CABARET et al., 2007). These experimental techniques mostly provide global information of the mixing performance and a qualitative observation of the flow patterns if transparent vessels and fluids are employed. For non-transparent tanks most techniques rely on the insertion of probes in the flow to measure pH or temperature which may alter the flow.

To properly design efficient mixers, local flow information is meaningful. Detailed experimental measurement techniques, such as laser Doppler anemometry (LDA) (WU and PATTERSON, 1989; DUCCI and YIANNESKIS, 2005), particle image velocimetry (PIV) (ESCUDIE and LIN, 2003), and laser-induced fluorescence (LIF) (DISTELHOFF and MARQUIS, 1998) are very helpful in resolving large-scale as well as small-scale flow structures in small vessels. However, the local parameters dominating the flow (vorticity, energy dissipation rates, shear rates, axial pumping rates) in the whole three dimensional tank are hardly accessible by these techniques not forgetting that they are unfeasible for reactors at the industrial size. Furthermore, in order to apply them, both the fluid and the vessel and sometimes the impeller need to

be optically transparent. Other techniques as radioactive particle tracking (RAMMOHAN et al., 2001) and electric resistance tomography (MANN et al., 1997; DUDUKOVIC, 2002) show promising results since they work very well for non-transparent material and vessels, but they are still limited due their costly or complex experimental procedures. Computational modeling is an alternative route to obtain local and global information of the flow field. With the convenience of high performance computers and the efficient implementation of accurate numerical algorithms, computational fluid dynamics (CFD) is a helpful tool to characterize mixing industrial equipment.

1.4 Challenges to numerically model transition flow regime in agitated tanks

The modeling of the isothermal single phase flow in agitated vessels is governed by the Navier-Stokes equations, namely:

$$\rho\left(\dot{\mathbf{v}} + \mathbf{v} \cdot \operatorname{grad} \mathbf{v}\right) - \mu \nabla^2 \mathbf{v} + \operatorname{grad} p = 0 \tag{1.1}$$

$$\operatorname{div} \mathbf{v} = 0 \tag{1.2}$$

These equations are capable to predict any flow regime. However, since the resolution is performed in finite precision computers, the continuum medium needs to be represented by a mesh consisting of several interconnected elements or cells. The

partial derivates are then approximated with help of a numerical scheme such as the finite element or finite volume methods to obtain an algebraic system of equations.

The accurate numerical modeling of transition flows in agitated tanks is still challenging, the main obstacle being the time and memory required to accurately predict the convective term ($v \cdot grad\, v$) in the Navier-Stokes equations which is not negligible in the transition regime. As shown in Figure 1-8, as the Reynolds number increases, the flow structures become more complex and the mesh size to represent the problem needs to be refined otherwise numerical instabilities arise when convection dominates the flow (ZIENKIEWICZ and TAYLOR, 2000). Furthermore, convection introduces a nonlinearity to the equations, requiring special handling. If implicit schemes are used then extra fixed point iterations are required. On the other hand, if explicit treatment is utilized, many time steps are necessary to satisfy the Courant-Friedrisch-Lewy condition.
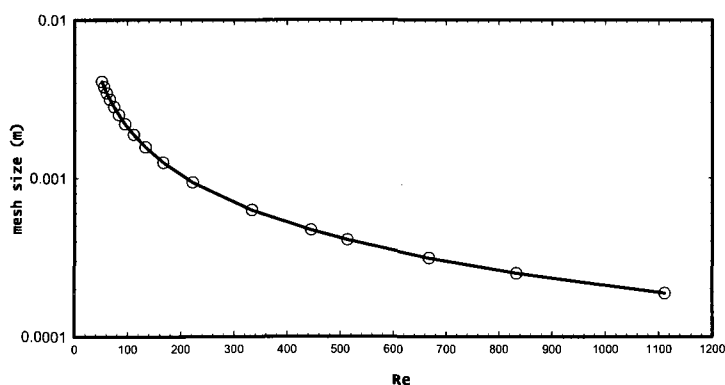
Figure 1-8: Mesh size requirement with respect to the Reynolds number for a 40 L. agitated tank

As already discussed in section 1.2, the geometries employed at this regime are generally complex, usually requiring locally refined unstructured grids with high aspect ratios to properly represent geometrical details such as the curved, angled shapes and small gaps of agitated tanks. Special handling is generally required to reproduce the motion of the impellers that may require extra time and memory.

Excessive waiting times are not efficient for process design. Taking into account that high performance computations have been successfully applied to several large-scale flow problems, it becomes necessary to design computational algorithms suited for multi-processor computers. Early applications in fluid mechanics were made by FARHAT et al. (1993) and JOHAN et al. (1995). Their works demonstrated the possibility to speed-up calculations and to reduce the memory per processor by the use of parallel computers.

1.5 General objective

The general scope of the project is to develop a numerical method to model the transition flow regime in novel mixing technologies exploiting the capabilities of parallel computers. The methodology will be designed to tackle two challenges of the present investigation:

- the increase in computation time and memory as mesh is refined

- the modeling of the motion of the agitators

Chapter 2.   Literature review

Based on the general objective of this thesis, the literature review is divided in three parts; transition flow regime in agitated tanks, parallel computing and numerical modeling of the agitator motion. The first section is intended to provide the state-of-the-art of the mixing in the transition regime. The purpose of the last two sections is to give a general background of the computational techniques required to develop a parallel algorithm capable to predict the hydrodynamics in stirred tanks.

2.1.   Transition flow regime in agitated tanks

The log-log plot of the Reynolds number with respect to the dimensionless power number is commonly used to identify the flow regime the mixing is performed. The Reynolds number is defined as:

$$Re = \frac{\rho ND^2}{\mu} \tag{2.1}$$

and the power number is expressed as:

$$Np = \frac{P}{\rho N^3 D^5} \tag{2.2}$$

The characteristic shape of this plot for different impellers is depicted in Figure 2-1.
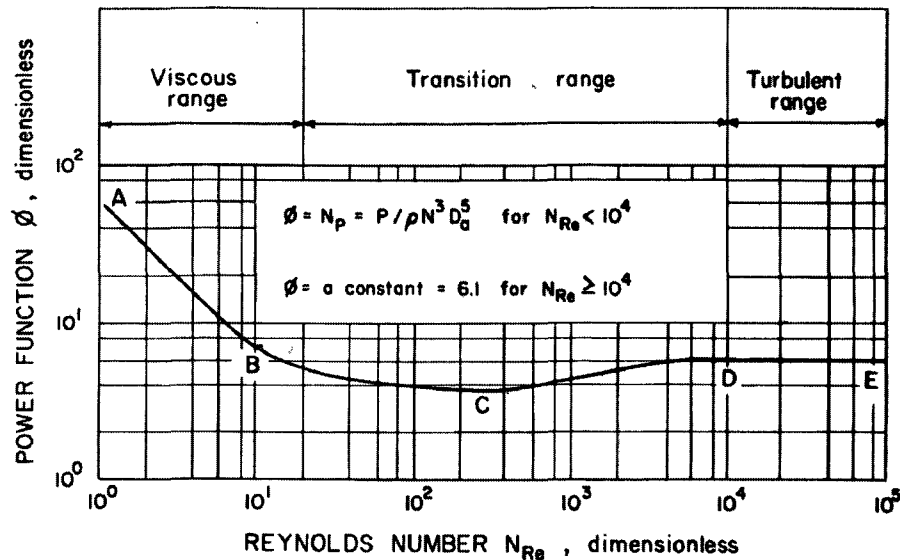
Figure 2-1: Flow regimes for standard agitated tank configuration (HOLLAND and

CHAPMAN, 1996)

Based on classical mixing theory, in the laminar regime (point A to B region in Figure

2-1) the slope of the regression $Np = Kp(\text{Re})^a$ is equal to -1. In the turbulent regime

(point D to E region in Figure 2-1) the power number is constant, i.e., the slope in

$Np = Kp(\text{Re})^a$ is zero. The region comprised from point B to D in Figure 2-1 defines the

transition regime.

2.1.1. Experimental studies

a) Macro-variables

Early studies of mixing in the transition regime are focused on the determination of

macro-variables such as the effective deformation rate generated within the mixing

tank. In laminar regime, this parameter is calculated with help of the relation given by METZNER and OTTO (1957):

$$\dot{\gamma}_a = K_s \cdot N \qquad (2.3)$$

By this approximation it is possible to define a modified Reynolds number for power law fluids as:

$$\mathrm{Re}_{MO} = \frac{\rho K_s^{1-n} N^{2-n} D^2}{m} \qquad (2.4)$$

However, as evidenced in the work of METZNER et al. (1961), relation (2.3) only holds in the laminar region. Literature points out that in the transition region the deformation rate increases with respect to the Reynolds number. For example, POLLARD and KANTYKA (1969) found that for anchor agitated tanks the average shear rate is proportional to almost the fourth power of the agitator speed as shown in Figure 2-2.
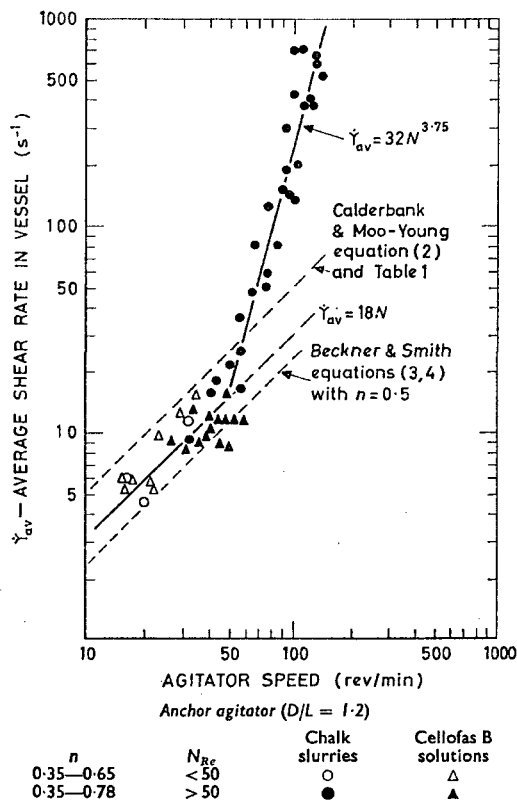
Figure 2-2: Effect of the agitator speed on the average shear rate in the laminar regime

(N<50 rev/min) and the transition regime (N>50 rev/min) (POLLARD and

KANTYKA, 1969)

In a different work WITCHERLE et al. (1984) reported deformation rate values in the vicinity of the turbine blade based on an electrochemical technique as presented in Figure 2-3.
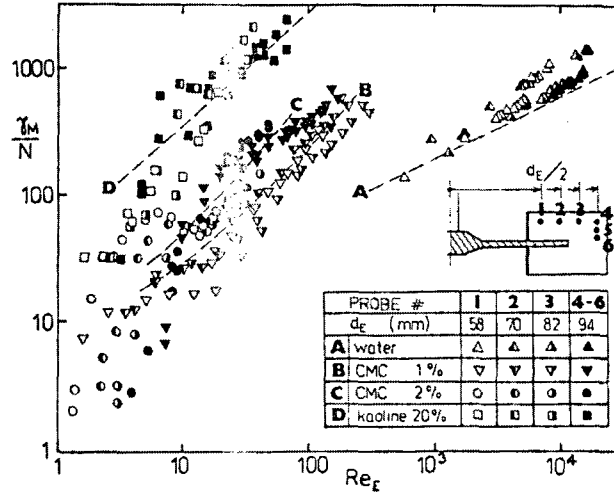
Figure 2-3: Dependence of the dimensionless shear rate $\dot{\gamma}_a/N$ with respect to Re in the

vicinity of the agitators blade (WITCHERLE et al., 1984)

They have proposed the following correlation for the average shear rate in the transition regime:

$$\dot{\gamma}_a = (1 + 5.3n)^{1/n} \left(\frac{\rho N^{2-n} D^2}{m} \right)^{1/(n+1)} N \tag{2.5}$$

Furthermore, JAHANGIRI et al. (2001) using laser Doppler anemometry observed that in the transition region (30<Re<2000) the variation of local deformation rate in an agitated tank with a Rushton turbine is well correlated by the following equation:

$$\dot{\gamma}_a = K_s' N^b \tag{2.6}$$

In view to determine the deformation rate, several methods have been proposed. ZEPPENFELD and MERSMANN (1988) presented an iterative procedure based on the increase of the mean flow velocity standardized with the stirrer tip velocity. Their technique requires several parameters such as the power characteristic of the impeller for the whole region from laminar to turbulent flow, the K_s constant, the turbulent pumping coefficient, and the dimensionless mean velocity. An alternative approach is proposed by FORSCHNER et al. (1992) who modified the Metzner-Otto equation utilizing a varying K_s parameter that is calculated from:

$$K_{transition} = K_2 K_s \, \text{Re}_{MO}^a \tag{2.7}$$

The empirical constants (K_2 and a) are determined from experimental data correlations. CHENG and CARREAU (1994) developed models to determine the effective deformation rates in the transition regime based on an analogy with the Couette flow. The first model is originated from the relation between the power consumption and the torque exerted on the inner cylinder producing the following equation:

$$\dot{\gamma}_a = \left[\frac{K p \, d_e^3}{\pi^2 d_e^2 H} \right]^{1/q} \left[\frac{d_e^2 \rho}{m} \right]^{(1-a)/q} N^{(2-a)/q} \tag{2.8}$$

where $q = n(1-a) + a$. In the same work, the authors proposed a model based on the helical flow between two concentric cylinders taking into account the contribution from the axial velocity:

$$\dot{\gamma}_a = \left[\frac{Kp'd_e^3}{\pi^2 d_e^2 H}\right]^{1/s} \left[\frac{d_e \rho}{m}\right]^{(1-a)/s} N^{(2-a)/s} \left[\left(\frac{d_e}{2\omega'}\right)\left(v_z'^2 + \left(\frac{d_e}{2}\right)^2 \omega'^2\right)^{0.5}\right]^{-n/s} \tag{2.9}$$

where $s = a(1-n)$ and the values of v_z' and ω' are calculated at the inner cylinder wall.

The predictions obtained with these models show very good agreement with data obtained from various non-Newtonian fluids as shown in Figure 2-4.
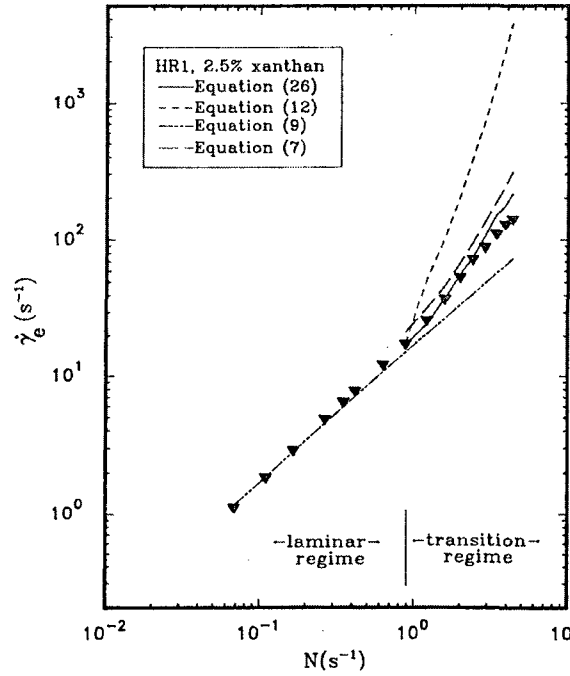
Figure 2-4: Comparison of the experimental deformation rate with the theoretical model predictions. Equation (9) and (26) are (2.8) and (2.9) in the text. (CHENG and CARREAU, 1994)

CHENG and CARREAU (1994) pointed out the necessity to improve the accuracy of numerical models to obtain a better estimation of the deformation rate in complex configurations. In the same study, they also observe a decay of the mixing time when Reynolds number increase in the transition region (Figure 2-5).
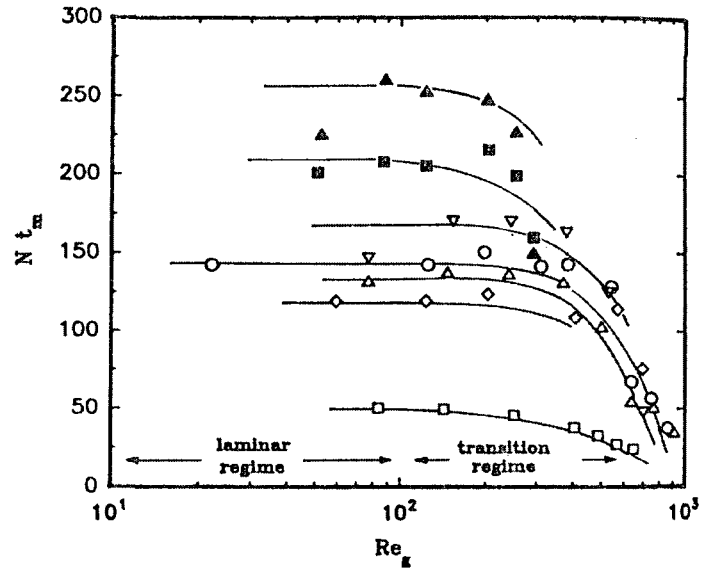
Figure 2-5: Reduction of the dimensionless mixing time (Nt_m) in the transition regime

(CHENG and CARREAU, 1994)

Later, WASSMER and HUNGENBERG (2005) developed a way to extend the Metzner-Otto method for both the transition and the turbulent flow regimes employing the relation between the effective shear stress and specific power input. They proposed an effective shear rate calculated by the following expression:

$$\dot{\gamma}_a = C_s \frac{\rho N_p N^2 D^5}{\eta_e V} \qquad (2.10)$$

where the constant C_s is determined with help of the following correlation:

$$C_s = c_{geom.} \frac{Ks}{Kp} \qquad (2.11)$$

As in the approach of ZEPPENFELD and MERSMANN (1988), an iterative procedure is used to calculate the η_e parameter.

b) Velocity measurements

Other studies are focused on the local hydrodynamic characterization of the flow close to the impeller with help of techniques such as laser Doppler anemometry (LDA) or particle image velocimetry (PIV). Table 2-1 summarizes the authors, the configurations, the flow conditions and the techniques used in these works. The main findings are resumed next.

Table 2-1: Experimental single phase mixing studies in the transition flow regime

Authors	Agitator type	Flow conditions
KOUTSAKOS et al. (1990)	Rushton turbine and baffles	Re=5-5000 (shear-thinning fluids)
DYSTER et al. (1993)	Rushton turbine and baffles	Re=5-5000 (water)
HOCKEY and NOURI (1996)	Pitched blade turbine and baffles	Re=200-5000 (water and maltose syrup)
MAVROS et al. (1996)	Radial and axial turbines	Re=480 (CMC solutions)
MONTES et al. (1997)	Pitched blade turbine and baffles	Re=300-1200 (water and glycerine)
SCHAFER et al. (1998)	Pitched blade turbine and baffles	Re=225-7500 (water)
JAHANGIRI (2006)	Rushton turbine	Re=35-1800 (Viscoelastic liquids)
JAHANGIRI (2007)	Helical ribbon impeller	Re=70-6700 (Viscoelastic liquids)
ESCUDIE et al. (2002)	Hydrofoil	Re=17-280

Laser Doppler anemometry measurements have been reported for agitated tanks operating in the transition regime by KOUTSAKOS et al. (1990) and DYSTER et al. (1993) who measured mean velocity profiles with help of LDA. They reported an increase in the radial pumping with respect to the Reynolds number as shown in Figure 2-6.
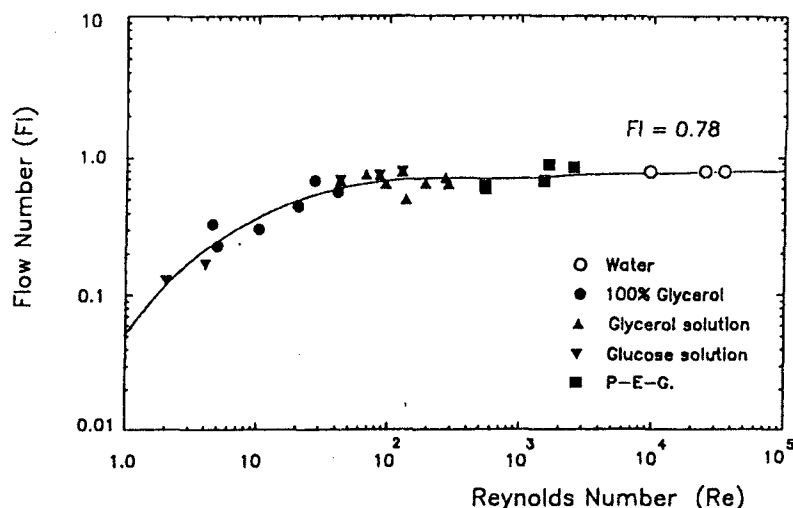
Figure 2-6: Flow number with respect to the Reynolds number in the laminar, transition

and turbulent regimes (DYSTER et al., 1993)

Other studies have reported the evolution of the flow from a primary pattern to a secondary one. HOCKEY and NOURI (1996) observed at Re=1200 a flow reorientation from radial to axial direction. This finding agrees with the velocity measurements of NOURI and WHITELAW(1990). MAVROS et al. (1996) reported a well-defined flow segregation when agitating non-Newtonian liquids with radial impellers. The authors have concluded that in the transition regime, non-Newtonian liquids have more difficulties to be pumped along the whole tank than a Newtonian liquid. MONTES et al. (1997) based on the unsteady analysis of the velocity near the impeller showed a non-stationary, pseudo-periodic instability at a frequency much lower than the blade passage frequency (6%), and linearly coupled with the impeller rotational speed. The same authors have noted that above Re=600, the main vortex in

the agitated tank was unstable; the fluctuations in the flow increased rapidly (as shown

in Figure 2-7), and the angle of the impeller discharge fluctuated.
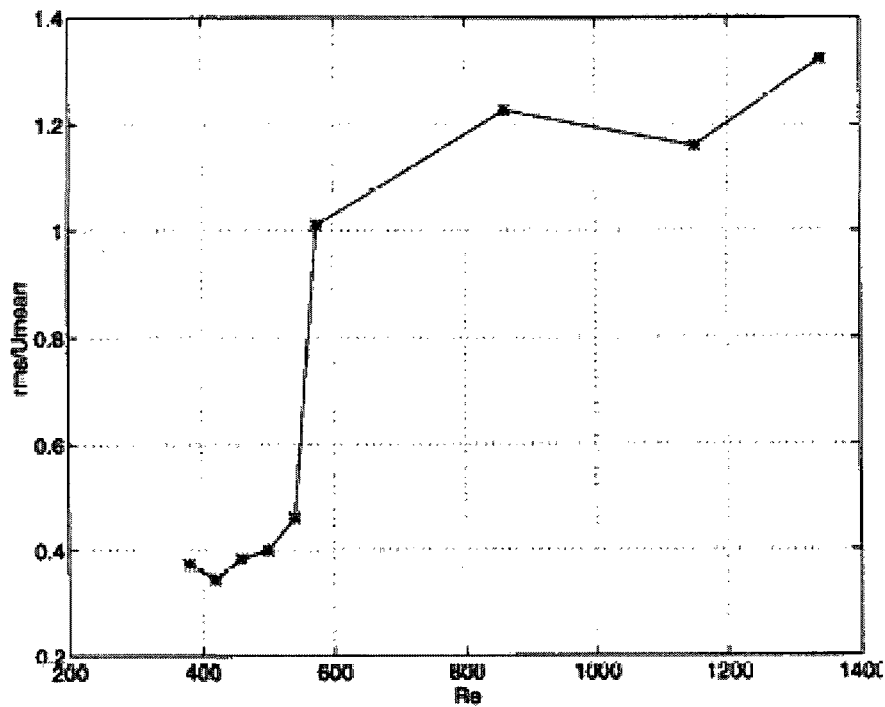
Figure 2-7: Velocity R.M.S. variations of the flow with respect to the Reynolds number

(MONTES et al., 1997)

As Re increases, the flow induced by a pitched blade turbine (PBT) evolves from one

single loop to a flow where many vortices structures appear in the upper part of the

vessel. SCHAFER et al. (1998) also observed the creation of secondary recirculation

zones as Reynolds number was increased. They also found out instabilities in the

impeller discharge flow direction at Re=500. ESCUDIE et al. (2002) with help of

particle image velocimetry have observed an increase of the radial component

magnitude and an increase in the pumping capacity of the agitator as the viscosity of the fluid decreases. Finally, they pointed out that the flow in turbulent regime is quite different than the flow produced in lower part of the transition regime.

2.1.2. Numerical studies

Table 2-2 summarizes the numerical models that have been developed to predict the hydrodynamics in agitated tanks in the transition regime. In Table 2-2, the label *laminar model* is used to indicate that the Navier-Stokes equations are considered without the addition of any turbulence model. The methods listed in the column 'agitator motion' are explained in section 2.3 of the present literature review.

Table 2-2: Computational models for the transition flow regime in agitated

Authors	Conditions	Model	Grid and number of equations	Agitator type	Agitator motion
VASCONCELOS et al. (1996)	Re=200-10000 (Newtonian fluid)	Compartmental model (without CFD)	Not applicable	Three-turbines stacked on single shaft	Not applicable
BAKKER et al. (1997)	Re=40-1200 (Newtonian fluid)	Laminar model Finite volume (FLUENT)	Not reported	Pitched blade turbine (PBT)	Sliding mesh
ZALC et al. (2001)	Re=20-200 (Newtonian fluid)	Laminar model Finite element (ORCA-CFD)	2M elements 370K nodes 1.48M equations Full tank geometry	Three-turbines stacked on single shaft	Rotating frame of reference
BARTELS et al. (2002)	Re=0.1-7000 (Newtonian fluid)	Laminar model Finite volume multi-grid (in-house)	2M cells 8M equations 1/2 tank geometry	Rushton turbine with baffles	Multiple frame of reference
MURTHY and JAYANTI (2002)	Re=0.5-500 (Newtonian fluid)	Low Reynolds k-ε model Finite volume (CFX)	172K cells 688K equations 1/8 tank geometry	Flat blade paddle	Sliding mesh

28

(Continuation of Table 2-2)

Authors	Conditions	Model	Grid and number of equations	Agitator type	Agitator motion
LETELLIER et al. (2002)	Re=1-250 (Newtonian and shear-thinning fluids)	Laminar model Finite volume (FLUENT)	200K cells 800K equations 1/2 tank geometry	Multi-stage agitator	Rotating frame of reference
KELLY and GIGAS (2003)	Re=25-400 (shear-thinning fluid)	Laminar model Finite volume (FLUENT)	158K cells 632K equations 1/4 tank geometry	Pitched blade turbine (PBT) and hydrofoil	Multiple frame of reference
CHOI et al. (2004)	Re=10-10000 (Newtonian fluid)	k-ε model Finite volume (FLUENT)	0.6M cells 2.4M equations Full tank geometry	Rushton turbine with baffles	Multiple frame of reference
RICCI and KELLY (2004)	Re=25-850 (shear-thinning fluid)	Laminar model Finite volume (FLUENT)	1.5M cells 6M equations 1/4 tank geometry	Pitched blade turbine (PBT)	Multiple frame of reference
ADAMS and BARIGOU (2007)	Re=7.3-163 (Bingham plastic fluid)	Laminar model Finite volume (CFX)	400K cells 1.6M equations 1/2 tank geometry	Pitched blade turbine (PBT)	Multiple frame of reference

The first attempt to develop a numerical model of the transition regime is presented by VASCONCELOS et al. (1996) who represented the hydrodynamics within the tank by a fixed cascade of well mixed compartments with backflow, where the backflow parameters are experimentally determined. A schematic representation of such model is shown in Figure 2-8.

a)   b)
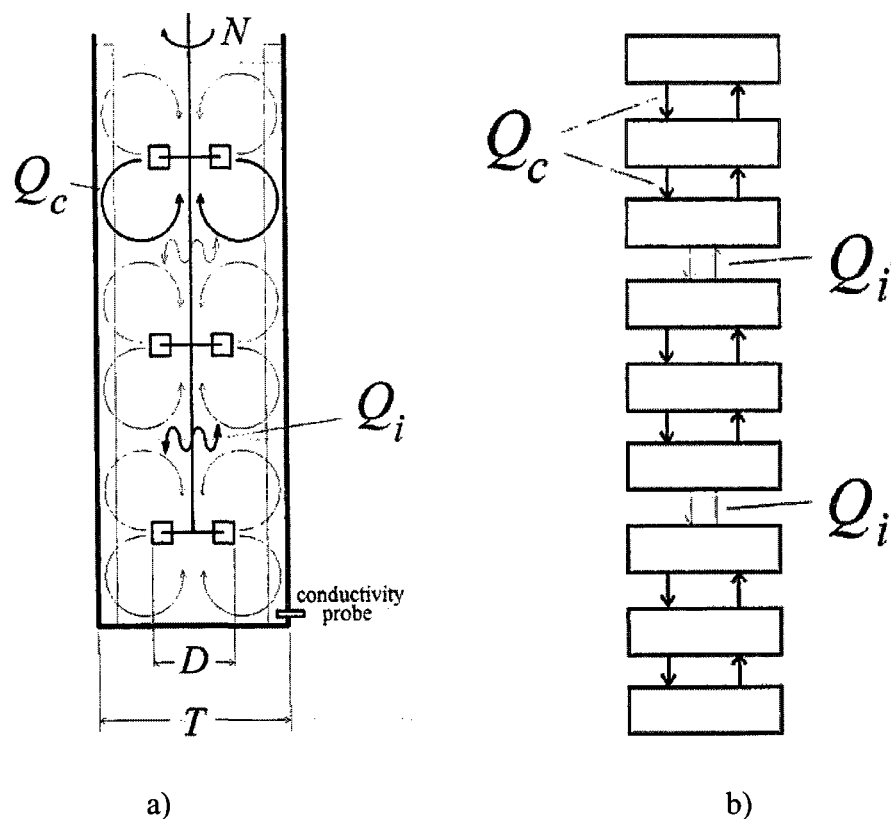
Figure 2-8: Simplification used to model transition regime in agitated tank a) Agitated tank with three turbines, b) structure of the compartment model for the agitated tank (VASCONCELOS et al., 1996)

They were able to predict the mixing time, power consumption and pumping capacity of the mixer in the upper transition region (Re>400) but not in the lower transition region. They found that the mixing time and power number depend on the Reynolds number as long as the full turbulent regime is inhibited by the viscosity. Later, BAKKER et al. (1997), with the objective to validate the sliding mesh technique in the context of agitated tanks, presented a CFD prediction of the pumping rate in the transition regime.
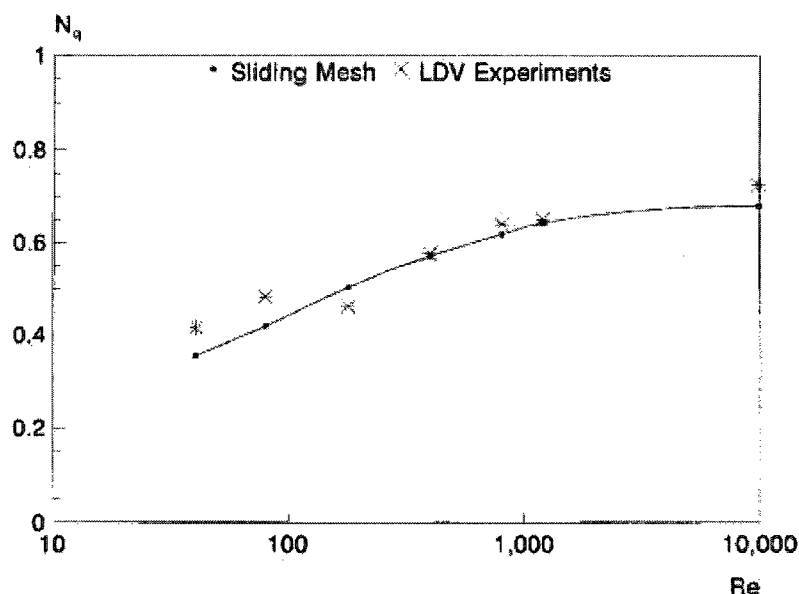
Figure 2-9: Comparison between experimental and CFD results for the pumping number with respect to the Reynolds number (BAKKER et al., 1997)

In order to capture the flow details generated in the transition regime, some authors resorted to turbulence models to simulate the transition regime. These works assumed that the flow structures and variations smaller than the mesh size can be well

represented by the turbulent contribution. MURTHY and JAYANTI (2002) employed a low Reynolds number version of the k-ε model to analyze the laminar and the transitional flow of an eight blade paddle impeller. They concluded that good results in the transition regime may be obtained with this approach. CHOI et al. (2004) also used turbulence model to predict the residence time distribution in a continuous reactor in the laminar and the transitional flow regime. They employed a standard k-ε model to simulate all the conditions (even the laminar) reporting good agreement between the experimental and numerical residence time distributions.

Most authors preferred to employ grids with small mesh sizes to avoid the re-laminarization effect. For example, ZALC et al. (2001) presented a finite element model for the laminar and the transition regime to predict the chaos in agitated tanks. Due to the large number of unknowns (370K nodes) in their simulations, they run their computations in parallel using eight processors per simulation. Based on the obtained hydrodynamics, they visualized the heterogeneous distribution of deformation rate produced within the mixing tank. Furthermore, they found that the pumping capacity of their configuration depends on Reynolds numbers as shown in Figure 2-10.
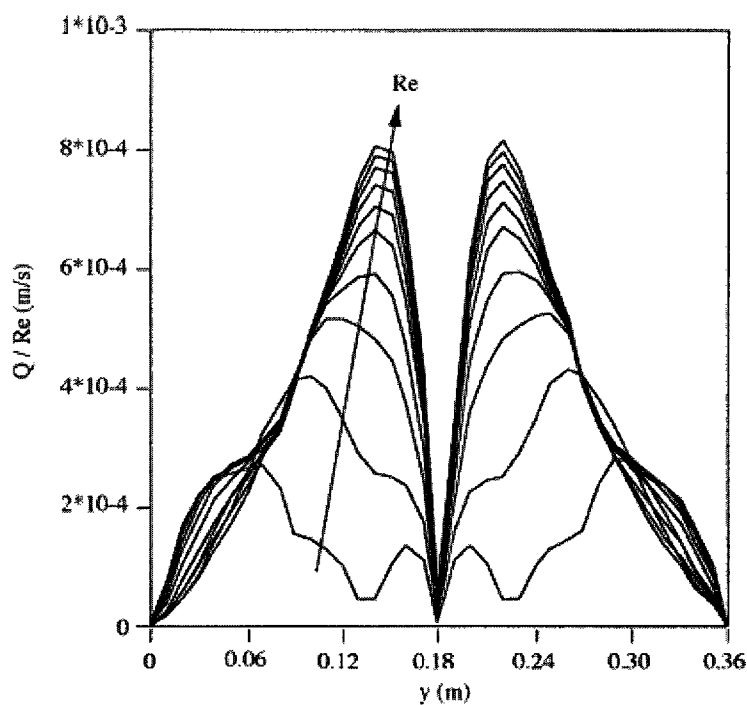
Figure 2-10: Increase of the pumping capacity with respect to Reynolds number in the

range 20-200 (ZALC et al., 2001)

Literature review shows that BARTELS et al. (2002) have used the most refined grids to predict the flow generated by a turbine in the transition regime. To accelerate their simulations they employed a parallel multi-grid finite volume code developed by DURST and SCHAFER (1996) on a 16 processors shared memory computer. With the results they observed an evolution of the flow with respect to the Reynolds number as shown in Figure 2-11 .

Re=10   Re=1000
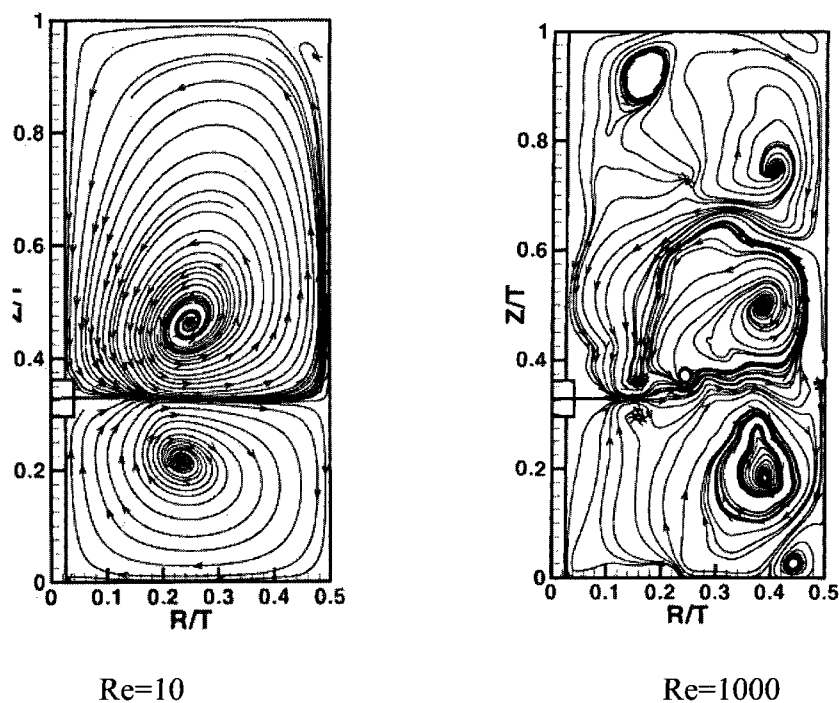
Figure 2-11: Flow streamlines at different Reynolds numbers generated in an agitated

tank (BARTELS et al., 2002)

CFD simulations involving non-Newtonian fluids in the transition flow regime have

also been performed. LETELLIER et al. (2002) reported the simulation of the flow in a

multi-stage agitator at three different scales. They assessed the effect of scale-up rules

over the flow patterns and pumping number in the laminar and the transition regimes.

They verified that the plot of the dimensionless pumping number with respect to the

Reynolds number was independent of the scale of the mixer. KELLY and GIGAS

(2003) and RICCI and KELLY (2004) have studied the effect of power law fluids in

the power characteristic and heat transfer of different stirred vessels. They found that

the power number and discharge angle of the agitator depends not only on the Reynolds number but also on the flow behaviour index. Furthermore, their results indicated that in the transition regime the average shear rate near the impeller increases not only with increasing the velocity of the agitator, but also with decreasing the flow behaviour index. ADAMS and BARIGOU (2007) have performed simulations of yield stress fluids to measure the size of the well mixed regions called caverns with respect to the Reynolds number. They concluded that the shape behaviour of the caverns is more complex than suggested by the toroidal cavern model.

2.2. Parallel computing

Parallel computing is a form of data processing in which many calculations are carried out simultaneously on several computer processors; operating on the principle that a problem can be partitioned into smaller ones. It allows reducing times and to solve problems that cannot be handled by single processor units due to excessive memory requirements.

2.2.1.   Types of parallel computers

Parallel computers can be divided in two main categories based on their architecture:

- A single computer with multiple processors interconnected to a shared address space, known as a *Shared Memory Multiprocessor* (Figure 2-12a).

- A set of computers interconnected through a network, known as a *Distributed Memory Multicomputer* (Figure 2-12b).
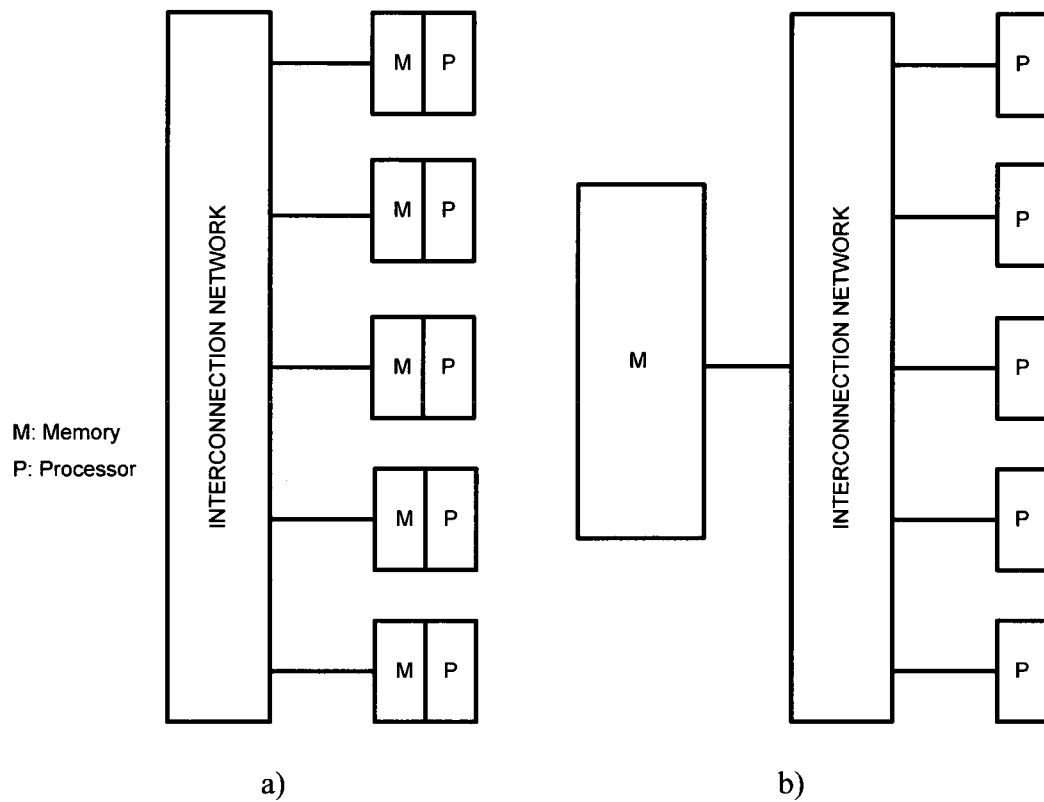
Figure 2-12: Parallel computer architectures: a) distributed memory computer b) shared memory computer

The advantages and disadvantages of shared and distributed memory computers are listed on Table 2-3 and Table 2-4.

Table 2-3: Advantages and disadvantages of shared memory computers.

Advantages	Disadvantages
Global address space provides a user-friendly programming perspective.	Lack of scalability between memory and CPUs. Adding more CPUs may geometrically increase traffic on the shared memory-CPU path.
Data sharing between tasks is both fast and uniform due to the proximity of memory to CPUs.	Computer price becomes excessive as the number of processor increases.

Table 2-4: Advantages and disadvantages of distributed memory computers.

Advantages	Disadvantages
Memory is scalable with number of processors. Augment the number of processors and the size of memory increases proportionately.	Difficult to adapt data structures and algorithms, based on shared memory, to distributed memory.
Each processor can easily access its own memory.	
Computer price is more affordable.	

2.2.2. *Performance of parallel systems*

There are various methods that are used to measure the performance of a parallel algorithm. Each of them reflects certain properties of the parallel code.

a) Run time

The simplest way to measure the performance of a parallel computer is the run time. The serial run time of a program (t_s) is the time elapsed between the beginning and the end of its execution on a sequential computer. The parallel run time (t_n) is the time that elapses from the moments that a parallel computations starts to the moments that the last processor finishes execution.

b) Speed-up

Speed-up is a measure that evidences the relative benefit of solving a problem in parallel. It is defined as the ratio of the time taken to solve a problem on single processors to the time required to solve the same problem on a parallel computer with p identical processors. Namely:

$$S(np) = \frac{t_s}{t_n} \qquad (2.12)$$

The ideal speedup is *np* when using *np* processors.

c)   Efficiency

The efficiency of a parallel system describes the fraction of the time that is being used by the processors for a given computation. It is defined as:

$$E(np) = \frac{t_s}{(np)(t_n)}$$ (2.13)

In practice, ideal behaviour is not achieved because while executing a parallel algorithm, the processors cannot devote one hundred percent of their time to the computations of the algorithm. Part of the time required by the processors is spent in communication.

2.2.3.   Causes of inefficiencies in parallel computing

In parallel computing science, overhead is defined as the collection of causes that produces non-optimal efficiency of the parallel system. The major sources of overhead in a parallel system are:

- *Inter-processor communication*: It is the most significant source of parallel processing overhead. It contains the time spent to communicate data between processors.

- *Load imbalance*: It is caused by the uneven partition of the problem that results in a disproportionate amount of work assigned between processors. If different

processors have different work loads, some processors may be waiting during part of the time that others are working on the problem.

- *Extra computation*: It is produced by the use of algorithms that may perform poorer compared to the best sequential algorithm but are easier to parallelize.

2.2.4. *Parallel algorithms to simulate flow problems*

Computational fluid dynamics (CFD) models are typically based on the solution of the Navier-Stokes equations with help of approximation schemes such as the finite volume or finite element method. As a result, a system of algebraic equations is obtained. Its solution is the most time consuming step for CFD codes. Several parallel algorithms have been proposed to reduce time and in some instances to reduce memory too. Most of them are based on domain decomposition methods which consist in the subdivision of the original computational domain into a set of interconnected subdomains. In this manner, internal unknowns are calculated in parallel, while the communications is restricted to the unknowns at the subdomain interfaces. Depending on the way the interfaces are handled they can be classified in overlapping and non-overlapping as shown in Figure 2-13.
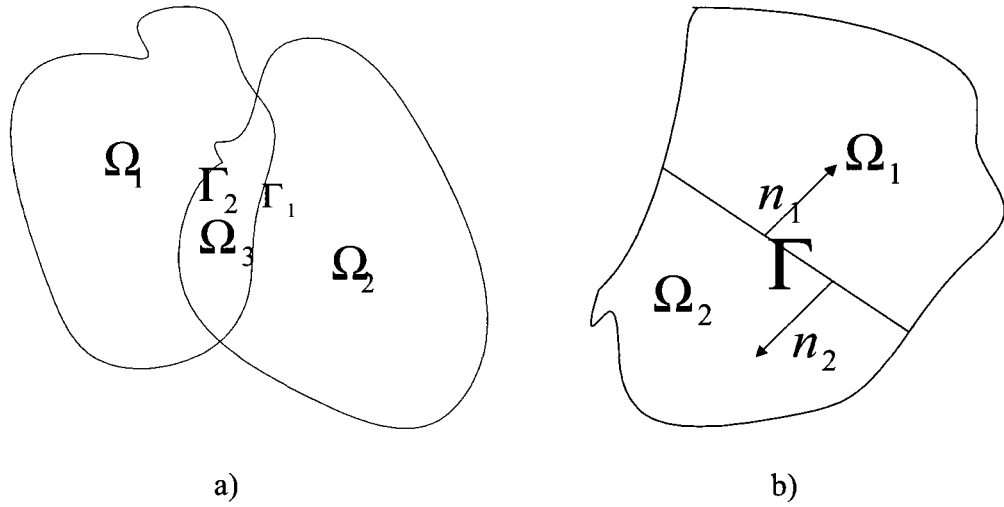
Figure 2-13: Schematic representation of domain decomposition: a) overlapping

partitions, b) non-overlapping partitions.

The most common techniques are described next.

a) Direct solvers

Direct solution methods based on the LU-decomposition of the global matrix and subsequent forward-backward substitution schemes are often selected as they are very robust especially for ill-conditioned problems. Parallel variants are the multi-frontal methods (SCOTT, 2003), the sparse Cholesky algorithms proposed in SuperLU software (LI and DEMMEL, 2003) or the tree assembly factorization presented by AMESTOY et al. (2000) for the MUMPS solver. The parallel efficiency of these methods depends on equations reordering and pivoting strategies as has been shown by GOULD et al. (2005).

Examples of the application of such methods in fluid dynamics are given by AGGARWAL et al. (1994) and HENRIKSEN and KEUNINGS (1994) who employed parallel direct solvers to simulate the flow of viscoelastic fluids. Recently, SAHIN and WILSON (2008) utilized MUMPS to simulate the viscoelastic flow past an array of circular cylinders in a channel. Unfortunately the large memory requirements limit the use of parallel direct solvers to massive parallel computing composed of hundreds or thousands of processors. For example, LI and DEMMEL (2003) required 32 processors to solve a system of approximately 10^6 equations (40K equations/processor).

b) Krylov iterative solvers

To overcome the memory limitations, at least partly, an alternative is to use preconditioned iterative Krylov subspace methods. With these methods, several algebra operations like sparse matrix-vectors products, inner products, vector updates and lower-upper solves need to be performed. The success of Krylov solvers depends highly on the preconditioner utilized. Preconditioning consists in transforming the coefficients matrix into one that has a lower condition number improving the convergence of the method. The transformation matrix is what is called the preconditioner. Their parallelization has been the subject of numerous investigations. For example, CAREY et al. (1998) presented the performance of a parallel diagonal preconditioner for a conjugate gradient solver using structured grids in the context of transport problems. Attempts to parallelize more robust preconditioners as incomplete lower-upper factorizations have been presented. DUTTO and HABASHI (1999)

proposed to reorder the variables by the so-called coloring techniques to facilitate parallelization of ILU. They showed that the approach is useful only for 4-6 processors when using ILU (0)-GMRES. WILLE et al. (2003) and STAFF and WILLE (2005) used domain decomposition, a priori pivoting and segregation of variables to parallelize the ILU preconditioning of conjugate gradient solver. Results presented for the Navier-Stokes equations, approximated with a mixed formulation, showed that the speed-up is limited due to the sequential characteristics of ILU algorithms as shown in Figure 2-14.
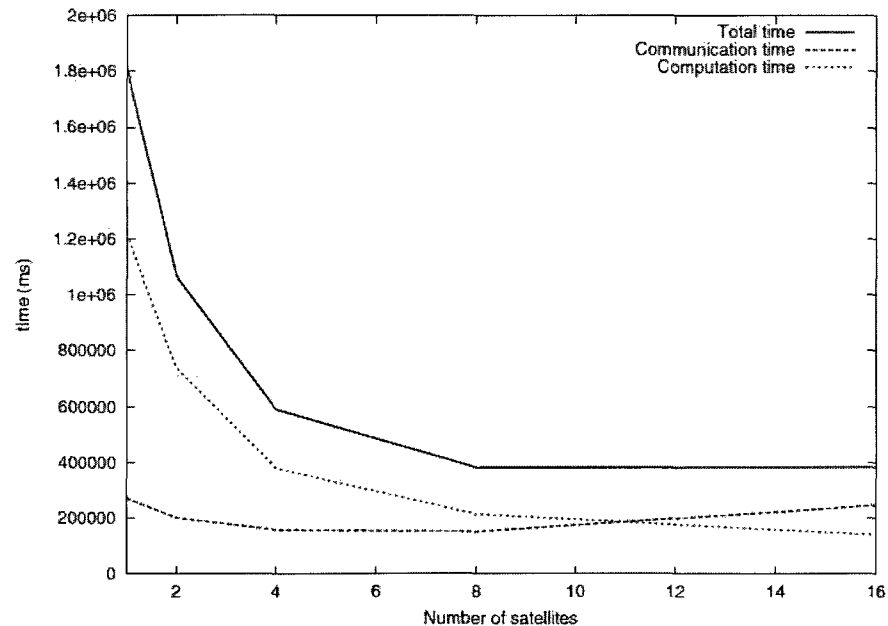
Figure 2-14: CPU time with respect to the number of processors (satellites) for parallel ILU preconditioning applied to Navier-Stokes problems (WILLE et al., 2003).

With the purpose to build highly parallel preconditioners, HUGHES et al. (1983) introduced the concept of element-by-element (EBE) preconditioners. It consists of

computing the preconditioner from the element matrix avoiding the storage of both the global matrix and preconditioner. This idea can be combined with domain decomposition to give better performance. Different variants such as the clustered-element-by-element (CEBE), the mixed CEBE and the cluster companion (CC) preconditioners were proposed by TEZDUYAR and LIOU (1989) and TEZDUYAR et al. (1992). KASHIYAMA et al. (2000) used an EBE preconditioner for the simulation of incompressible flow on benchmark cases. SHEU et al. (1999) developed a finite element model of the three-dimensional incompressible flow in a cavity using an EBE preconditioned BiCGSTAB solver. A maximum speed-up of four was obtained as shown in Figure 2-15.
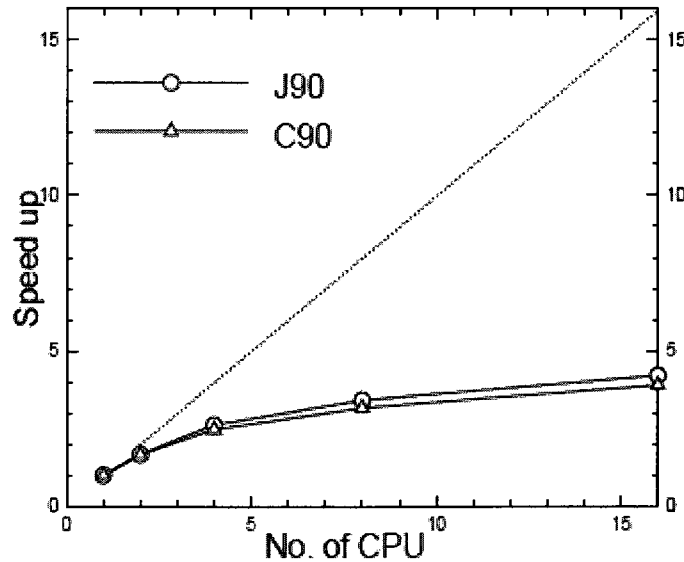
Figure 2-15: Speed-up of element-by-element preconditioned BiCGSTAB for the lid-driven cavity flow case (SHEU et al., 1999)

c) Overlapping domain decomposition methods

A well known domain decomposition approach based on overlapping partitions is the additive Schwarz method. This technique has been used to build parallel preconditioners for Krylov solvers. An excellent introduction and application of Schwarz methods is presented by SMITH et al. (1996). Figure 2-16 exemplifies a three overlapped partitions and their communication pattern.
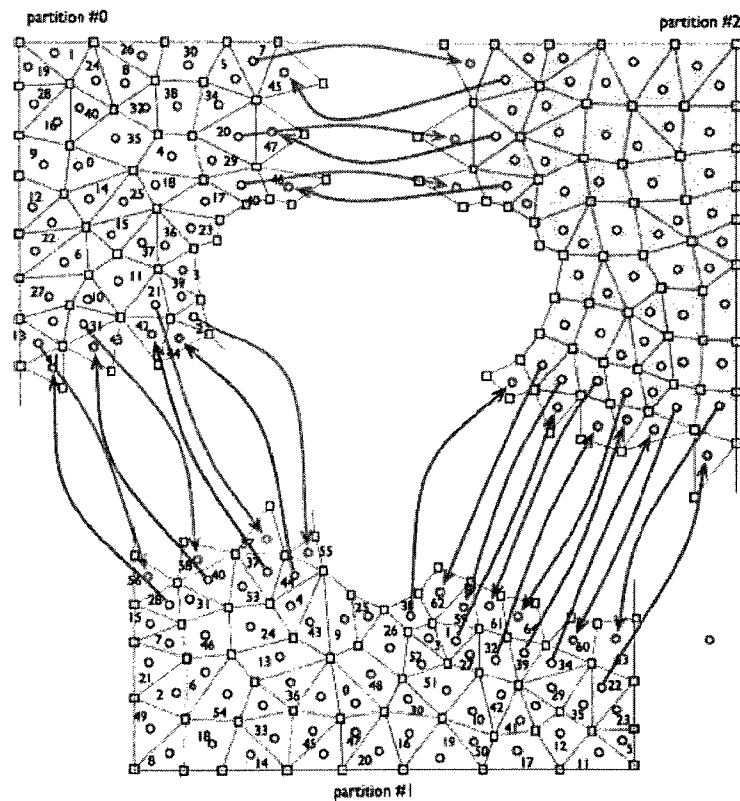
Figure 2-16: Three overlapping partitions and their communications patterns

(DARWISH et al., 2008)

Examples of overlapping Schwarz domain decomposition for the simulation of incompressible flows are given next. BRAKKEE et al. (1998) compared the performance of Schwarz domain decomposition in combination with CG and GMRES solver to reduce the computational time with respect to direct methods. GROPP et al. (2001) examined several tuning parameters such as the partitioning and the ordering of variables of an additive Schwarz ILU-GMRES solver to simulate a large CFD case containing 2.8M nodes. BORELLO et al. (2003) used an explicit Schwarz algorithm and GMRES solver to speed-up the solution of turbulent flows in turbo-machinery. CHAU et al. (2007) proposed an explicit alternating Schwarz domain decomposition that runs on asynchronous mode, where all the synchronization points are skipped and updated with the most recent information available.

Overlapping domain decomposition suffers from an increase in the number of iterations as the number of subdomains increases. The problem comes from the fact that the information at one node is conveyed through to another node only by passing through all the intermediate subdomains, each of which retards the transfer of information (SMITH et al., 1996). To alleviate this problem, many works have proposed the use of several levels of grids in a similar way than multi-grid techniques. It has been proved that the condition number of a two-level overlapping Schwarz method, for symmetric positive definite problems and generous overlap between subdomains, is bounded independently of the number of subdomains and the mesh size (DRYJA and WIDLUND, 1987). Examples of hybrid multi-grid and Schwarz solvers for fluid flow

simulations are widely found in literature. CAOLA et al. (2001) and CAOLA and BROWN (2002) utilized a two-level additive Schwarz, Newton method and BiCGSTAB solver to solve buoyancy driven convection and viscoelastic flows. CAI et al. (2002) and HWANG and CAI (2005) combined two-level Schwarz methods, GMRES and inexact Newton schemes to predict the flow at high Reynolds numbers in cavities. VAINIKKO and GRAHAM (2004) used a two level additive Schwarz preconditioner with GMRES applied to the solution of the Navier-Stokes equations with mixed discontinuous pressure elements. DOLEAN and LANTERI (2004) showed the usefulness of a parallel multi-grid and additive Schwarz domain decomposition for the simulation of unsteady flows on unstructured grids. LIN et al. (2006) studied the performance of a Newton-Krylov method in the finite element context using three levels of the algebraic multi-grid loop. Recently, DARWISH et al. (2008) compared different algebraic multi-grid techniques for overlapping partitions to improve the parallel efficiency of a finite volume parallel solver. These works show that the parallelization of multi-grid techniques is not straightforward. As pointed out by JOHN and TOBISKA (2000), multi-grid methods contradict the optimal condition for high parallel efficiency, which is data locality. The calculations on the grids that are coarser than the finest tend to show a bad parallel performance (JOHN and TOBISKA, 2000).

d) *Non-overlapping domain decomposition methods*

Non-overlapping approaches are based on the resolution of independent set of adjacent partitions and an interface problem. TOSELLI and WIDLUND (2005) presented a

complete mathematical description of these methods in their book. The most common non-overlapping domain decomposition technique is based on the introduction of Lagrange multipliers constraints to ensure continuity of the variables at the interface. There exist two approaches for solving such methods. One is based on the elimination of the degrees of freedom internal to the subdomains in order to solve an interface problem by an iterative algorithm (FARHAT and ROUX (1991); ACHDOU et al. (1995); HU et al. (2004)) as in the finite element tearing and interconnecting (FETI) method. Similar algorithms applied to incompressible flow simulations are highlighted next. GLOWINSKI et al. (1995) presented the use of Lagrange multiplier for domain decomposition in combination with fictitious domain methods. In their work, the Lagrange multipliers were obtained through a conjugate gradient algorithm. VANDERSTRAETEN and KEUNINGS (1998) reported flow simulations using a direct method to solve the internal equations and a parallel GMRES to solve the corresponding Lagrange multiplier equations. CALGARO and LAMINIE (2000) developed a non-overlapping domain decomposition method for the Stokes equations where preconditioned conjugate gradient was used for the interface equation. The velocity and pressure were obtained by means of Uzawa iterations or penalty methods. ZSAKI et al. (2003) implemented a CFD solver based on Uzawa iterations to uncouple the pressure from the mixed velocity-pressure problem. After each pressure update, the FETI algorithm was used to solve for the velocity and Lagrange multiplier unknowns. VEREECKE et al. (2003) extended the two-level FETI method for nearly incompressible problems.

The second option is to directly solve the full saddle-point problem by a preconditioned iterative method. This has the advantage of allowing the use of inexact low memory Krylov solvers for both the interior and multiplier variables. This approach has been applied to solve the diffusion equation on non-matching grids (KUZNETSOV, 1995), elasticity problems (KLAWONN and WIDLUND, 2000; KLAWONN and RHEINBACH, 2007) and elliptic problems with variables coefficients (HU et al., 2004). For preconditioning, KUZNETSOV (1995) proposed block preconditioners. KLAWONN and WIDLUND (2000) utilized block preconditioners combining different versions of incomplete LU factorization of the global matrix. No applications of this second approach were found in the literature for the Navier-Stokes equations.

2.3. Numerical modeling of the agitators motion

The treatment of the agitator periodic motion within a stirred tank provided with baffles is particularly critical for the accurate prediction of the flow. As the agitator moves, the position of the boundary of the problem changes as shown in Figure 2-17.

| time step 1 | time step 2 | time step 3 |
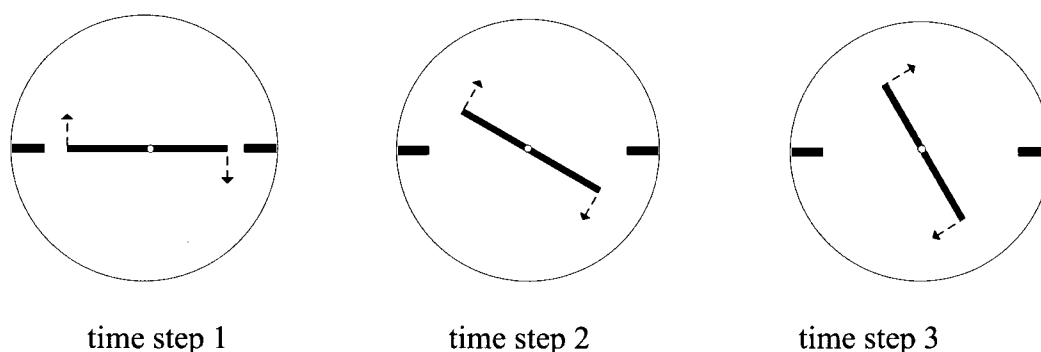
Figure 2-17: Unsteady motion of a paddle impeller on a two-baffle tank at three time steps.

Several simplifications and techniques have been developed through the years to handle such conditions. The most popular methods are outlined in the next paragraphs.

2.3.1. Black box approach

An early approach to handle the motion of impellers consisted in excluding the impeller swept volume from the computational domain. Boundary conditions in the black box region were prescribed from time averaged experimental data or empirical functions as shown in Figure 2-18. The task of the CFD solver was to compute a steady state average flow in the remainder of the tank.
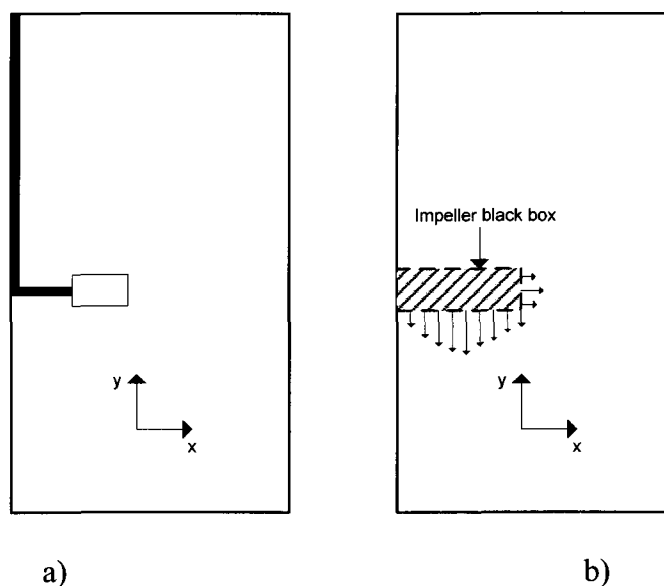
Figure 2-18: Schematic representation of the black box approach. a) Half of an agitated

tank; b) Computational domain used for the half on the domain in the black box

approach.

HARVEY and GREAVES (1982) utilized this approach to model the two-dimensional flow produced by an agitator. They employed parabolic profile for the radial and axial velocity assuming rigid body motion profile for the tangential velocity in the impeller swept region. The turbulent quantities at the boundary of the agitators were set to zero. MIDDLETON et al. (1986) extended this technique for three-dimensional flow in mixing tanks using a finite volume code. The experimental data used for boundary conditions in the impeller region were obtained from laser anemometry. RANADE and JOSHI (1990) described a computer code to simulate turbulent flows in agitated tanks based on k-ε model. Their model approximates the partial differential equations using finite volume method coupled with a Gauss-Seidel linear solver. Unlike the work of

HARVEY and GREAVES (1982), they used non-zero boundary conditions for the turbulent levels on the impeller region. GOSMAN et al. (1992) presented a computational procedure based on the finite volume method for the prediction of multi-phase turbulent flows in baffled, impeller-stirred vessels. Their resolution algorithm was based on two phase implicit velocity-pressure coupling and the k-e model. The main limitations of the black box approach are that only steady state solutions are obtained and it requires experimental data which is not always available.

2.3.2.   Rotating frame of reference

A more general approach is to simulate the flow using the exact shape of the impellers. A simplification that removes time dependency for some cases is the rotating or Lagrangian frame of reference model. It consists in solving the steady-state momentum equations for the entire domain in a rotating frame. Due to the change of frame of reference, the Coriolis and centrifugal forces need to be included in the equations of change. Problems solved in a rotating frame typically use the angular velocity of the impeller as the angular velocity of the frame. Thus, the impeller is at rest in the rotating frame of reference while the wall of the tanks rotate at the angular speed of the agitator, as shown in Figure 2-19.

a)   b)
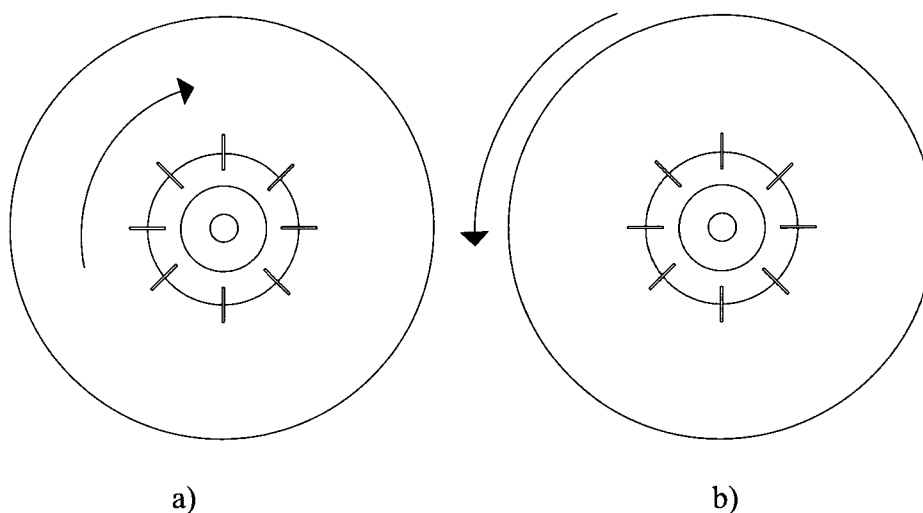
Figure 2-19: Rotating frame of reference approach. a) The impeller rotates in the

laboratory frame of reference; b) The walls rotate in the rotating frame of reference

A rotating frame of reference has been utilized in several works where the geometry of

the tank is symmetric. For example, TANGUY et al. (1992) utilized this technique to

simulate the flow of a helical ribbon impeller vessel with the help of the finite element

method. ZALC et al. (2001) used this approach to model the flow generated by several

turbines on a single shaft positioned at the center of the tank.

2.3.3.   Techniques based on body forces

A different approach is to introduce body forces in the Eulerian version of the

momentum equations to emulate the effect of the moving impellers over a background

mesh. PERICLEOUS and PATEL (1987) presented a technique for the solution of the

time averaged Navier-Stokes equations describing the flow in the reactor. The impellers were represented as sources of tangential, axial or radial momentum and similarly flow resistances such as baffles were represented as momentum sinks. The momentum terms were computed from correlations involving variables such as drag coefficients, number of baffles or blades and time average area of the object. The resulting partial differential equations were solved numerically using a finite difference solver. They have applied their model to simulate the flow in a bioreactor composed of three-turbines stacked on a single shaft. RANADE and DOMMETI (1996) developed a steady-state three-dimensional finite volume model for stirred tank simulation. In this approach, impeller blades were considered as fixed at one particular position. The influence of the blade rotation is modeled by mass sources in front of and behind the impeller based on an empirical approximation of the time derivative as shown in Figure 2-20.

Figure 2-20: Computational snapshot model (RANADE et al., 2002)

Another example is the immersed boundary method developed by PESKIN and MCQUEEN (1989) for the simulation of blood flow in the human heart. Their model consisted in representing the moving bodies by a set of control points on which body forces are imposed. These forces were not known a priori and were calculated using theoretical models. Variants of this method are the immersed interface method of LEVEQUE and LI (1994) and the immersed finite element method of ZHANG et al. (2004). REVSTEDT and FUCHS (2001) employed a similar approach in combination with large eddy simulations to model the turbulent flow produced in a baffled tank agitated by a turbine. Their model was based on finite difference method on Cartesian grids and a multi-grid solver. The boundary conditions on the solid boundaries were applied by replacing the boundary with a surface force distribution. These artificial forces were obtained iteratively based on the defect in satisfying the boundary

conditions. VERZICCO et al. (2004) presented an immersed boundary technique for the resolution of turbulent flows in agitated tanks. Their approach resembles the technique of REVSTEDT and FUCHS (2001); a body force iteratively computed was used to impose the effect of the moving agitator over the flow. Their model relies on large eddy simulations and a second order finite difference approximation on structured grids. The equations were integrated in time using a fractional step method where the viscous terms were computed implicitly and the convective terms explicitly.

In the finite element context, the fictitious domain method of GLOWINSKI et al. (1994) operates in an analogous way to the method proposed by PESKIN and MCQUEEN (1989) with the difference that this approach does not resort to empirical forces but rather to Lagrange multipliers to enforce the velocity constraints at the moving surfaces. One important issue of this approach is the evaluation of surface integrals which are computationally expensive and not necessarily easy to compute for three-dimensional complex geometries. A different (and independent) approach was proposed by BERTRAND et al. (1997) based on a collocation method to impose the surface constraints point-wise by the use of Dirac functions as shown in Figure 2-21. Briefly, their approach consists in the imposition of the impeller kinematics by means of a set of control points distributed along the surface of the impeller (this is done using Lagrange multipliers and penalty techniques). At each time step, the velocity and position of the control points are updated and a new optimization problem is solved. The method was called by the authors the virtual finite element method (VFEM).
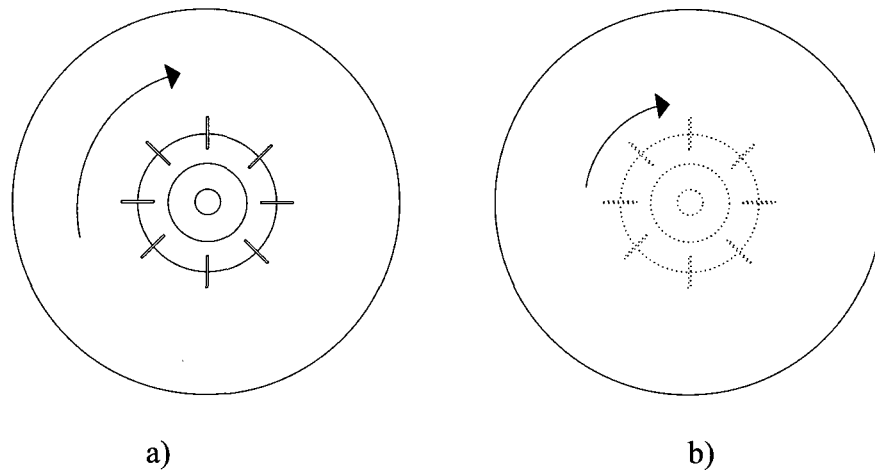
Figure 2-21: Virtual finite element method. a) six-blade turbine rotating in a tank; b) control points used by VFEM to discretize the surface of the rotating impeller.

This technique has been successfully employed to simulate the flow of mixers in laminar regime with multiple agitators and unconventional motions (TANGUY et al., 1996; BERTRAND et al., 1997). The algorithm used computes the Lagrange multiplier from Uzawa algorithm. Recently, in an effort to reduce computational times, COESNON et al. (2008) reformulated the algorithm using a fully coupled approach calculating the velocity, pressure and Lagrange multipliers simultaneously with the help of preconditioned Krylov iterative methods. They reported a reduction of the CPU time for the studied scenarios. The main advantage of the techniques based on body forces is the simplification of mesh generation and possibility to model the flow of a wide range of complex geometries and motions. Its main disadvantage is that in some cases, it may require special mesh refinement techniques in the regions near the moving

agitator surface to ensure accurate results as shown in the work of RIVERA et al. (2004) for fictitious domain methods.

2.3.4. Techniques based on domain decomposition

An interesting alternative is the use of domain decomposition methods. The basic idea is to use two grids, one corresponding to the rotating part and another one to the stationary part. These techniques allow the preservation of the exact shape of the moving boundaries as the object rotates without re-meshing. Based on this type of partitioning, several techniques and simplifications have been proposed.

a) Multiple frame of reference (MFR)

A hybrid method between the rotating frame model and domain decomposition techniques is the multiple frame of reference approach proposed by LUO et al. (1993). The method consists in utilizing more than one reference frame in order to obtain a steady-state model. The mesh utilized for a MRF simulation requires a non-overlapping partition that splits the region that rotates from the stationary zone as shown in Figure 2-22.
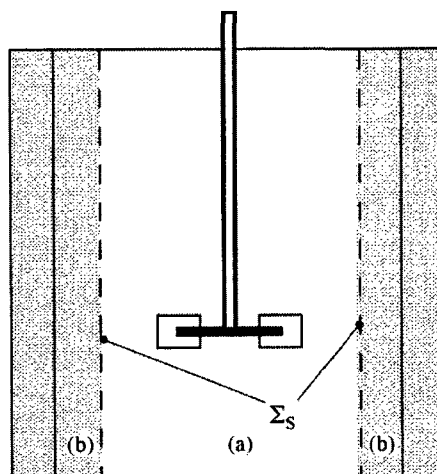
Figure 2-22: Domain decomposition for multiple frames of reference approach. (a)

Impeller region; (b) baffles region (BRUCATO et al., 1998)

The momentum equations inside the rotating partition are solved in a Lagrangian frame of reference while those outside the rotating frame are solved in the Eulerian frame. This means that in the rotating zone, the Coriolis and centrifugal forces must be added to the Navier-Stokes equations. This steady-state approach permits for the modeling of baffled stirred tanks. Since this technique allows computing steady-state solutions, the time required for a simulation with this model is normally shorter than the one required for a non-steady simulation. However, it only provides an average flow and it is very difficult to observe interaction between the baffles and the agitator. For that reason this model is recommended for simulations in which the impeller-baffle interaction is weak or inexistent.

b) Chimera or composite overset methods

One way to apply domain decomposition techniques is to overlap independent three-dimensional grids by means of composite overset or Chimera methods (STEGER et al., 1983). This model is a time dependent unsteady approach. It requires a background mesh and patch grids. The grids are not required to align with neighboring grids in any special way. The idea of the method is to remove some elements from the background mesh in order to generate an apparent interface. The nodes in the background mesh that form this interface are referred as fringe nodes. This procedure is called hole cutting and the nodes of the elements removed are denominated holes or ghost nodes. Suitable transfer conditions are exchanged at the interface between the outer boundary of the patch and the apparent interface. At each time step, the patch grids move, a new apparent interface is defined and a new problem is solved.
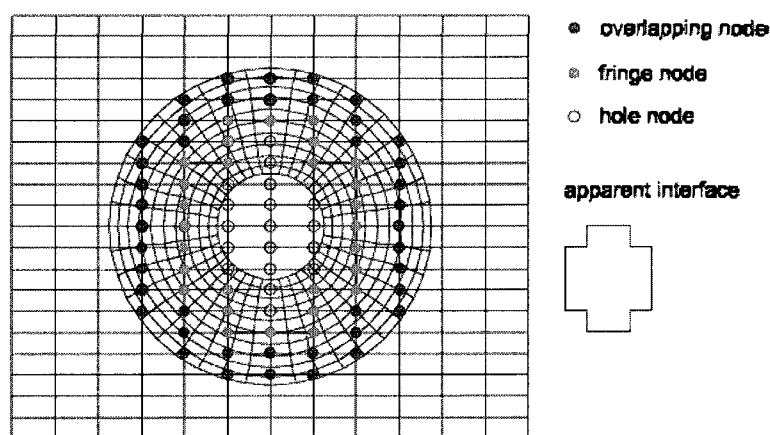
Figure 2-23: The apparent interface formed by a patch grid (circular mesh) over a background mesh required for the Chimera method (rectangular mesh) (HOUZEAUX and CODINA, 2003).

Based on similar ideas, TAKEDA et al. (1993) presented a multi-block technique based on finite difference method capable to handling overlapping partitions. They applied their model to the simulation of agitated tank with baffles and multiple impellers. HOUZEAUX and CODINA (2003) also employed this technique to simulate incompressible fluid flows in agitated vessels with help of a stabilized finite element method. They proposed a method based on an iteration-by-subdomain algorithm and Dirichlet/Neumann coupling to handle each independent grid.

The advantage of the composite overset method is that it allows simulating any type of motion. However, the coupling between the different meshes requires a hole cutting strategy to generate an overlapping interface among the grids that may entail to complex coding. Furthermore, the forth and back interpolations between the moving and background meshes in the overlap region may be a computationally costly procedure.

c) Sliding mesh technique

The sliding mesh technique is a time-dependent model based on the decomposition of the original mesh into stationary and moving grids interconnected by a sliding interface. As time advances, the moving grid slides along the sliding interface as shown in Figure 2-24.
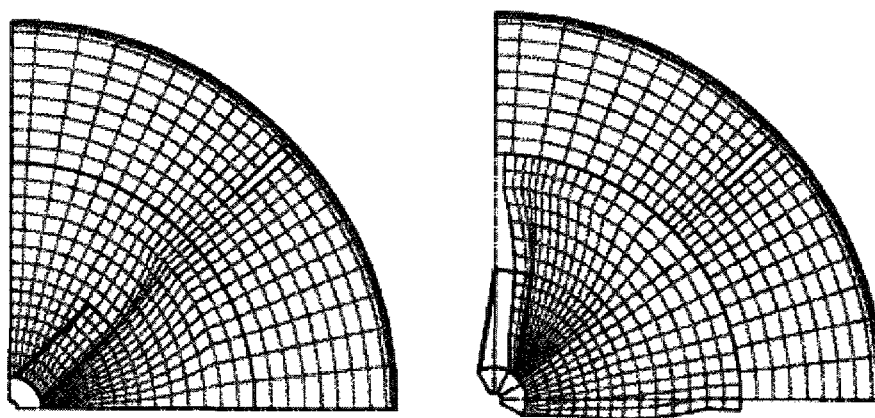
Figure 2-24: Grid used in the sliding mesh method at two different time step. The grid in the impeller region moves with the impeller and slides past the stationary grid for the rest of the tank (BAKKER et al., 1997)

Examples of this technique are found in wide variety of applications. WAYMEL et al. (2006) proposed a sliding mesh finite volume model to simulate the flow around trains. Their method was based on a two-dimensional face reconstruction of the contact boundaries. The velocity components at the interface faces were obtained from a linear interpolation of the velocity at the center of the cells, corrected by a third order pressure gradient term. GARTLING (2005) presented a finite element sliding mesh algorithm to solve moving body thermal and flow problems. The algorithm was based on an efficient node-in-mesh search procedure and penalty type constraints to enforce the continuity of the primary variables. FENWICK and ALLEN (2006), in a work involving the simulation of the flow around the wings of an airplane, studied different finite volume interpolation techniques for the sliding mesh technique. BLADES and

MARCUM (2007) presented a parallel sliding mesh finite volume model to determine the flow around a missile. At the subdomain interfaces, the faces along interfaces were extruded into the adjacent subdomain to create new volume cells forming a one-cell overlap. These new volume elements were then used to compute a flux across the subdomain interface. The values at the new cells were obtained through linear interpolation. STEIJL and BARAKOS (2008) developed a parallel finite volume sliding mesh with non-matching cell faces to model the hydrodynamics around the blades of helicopters.

The application of the sliding mesh technique to mixing tanks was presented by LUO et al.(1993) who implemented a finite volume sliding mesh technique in the code STAR-CD, to predict the flow of a four-baffle tank stirred by a six-blade turbine. The computation was based on half of the domain.

A variant of the sliding mesh is presented by PERNG and MURTHY (1993), who developed a moving-deforming mesh technique for the commercial finite volume code FLUENT to simulate the unsteady flow in mixing tanks with a four-blade turbine. A single mesh and a single reference frame were used for stationary and moving parts, but the grid cells associated with the impeller is rotating with it, causing the interfacial mesh to deform. When the mesh distortion became excessive, the mesh at the interface is regenerated. Later, FLUENT replaced this technique by a sliding grid technique described by MURTHY et al. (1994). Following the basic idea of the sliding mesh

technique, the moving grid was allowed to slide with respect to the stationary one, with no mesh distortion, and a conservative interpolation was used to obtain flow variables and face fluxes across the slip surface. They have applied their model to simulate the flow in a six-baffled mixing tank with a six-blade turbine. The computational domain was limited to a one sixth of the whole tank. BAKKER et al. (1997) validated this sliding mesh model for a mixing tank agitated by a pitched-blade turbine based on the comparison of the numerical and experimental pumping capacity of the impeller. In a different work, BRUCATO et al. (1998) compared the MFR and the sliding mesh methods. They found that the best results were obtained by the sliding mesh method. However, they mentioned the high computational cost of this technique due its time dependence.

One particular simplification of the sliding mesh method is the clicking mesh method (BOHM et al., 1998; WECHSLER et al., 1999) where the grid movement is such that the boundary nodes must match at the interfaces at any time step. As it can be difficult and tedious to ensure this condition, most finite element sliding mesh implementations are extensions of the mortar method developed by BERNARDI et al. (1994) to couple non-matching grids. They are usually based on the imposition of linear multi-point constraints at the interfaces such as Lagrange multipliers, penalty methods or master-slaves elimination.

2.4. Synthesis

The literature review has shown that the transition flow regime in stirred tank has not been extensively studied. Most studies in mixing science are focused on fully laminar or turbulent conditions. Experimental investigations working in the transition regime have studied standard mixing configurations such as agitated tanks equipped with turbines or hydrofoils. Special attention has been given to the determination of an average deformation rate within the mixing tank for which many empirical and theoretical models were found. These models follow the trend observed in the experimental data which indicate that in the transition regime, the deformation rate increases with respect to the Reynolds number. A deeper understanding of the flow complexity has been obtained from the analysis of the velocity field obtained from laser Doppler anemometry (LDA). The main limitation of LDA is that the velocity is measured in a few points localized in a small region close to the agitator. The main conclusion from the experimental studies is that in the transition regime, the flow is completely different than the laminar one. The pumping capacity and the deformation rates increase as a function of the Reynolds number which have a direct impact on the mixing and circulation times.

Numerical simulations reported in literature have also utilized standard mixing tanks configurations using commercial CFD codes such as FLUENT or CFX. To model the transition regime, two approaches have been found. A few authors have opted to use steady-state simulations with the k-e turbulence model. However, only an average

steady-state flow field is obtained and the turbulence models may alter the flow pattern due to the re-laminarization effect. In view of that, other authors have resorted to small mesh sizes in order to capture the flow structures found in the transition regime. Most of the studies have assumed symmetry of the flow in order to reduce the computational cost of the simulations, allowing them to simulate only a fraction of the vessel. Furthermore, in the multiple frame of reference approach the unsteadiness of the flow caused by the motion of the blades has been neglected. The literature is not limited to Newtonian fluids; simulations involving non-Newtonian fluids have also been reported. These studies have shown the effect of shear-thinning behaviour over the hydrodynamics in the transition regime, concluding that the non-Newtonian behaviour delays the onset of the transition regime.

As discussed in the introduction of this thesis, stirred tank with multiple impellers are a good choice to operate in the transition region. Nonetheless, the majority of authors have focused on standard mixing tank configurations. A deeper understanding is needed about the mixing hydrodynamics in multiple impeller configurations in the transition regime. As shown by the literature review, numerical simulations are capable to provide us with both global and local information of the hydrodynamics in agitated tanks. From the obtained hydrodynamics, it is possible to reproduce the mixing tests performed in pilot rigs without the complications of laboratory procedures.

The main obstacle for CFD simulations is the limited memory and processor speed of computers. As a consequence, the CFD simulations of the flow in a mixer take significant amounts of time and memory. To deal with this problem, simplifications in the simulation of stirred tanks are commonly used such as:

- The simulation of a fraction of the tank, assuming flow symmetry in the vessel;

- The assumption of steady-state flow even if the flow in an agitated tank is unsteady.

These simplifications help in reducing computational cost but they also restrict the information that is possible to extract from the simulations. For example, removing the unsteadiness of the flow may alter the trajectories followed by a tracer dispersed by the flow. As a consequence, mixing times obtained from steady hydrodynamics may differ from the ones obtained in the laboratory. In view of the necessity to take into account these effects, parallel computing becomes a requirement for CFD simulations of agitated tanks in the transition regime. In the context of the finite element method, the possibility to solve problems for larger number of unknowns also open the possibility of using more accurate finite element approximations.

The parallelization of CFD solvers is based on domain decompositions which consist in partitioning the computational domain into a set of subdomains interconnected by an interface. They can be categorized in overlapping and non-overlapping methods and can be combined with direct or iterative solvers. Direct solvers are very robust for difficult problems. Unfortunately, for cases comprising several millions of unknowns,

their large memory requirements limits their use to parallel computers composed of hundreds or thousands of processors. On the other hand, iterative solvers are less memory demanding. The key ingredient of any iterative solvers is the preconditioning step and many strategies have been proposed. The majority of authors have opted for iterative solvers with overlapping domain decomposition. However, the convergence rate of these methods decays with respect to the number of processor used. Multigrid techniques have been incorporated into these algorithms to improve the convergence rate at the cost of a more complicated algorithm with lower parallel efficiency. Another point to consider is that from the programming point of view, overlapping data structures are more complex to handle than non-overlapping ones, mainly on unstructured grids. In view of that, and the fact that algorithms combining non-overlapping techniques and iterative methods have not been widely investigated in the context of fluid flow problems, it becomes interesting to explore them in this thesis.

Another important issue in the modelling of agitated tanks is the treatment of agitators motion. A suitable modeling strategy must be capable to take into account the unsteady interaction between agitators since it is critical for the mixing. The literature review has shown that sliding mesh techniques are very accurate methods to predict the flow field unsteadiness. However, it is know to be very costly in terms of CPU times. In view of the fact that both the parallel solver and the sliding mesh techniques are based on domain decomposition, it is a good opportunity to formulate a sliding mesh technique

that not only helps to decouple the computational domain into rotating and stationary subdomains, but also facilitates its parallelization.

Chapter 3. Specific objectives

Based on the information already presented, the specific objectives of this thesis are:

1. To develop a parallel finite element algorithm capable of predicting the hydrodynamics of three-dimensional incompressible fluid flow problems on unstructured grids.

2. To develop a parallel sliding mesh technique capable of predicting the unsteady hydrodynamics caused by the rotation of the agitators.

3. To characterize the hydrodynamics and mixing mechanisms of a multiple impeller mixer operating in the transition flow regime utilizing the developed algorithms on high performance parallel computers.

Chapter 4. Overall methodological approach

In this chapter the hardware and the strategy of development to accomplish the general objective of this project is presented.

4.1. Computational resources

The parallel computer used in this project was the IBM-P690 computer, better known as Regatta. This computer is a 64-bit multiprocessing UNIX server with 16 RISC POWER4 processors sharing 128GB of RAM memory. The transfer rate among the processors is about 204 GB/s.
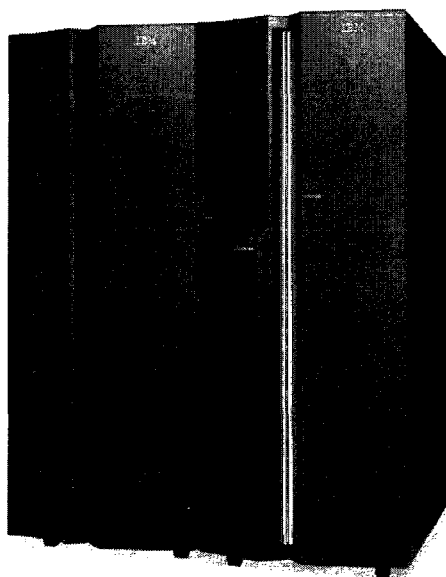
Figure 4-1: IBM-P690 computer (IBM)

4.2. Program development strategy

The overall methodology was based on the modification of the POLY3D software (Rheosoft, Inc.) written in FORTRAN 70, developed in the 90s by the URPEI research group of the Ecole Polytechnique of Montreal. This code is a sequential three-dimensional finite element flow and thermal solver for unstructured tetrahedral grids with several finite element approximations for the velocity and pressure variables. It is equipped with sequential iterative Krylov and direct methods for the resolution of the discrete linear system of equations.

The sequence of steps required to run a simulation is as follows. The first step consists in creating a mesh for the domain of the problem. This task is carried out with the help of the commercial software I-DEAS (EDS) or Gambit (Ansys). From that step, further pre-processing steps are necessary which are schematically represented in Figure 4-2.
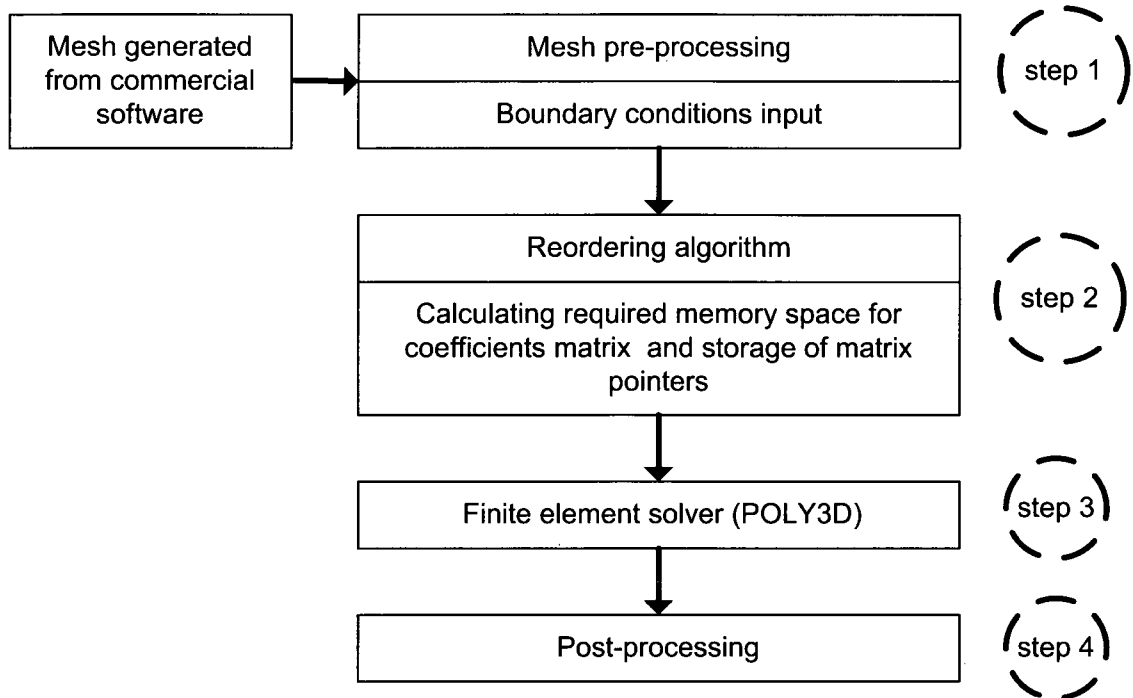
Figure 4-2: Standard procedure to run a simulation with the software POLY3D.

In Figure 4-2, step 1 involves the processing of both the mesh and the boundary conditions. In a similar manner, in step 2, both the reordering algorithm and the memory requirements of the global finite element matrix are calculated. Thus, if a simulation requires a modification in the boundary conditions, step 1 and 2 need to be repeated before running a simulation. Step 2 is very costly in term of time due the reordering algorithm used by POLY3D. In view of that, a different paradigm was followed in this work in order to increase the flexibility of the code. Figure 4-3 shows the proposed procedure:
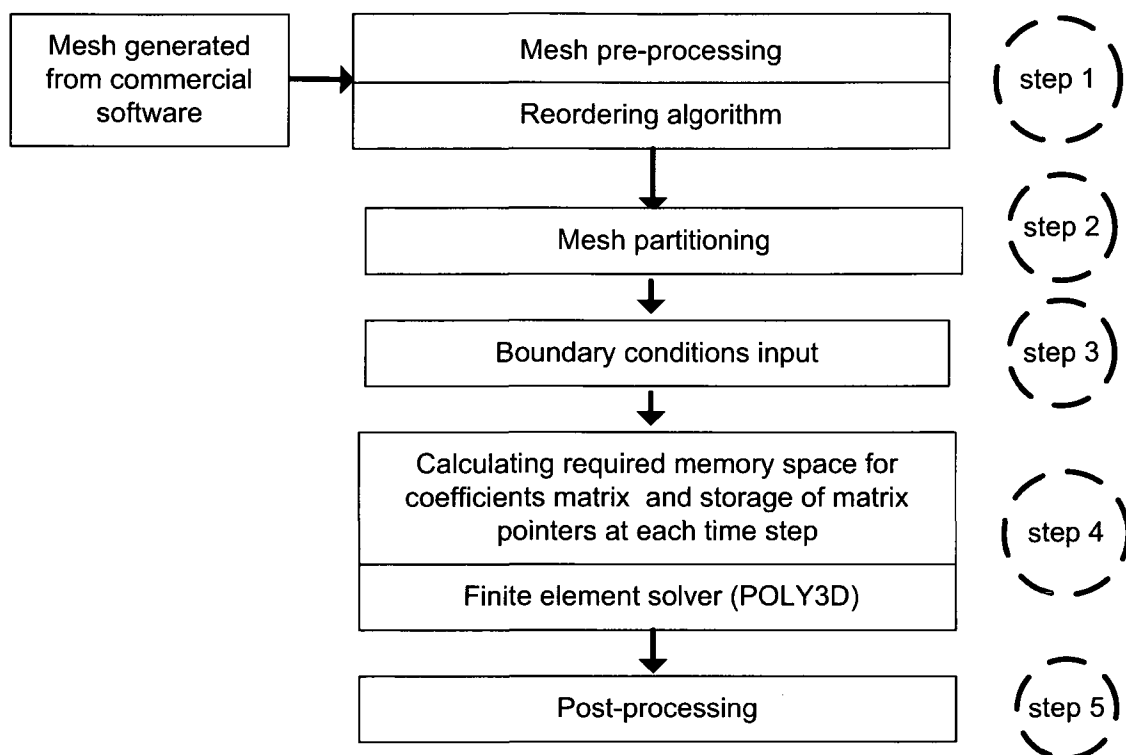
Figure 4-3: Proposed procedure to run a simulation in this thesis.

In the strategy proposed in Figure 4-3, the first major change is that the reordering algorithm is performed in the first step together with the mesh pre-processing. The second step consists in the mesh partitioning required for the parallelization of the code. The Chaco (HENDRIKSON and LELAND, 1993) and the Metis (KARYPIS and KUMAR, 1998) softwares are used for this purpose. The partitioning will be discussed in more detail in the next chapter. The third step involves the input of boundary conditions by the user. This step is completely independent of the other steps. In this way, if boundary conditions are required to change, the only step to repeat is step 3. The second major change is the inclusion of subroutines related with the memory

requirements for the global finite element matrix in the main solver (step 4). This modification opens the possibility to add or eliminate equations from the global matrix at each time step. The implications of such change will be easier to understand after the next two chapters. This thesis focuses on the parallelization of step 4 of the proposed procedure. Finally, for the visualization of the results, the Ensight software (CEI) was employed (step 5).

The programs and subroutines employed in this work were programmed using the FORTRAN 90 language. The dynamic memory allocation features included in this programming language were highly exploited with the help of the ALLOCATE ( ) and DEALLOCATE ( ) subroutines. In order to create a readable code, GOTO statements were avoided as much as possible. To ensure portability of the code, a message based memory distributed model with MPI was employed.

Chapter 5. Parallel finite element simulations of incompressible viscous fluid flow by domain decomposition with Lagrange multipliers

Authors: Christian A. Rivera[1], Mourad Heniche[1], Roland Glowinski[2] and Philippe A. Tanguy[1]

[1] *Research Center for Industrial Flows Processes (URPEI),*

Department of Chemical Engineering, École Polytechnique of Montreal, Canada

[2] *Department of Mathematics, University of Houston, USA*

KEYWORDS: Lagrange multiplier method; finite element method; parallel computing; Krylov methods; domain decomposition method, mesh partition, ILU preconditioning, Stokes equations.

5.1. Presentation of the article

This article was submitted to the Journal of Computational Physics. It comprises the development of the finite element parallel solver that is used in the next chapters to predict the hydrodynamics in agitated tanks. A characterization is performed to know the parallel behaviour of the solver on benchmark cases. Guidelines to improve the parallel performance of the solver are given at the end of the article.

5.2. Abstract

A parallel approach to solve three-dimensional viscous incompressible fluid flow problems using discontinuous-pressure finite elements and a Lagrange multiplier technique is presented. The strategy is based on non-overlapping domain decomposition methods, and Lagrange multipliers are used to enforce continuity at the boundaries between subdomains. The novelty of the work is the coupled resolution of the velocity-pressure-Lagrange-multiplier system of the discrete Navier-Stokes equations by a distributed memory parallel ILU (0) preconditioned Krylov method. A penalty function on the interface constraints equations is introduced to avoid the locking of the ILU factorization algorithm. To ensure portability of the code, a message based memory distributed model with MPI is employed. The method has been tested over different benchmark cases such as the lid-driven cavity and the pipe flow with unstructured tetrahedral grids. It is found that the partition algorithm and the ordering

of the physical variables are central to parallelization performance. A speed-up in the range of 5 to 13 is obtained with 16 processors.

5.3. Introduction

Computational fluid dynamics (CFD) models are typically based on the solution of the Navier-Stokes equations with the help of discretization schemes such as the finite volume or finite element method. In most practical situations, the mesh needs to be highly refined to capture the physics of the problem, making the computations highly demanding in memory and time. To address this issue, parallel finite element computations have been developed and successfully applied to several large-scale flow problems. Some early applications in fluid mechanics were made by FARHAT et al. (1993) and JOHAN et al. (1995). These applications demonstrated the possibility to speed-up calculations by the use of several CPU processors.

The most time-consuming part of the simulation is the resolution of the generated algebraic system of equations. Several parallel algorithms have been proposed to reduce time and memory. Most of them are based on domain decomposition methods which consist in the subdivision of the original computational domain into a set of interconnected subdomains. In this manner, internal unknowns are calculated in parallel, while the inter-processor communications is restricted to the unknowns at the subdomain interfaces.

Direct solution methods based on the LU-decomposition of the matrix and subsequent forward-backward substitution schemes are often selected as they are very robust especially for ill-conditioned problems. Parallel variants can be found in the case of multi-frontal methods (SCOTT, 2003), or sparse Cholesky algorithms as in the SuperLU software (LI and DEMMEL, 2003). An evaluation of several solvers such as PARDISO, MA57 and BSLIB-EXT for the direct solution of large sparse linear systems can be found in GOULD et al. (2005). They concluded that the parallel efficiency of these methods depends on equations reordering and pivoting strategies. AGGARWAL et al. (1994) and HENRIKSEN and KEUNINGS (1994) have employed these solvers to simulate the flow of viscoelastic fluids. Unfortunately the large memory requirements limit its use to massive parallel computing composed of hundreds of processors. LI and DEMMEL (2003) required 32 processors to solve a system of approximately 10^6 equations (40K equations/processor).

To overcome the memory limitations, at least partly, an alternative is to use preconditioned iterative Krylov subspace methods. With these methods, several algebra operations like sparse matrix-vectors products, inner products, vector updates and forward and backward substitutions need to be performed. Their parallelization has been the subject of numerous investigations. For example, one option to facilitate parallelization is to reorder the variables by the so-called coloring techniques (DUTTO and HABASHI, 1999). They show that the approach is useful only for 4-6 processors

when using ILU(0)-GMRES. WILLE et al. (2003) and STAFF and WILLE (2005) used domain decomposition, a priori pivoting and segregation of variables to parallelize the ILU preconditioning of an conjugate gradient solver. Results presented for the Navier-Stokes equations showed that the speed-up is limited due to the sequential characteristics of ILU algorithms. HUGHES et al. (1983) introduced the concept of element-by-element (EBE) preconditioners. It consists of computing the preconditioner from the element matrix, avoiding the storage of both the global matrix and the preconditioner. This idea can be combined with domain decomposition to give better performance. Different variants such as the clustered-element-by-element (CEBE), the mixed CEBE and the cluster companion (CC) preconditioners were proposed by TEZDUYAR and LIOU (1989) and TEZDUYAR et al. (1992). However, the effectiveness of the EBE technique is limited because it does not often provide a substantial improvement in CPU time with respect to fast sequential techniques (DUFF and VAN DER VORST, 1999).

A well known domain decomposition approach based on overlapping partitions is the Schwarz method. An excellent introduction and application of this method is presented by SMITH et al. (1996). It has been applied to solve incompressible Navier-Stokes equations in various situations: flows in turbomachinery (BORELLO et al., 2003), viscoelastic fluid flows (CAOLA et al., 2001; CAOLA and BROWN, 2002), high Reynolds number flows (CAI et al., 2002; HWANG and CAI, 2005), backward flow step (VAINIKKO and GRAHAM, 2004), multi-physics problems (SHADID et al.,

2005), and large scale computing (GROPP et al., 2001). Nevertheless, Schwarz methods require a larger amount of inter-processor communications with respect to non-overlapping techniques. Additionally, the data structure required by an overlapping partition is always more difficult to handle than the one employed by a non-overlapping one.

Non-overlapping approaches are based on the resolution of independent sets of adjacent partitions with the subsequent resolution of an interface problem. TOSELLI and WIDLUND (2005) give a complete mathematical description of these methods. They are normally based on Lagrange multipliers. There are different approaches for implementing Lagrange multiplier based methods. One is based on the elimination of the degrees of freedom internal to the subdomains in order to solve an interface problem by a conjugate gradient algorithm (FARHAT and ROUX, 1993; ACHDOU et al., 1995; HU et al., 2004) as in the finite element tearing and interconnecting (FETI) method of FARHAT and ROUX (1993). It is worth noting that this method has been applied to incompressible flow in the work presented by VANDERSTRAETEN and KEUNINGS (1998), ZSAKI et al. (2003) and VEREECKE et al. (2003). A similar approach is presented by GLOWINSKI et al. (1995) in combination with fictitious domain methods. The main drawback of FETI algorithm is that it requires direct method solvers that may demand a large amount of memory. One way to alleviate this shortcoming is to directly solve the saddle-point problem by a preconditioned iterative method. This has the advantage of allowing the use of inexact low memory Krylov

solvers for both the interior and multiplier variables. This type of domain decomposition has been applied to solve the diffusion equation on non-matching grids (KUZNETSOV, 1995), elasticity problems (KLAWONN and WIDLUND, 2000; KLAWONN and RHEINBACH, 2007) and elliptic problems with variable coefficients (HU et al., 2004).

In this work we present a domain decomposition method based on Lagrange multipliers in the context of the finite element solution of the Stokes equations (laminar flows). The particular motivation is the study of viscous fluid mixing, where computer resources needed dramatically increase when attempting to simulate industrial problems. To benefit from the full computational potential of nowadays multi-processor machines, it is mandatory to develop a parallel solver with distributed memory so that it enables to perform large simulations on very refined grids that can hardly be handled on a single processor. For that purpose, a parallel finite element solver for the Navier-Stokes equations based on non-overlapping partitions is developed to speed-up computations and to reduce memory requirements per processor. The continuity at the interface is enforced by a set of Lagrange multipliers located at the subdomains interfaces. This method can be seen as a variant of the FETI technique. The novelty of the work is that the velocity-pressure-Lagrange multiplier system arising from the finite element discretization of the Navier-Stokes equations is solved simultaneously by a distributed memory parallel ILU(0) preconditioned Krylov method. As presented by COESNON et al. (2008), a penalty parameter is introduced on the

interface constraints to avoid zero entries on the diagonal of the global matrix that prohibits the ILU factorization. To ensure code portability, a message passing interface (MPI) communication protocol is employed. The finite element parallel solver was implemented in the POLY3D (Rheosoft Inc.) software. The organization of the paper is as follows; in section 2 we describe the proposed numerical model with emphasis on the domain decomposition mathematical formulation. Section 3 presents the details about the parallelization of the method using MPI. Section 4 shows results for three-dimensional benchmark cases as the pipe and cavity flows. The effect of several partitioning algorithms and reordering of variables is described.

5.4. Parallel numerical model

5.4.1. One-domain variational formulation

For the sake of brevity the mathematical formulation is presented for the steady Stokes problem in a computational domain Ω with boundary $\partial\Omega$ (Figure 5-1a).

a)

b)
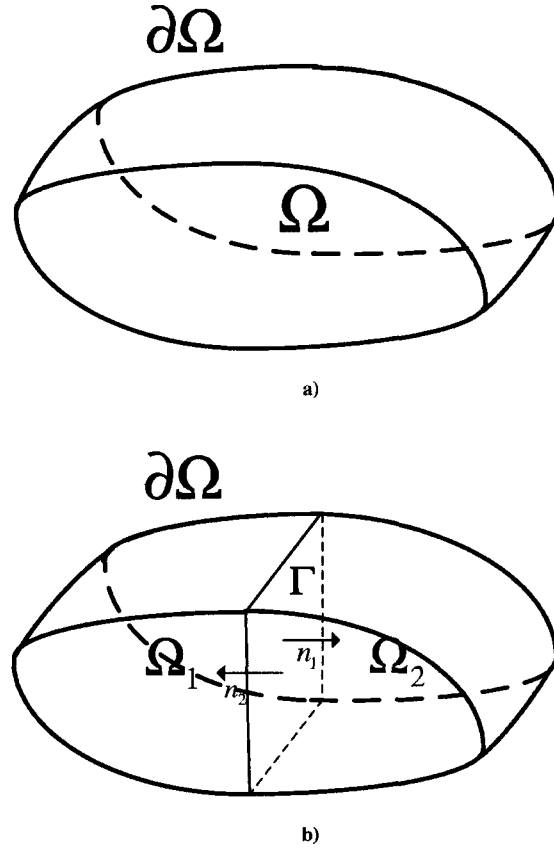
Figure 5-1: Three-dimensional domain Ω with boundary $\partial\Omega$: a) one partition; b)

partitioning into two subdomains Ω_1 and Ω_2 .

$$\mu\nabla^2\mathbf{v} + grad\ p = \mathbf{f}, \text{ in } \Omega, \tag{5.1}$$

$$\text{div } \mathbf{v} = 0, \text{ in } \Omega. \tag{5.2}$$

where $\mathbf{v}$ stands for the velocity, $\mathbf{f}$ the body force, p the pressure and μ the Newtonian

fluid viscosity. It is well known that problem (5.1) and (5.2) is equivalent to finding the

functions $\mathbf{v}$ and p from the following saddle-point problem defined for any admissible $\mathbf{w}$ and q functions.

$$\inf_{\mathbf{w} \in \left[H_0^1(\Omega)\right]^3} \sup_{q \in L^2(\Omega)} L(\mathbf{w}, q), \text{ in } \Omega, \tag{5.3}$$

where:

$$L(\mathbf{w}, q) = \frac{\mu}{2} \int_\Omega |\text{grad } \mathbf{w}|^2 \, d\Omega - \int_\Omega q \, \text{div } \mathbf{w} \, d\Omega - \int_\Omega \mathbf{f} \cdot \mathbf{w} \, d\Omega, \text{ in } \Omega, \tag{5.4}$$

This last expression is known as the Lagrangian functional. After derivation with respect to each variable, the Euler-Lagrange equations are obtained:

$$a(\mathbf{v}, \psi) - b(\psi, p) = (\mathbf{f}, \psi), \quad \forall \psi \in \left[H_0^1(\Omega)\right]^3, \text{ in } \Omega, \tag{5.5}$$

$$b(\mathbf{v}, \varphi) = 0, \quad \forall \varphi \in L^2(\Omega), \text{ in } \Omega \tag{5.6}$$

where

$$a(\mathbf{v}, \psi) = \mu \int_\Omega \text{grad } \mathbf{v} \cdot \text{grad } \psi \, d\Omega, \tag{5.7}$$

$$b(\mathbf{v}, \varphi) = \int_\Omega \varphi \cdot \text{div } \mathbf{v} \, d\Omega, \tag{5.8}$$

and $(.,.)_\Omega$ is the scalar product in $L^2(\Omega)$:

$$(\mathbf{u}, \mathbf{v})_\Omega = \int_\Omega \mathbf{u} \cdot \mathbf{v} \, d\Omega, \quad \forall \mathbf{u}, \mathbf{v} \in L^2(\Omega) \tag{5.9}$$

in (5.5)-(5.8) ψ and φ stand for the shape functions for the velocity and pressure respectively.

5.4.2. Two-domain decomposition method with Lagrange multipliers

First, a partition of the domain is introduced. For instance, let us consider two subdomains (Figure 5-1b). Due to the decomposition, the coupled problem defined by equations (5.1) and (5.2) is equivalent to:

$$-\mu\Delta\mathbf{v}_i + \operatorname{grad} p_i = \mathbf{f}_i, \text{ in } \Omega_i \text{ for } i = 1,2 \tag{5.10}$$

$$\operatorname{div}\mathbf{v}_i = 0, \text{ in } \Omega_i, \text{ for } i = 1,2 \tag{5.11}$$

$$\mathbf{v}_1 = \mathbf{v}_2, \text{ in } \Gamma \tag{5.12}$$

$$\frac{\partial\mathbf{v}_1}{\partial\mathbf{n}_1} = -\frac{\partial\mathbf{v}_2}{\partial\mathbf{n}_2}, \text{ in } \Gamma \tag{5.13}$$

where $\mathbf{n}_i$ stands for the outward normal to the subdomain interface Γ. Dirichlet boundary conditions are assumed on the domain boundary. Thus, the domain decomposition removes the strong point-wise continuity at the parallel boundary by a weak integral condition generating extra constraints over the subdomains interface [Equations (5.12) and (5.13)]. We resort to a Lagrange multiplier method and constrained optimization techniques to reformulate the problem in (5.10)-(5.13) to find

the solutions $\mathbf{v}$, p and λ of the modified saddle point problem defined for any admissible functions $\mathbf{w}$, q and $\boldsymbol{\mu}$:

$$\inf_{\mathbf{w} \in \left[H_0^1(\Omega)\right]^3} \sup_{q \in L^2(\Omega)} \sup_{\boldsymbol{\mu} \in [L^2(\Gamma)]^3} L_{p_i}(\mathbf{w}_i, q_i, \boldsymbol{\mu}) \text{ in } \Omega_i \text{ for } i = 1, 2 \tag{5.14}$$

where,

$$L_p(\mathbf{w}, q, \boldsymbol{\mu}) = L_i(\mathbf{w}, q) - \int_\Gamma \boldsymbol{\mu} \cdot (\mathbf{w}_1 - \mathbf{w}_2) \, d\Gamma \tag{5.15}$$

In (5.15) we introduce a Lagrange multiplier function $\boldsymbol{\mu}$ associated with the interface boundary condition. The Euler-Lagrange equations corresponding to this constrained problem are given by

$$a\left(\mathbf{v}_i, \psi\right) = \left(\mathbf{f}_i, \psi\right) + b(\psi, p_i) + (\lambda, \psi)_\Gamma \ , \forall \, \psi \in \left[H_0^1(\Omega_i)\right]^3, \text{ in } \Omega_i \text{ for } i = 1, 2 \tag{5.16}$$

$$b\left(\mathbf{v}_i, \varphi\right) = 0, \ \forall \, \varphi \in L^2(\Omega_i), \text{ in } \Omega_i \text{ for } i = 1, 2 \tag{5.17}$$

$$\left((\mathbf{v}_1 - \mathbf{v}_2), \xi\right)_\Gamma = 0, \ \forall \, \xi \in \left[L^2(\Gamma)\right]^3 \quad at \quad \Gamma \tag{5.18}$$

where ξ stands for the shape function of the Lagrange multiplier space. The solution of the Lagrange multiplier function λ is nothing but the jump of normal derivates at the subdomain interface GLOWINSKI et al. (1995). To connect multiple subdomains (as in the simple example of Figure 5-2), the only valid constraints to impose are the ones

where a face (edge for two-dimensional problems) connecting subdomains exists. Thus

in our example, only the following constraints are considered.

$$\int_{\Gamma_{12}} \mu_{12} \cdot (w_1 - w_2) d\Gamma_{12} , \qquad (5.19)$$

$$\int_{\Gamma_{14}} \mu_{14} \cdot (w_1 - w_4) d\Gamma_{14} , \qquad (5.20)$$

$$\int_{\Gamma_{23}} \mu_{23} \cdot (w_2 - w_3) d\Gamma_{23} , \qquad (5.21)$$

$$\int_{\Gamma_{34}} \mu_{34} \cdot (w_3 - w_4) d\Gamma_{34} . \qquad (5.22)$$
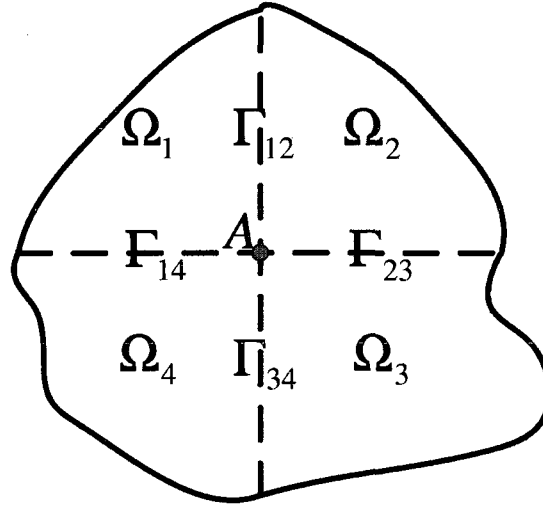
Figure 5-2: Multiple domain decomposition of a 2D computational domain Ω in four

Ω_i subdomains and respective boundaries Γ_{ij}.

This is in agreement with the discussion presented by FARHAT and ROUX (1991) for the FETI method. As they pointed out, this particularity helps to reduce communication between processors improving parallel computing performance.

5.4.3.   Finite element discretization

In the present work, P_1^+-P_0 (Figure 5-3a) (BERTRAND et al., 1992) and P_2^+-P_1 (Figure 5-3b) (CROUZEIX and RAVIART, 1973) tetrahedral finite elements approximations are used. The former is an enriched version of the P_1-P_0 finite element. Extra degrees of freedom are added at the middle of each face and the pressure is assumed constant at each element. The latter element approximates the velocity by continuous quadratic shape functions, while the pressure and its gradients are computed inside each element. Both elements belong to the class of discontinuous pressure elements that satisfies the Brezzi-Babuska condition ensuring numerical stability.
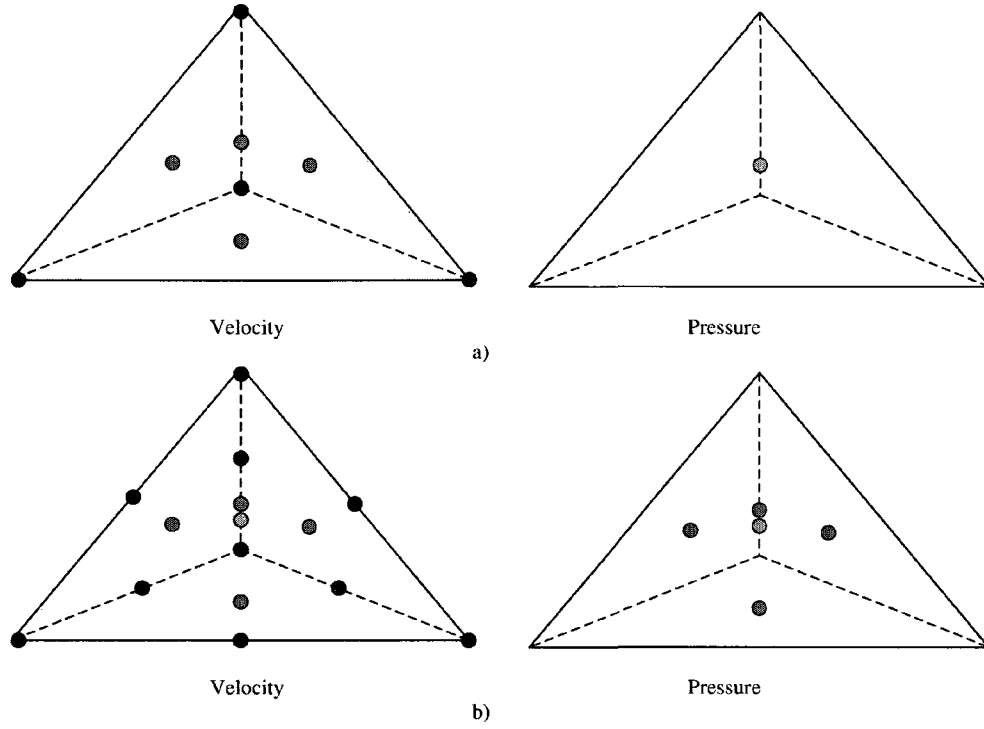
Figure 5-3: Tetrahedral finite element approximations a) $P1^+$-P0; b)$P2^+$-P1.

The Lagrange multiplier space Λ is discretized using Dirac functions that are defined by:

$$\delta(\mathbf{x} - \mathbf{x}_i) = \begin{cases} +\infty & \textit{if } \mathbf{x} = \mathbf{x}_i \\ 0 & \textit{if } \mathbf{x} \neq \mathbf{x}_i \end{cases} \tag{5.23}$$

The use of Dirac functions is inspired by the fictitious domain method (BERTRAND et al., 1997; COESNON et al., 2008). This is done with the purpose to simplify the discretization of the constraint in (5.18) allowing its imposition point-wise, and therefore eliminating the need to compute surface integrals at the subdomain interface.

Thus for each constraint distributed over the set of nodes $\{x_i\}_{i=1}^{N}$ that lie over the interface between subdomains, we have,

$$v_1(x_i) = v_2(x_i) \tag{5.24}$$

where subscripts 1 and 2 stand for subdomain labels.

A fully coupled approach is used to solve the set of equations (5.16)-(5.18), meaning that velocity, pressure and multipliers are solved simultaneously. The matrix form of the problem is the following

$$\begin{bmatrix} A_1 & B_1^T & 0 & 0 & -K_{\Lambda 1}^T \\ B_1 & 0 & 0 & 0 & 0 \\ 0 & 0 & A_2 & B_2^T & K_{\Lambda 2}^T \\ 0 & 0 & B_2 & 0 & 0 \\ -K_{\Lambda 1} & 0 & K_{\Lambda 2} & 0 & 0 \end{bmatrix} \begin{Bmatrix} U_1 \\ P_1 \\ U_2 \\ P_2 \\ \Lambda \end{Bmatrix} = \begin{Bmatrix} F_1 \\ 0 \\ F_2 \\ 0 \\ 0 \end{Bmatrix} \tag{5.25}$$

where A_i stands for the convection-diffusion matrix, B_i the matrix obtained from the incompressibility constraint, B_i^T the transpose of B_i, $K_{\Lambda i}$ the matrix from the interface constraint, U_i, P_i, Λ and F_i stand for the velocity, pressure, Lagrange multipliers and body forces respectively.

Although the mathematical formulation is well-posed, the presence of zeros on the main diagonal makes the ILU preconditioning fail due to the lack of pivoting during the

ILU decomposition. To overcome this problem, we introduce penalty parameters in (5.25) for both the divergence and Lagrange multipliers equations. In this way, equations (5.17) (pressure p) and (5.18) (Lagrange multiplier λ) are replaced by

$$b\left(\mathbf{v}_i, \varphi\right) = -\left(p_i, \varphi\right)/\varepsilon_p, \ \forall \ \varphi_h \in P_h, \text{ in } \Omega_i \text{ for } i = 1, 2 \tag{5.26}$$

$$\left(\left(\mathbf{v}_1 - \mathbf{v}_2\right), \xi\right)_\Gamma = -\left(\lambda, \xi\right)_\Gamma/\varepsilon_\lambda, \ \forall \ \xi_h \in \Lambda_h, \tag{5.27}$$

where ε_p and ε_λ are penalty parameters. According to (5.26) and (5.27), the matrix form (5.25) is rewritten as follows

$$\begin{bmatrix} \mathbf{A}_1 & \mathbf{B}_1^T & 0 & 0 & -\mathbf{K}_{\Lambda 1}^T \\ \mathbf{B}_1 & \varepsilon_p^{-1} & 0 & 0 & 0 \\ 0 & 0 & \mathbf{A}_2 & \mathbf{B}_2^T & \mathbf{K}_{\Lambda 2}^T \\ 0 & 0 & \mathbf{B}_2 & \varepsilon_p^{-1} & 0 \\ -\mathbf{K}_{\Lambda 1} & 0 & \mathbf{K}_{\Lambda 2} & 0 & \varepsilon_\lambda^{-1} \end{bmatrix} \begin{Bmatrix} \mathbf{U}_1 \\ \mathbf{P}_1 \\ \mathbf{U}_2 \\ \mathbf{P}_2 \\ \Lambda \end{Bmatrix} = \begin{Bmatrix} \mathbf{F}_1 \\ 0 \\ \mathbf{F}_2 \\ 0 \\ 0 \end{Bmatrix} \tag{5.28}$$

In this work, penalty parameters are defined by the expressions given in (5.26) and (5.27).

$$\varepsilon_p = 10^{-\alpha}/\rho\mu \tag{5.29}$$

$$\varepsilon_\lambda = 10^{-\beta} h /\rho\mu \tag{5.30}$$

where α and β has been heuristically determined to be between 6 and 12. In this work, a value of 8 is taken for both parameters. A fixed-point Newton iterative algorithm is chosen to solve the problem in incremental form to give the Algorithm 5-1. It must be remarked that only one fixed point iteration is required for linear problems.

0.   Given $U^{(0)}$, $P^{(0)}$ and $\Lambda^{(0)}$.

1.   For n = 1, 2, ..., until convergence:

     1.1. Solve simultaneously for δU, δP and $\delta \Lambda$:

$$
\begin{bmatrix}
\mathbf{A}_1 & \mathbf{B}_1^T & 0 & 0 & -\mathbf{K}_{\Lambda 1}^T \\
\mathbf{B}_1 & \varepsilon_p^{-1}\mathbf{I} & 0 & 0 & 0 \\
0 & 0 & \mathbf{A}_2 & \mathbf{B}_2^T & \mathbf{K}_{\Lambda 2}^T \\
0 & 0 & \mathbf{B}_2 & \varepsilon_p^{-1}\mathbf{I} & 0 \\
-\mathbf{K}_{\Lambda 1} & 0 & \mathbf{K}_{\Lambda 2} & 0 & \varepsilon_\lambda^{-1}\mathbf{I}
\end{bmatrix}
\begin{Bmatrix}
\delta U_1 \\
\delta P_1 \\
\delta U_2 \\
\delta P_2 \\
\delta \Lambda
\end{Bmatrix}
=
\begin{Bmatrix}
\mathbf{R}_{v1^{(n)}} \\
\mathbf{R}_{p1^{(n)}} \\
\mathbf{R}_{v2^{(n)}} \\
\mathbf{R}_{p2^{(n)}} \\
\mathbf{R}_{\lambda^{(n)}}
\end{Bmatrix}
$$

$$
\begin{Bmatrix}
\mathbf{R}_{v1^{(n)}} \\
\mathbf{R}_{p1^{(n)}} \\
\mathbf{R}_{v2^{(n)}} \\
\mathbf{R}_{p2^{(n)}} \\
\mathbf{R}_{\lambda^{(n)}}
\end{Bmatrix}
=
\begin{Bmatrix}
\mathbf{F}_1 \\
0 \\
\mathbf{F}_1 \\
0 \\
0
\end{Bmatrix}
-
\begin{bmatrix}
\mathbf{A}_1 & \mathbf{B}_1^T & 0 & 0 & -\mathbf{K}_{\Lambda 1}^T \\
\mathbf{B}_1 & \varepsilon_p^{-1}\mathbf{I} & 0 & 0 & 0 \\
0 & 0 & \mathbf{A}_2 & \mathbf{B}_2^T & \mathbf{K}_{\Lambda 2}^T \\
0 & 0 & \mathbf{B}_2 & \varepsilon_p^{-1}\mathbf{I} & 0 \\
-\mathbf{K}_{\Lambda 1} & 0 & \mathbf{K}_{\Lambda 2} & 0 & \varepsilon_\lambda^{-1}\mathbf{I}
\end{bmatrix}
\begin{Bmatrix}
\mathbf{U}_1^{(n)} \\
\mathbf{P}_1^{(n)} \\
\mathbf{U}_2^{(n)} \\
\mathbf{P}_2^{(n)} \\
\Lambda^{(n)}
\end{Bmatrix}
$$

     1.2. Update $\mathbf{U}_i^{(n)}$, $\mathbf{P}_i^{(n)}$ and $\Lambda^{(n)}$:
$$
\begin{cases}
\mathbf{U}_i^{(n+1)} = \mathbf{U}_i^{(n)} + \delta U_i \\
\mathbf{P}_i^{(n+1)} = \mathbf{P}_i^{(n)} + \delta P_i \\
\Lambda^{(n+1)} = \Lambda^{(n)} + \delta \Lambda
\end{cases}
$$

     1.3.   in Ω_i for $i = 1, 2$

Algorithm 5-1: Two-domain fixed-point solution algorithm

5.5. Parallel implementation

The parallel implementation of the Algorithm 5-1 is composed of several key elements; in this section we describe the particularities for each one of them.

5.5.1. Matrix partition

The block structure of the matrix for each subdomain can be exploited to adapt iterative methods to the capabilities of parallel computers. To allow efficient parallelization, each block A_i has been subdivided into smaller blocks, depending whether the equations belongs to internal or interface.

$$A_i = \begin{bmatrix} A_{int} & H \\ G & A_{iface} \end{bmatrix} \quad (5.31)$$

In (5.31) the subscripts *int* and *iface* refer to internal and interface equations respectively while matrices **H** and **G** correspond to the coupling between internal and interface equations (for symmetric problems $H = G^T$). In this way, computations can be done in parallel for A_{int} block variables, being the communication limited to the equations let in the A_{iface} block. Thus each processor stores and computes the data related to the block structure.

$$
\begin{bmatrix}
\mathbf{A}_{int(i)} & \mathbf{H}_{(i)} & \mathbf{B}^T_{int(i)} & -\mathbf{K}_{\Lambda(j)} \\
\mathbf{G}_{(i)} & \mathbf{A}_{int(i)} & \mathbf{B}^T_{iface(i)} & \mathbf{K}^T_{\Lambda(i)} \\
\mathbf{B}_{int(i)} & \mathbf{B}_{iface(i)} & \varepsilon^{-1}_{p(i)}\mathbf{I} & 0 \\
-\mathbf{K}_{\Lambda(j)} & 0 & \mathbf{K}_{\Lambda(i)} & \varepsilon^{-1}_{\lambda(i)}\mathbf{I}
\end{bmatrix}
\begin{Bmatrix}
\mathbf{U}_{int} \\
\mathbf{U}_{iface} \\
\mathbf{P}_i \\
\mathbf{\Lambda}_{ij}
\end{Bmatrix}
=
\begin{Bmatrix}
\mathbf{F}_{int} \\
\mathbf{F}_{iface} \\
0 \\
0
\end{Bmatrix}
\tag{5.32}
$$

In (5.32), the subscript (i) refers to the entries that belong to subdomains i and subscript (j) refers to the entries that belong to subdomains j connected to subdomain i where $j<i$. Although not performed in practice, the union of all blocks distributed in the processors regenerates the global system of equations presented in Algorithm 5-1.

5.5.2. Mesh partitioning schemes

To partition the computational domain several mesh partitioning schemes such as the coordinate recursive bisection, the multilevel k-way (KARYPIS and KUMAR, 1998), the multilevel-KL (HENDRIKSON and LELAND, 1993) and the spectral octasection partitioning method (HENDRIKSON and LELAND, 1993) were considered. Furthermore Kernigham-Lin local refinement (KERNIGHAN and LIN, 1970) and terminal propagation (DUNLOP and KERNIGHAN, 1985) were also investigated in combination with spectral methods. Kernigham-Lin local refinement is nothing but a greedy local smoothing strategy, moving elements between subdomains in an effort to reduce the amount of interfacial area. Terminal propagation is another technique that yields a partition connectivity suitable for the machine architecture. In our case, we use

this feature to simplify as much as possible the connectivity of the partition generating

stripped partitions. The multilevel k-way partitioning technique is available from Metis

software (KARYPIS and KUMAR, 1998). Multilevel-KL and all spectral partitioning

techniques are available in the Chaco software (HENDRIKSON and LELAND, 1993).

To characterize how well the computational work is uniformly distributed among the

processors, we define the load distribution that can be computed by

$$load\ distribution = \min(NNZ)/\max(NNZ) \tag{5.33}$$

where NNZ stands for a list that contains the number of non-zero entries in each

submatrix. The size of each sub-matrix is determined by NNZ instead of number of

equations (NEQ) because the demand for CPU and memory resources is directly

related to NNZ, and not to NEQ. In this way, the load distribution takes values between

0 and 1; a value of 1 corresponds to the ideal load distribution and a value of 0

corresponds to the worst case scenario.

5.5.3.   Krylov subspace iterative solvers

The system of equations of Algorithm 5-1 is solved by an iterative Krylov method,

which is composed of parallelizable algebra operations like matrix-vector products,

inner products and vector updates. This approach is characterized by its low memory

requirements allowing the solution of a larger number of equations per processor than

with direct methods. The choice of iterative methods for the systems arising from the finite element discretization of the Navier-Stokes equations is restricted by the non-symmetry and non-definite positiveness properties of the matrix. The conjugate gradient method, very efficient for symmetric matrices, becomes inapplicable. One should use variants based on the Quasi-Minimal Residuals (QMR) or the Biconjugate Gradient Stabilized approach (BiCGSTAB).

Preconditioning is a central issue because in many cases it makes a diverging problem converging. In this work, an incomplete factorization with zero fill-ins (ILU(0)) was selected due to its well known robustness in comparison to other techniques (e.g. diagonal preconditioners), low memory requirements and reduced operations counts with respect to their fill-in counterparts (SAAD, 2003). Matrix factorization and forward-backward substitution operations on a memory distributed parallel environment has been performed based on algorithms presented by SAAD (2003).

5.5.4. Ordering of variables

The ordering of variables inside each sub-matrix can play a critical role in the convergence rate behaviour of the Krylov solver as shown in HENICHE et al. (2001). It consists in reordering internal velocity (Ux, Uy, Uz), interface velocity (I), pressure (P) and Lagrange multipliers (LM) sub-blocks in each of the sub-systems that form the global system of equations.

Five configurations were tested based on modifying the structure of the internal velocity and pressure sub-blocks. Lagrange multiplier and interface velocity sub-blocks were not modified since parallel efficiency depends on them. One option is to keep contiguous each component of the velocity for each node in the mesh while the pressure is kept in a separate block; this creates two orderings depending if the pressure sub-block is located after or before the interface velocity, represented as follows,

$$UxUyUz - I - P - LM \rightarrow \left\langle \begin{matrix} u_{\text{int}x1}, u_{\text{int}y1}, u_{\text{int}z1}, ..., u_{\text{int}xn}, u_{\text{int}yn}, u_{\text{int}zn}, \\ u_{ifacex1}, u_{ifacey1}, u_{ifacez1}, ..., u_{ifacexm}, u_{ifaceym}, u_{ifacezm}, \\ p_1, ..., p_n, \\ \lambda_{x1}, \lambda_{y1}, \lambda_{z1}, ..., \lambda_{xm}, \lambda_{ym}, \lambda_{zm} \end{matrix} \right\rangle \qquad (5.34)$$

$$UxUyUz - P - I - LM \rightarrow \left\langle \begin{matrix} u_{\text{int}x1}, u_{\text{int}y1}, u_{\text{int}z1}, ..., u_{\text{int}xn}, u_{\text{int}yn}, u_{\text{int}zn}, \\ p_1, ..., p_n, \\ u_{ifacex1}, u_{ifacey1}, u_{ifacez1}, ..., u_{ifacexm}, u_{ifaceym}, u_{ifacezm}, \\ \lambda_{x1}, \lambda_{y1}, \lambda_{z1}, ..., \lambda_{xm}, \lambda_{ym}, \lambda_{zm} \end{matrix} \right\rangle \qquad (5.35)$$

Another variant was to consider a sub-block for each component of the velocity and pressure; this was denoted as Ux-Uy-Uz-I-P-LM.

$$Ux - Uy - Uz - I - P - LM \rightarrow \left\langle \begin{matrix} u_{\text{int}x1}, \ldots, u_{\text{int}xn}, u_{\text{int}y1}, \ldots, u_{\text{int}yn}, u_{\text{int}z1}, \ldots, u_{\text{int}zn}, \\ p_1, \ldots, p_n, \\ u_{ifacex1}, u_{ifacey1}, u_{ifacez1}, \ldots, u_{ifacexm}, u_{ifaceym}, u_{ifacezm}, \\ \lambda_{x1}, \lambda_{y1}, \lambda_{z1}, \ldots, \lambda_{xm}, \lambda_{ym}, \lambda_{zm} \end{matrix} \right\rangle \quad (5.36)$$

Another option was to consider a single sub-block for both velocity and pressure where each component of the velocity and pressure equations are kept adjacent for each node in the mesh; this was referred to as UxUyUzP-I-LM.

$$UxUyUzP - I - LM \rightarrow \left\langle \begin{matrix} u_{\text{int}x1}, u_{\text{int}y1}, u_{\text{int}z1}, p_1, \ldots, u_{\text{int}xn}, u_{\text{int}yn}, u_{\text{int}zn}, p_n, \\ u_{ifacex1}, u_{ifacey1}, u_{ifacez1}, \ldots, u_{ifacexm}, u_{ifaceym}, u_{ifacezm}, \\ \lambda_{x1}, \lambda_{y1}, \lambda_{z1}, \ldots, \lambda_{xm}, \lambda_{ym}, \lambda_{zm} \end{matrix} \right\rangle \quad (5.37)$$

Finally the pressure sub-block was positioned before the internal velocity in the ordering named P-UxUyUz-I-LM.

$$P - UxUyUz - I - LM \rightarrow \left\langle \begin{matrix} p_1, \ldots, p_n, u_{\text{int}x1}, u_{\text{int}y1}, u_{\text{int}z1}, \ldots, u_{\text{int}xn}, u_{\text{int}yn}, u_{\text{int}zn}, \\ u_{ifacex1}, u_{ifacey1}, u_{ifacez1}, \ldots, u_{ifacexm}, u_{ifaceym}, u_{ifacezm}, \\ \lambda_{x1}, \lambda_{y1}, \lambda_{z1}, \ldots, \lambda_{xm}, \lambda_{ym}, \lambda_{zm} \end{matrix} \right\rangle \quad (5.38)$$

5.5.5. Communications

The communication pattern is governed by the forward/backward parallel substitution algorithms presented in SAAD (2003) that were adapted to the linear system in Algorithm 5-1. They consist in two steps. The first one consists in sending the interface

velocity from subdomain i to subdomains j where $j>i$ (forward communication). The second step requires to send the Lagrange multiplier values from subdomain i to subdomains j where $j<i$ (backward communication). Figure 5-4 presents a schematic representation of this process for the case of two partitions.
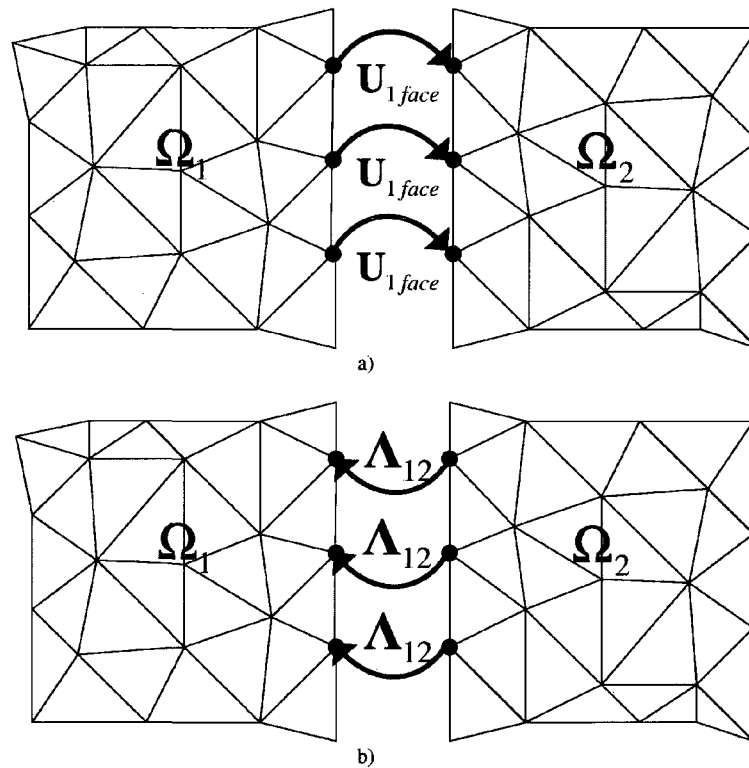
Figure 5-4: Schematic representation of the communication between two subdomains a) forward communication for the interface velocities; b) backward communication for the Lagrange multipliers

In the case of multiple partitions as shown in Figure 5-5, it is necessary to communicate data to only certain partitions. One way is to communicate from the sender partition to the receivers (the ones that are related with the sender) making a send-receive call at each time a partition communicates to other partitions. By experience this is a very inefficient procedure in terms of communication and overhead time. A better option is to use the MPI_BROADCAST routine, which allows sending data in an optimized way from a 'sender' process to the rest of partitions included in the communicator. The communicator here is defined as a collection of processes that can send messages to each other. By default MPI uses MPI_COMM_WORLD communicator where all the processes in the computation are included. For our application the use of a unique MPI_COMM_WORLD communicator in the broadcast of information would generate overhead time for the processes that are not related to the sender. This is caused by the fact that the broadcast function would not return until all the data is send to all receiver processes included in MPI_COMM_WORLD. To avoid this, we have defined several sets of communicators, one for each process, which is composed of the partitions that are related. Figure 5-5 exemplifies the set of subdomains that compose the communicator for subdomains 2 and 3. In this way, in the case of several subdomains, broadcast operations make use of these particular communicators instead of MPI_COMM_WORLD. Thus, processes that are not related to the sender can continue their work while processes that are connected can receive their information.
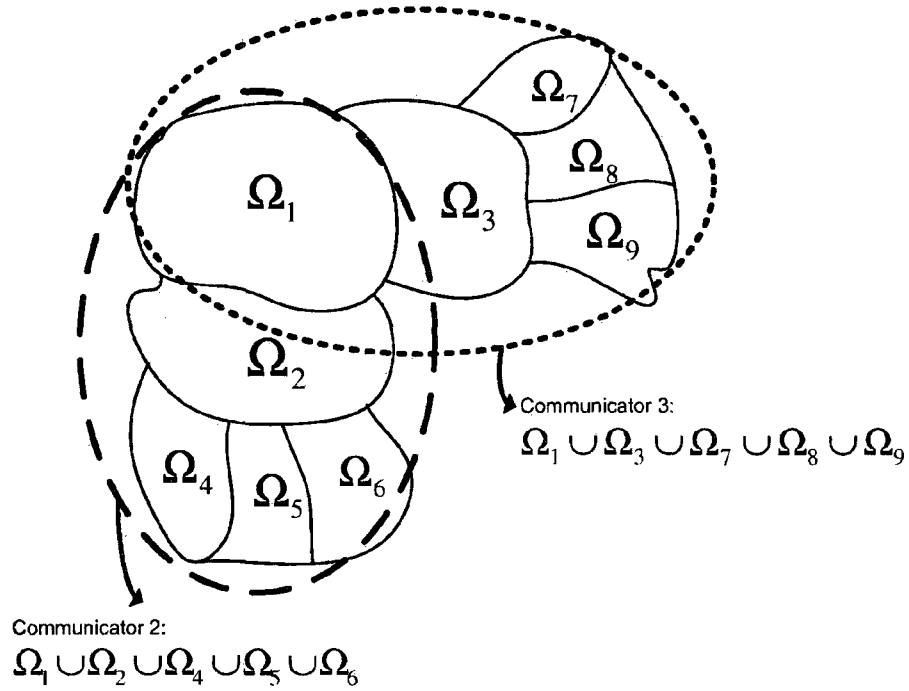
Figure 5-5: Schematic representation of a domain partitioned into 9 subdomains, that exemplifies the set of subdomains that define communicators for subdomain 2 (broken line) and 3 (dotted line).

5.6. Three-dimensional benchmark cases

The proposed numerical methodology was tested on two benchmark problems, namely the flow in a pipe and the lid driven cavity flow, with the purpose to analyze the effect of the shape of the geometry over the parallel performance. Since the convective term was not considered at this point, Stokes flows (linear problems) were solved by means of the Lagrange multiplier based parallel conjugate gradient Krylov solver developed in this work. Furthermore, the solutions obtained by the CG Krylov solver were

considered converged when the norm ratio between the last residual (r^i) and the first residual (r^0) satisfies the following:

$$\|r^i\|/\|r^0\| < 10^{-6} \qquad (5.39)$$

where $\|\cdot\|$ stands for the Euclidean norm. The initial solution for all cases was set to zero. The simulations were run on a 16 processor IBM-P690 with 64 GB of shared memory. In section 4.1 and 4.2 Metis was used for partitioning and the variables were UxUyUz-I-P-LM ordered.

5.6.1. Flow in a pipe

The partitioning for the pipe flow consisted in simply connected strips where each interface connects only two subdomains avoiding the multiple subdomain issue described in 2.4. The total number of elements, number of equations, number of non-zero entries in the matrix and time required to solve the problem in sequential mode for each of the computational grid can be found in Table 5-1. A characteristic of the method is the growth in size of the global system of equations due to the addition of the Lagrange multipliers equations with respect to the number of subdomains, as can be seen on Figure 5-6. As was already discussed, the partitioning was performed using Metis that distributes in an almost uniform fashion the number of elements in the subdomains. This characteristic can be better observed with the help of the load balance ratio, as shown in Table 5-2.

Table 5-1: Number of equations and size of the matrix for the pipe flow test case.

Nomination	Finite element	# Elements	# Nodes	v-p equations $(x10^6)$	NNZ $(x10^6)$	CPU time(min)
Mesh1	$P1^+$-$P0$	100k	338.5k	0.7	28.7	3.30
Mesh2		200k	646.8k	1.4	256.8	43.28
Mesh3		400k	1.32M	2.9	545.9	43.87
Mesh1	$P2^+$-$P1$	100k	474.6k	1.6	128.5	30.85
Mesh2		200k	903.7k	3.1	256.5	176.56
Mesh3		400k	1.84M	6.5	545.9	255.34

Table 5-2: Ratio between minimum and maximum number of NNZ in the subdomains

for the pipe flow test case.

Partitions	mesh1	mesh2	mesh3
2	0.985	0.998	0.997
4	0.973	0.990	0.979
8	0.951	0.940	0.964
16	0.941	0.910	0.939
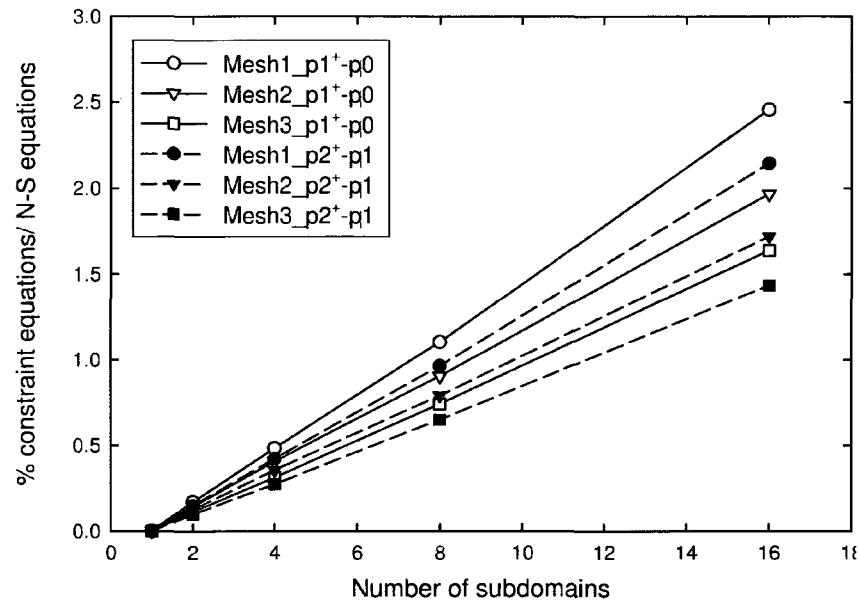
Figure 5-6: Increase of the number of equations due to the introduction of Lagrange multiplier constraints at the interface with respect to the number of subdomains for the P1$^+$-P0 and P2$^+$-P1 finite elements for the pipe flow test case

Figure 5-7 presents the speed-up per CG iteration with respect to the CPU time to solve the problem by a sequential ILU(0)-CG solver. A value close to 12 was obtained with P2$^+$-P1 element, while the maximum speed-up/iteration with P1$^+$-P0 was around 11.3. It can be noted that the speed-up is not linear due to: i) the overhead generated in each matrix-vector and preconditioning operations; ii) the increase in the number of conjugate gradient iterations required to reach convergence with respect to the number of partitions (Table 5-3). In some cases one observes a decrease of the number of iterations as the number of partitions increases (mesh3/P1$^+$-P0 and mesh2/P2$^+$-P1), but

overall, a slight increase (around 1.5 times for 16 partitions) in the number of iterations

is observed as the number of partitions increases. A normal result considering the fact

that the number of Krylov iterations grows with respect to the number of equations.

Finally, we present in Table 5-4 the overall speed-up that combines both the

convergence rate deterioration due to the overhead and the increment in conjugate

gradient iterations with respect to the lowest CPU time we could obtain for an ILU(0)-

CG solver running in sequential mode. The speed-up for the maximum number of

partitions employed (16) varies in the range of 8 to 14, leading to a parallel efficiency

of 50 to 88%.
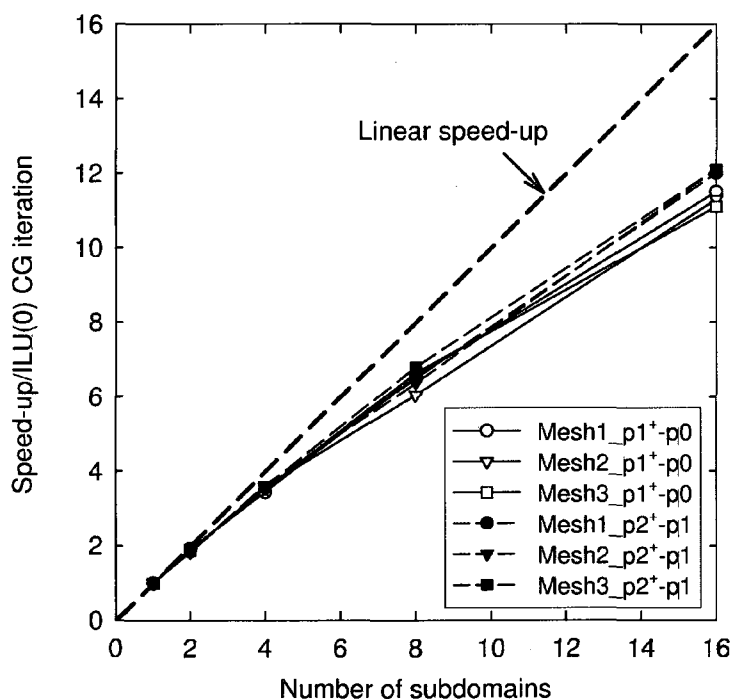
Figure 5-7: Speed-up per ILU(0) preconditioned conjugate gradient iteration for the

pipe flow test case with $P1^+$-P0 and $P2^+$-P1 finite elements.

Table 5-3: Number of conjugate gradient iterations to solve the pipe flow test case.

Partitions	mesh1	mesh2	mesh3	mesh1	mesh2	mesh3
	$P1^+$-$P0$			$P2^+$-$P1$		
1	284	1894	826	567	1530	1084
2	333	2913	596	615	1615	1440
4	341	2697	629	718	1793	1100
8	351	2230	623	669	1345	1146
16	372	2793	643	683	1249	1503

Table 5-4: Overall speed-up for pipe flow test case (CPU time in seconds in parenthesis).

Partitions	mesh1	mesh2	mesh3	mesh1	mesh2	mesh3
	$P1^+$-$P0$			$P2^+$-$P1$		
2	1.6 (118)	1.2 (2116)	2.6 (1012)	1.7 (1079)	1.7 (6034)	1.4 (10779)
4	2.9 (67)	2.5 (1030)	4.6 (572)	2.8 (651)	3.1 (3414)	3.5 (4333)
8	5.3 (36)	5.1 (504)	8.8 (298)	5.6 (330)	7.2 (1461)	6.5 (2366)
16	8.8 (21)	7.7 (336)	14.3 (182)	10.1 (182)	14.9 (709)	8.8 (1734)

5.6.2.   Lid-driven cavity flow

The objective of this second example is to apply the parallel computational method developed in this work to the lid-driven cavity flow case where the hydrodynamics are more complex. Three unstructured meshes were employed to conduct the analysis. The Metis-based partitions into 2, 4, 8, 16 subdomains are presented in Figure 5-8.
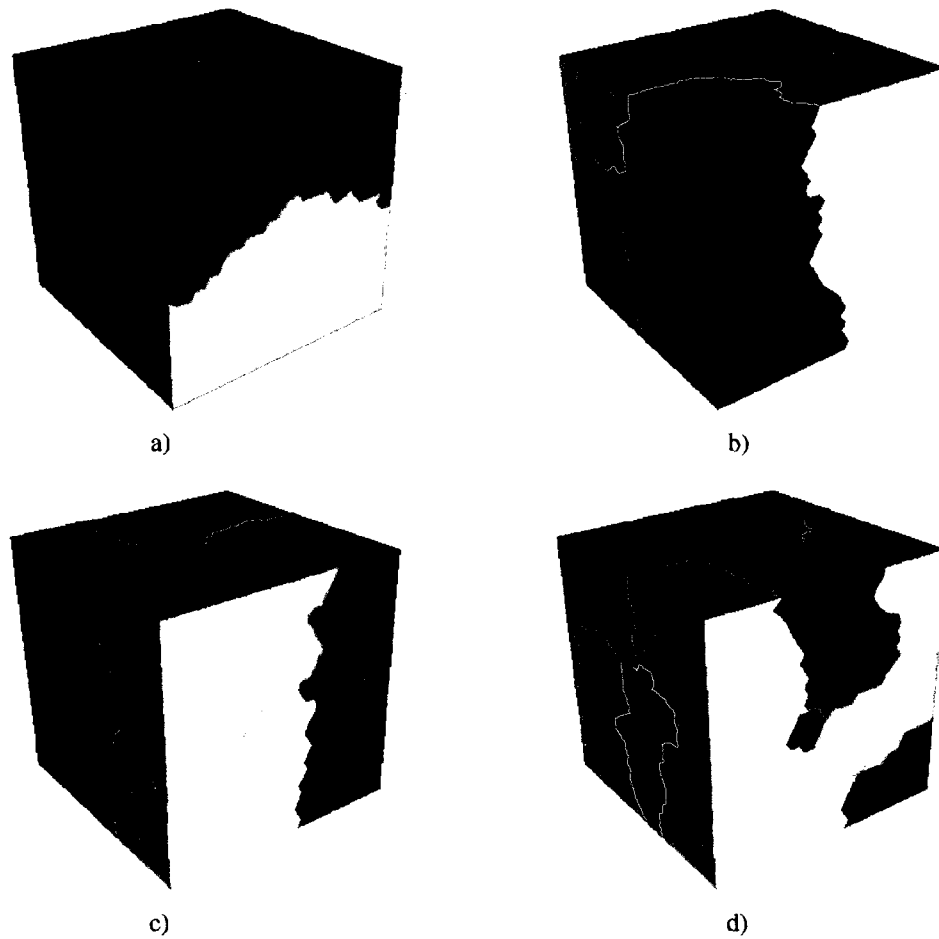
Figure 5-8: Partitions generated by METIS: a) 2 partitions, b) 4 partitions, c) 8

partitions, d) 16 partitions

In comparison to the pipe flow, this problem has the particularity that the subdomains are highly interconnected yielding several nodes that connects multiple subdomains requiring a more complicated communication pattern. Table 5-5 presents the total number of elements, number of equations, the number of non-zero entries in the matrix

and time required to solve the problem in sequential mode for each of the computational grids.

Table 5-5: Number of equations per mesh used and corresponding CPU time required to solve the cavity flow test case with a single processor.

Nomination	Finite element	# Elements	# Nodes	Equations (x10^6)	NNZ (x10^6)	CPU time(min.)
Mesh1	$P1^+$-$P0$	100k	360.1k	0.8	36.4	4.83
Mesh2		200k	685.9k	1.5	71.0	13.66
Mesh3		400k	1.303M	3.0	137.2	171.47
Mesh1	$P2^+$-$P1$	100k	498.6k	1.8	159.7	48.63
Mesh2		200k	947.4k	3.5	310.6	136.49
Mesh3		400k	1.79M	6.7	599.4	541.60
Mesh4		800k	3.69M	13.9	625.9	912.35

Figure 5-9 presents the percentage of Lagrange multiplier equations obtained for both type of finite element discretizations used in this work. It can be observed that the amount of constraints required for this case is larger than for the pipe flow since the interfacial area is considerably superior. Table 5-6 provides the sub-matrices balance defined in the same way as in the previous section. It is worth to underline that it is hard to obtain a good load distribution ratio as the partitions increases varying from 0.97 for 2 subdomains to around 0.778-0.84 for 16 subdomains.
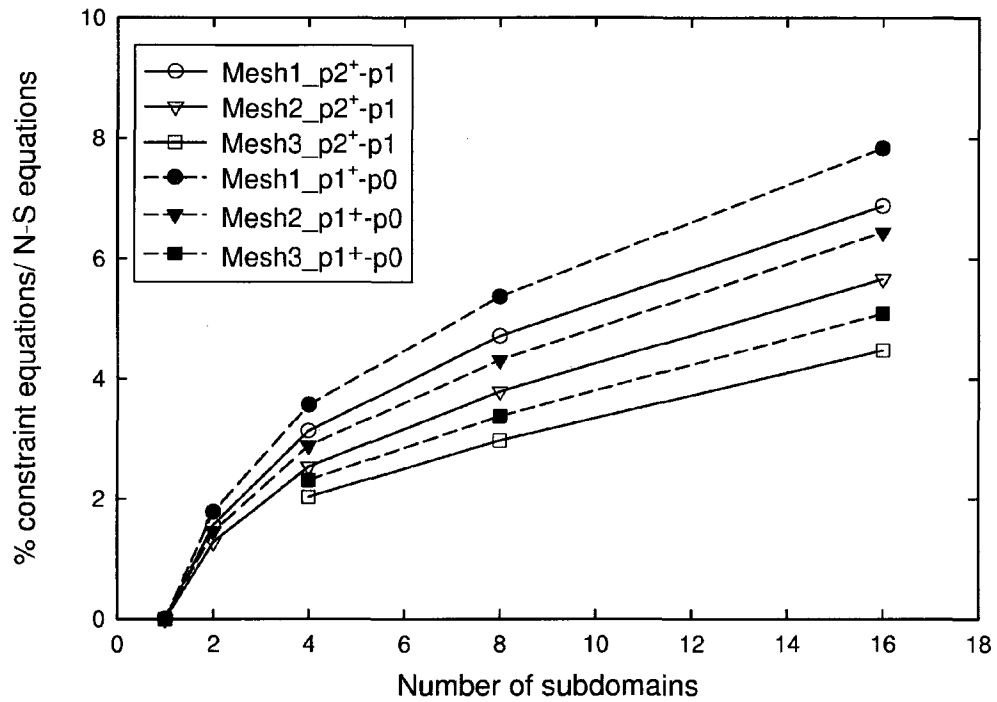
Figure 5-9: Increase of the number of equations due Lagrange multiplier constraints at

the interface for $P1^+$-P0 and $P2^+$-P1 finite element for the cavity flow test case

Table 5-6: Ratio between minimum and maximum number of NNZ in the subdomains

for the cavity flow test case.

Partitions	Mesh1	Mesh2	Mesh3	Mesh1	Mesh2	Mesh3
	$P1^+$-P0			$P2^+$-P1		
2	0.985	0.974	-	0.986	0.976	-
4	0.913	0.976	0.963	0.917	0.978	0.964
8	0.869	0.945	0.902	0.878	0.951	0.908
16	0.779	0.821	0.800	0.804	0.840	0.820

Figure 5-10 presents the speed-up per conjugate gradient iteration with respect to the

sequential ILU(0)-CG solver. As should be expected, the speed-up is lower than for the

pipe flow problem due the larger connectivity between sub-matrices taking values in

the range of 9.5 to 11 with 16 processors. It can also be observed that the expected

increase in parallel efficiency as the problem becomes larger (increasing NEQ values).

Table 5-7 presents the number of iterations to reach convergence. Contrary to the pipe

flow case, the number of iterations tends to increase in a more regular fashion with

respect to the partitions. The overall speed-up with respect to the sequential run is in

the range of 5-5.5 for 16 processors (Table 5-8). The differences between the iteration

speed-up and the overall speed-up are discussed in 4.4.
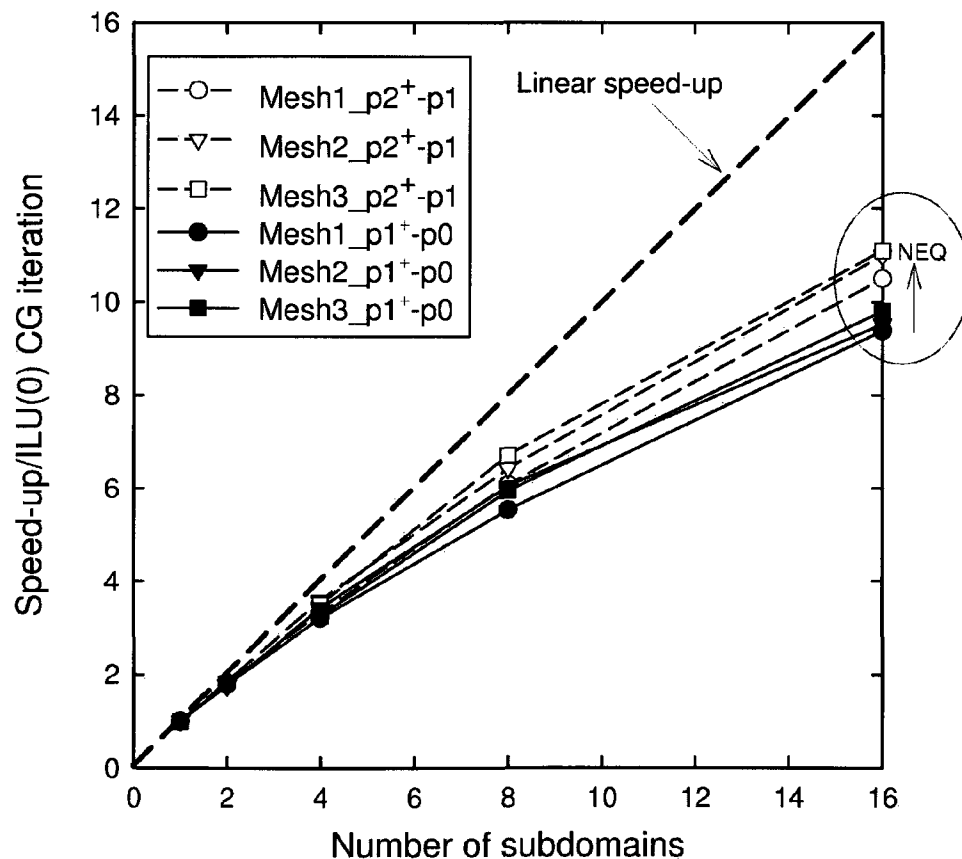
Figure 5-10: Speed-up per ILU(0) preconditioned conjugate gradient iteration for the

cavity flow test case with $P1^+$-P0 and $P2^+$-P1 finite elements.

Table 5-7: Number of conjugate gradient iterations to solve the cavity flow test case.

Subdomains	Mesh1	Mesh2	Mesh3	Mesh1	Mesh2	Mesh3
	$P1^+$-$P0$			$P2^+$-$P1$		
1	316	432	3076	685	961	1908
2	422	537	Not run	867	1146	Not run
4	487	628	4091	1064	1585	2577
8	523	715	4160	1138	1528	2713
16	587	754	5001	1440	1831	3823

Table 5-8: Overall speed-up for cavity flow test case (CPU time in seconds in

parenthesis).

Subdomains	Mesh1	Mesh2	Mesh3	Mesh1	Mesh2	Mesh3
	$P1^+$-$P0$			$P2^+$-$P1$		
2	1.3 (202)	1.4 (553)	Not run	1.4 (1950)	1.6 (5134)	Not run
4	2.1 (131)	2.4 (332)	2.5 (4172)	2.1 (1308)	2.1 (3661)	2.5 (12343)
8	3.3 (82)	3.7 (215)	4.4 (2329)	3.7 (767)	4.0 (1971)	4.7 (6782)
16	5.0 (54)	5.5 (144)	5.5 (1850)	5.0 (560)	5.8 (1374)	5.5 (5772)

a) Effect of the ordering of the variables

As a preliminary test it was necessary to know the optimal way to order the unknowns in the system of equations. We present in Figure 5-11 the convergence rates of ILU(0)-CG when 16 partitions are employed for the studied configurations. It is observed that UxUyUz-I-P-LM produces the best results. Similar trends were observed when the number of partitions was varied. This is the ordering that is used in the next section.
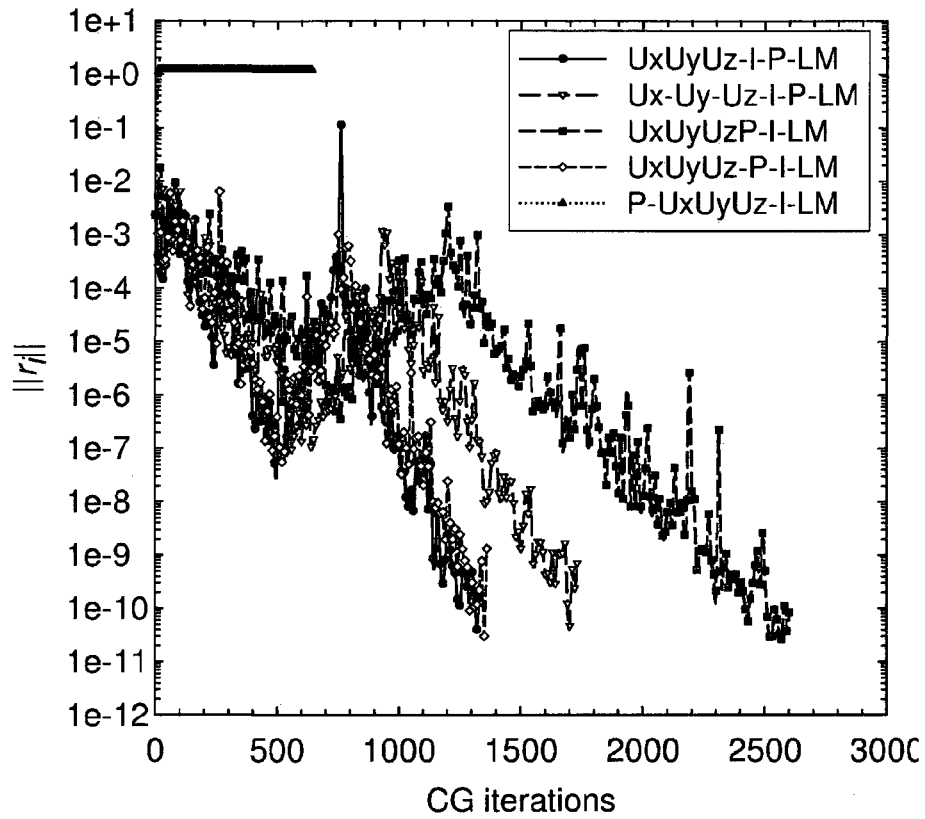
Figure 5-11: ILU(0)-CG convergence rate for different ordering of internal velocity

(UxUyUz), interface velocity (I), pressure (P) and Lagrange multiplier (LM) unknowns

for 16 partitions on the cavity flow test case.

b) Effect of the partitioning schemes

Two factors limit the overall speed-up of the method. The first factor is dealing with

the parallel implementation of the linear algebra where the main parameter to consider

is the speed-up per iteration. It is dominated by the parallel efficiency of the employed

parallel algebra operations, where parallel matrix-vector products and ILU

preconditioning operations are the most time consuming as evidenced in Figure 5-12. It

must be remarked that the ideal linear speed-up is very difficult to obtain due to the

unbalanced charge loading when using unstructured meshes.
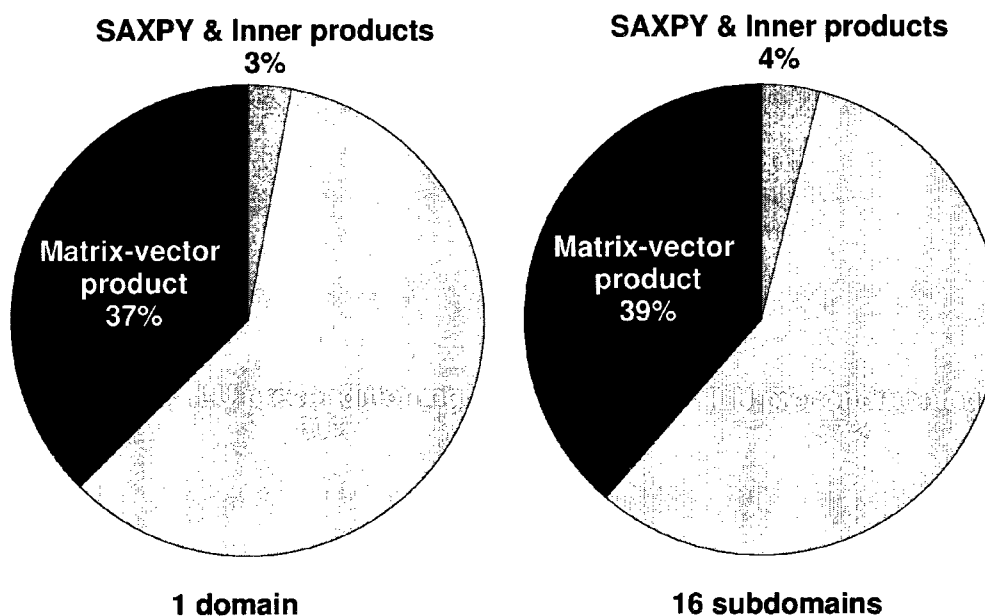
Figure 5-12: CPU time distribution at each conjugate gradient iteration

The second factor is dealing with the numerical scalability governed by the number of

iterations required to reach convergence. The general trend is that the number of CG

iterations increases with respect to partitioning. One cause of this trend could be

attributed to the increase in the total number of equations. It is also expected that the

global matrix structure plays a role in the numerical performance since it affects the

quality of the ILU preconditioner (BENZI et al., 1999; OLIKER et al., 2002). Figure

5-13 and Figure 5-14 illustrate how the matrix structure evolves as the number of

partitions increases, having an impact on the quality of the ILU preconditioner. Another factor that could affect the parallel scalability is the smoothness of the interfaces. To observe its effect over the speed-up, a 100K element block structured mesh was discretized using $P2^+$-P1 finite elements. Coordinate recursive bisection was employed producing smooth partitions as evidenced in Figure 5-15a in opposition to the irregular ones presented in Figure 5-15b. This latter configuration was attained by the coordinate recursive bisection method applying a small perturbation that produces an irregular subdomain interface shape. It was important to use the same partitioning method to keep the subdomains connectivity unchanged. As can be observed in Figure 5-16, the alteration of the interface smoothness causes a considerable increase of the number of iterations. As the interface becomes more irregular, the number of Lagrange multiplier equations increases, inducing a decay of the convergence rate.
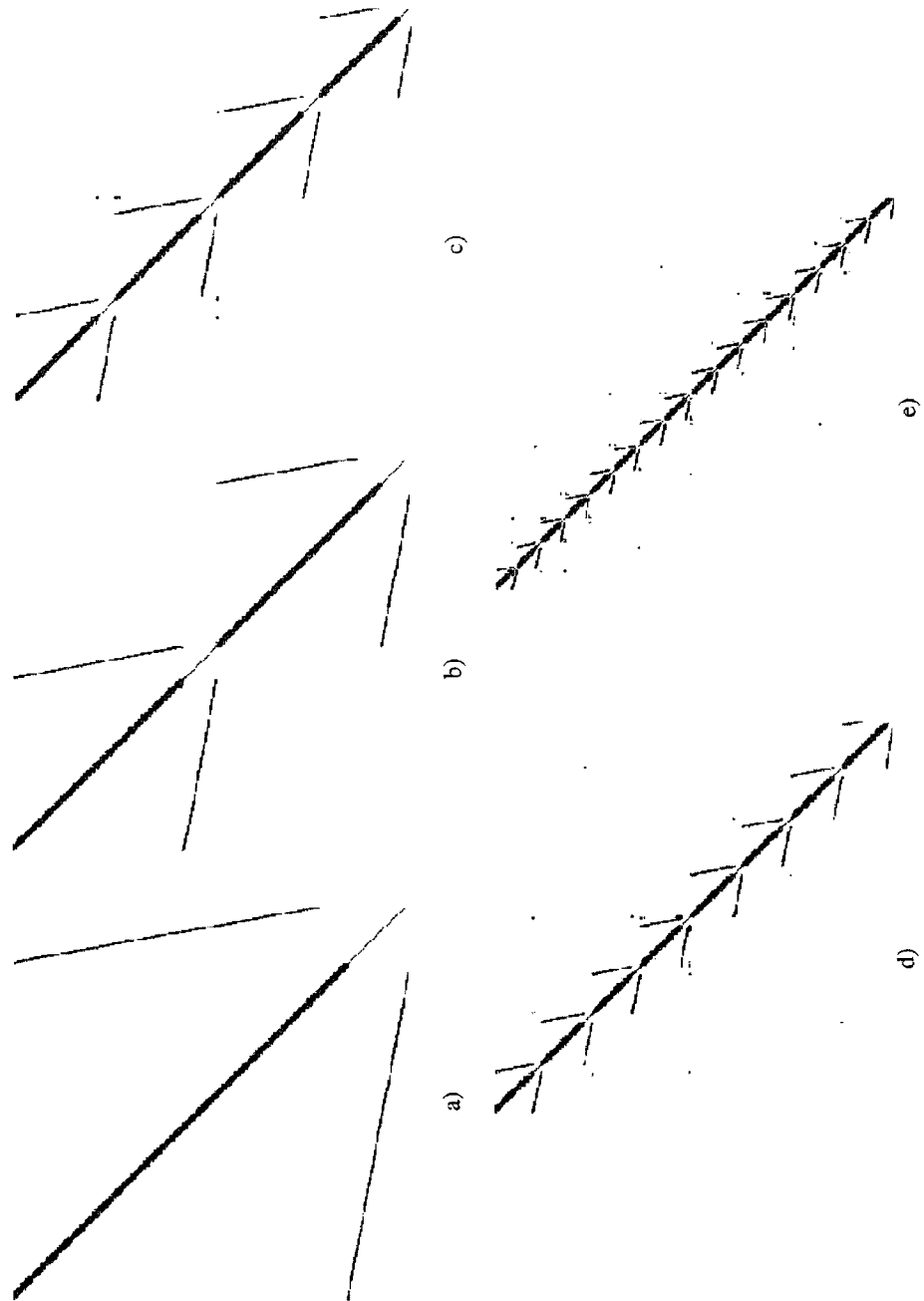
Figure 5-13: Matrix non-zero entries for the pipe flow test case a) 1 domain; b) 2 domains; c) 4 domains; d) 8 domains; e) 16 domains.
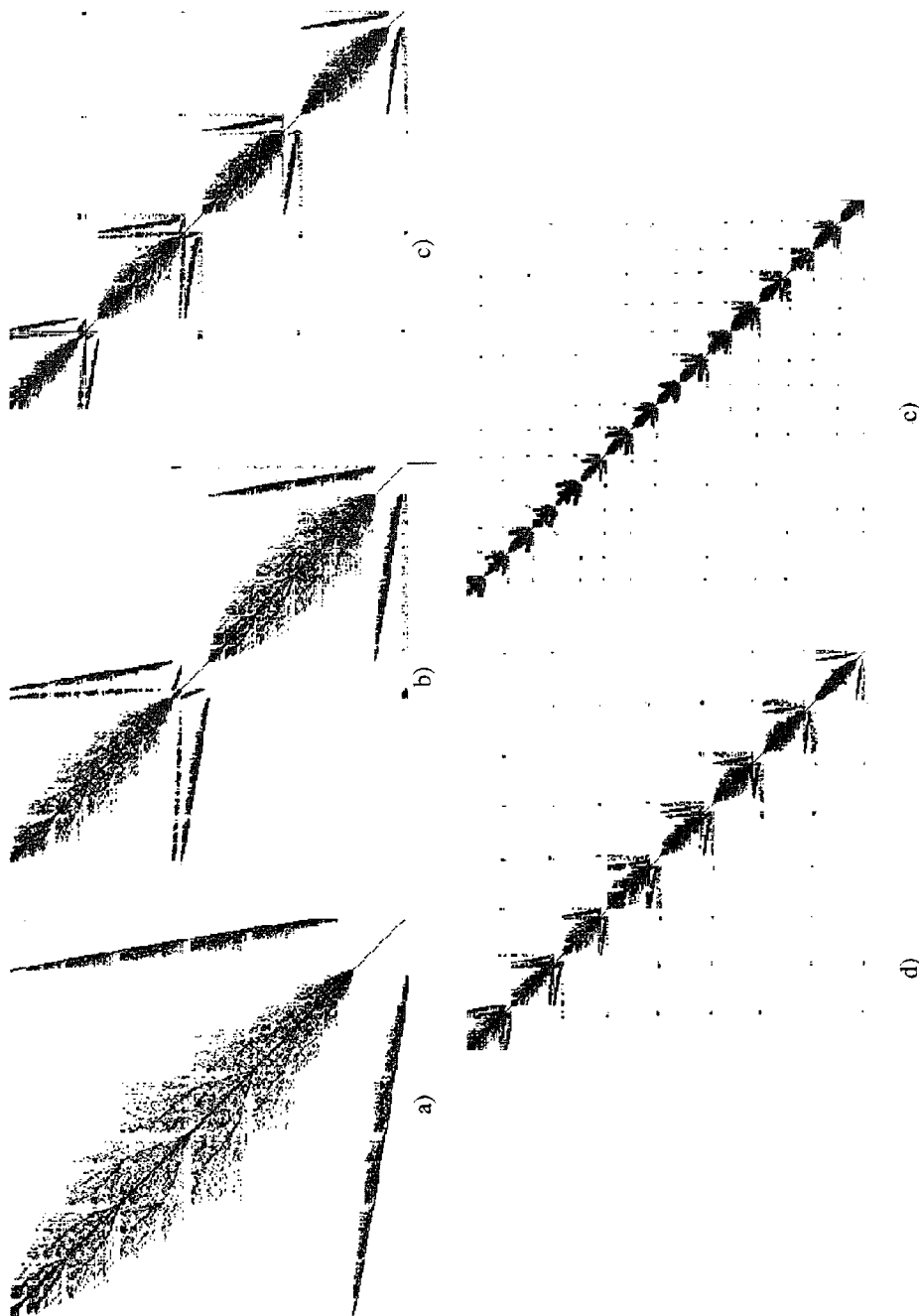
Figure 5-14: Matrix non-zero entries for the cavity flow test case a) 1 domain; b) 2 domains; c) 4 domains; d) 8 domains; e) 16 domains.

8 partitions

16 partitions

a)

8 partitions

16 partitions

b)
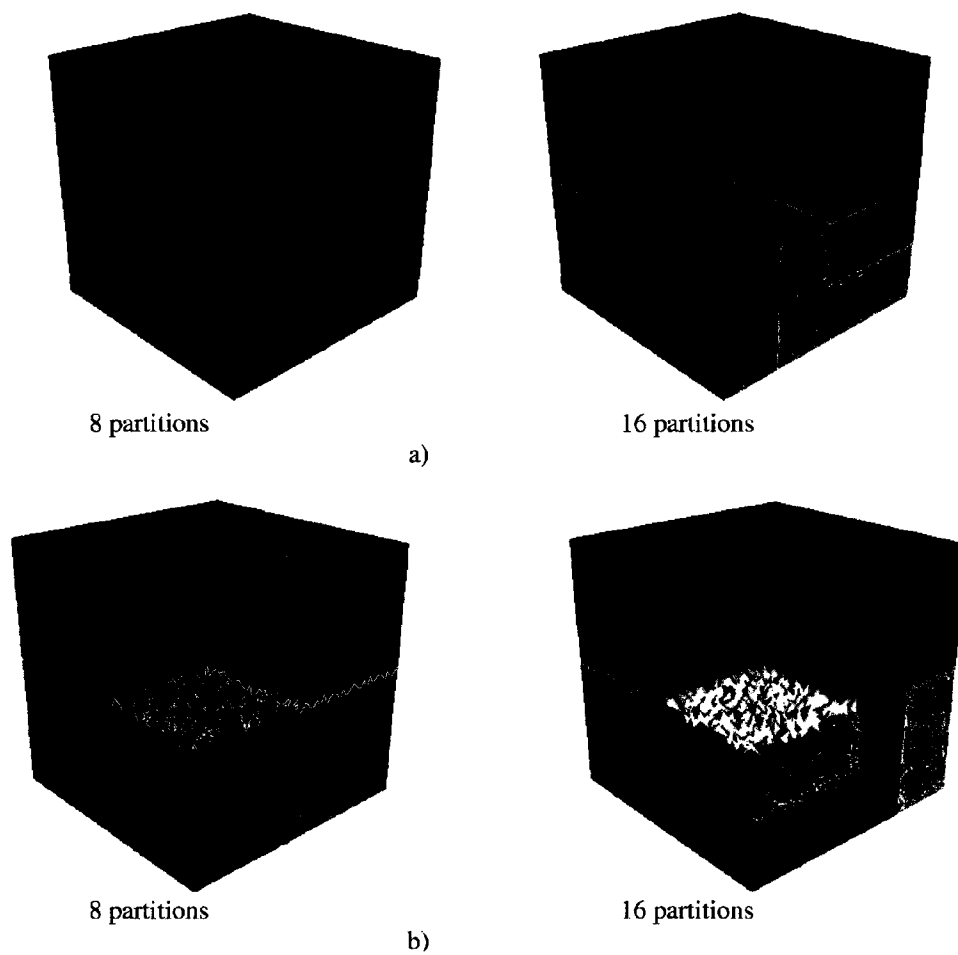
Figure 5-15: Partitions generated by the recursive bisection technique: a) smooth

interfaces b) irregular interfaces.
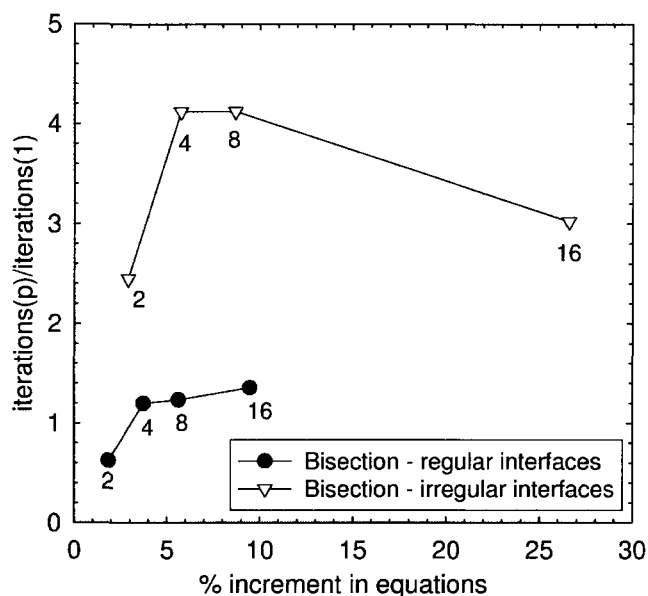
Figure 5-16: Normalized variation in iterations for the cavity flow test case

(Numbers close to symbols indicate the number of partitions used for each point in the graph).

The convergence rate is also associated with the structure of the global matrix for the already discussed reasons. To demonstrate that, we have run some experiments using different partition schemes to solve the cavity flow case. The purpose of the experiments is to show that different partition algorithms produce different amount of multiplier equations and non-zero matrix entries patterns allow to check their respective influence. Table 5-9 shows the obtained results, where spectral octasection with terminal propagation and Kerninghan-Lin smoothing being the one that gives the best results in terms of number of iterations and overall speed-up (8.9), even faster than the case were smooth interfaces where employed (8.4). When considering spectral-octasection parallel performance, it is interesting to mention that a good speed-up per

iteration does not imply a good overall speed-up. The results confirm that both the amount of Lagrange multipliers and the matrix structure (average number of adjacent subdomains) influence the overall performance of the method. The data suggests that irregular subdomains connectivity with large non-smooth interfacial area induce a deterioration in the convergence rate. When comparing the performance of spectral methods, it appears that the interface smoothing, by Kernighan-Lin heuristics, is critical to reduce the number of CG iterations. The smoothing action of Kerninghan-Lin rule can be observed in Figure 5-17. Furthermore, the speed-up per iteration remains almost constant for the different schemes studied. Finally, we have run again the cases presented in Table 5-5 with this new partitioning strategy (spectral method-Kernighan-Lin refinement- terminal propagation) to verify the validity of our findings. Table 5-10 summarizes the new speed-ups for these cases using 16 partitions. They show a significant improvement with respect to the ones in Table 5-8, confirming our preliminary observations. It is worth mentioning the results of KLAWONN and WIDLUND (2000) who used a similar method applied to elasticity problems over structured grids. They also observed an increase in iterations and concluded that there is a strong indication that this problem would be cured by the use of a better block preconditioner as algebraic multi-grid instead of ILU. We have demonstrated in this work that this situation can also be controlled by the use of suitable partitioning strategies in the case of unstructured meshes where the smoothness of the interface and partition connectivity are key parameters to obtain good performance even at the cost of larger interfacial area.

Table 5-9: Summary of the speed-ups obtained for the different partitioning schemes investigated of the cavity flow test case

when running on 16 processors.

Partition method	Refinement	Increase in equations (%)	Average adjacent subdomains	Iterations(p)/ iteration(1)	speed-up/iteration	overall speed-up	CPU time (s)
Spectral-octasection	Kernighan-Lin + Terminal propagation	19	2.375	1.179	10.5	8.9	427
Coordinate recursive bisection	regular interfaces	9	4.375	1.355	11.3	8.4	456
Spectral-octasection	Terminal propagation	20	2.500	1.404	10.9	7.8	484
Spectral-octasection	Kernighan-Lin	11	4.250	1.422	10.2	7.2	531
Multilevel-k-way	None	7	6.250	1.518	10.8	7.1	536
Spectral-octasection	None	11	4.125	2.314	11.3	5.1	754
Coordinate recursive bisection	irregular interfaces	27	4.375	3.022	10.1	3.4	1143
Multilevel-octasection	Kernighan-Lin	10	7.875	No convergence	10.0	No convergence	No convergence

a)

b)

c)

d)
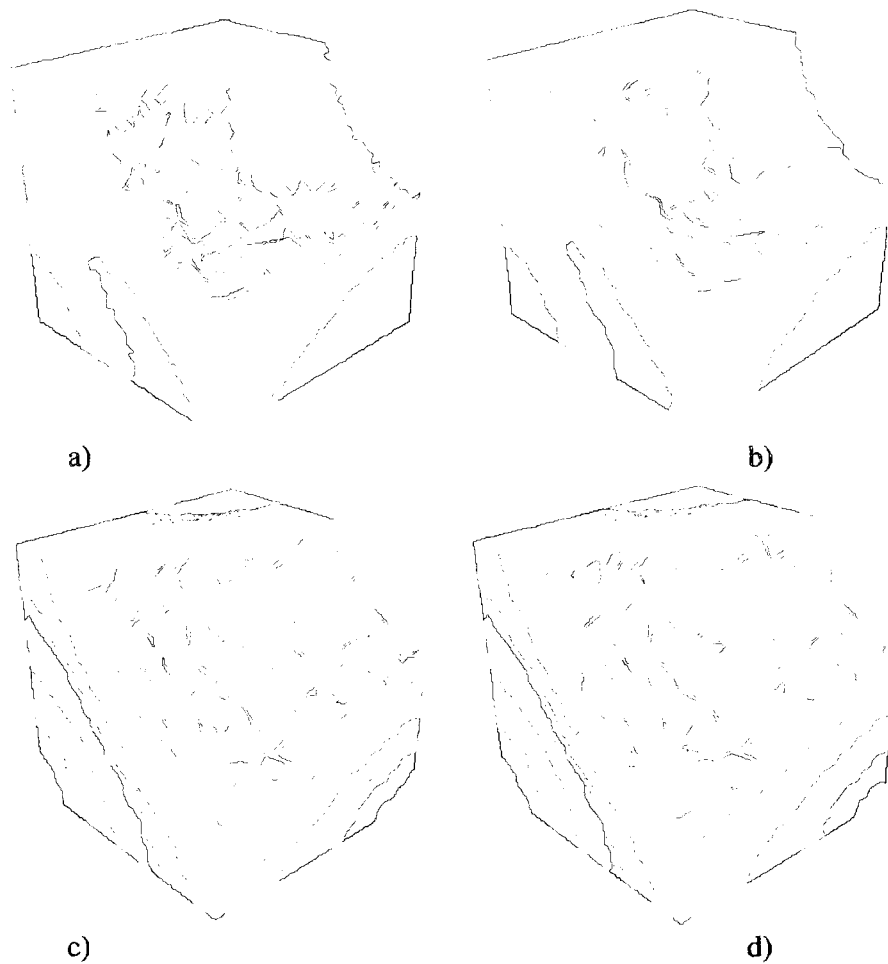
Figure 5-17: Smoothing effect over the interfaces due to Kernighan-Lin heuristics for

16 partitions in the cavity flow test case a) spectral octasection without Kernighan-Lin;

b) spectral octasection with Kernighan-Lin; c) spectral octasection and terminal

propagation without Kernighan-Lin; d) spectral octasection and terminal propagation

with Kernighan-Lin.

Table 5-10: Overall speed-up obtained from the 16 partition cases described in Table 5-5.

Mesh	Finite element	v-p equations (x10⁶)	Increase in equations (%)	Average adjacent subdomains	iterations(p) /iterations(1)	Overall Speed-up	CPU time (s)
mesh1		0.8	21	2.125	1.8	5.5	49
mesh2	$P1^+$-$P0$	1.5	17	1.875	1.5	7.3	108
mesh3		3.0	14	1.875	1.0	10.0	1020
mesh1		1.8	19	2.125	1.5	7.5	373
mesh2		3.5	15	1.875	1.4	8.8	900
mesh3	$P2^+$-$P1$	6.7	12	1.875	1.1	11.0	2888
mesh4		13.9	10	1.875	1.4	8.9	6158

5.7. Conclusions

The objective of this paper was to present a method to parallelize a finite element Navier-Stokes solver based on non-overlapping domain decomposition and Lagrange multiplier for the simulation of viscous fluid flows. It was done with the aim to distribute the memory and speed-up calculations to solve large problems unfeasible on a single processor. The novelty of the work is that the velocity-pressure-Lagrange multiplier system of Navier-Stokes equations is solved simultaneously by a distributed memory parallel ILU(0) preconditioned Krylov method. A penalty technique applied to the Lagrange multipliers equations is introduced to avoid ill-conditioning of the matrix that threats the ILU factorization of the global system of equations. The method was tested over two benchmark cases (pipe and cavity flow) employing discontinuous pressure finite element approximations ($P1^+$-$P0$/$P2^+$-$P1$) on unstructured tetrahedral grids. It was found that the proposed approach can solve problems around 5 to 13 times faster than the sequential ILU-Krylov subspace solver running on 16 processors. The

speed-up is mainly affected by the load distribution balance and convergence rates which decay as the number of partitions increases. The ordering of physical variables and partitioning strategy are critical to obtain good convergence rate. It was found that the UxUyUz-I-P-LM ordering combined with the spectral octasection with terminal propagation and Kerninghan-Lin smoothing partitioning scheme produced the most promising speed-up performance.

5.8. Acknowledgments

5.9. References

ACHDOU, Y., KUZTETSOV, Y. A., PIRONNEAU, O. (1995). Substructuring preconditioners for the Q1 mortar element method. *Numerische Mathematik, 71*, 419-449.

AGGARWAL, R., KEUNINGS, R., ROUX, F. X. (1994). Simulation of the flow of integral viscoelastic fluids on a distributed memory parallel computer. *Journal of Rheology, 38*(2), 405-419.

BENZI, M., SZYLD, D. B., VAN DUIN, A. (1999). Orderings for incomplete factorization preconditioning of nonsymmetric problems. *SIAM Journal on Scientific Computing, 20*(5), 1652-1670.

BERTRAND, F. H., GADBOIS, M. R., TANGUY, P. A. (1992). Tetrahedral elements for fluid flow. *International Journal for Numerical Methods in Engineering, 33*(6), 1251-1267.

BORELLO, D., CORSINI, A., RISPOLI, F. (2003). A finite element overlapping scheme for turbomachinery flows on parallel platforms. *Computers and Fluids, 32*(7), 1017-1047.

CAI, X.-C., KEYES, D. E., MARCINKOWSKI, L. (2002). Non-linear additive Schwarz preconditioners and application in computational fluid dynamics. *International Journal Numerical Methods Fluids, 40*, 1463-1470.

CAOLA, A. E., JOO, Y. L., ARMSTRONG, R. C., BROWN, R. A. (2001). Highly parallel time integration of viscoelastic flows. *Journal of Non-Newtonian Fluid Mechanics, 100*(1-3), 191-216.

CAOLA, A. E., BROWN, R. A. (2002). Robust iterative methods for solution of transport problems with flow: A block two-level preconditioned Schwarz-domain decomposition method for solution of nonlinear viscous flow problems. *Chemical Engineering Science, 57*(21), 4583-4594.

COESNON, B., HENICHE, M., DEVALS, C., BERTRAND, F., TANGUY, P. A. (2008). A fast and robust fictitious domain method for modelling viscous flows in complex mixers: The example of propellant make-down. *International Journal for Numerical Methods in Fluids, 58*(4), 427-449.

CROUZEIX, M., RAVIART, P. (1973). Conforming and non-conforming finite element methods for solving the stationary Stokes equations. *RAIRO analyse numerique, 7*, 33-76.

DUFF, I. S., VAN DER VORST, H. A. (1999). Developments and trends in the parallel solution of linear systems. *Parallel Computing, 25*(13), 1931-1970.

DUNLOP, A. E., KERNIGHAN, B. W. (1985). A procedure for placement of standard-cell VLSI circuits. *IEEE Transactions on Computer-Aided Design of Integrated Circuits and Systems, CAD-4*(1), 92-98.

DUTTO, L. C., HABASHI, W. G. (1999). Parallelization of the ILU(0) preconditioner for CFD problems on shared-memory computers. *International Journal for Numerical Methods in Fluids, 30*(8), 995-1008.

FARHAT, C., ROUX, F.-X. (1991). Method of finite element tearing and interconnecting and its parallel solution algorithm. *International Journal for Numerical Methods in Engineering, 32*(6), 1205-1227.

FARHAT, C., FEZOUI, L., LANTERI, S. (1993). Two-dimensional viscous flow computations on the Connection Machine: unstructured meshes, upwind schemes and massively parallel computations. *Computer Methods in Applied Mechanics and Engineering, 102*(1), 61-88.

GLOWINSKI, R., PAN, T. W., KEARSLEY, A. J., PERIAUX, J. (1995). *Fictitious domain methods for viscous flow simulation.* Houston: Rice University.

GLOWINSKI, R., PAN, T. W., PERIAUX, J. (1995). Fictitious domain/domain decomposition methods for partial differential equations. *Domain-based parallelism and problem decomposition method in computational science and engineering, Philadelphia* (pp. 177-192)SIAM.

GOULD, N. I. M., HU, Y., SCOTT, J. A. (2005). *A numerical evaluation of sparse direct solvers for the solution of large sparse, symmetric linear systems of equations.* Oxfordshire: CCLRC Rutherford Appleton Laboratory.

GROPP, W. D., KAUSHIK, D. K., KEYES, D. E., SMITH, B. F. (2001). High-performance parallel implicit CFD. *Parallel Computing, 27*(4), 337-362.

HENDRIKSON, B., LELAND, R. (1993). *The Chaco user guide, version 1.0.* Alburquerque: Sandia Laboratories.

HENICHE, M., SECRETAN, Y., LECLERC, M. (2001). Efficient ILU preconditioning and inexact-Newton-GMRES to solve the 2D steady shallow equations. *Communications in Numerical Methods Engineering, 17*, 69-75.

HENRIKSEN, P., KEUNINGS, R. (1994). Parallel computation of the flow of integral viscoelastic fluids on a heterogeneous network of workstations. *International Journal for Numerical Methods in Fluids, 18*(12), 1167-1183.

HU, Q., SHI, Z., YU, D. (2004). Efficient solvers for saddle-point problems arising from domain decompositions with lagrange multipliers. *SIAM Journal on Numerical Analysis, 42*(3), 905-933.

HUGHES, T. J. R., LEVIT, I., WINGET, J. (1983). An element-by-element solution algorithm for problem of structural and solid mechanics. *Computer Methods in Applied Mechanics and Engineering, 36,* 241-254.

HWANG, F.-N., CAI, X.-C. (2005). A parallel nonlinear additive Schwarz preconditioned inexact Newton algorithm for incompressible Navier-Stokes equations. *Journal of Computational Physics, 204*(2), 666-691.

JOHAN, Z., MATHUR, K. K., JOHNSSON, S. L., HUGHES, T. J. R. (1995). A case study in parallel computation: viscous flow around an ONERA M6 wing. *International Journal for Numerical Methods in Fluids, 21,* 877-884.

KARYPIS, G., KUMAR, V. (1998). *METIS: A software package for partitioning unstructured graphs, partitioning meshes, and computing fill-reducing orderings of sparse matrices.* Minnesota: University of Minnesota.

KERNIGHAN, B. W., LIN, S. (1970). An efficient heuristic procedure for partitioning graphs. *Bell System Technical Journal, 49*(2), 291-308.

KLAWONN, A., WIDLUND, O. B. (2000). A domain decomposition method with Lagrange multipliers and inexact solvers for linear elasticity. *SIAM Journal on Scientific Computing, 22*(4), 1199-1219.

KLAWONN, A., RHEINBACH, O. (2007). Inexact FETI-DP methods. *International Journal for Numerical Methods in Engineering, 69*(2), 284-307.

KUZNETSOV, Y. A. (1995). Efficient iterative solvers for elliptic finite element problems on non-matching grids. *Russian Journal Numerical Analysis Mathematical Modeling, 10,* 187-211.

LI, X. S., DEMMEL, J. W. (2003). SuperLU_DIST: a scalable distributed-memory sparse direct solver for unsymmetric linear systems. *ACM Transactions on Mathematical Software, 29*(2), 110-140.

OLIKER, L., XIAOYE, L., HUSBANDS, P., BISWAS, R. (2002). Effects of ordering strategies and programming paradigms on sparse matrix computations. *SIAM Review, 44*(3), 373-393.

SAAD, Y. (2003). *Iterative methods for sparse linear systems* (2nd ^{e} éd.). Philadelphia: SIAM.

SCOTT, J. A. (2003). Parallel frontal solvers for large sparse linear systems. *ACM Transactions on Mathematical Software, 29*(4), 395-417.

SHADID, J. N., TUMINARO, R. S., DEVINE, K. D., HENNIGAN, G. L., LIN, P. T. (2005). Performance of fully coupled domain decomposition preconditioners for finite element transport/reaction simulations. *Journal of Computational Physics, 205*(1), 24-47.

SMITH, B. F., BJORSTAD, P., GROPP, W. D. (1996). *Domain decomposition: parallel multilevel methods for elliptic partial differential equations* (1rst^e éd.). Cambridge: Cambridge university press.

STAFF, O., WILLE, S. (2005). Parallel ILU preconditioning and parallel mesh adaptation with load balancing for general domain decompositions for the Navier-Stokes equations. *International Journal for Numerical Methods in Fluids, 47*(10-11), 1301-1306.

TEZDUYAR, T. E., LIOU, J. (1989). Grouped element-by-element iteration schemes for incompressible flow computations. *Computer Physics Communications, 53*(1-3), 441-453.

TEZDUYAR, T. E., BEHR, M., ALIABADI, S. K., MITTAL, S., RAY, S. E. (1992). New mixed preconditioning method for finite element computations. *Computer Methods in Applied Mechanics and Engineering, 99*(1), 27-42.

TOSELLI, A., WIDLUND, O. B. (2005). *Domain decomposition methods algorithms and theory* (1rst^e éd.). Berlin: Springer-Verlag.

VAINIKKO, E., GRAHAM, I. G. (2004). A parallel solver for PDE systems and application to the incompressible Navier-Stokes equations. *Applied Numerical Mathematics, 49*(1), 97-116.

VANDERSTRAETEN, D., KEUNINGS, R. (1998). A parallel solver based on the dual Schur decomposition of general finite element matrices. *International Journal for Numerical Methods in Fluids, 28*(1), 23-46.

VEREECKE, B., BAVESTRELLO, H., DUREISSEIX, D. (2003). An extension of the FETI domain decomposition method for incompressible and nearly incompressible problems. *Computer Methods in Applied Mechanics and Engineering, 192*(31-32), 3409-3429.

WILLE, S. O., STAFF, O., LOULA, A. F. D. (2003). Parallel ILU preconditioning, a priori pivoting and segregation of variables for iterative solution of the mixed finite element formulation of the Navier-Stokes equations. *International Journal for Numerical Methods in Fluids, 41*(9), 977-996.

ZSAKI, A., RIXEN, D., PARASCHIVOIU, M. (2003). A substructure-based iterative inner solver coupled with Uzawa's algorithm for the Stokes problem. *International Journal for Numerical Methods in Fluids, 43*(2), 215-230.

129

Chapter 6. A Parallel Finite Element Sliding Mesh Technique for the Navier-Stokes Equations

Authors: Christian A. Rivera[1], Mourad Heniche[1], François Bertrand[1], Roland Glowinski[2] and Philippe A. Tanguy[1]

[1] *Research Center for Industrial Flows Processes (URPEI)*

Department of Chemical Engineering, École Polytechnique Montreal, Canada

[2] *Department of Mathematics, University of Houston, USA*

KEYWORDS: Lagrange multiplier method; finite element method; parallel computing; Navier-Stokes equations; sliding grids; domain decomposition, agitated tanks, fluid mixing

6.1. Presentation of the article

This article was submitted to the Journal of Computational Physics. It explains the sliding mesh technique used to reproduce the unsteady motion of the agitator. A validation of the method is presented for two examples. The parallel performance is examined at the end of the article.

6.2. Abstract

A sliding mesh algorithm for the finite element simulation of three-dimensional incompressible viscous flows on unstructured grids is presented. Lagrange multipliers are used at the sliding interfaces to enforce the continuity between the fixed and moving subdomains. The novelty of the method consists in the coupled solution of the resulting velocity-pressure-Lagrange multipliers system of equations by an ILU(0)-QMR solver. A penalty parameter is introduced for both the interface and the incompressibility constraints to avoid pivoting problems in the ILU(0) algorithm. To handle the convective term, both the Newton-Raphson scheme and a semi-implicit linearization are tested. The method is validated for concentric cylinders and stirred tank flows. Furthermore, this approach allows additional partitioning for both sliding and fixed subdomains if parallelization is required.

6.3. Introduction

Many industrial flows are driven by the motion of mechanical components such as agitators in stirred tanks, pistons in internal combustion engines or screws in extruders to name a few. In some instances, more than one kinematics is involved. This is particularly true in the case of the mixing of viscous fluids where the lack of turbulence requires the combination of different types of impellers distributed in the tank that are rotating at different speeds to improve mixing (ESPINOSA-SOLARES et al., 1997; FOUCAULT et al., 2006). The simulation of such flows poses special challenges due to the difficulties of taking into account the time varying position of the boundaries. One early method was to resort to a Lagrangian frame of reference to ease their handling as presented by TANGUY et al. (1992) for symmetric geometrical configurations.

Various techniques have also been introduced, which are based on re-meshing algorithms. For example, BRAVO et al. (2000) regenerate the full three-dimensional mesh at each time step by an automatic mesh generator in the simulation of flows in extruders. To avoid complete re-meshing, BEHR and TEZDUYAR (1999) propose the shear-slip mesh update method where a local re-meshing in a small overlapping region is performed as the objects rotate. More widespread techniques are based on the arbitrary Lagrangian-Eulerian (ALE) formulation where the fluid mesh deforms as the object moves. This technique has been employed to study hydro-structural problems (BELYTSCHKO and KENNEDY, 1975), free surface flows (HUERTA and LIU, 1988;

SOULAIEMANI et al., 1991), flows around parachutes (TEZDUYAR et al., 2006) and sedimentation problems (SAKSONO et al., 2007) among others. Its main drawback is that a complete re-meshing is necessary when displacements are large, to avoid mesh distortion. AVALOSSE and CROCHET (1997) propose a mesh superposition technique without re-meshing at each time step to simulate the flow in twin-screw extruders. The technique consists in locating the elements that are crossed by the moving object boundary. The velocity of the moving object is then imposed by a penalty method over each node of these elements. CONNELLY and KOKINI (2006) used the same technique to simulate the three-dimensional flow of a viscous fluid in a sigma blade mixer.

A different approach is to introduce body forces in the momentum equations to emulate the effect of the moving body over a background mesh. PERICLEOUS and PATEL (1987) modeled the flow in multi-stage agitators as distributed sources of momentum that were computed from drag coefficients. Another example is the immersed boundary method developed by PESKIN and MCQUEEN (1989) for the simulation of blood flows in the human heart. It consists in representing the moving bodies by a set of control points on which body forces are imposed. These forces are not known a priori and are calculated using theoretical models. Variants of this method are the "immersed interface method" of LEVEQUE and LI (1994) and the immersed finite element method of ZHANG et al. (2004). A similar technique is the fictitious domain method of GLOWINSKI et al. (1994) with the difference that this approach does not resort to

empirical forces but rather to Lagrange multipliers to enforce the velocity constraints at the moving surfaces. One important issue of this approach is the evaluation of surface integrals which are computationally expensive and not necessarily easy to compute for 3D complex geometries. A different (and independent) approach was followed by the group of Tanguy in the 90's, based on a collocation method to impose the surface constraints point-wise by the use of Dirac functions. This technique has been successfully employed to simulate the flow of mixers in laminar regime (TANGUY et al., 1996; BERTRAND et al., 1997; JONGEN, 2000; RIVERA et al., 2004 and 2006). VAN LOON et al. (2004) have also applied this technique for fluid-structure interactions in heart valves. They pointed out the necessity of mesh adaptation in order to improve the accuracy of this method close to the fluid-structure interface.

An interesting alternative is the use of domain decomposition methods. They allow preserving the exact shape of the moving boundaries as the object rotates without re-meshing. One way to apply these techniques is to overlap independent three-dimensional grids by means of overset or Chimera methods (STEGER et al., 1983). TAKEDA et al. (1993) and HOUZEAUX and CODINA (2003) have applied this type of technique to simulate incompressible fluid flows in agitated vessels. The advantage of this approach is that it allows simulating any type of motion. However, the coupling between the different meshes requires a hole cutting strategy to generate an overlapping interface among the grids that may lead to complex coding. Furthermore, the forth and back interpolations between the moving and background meshes in the overlap region

may be a computationally costly procedure. An alternative solution is to decompose the original mesh into static and moving subdomains allowing them to slide along their common interfaces. This is the principle of the sliding mesh techniques introduced in the finite volume context in the 90's (RAI, 1985; LUO et al., 1993; PERNG and MURTHY, 1993). One particular simplification of the sliding mesh method is the clicking mesh method (BOHM et al., 1998; WECHSLER et al., 1999) where the grid movement is such that the boundary nodes must match at the interfaces at any time step. As it can be difficult and tedious to ensure this condition, most of sliding mesh implementations are extensions of the mortar element method developed by BERNARDI et al. (1994) to couple non-matching grids. They are usually based on the imposition of linear multi-point constraints at the interfaces by Lagrange multipliers, penalty methods or master-slaves elimination. The reader is referred to GARTLING (2005) for the application of sliding mesh techniques in the finite element framework to solve moving body thermal and flow problems.

The objective of this paper is to present a sliding mesh algorithm for the simulation of incompressible fluid flows around moving bodies by discontinuous pressure finite elements and Lagrange multipliers. The novelty of the method consists in the coupled resolution of the velocity-pressure-Lagrange multipliers system of equations by an ILU(0)-QMR solver. A penalty parameter is introduced for both the interface and the incompressibility constraints to avoid ILU(0) failure due to the lack of pivoting. Furthermore, this approach allows additional partitioning for both the sliding and fixed

subdomains in the case of parallel computing. The proposed sliding mesh technique has been implemented to run in sequential or parallel mode using FORTRAN and MPI in the POLY3D software (*Rheosoft Inc.*).

The organization of the paper goes as follows; in section 2, the domain decomposition formulation, sliding interface methodology and resolution schemes are introduced. Section 3 presents the parallelization procedure of the sliding mesh algorithm. Section 4 shows a validation of the proposed approach for the concentric cylinders and stirred tank flows on three-dimensional grids. Finally, section 5 presents the time reduction obtained when running on parallel computers for the simulation of the unsteady flows in a stirred tank with baffles.

6.4. Numerical method

6.4.1. Domain decomposition for sliding mesh techniques

Let Ω be the computational domain with boundary $\partial\Omega$ presented in Figure 6-1. Since in sliding mesh technique, the mesh is rotated in one of the subdomains, the arbitrary Lagrangian-Eulerian (ALE) formulation of the incompressible Navier-Stokes equations is employed, which reads as:

$$\rho\left(\dot{\mathbf{v}} + (\mathbf{v} - \mathbf{v}_m) \cdot \operatorname{grad} \mathbf{v}\right) - \mu\nabla^2\mathbf{v} + \operatorname{grad} p = \mathbf{f} \text{ , in } \Omega, \tag{6.1}$$

$$\operatorname{div} \mathbf{v} = 0 \text{ , in } \Omega, \tag{6.2}$$

where $\mathbf{v}$ is the velocity, $\mathbf{v}_m$ is the mesh velocity, $\dot{\mathbf{v}}$ the velocity time derivative, $\mathbf{f}$ a body force, p the pressure, μ the Newtonian viscosity and ρ the fluid density. Suitable initial conditions and boundary conditions must also be applied for mathematical well-posedness. A partition of the domain is introduced as in Figure 6-2b.
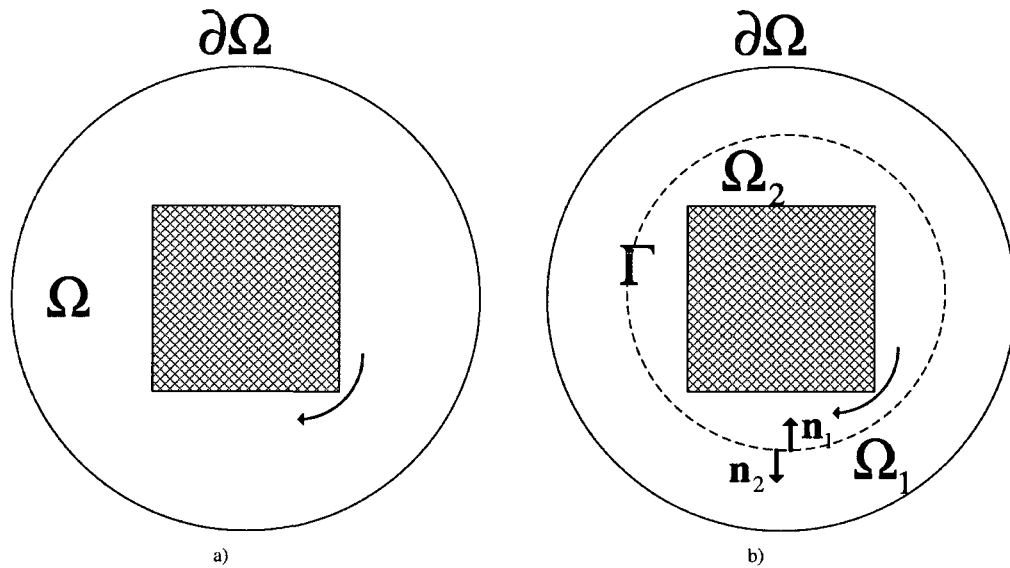
Figure 6-1. Schematic representation of the sliding mesh technique; a) domain Ω with boundary$\square$ $\partial\Omega$ and a squared rotating object; b) domain decomposition of Ω into Ω_{fix} and Ω_{rot} by a sliding interface Γ.

For sake of brevity, we will limit ourselves to two subdomains. Extra moving bodies can be added on the condition that they do not intersect. Due to the decomposition, the coupled problem defined by equations (6.1) and (6.2) is equivalent to the following problem

$$\rho\left(\dot{\mathbf{v}}_i + (\mathbf{v}_i - \mathbf{v}_{mi}) \cdot \operatorname{grad} \mathbf{v}_i\right) - \mu\,\Delta\mathbf{v}_i + \operatorname{grad} p_i = \mathbf{f}_i,\text{ in }\Omega_i\text{ for }i = 1,2 \tag{6.3}$$

$$\operatorname{div} \mathbf{v}_i = 0\text{, in }\Omega_i\text{, for }i = 1,2 \tag{6.4}$$

$$\mathbf{v}_1 = \mathbf{v}_2\text{, in }\Gamma \tag{6.5}$$

$$\mu\,\partial\mathbf{v}_1/\partial\mathbf{n}_1 = -\mu\,\partial\mathbf{v}_2/\partial\mathbf{n}_2\text{ , in }\Gamma \tag{6.6}$$

where $\mathbf{n}_i$ is an outward normal to the interface Γ. Dirichlet boundary conditions are assumed on the domain boundary. Let us introduce the following constraint in the energy principle of equation (6.3):

$$\int_\Gamma \lambda \cdot (\mathbf{v}_1 - \mathbf{v}_2)\,\mathrm{d}\Gamma = \mathbf{0} \tag{6.7}$$

where λ is a Lagrange multiplier that satisfies the Steklov-Poincare interface equation associated with the interface boundary conditions. According to GLOWINSKI et al. (1995) by choosing (6.7), (6.5) and (6.6) are simultaneously satisfied. In addition, we have:

$$\lambda = \mu \ \partial \mathbf{v}_1 / \partial \mathbf{n}_1 = -\mu \ \partial \mathbf{v}_2 / \partial \mathbf{n}_2 \tag{6.8}$$

The variational form corresponding to this modified problem is given by:

$$\left(\dot{\mathbf{v}}_i, \psi\right) + a\left(\mathbf{v}_i, \psi\right) = \left(\mathbf{f}_i, \psi\right) + b(\psi, p_i) + (\lambda, \psi)_\Gamma \ , \forall \ \psi \in \left[H_0^1(\Omega_i)\right]^3, \text{ in } \Omega_i \text{ for}$$
$$i = 1, 2 \tag{6.9}$$

$$b\left(\mathbf{v}_i, \varphi\right) = 0, \ \forall \ \varphi \in L^2(\Omega_i), \text{ in } \Omega_i \text{ for } i = 1, 2 \tag{6.10}$$

$$\left(\left(\mathbf{v}_1 - \mathbf{v}_2\right), \xi\right)_\Gamma = 0, \ \forall \ \xi \in \left[L^2(\Gamma)\right]^3 \quad on \quad \Gamma \tag{6.11}$$

where

$$a\left(\mathbf{v}, \psi\right) = \mu \int_\Omega \text{grad } \mathbf{v} \cdot \text{grad } \psi \, d\Omega + \rho \int_\Omega \psi \cdot \left(\mathbf{v} - \mathbf{v}_m\right) \cdot \text{grad } \mathbf{v} \, d\Omega \tag{6.12}$$

$$b\left(\mathbf{v}, \varphi\right) = \int_\Omega \varphi \cdot \text{div } \mathbf{v} \, d\Omega, \tag{6.13}$$

and $(.,.)_\Omega$ is the scalar product in $L^2(\Omega)$:

$$\left(\mathbf{u}, \mathbf{v}\right)_\Omega = \int_\Omega \mathbf{u} \cdot \mathbf{v} \, d\Omega, \ \forall \ \mathbf{u}, \mathbf{v} \in L^2(\Omega), \tag{6.14}$$

where ψ, φ and ξ are suitable interpolation functions for the velocity, pressure and Lagrange multiplier spaces respectively. YOTOV (1996) provides theoretical basis for the use of these techniques to handle non-matching grids in the context of flow problems.

6.4.2. Finite element discretization

In the present work, P_1^+-P_0 (BERTRAND et al., 1992) and P_2^+-P_1 (CROUZEIX and RAVIART, 1973) tetrahedral finite element approximations are used. The former is an enriched version of the linear element P_1-P_0. Extra degrees of freedom are added at the middle of each face and the pressure is assumed constant on each element. The latter element approximates the velocity by continuous quadratic shape functions, while the pressure is approximated by linear discontinuous functions. They belong to the class of discontinuous pressure elements that satisfies the Brezzi-Babuska condition ensuring numerical stability.

The transient term is discretized by an implicit k-step method based on backward differentiation formulas (BDF), as first proposed by GEAR (1971), which is less restricted to the Courant-Friedrichs-Levy (CFL) condition for explicit schemes. These types of methods can be proven to be A-stable for $k<7$ so that the error tends to zero as the time goes to infinity (SMITH, 1985; DEUFLHARD and FOLKMAR, 2002). This opens the possibility to use larger time steps than those required by explicit schemes to ensure convergence. In this work, a second-order-three-level-step approximation is used where the transient term is approximated by

$$\dot{v} = \left(v^t - v^{t-1} \right) \Big/ \Delta t + \Delta t \left(v^t - 2v^{t-1} + v^{t-2} \right) \Big/ 2\Delta t^2 + O(\Delta t^2)$$
$$= 1 \Big/ \Delta t \left(3/2\, v^t - 2v^{t-1} + 1/2\, v^{t-2} \right) + O(\Delta t^2)$$

(6.15)

6.4.3. Sliding interface

In our partitioned domain, the sliding interface is composed of the faces that connect the moving and static grids. When the sliding grid is moving, holes are created between the sliding and fixed subdomains, as can be observed in Figure 6-2a.
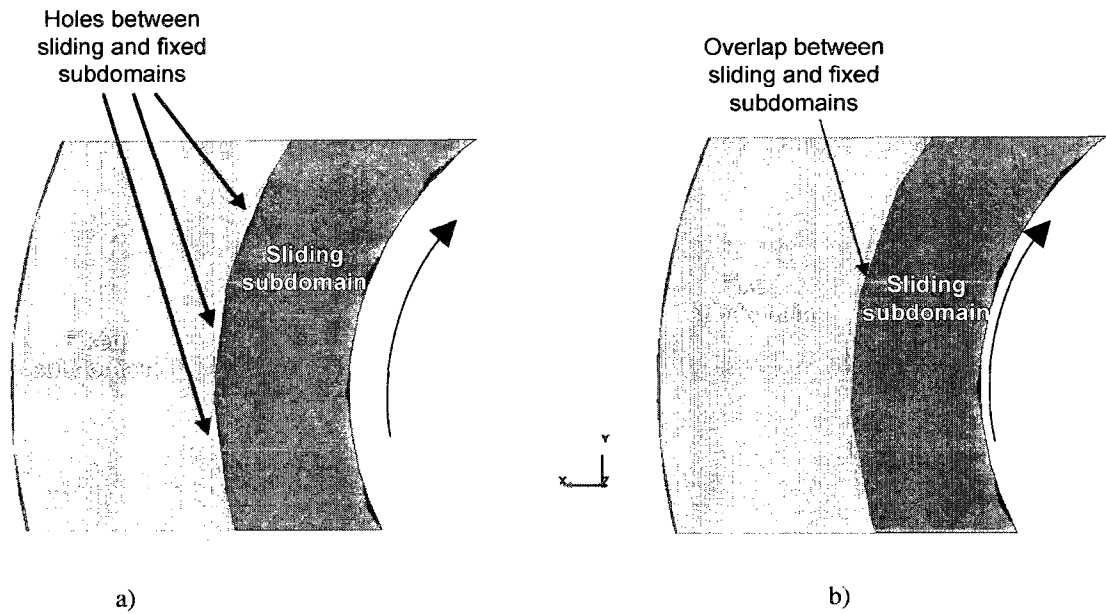
Figure 6-2. a) Holes generated between sliding and fixed subdomains due geometrical approximation error; b) Overlapping between fixed and sliding partitions that prevents holes.

As the existence of holes between sliding and fixed subdomains violates the finite element method principle of interface connection, a conservative treatment of the interface based on Lagrange multipliers is introduced. To simplify the computation of surface integrals required by constraint (6.11), Lagrange multipliers are enforced point-wise over an independent set of points $\left\{\mathbf{x}_i\right\}_{i=1}^{N}$ hereafter called *sliding points,* which are

located on the nodes along the interface of the fixed grid. The finite elements that contain sliding points will be referred as *host elements*. This approach is reminiscent of the virtual finite element method of BERTRAND et al. (1997). It is equivalent to (6.11) if the Lagrange multipliers Λ space, is discretized using Dirac functions defined by

$$\delta(\mathbf{x}-\mathbf{x}_i) = \begin{cases} +\infty & \textit{if } \mathbf{x}=\mathbf{x}_i \\ 0 & \textit{if } \mathbf{x} \neq \mathbf{x}_i \end{cases} \tag{6.16}$$

As the time advances, the sliding grid moves and the host elements change. In this respect, a point-to-element algorithm is used at each time step to determine the host element of each sliding point (LOHNER, 2007; STOBIAC et al., 2008). One issue is the likely loss of sliding points by the search algorithm due to round-off errors and the presence of holes caused by the geometrical approximation, as depicted in Figure 6-2a. Since sliding points are used to represent the sliding interface, failure to locate them appropriately may lead to a loss in the overall accuracy of the method. In this work, it is proposed to geometrically expand the sliding subgrid by some factor to remove the holes between the fixed and moving domains, thus increasing the success of the point-to-element search algorithm (see Figure 6-2b). The geometric factor is obtained heuristically through the following formula,

$$\alpha = 1 \pm \beta h / R_{si} \tag{6.17}$$

where h is an average mesh size, R_{si} is the radius of curvature of the sliding interface and β is a factor that should be as small as possible to avoid excessive changes in the subdomain dimensions but large enough to help the search algorithm in its accuracy. In the case the inner subdomain is the one that rotates, the sign in (6.17) becomes positive (expansion), otherwise it is taken negative (contraction). Tests were run to find a suitable β value using different mesh sizes over two concentric cylinders. It was found that $\beta = 0.1$ is the minimum value required to keep the loss of sliding points by the search algorithm close to zero, as shown in Figure 6-3. It must be noticed that as the mesh size (h) decreases, the geometric factor comes closer to unity.
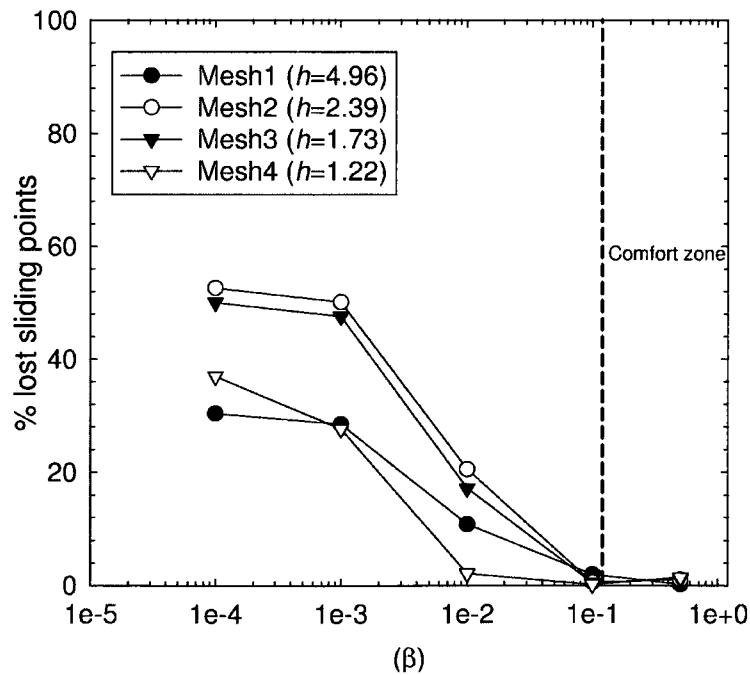
Figure 6-3. Effect of β on the loss of sliding points by the point- to-element search algorithm (Dimensions of mesh size (h) are in mm).

6.4.4. Matrix formulation and algorithm

A fully coupled approach is used to solve equations (6.9), (6.10) and (6.11). It means that velocity, pressure and multipliers are solved simultaneously. The matrix version for a two-domain problem is

$$
\begin{bmatrix}
\mathbf{A}_1 + \frac{3}{2}\Delta t^{-1}\mathbf{M} & \mathbf{B}_1^T & 0 & 0 & -\mathbf{K}_{\Lambda 1}^T \\
\mathbf{B}_1 & 0 & 0 & 0 & 0 \\
0 & 0 & \mathbf{A}_2 + \frac{3}{2}\Delta t^{-1}\mathbf{M} & \mathbf{B}_2^T & \mathbf{K}_{\Lambda 2}^T \\
0 & 0 & \mathbf{B}_2 & 0 & 0 \\
-\mathbf{K}_{\Lambda 1} & 0 & \mathbf{K}_{\Lambda 2} & 0 & 0
\end{bmatrix}
\begin{Bmatrix}
\mathbf{U}_1^t \\
\mathbf{P}_1 \\
\mathbf{U}_2^t \\
\mathbf{P}_2 \\
\Lambda
\end{Bmatrix}
=
\begin{Bmatrix}
\mathbf{F}_1 \\
0 \\
\mathbf{F}_2 \\
0 \\
0
\end{Bmatrix}
+
\begin{Bmatrix}
\Delta t^{-1}\mathbf{M}\left(2\mathbf{U}_1^{t-1} - \frac{1}{2}\mathbf{U}_1^{t-2}\right) \\
0 \\
\Delta t^{-1}\mathbf{M}\left(2\mathbf{U}_2^{t-1} - \frac{1}{2}\mathbf{U}_2^{t-2}\right) \\
0 \\
0
\end{Bmatrix}
\quad (6.18)
$$

where $\mathbf{A}_{i=1,2}$ stands for the convection-diffusion matrix, $\mathbf{M}$ a mass matrix that comes from the Gear time discretization scheme (6.15), Δt the time step, $\mathbf{B}_i$ the matrix obtained from the incompressibility constraint, $\mathbf{B}_i^T$ the transpose of $\mathbf{B}_i$, $\mathbf{K}_{\Lambda i}$ the matrix coming from the interface constraint and $\mathbf{U}_i$, $\mathbf{P}_i$, Λ and $\mathbf{F}_i$ stand for the velocity, pressure, Lagrange multipliers and body forces respectively. Note that this implicit time scheme improves the conditioning of the matrix, thanks to the addition of a mass matrix $\frac{3}{2}\Delta t^{-1}\mathbf{M}$ on the main diagonal of $\mathbf{A}_{i=1,2}$. Another issue that must be addressed is the presence of zeros along the main diagonal, which leads to the failure of the ILU preconditioning because pivoting is not possible. To cure the problem, penalty parameters are introduced for both the divergence and Lagrange multipliers equations. As a result, the discretized equations corresponding to (6.10) (pressure p) and (6.11) (Lagrange multiplier λ) become, respectively:

$$b\left(\mathbf{v}_i,\varphi\right)=-\left(p_i,\varphi\right)\big/\varepsilon_p \ , \ \forall\,\varphi\in L^2(\Omega_i), \text{ in } \Omega_i \text{ for } i=1,2 \tag{6.19}$$

$$\left(\left(\mathbf{v}_1-\mathbf{v}_2\right),\xi\right)_\Gamma=-\left(\lambda,\xi\right)_\Gamma\big/\varepsilon_\lambda, \ \forall\,\xi\in\left[L^2(\Gamma)\right]^3 \quad on \quad \Gamma \tag{6.20}$$

where ε_p and ε_λ are penalty parameters. This leads to the matrix system:

$$\begin{bmatrix} \mathbf{A}_1+\tfrac{3}{2}\Delta t^{-1}\mathbf{M} & \mathbf{B}_1^T & 0 & 0 & -\mathbf{K}_{\Lambda 1}^T \\ \mathbf{B}_1 & \varepsilon_p^{-1} & 0 & 0 & 0 \\ 0 & 0 & \mathbf{A}_2+\tfrac{3}{2}\Delta t^{-1}\mathbf{M} & \mathbf{B}_2^T & \mathbf{K}_{\Lambda 2}^T \\ 0 & 0 & \mathbf{B}_2 & \varepsilon_p^{-1} & 0 \\ -\mathbf{K}_{\Lambda 1} & 0 & \mathbf{K}_{\Lambda 2} & 0 & \varepsilon_\lambda^{-1} \end{bmatrix}\begin{Bmatrix} \mathbf{U}_1^t \\ \mathbf{P}_1 \\ \mathbf{U}_2^t \\ \mathbf{P}_2 \\ \Lambda \end{Bmatrix}=\begin{Bmatrix} \mathbf{F}_1 \\ 0 \\ \mathbf{F}_2 \\ 0 \\ 0 \end{Bmatrix}+\begin{Bmatrix} \Delta t^{-1}\mathbf{M}\left(2\mathbf{U}_1^{t-1}-\tfrac{1}{2}\mathbf{U}_1^{t-2}\right) \\ 0 \\ \Delta t^{-1}\mathbf{M}\left(2\mathbf{U}_2^{t-1}-\tfrac{1}{2}\mathbf{U}_2^{t-2}\right) \\ 0 \\ 0 \end{Bmatrix} \tag{6.21}$$

The scaling of the penalty parameters is done in such a way they remain dimensionally consistent:

$$\varepsilon_p=10^{-\alpha}\big/\rho\mu \tag{6.22}$$

$$\varepsilon_\lambda=10^{-\beta}h\big/\rho\mu \tag{6.23}$$

The α and β parameters require to take values as large as possible to ensure good accuracy. However, excessive large values can produce a break-down in the ILU algorithm since ε_λ and ε_p become too small. In this work, it has been heuristically determined a value of 8 for both parameters.

In flows where the convection term is not negligible, the system of equations in (6.21) is nonlinear. One way to handle such problems is by means of fully nonlinear Newton-Raphson type scheme. A Newton-Raphson scheme for the velocity can be written as:

For k = 1, 2,… until convergence do

$$\text{Solve } \mathbf{T}_i \Delta \mathbf{U}_k = -\mathbf{A}_i \mathbf{U}_k \tag{6.24}$$

$$\text{Update } \mathbf{U}_{k+1} = \mathbf{U}_k + \Delta \mathbf{U}_k$$

where $\mathbf{A}_i$ stands for the convection-diffusion matrix and $\mathbf{T}_i$ the tangent matrix, namely:

$$\mathbf{A}_i = \mu(\text{grad}\,\psi \cdot \text{grad}\,\psi) + \rho\psi(\mathbf{U}_i) \cdot \text{grad}\,\psi - \rho\psi(\mathbf{v}_m \cdot \text{grad}\,\psi) \tag{6.25}$$

$$\mathbf{T}_i = \mu(\text{grad}\,\psi \cdot \text{grad}\,\psi) + \rho\psi(\mathbf{U}_i \cdot \text{grad}\,\psi + \psi \cdot \text{grad}\mathbf{U}_i) - \rho\psi(\mathbf{v}_m \cdot \text{grad}\,\psi) \tag{6.26}$$

Another manner to deal with the convection term is based on semi-implicit schemes presented by TUREK (1996) where the convection term is linearized by extrapolation in time as:

$$\mathbf{v}^t \cdot \text{grad}\,\mathbf{v}^{t+1} \tag{6.27}$$

The semi-implicit treatment of the convective term allows solving linearized problems at each time step; nonetheless, the accuracy is expected to be highly dependent on the size of the time step due the dependence of (6.27) on the velocity field computed at the last time step (v') . Furthermore, they can only be used for unsteady simulations. For this scheme, the matrix $\mathbf{C}_i$ and $\mathbf{A}_i$ become:

$$\mathbf{T}_i = \mathbf{A}_i = \mu(\mathrm{grad}\,\psi \cdot \mathrm{grad}\,\psi) + \rho\psi\mathbf{U}_i^t \cdot \mathrm{grad}\,\psi - \rho\psi\left(\mathbf{v}_m \cdot \mathrm{grad}\,\psi\right) \tag{6.28}$$

Both techniques are tested for the stirred tank without baffles case presented in the next section. The general algorithm of the sliding mesh technique is presented in Algorithm 6-1.

0. Given $U^{(0)}$, $P^{(0)}$ and $\Lambda^{(0)}$.

1. For t = 1, 2, ..., total number of time steps

    1.1 Rotate the sliding sub-grids and identify host elements

    1.2 Update velocity at the boundaries of the sliding sub-grids

    1.3 Compute mesh velocity v_m

    1.4 For n = 1, 2, ..., until convergence:

    1.4.1 Solve simultaneously for δU, δP and $\delta\Lambda$:

$$\begin{bmatrix} T_1 + \tfrac{3}{2}\Delta t^{-1}M & B_1^T & 0 & 0 & -K_{\Lambda 1}^T \\ B_1 & \varepsilon_p^{-1}I & 0 & 0 & 0 \\ 0 & 0 & T_2 + \tfrac{3}{2}\Delta t^{-1}M & B_2^T & K_{\Lambda 2}^T \\ 0 & 0 & B_2 & \varepsilon_p^{-1}I & 0 \\ -K_{\Lambda 1} & 0 & K_{\Lambda 2} & 0 & \varepsilon_\lambda^{-1}I \end{bmatrix} \begin{Bmatrix} \delta U_1 \\ \delta P_1 \\ \delta U_2 \\ \delta P_2 \\ \delta\Lambda \end{Bmatrix} = \begin{Bmatrix} R_{v1}^{(n)} \\ R_{p1}^{(n)} \\ R_{v2}^{(n)} \\ R_{p2}^{(n)} \\ R_{\lambda}^{(n)} \end{Bmatrix}$$

$$\begin{Bmatrix} R_{v1}^{(n)} \\ R_{p1}^{(n)} \\ R_{v2}^{(n)} \\ R_{p2}^{(n)} \\ R_{\lambda}^{(n)} \end{Bmatrix} = \begin{Bmatrix} F_1 \\ 0 \\ F_1 \\ 0 \\ 0 \end{Bmatrix} - \begin{bmatrix} A_1 + \tfrac{3}{2}\Delta t^{-1}M & B_1^T & 0 & 0 & -K_{\Lambda 1}^T \\ B_1 & \varepsilon_p^{-1}I & 0 & 0 & 0 \\ 0 & 0 & A_2 + \tfrac{3}{2}\Delta t^{-1}M & B_2^T & K_{\Lambda 2}^T \\ 0 & 0 & B_2 & \varepsilon_p^{-1}I & 0 \\ -K_{\Lambda 1} & 0 & K_{\Lambda 2} & 0 & \varepsilon_\lambda^{-1}I \end{bmatrix} \begin{Bmatrix} U_1^{(n,t)} \\ P_1^{(n)} \\ U_2^{(n,t)} \\ P_2^{(n)} \\ \Lambda^{(n)} \end{Bmatrix} + \begin{Bmatrix} \Delta t^{-1}M\left(2U_1^{t-1} - \tfrac{1}{2}U_1^{t-2}\right) \\ 0 \\ \Delta t^{-1}M\left(2U_2^{t-1} - \tfrac{1}{2}U_2^{t-2}\right) \\ 0 \\ 0 \end{Bmatrix}$$

    1.4.2 Update $U_i^{(n)}$, $P_i^{(n)}$ and $\Lambda^{(n)}$:

$$\begin{cases} U_i^{(n+1)} = U_i^{(n)} + \delta U_i \\ P_i^{(n+1)} = P_i^{(n)} + \delta P_i \\ \Lambda^{(n+1)} = \Lambda^{(n)} + \delta\Lambda \end{cases} \quad \text{in } \Omega_i \text{ for } i = 1,2$$

Algorithm 6-1. Solution algorithm for the sliding mesh technique, for sliding and fixed subdomains.

If the Newton-Raphson scheme is used, the number of fixed-point iterations is greater than one, depending on the nonlinearity of the problem. On the other hand, the semi-implicit scheme requires only one fixed-point iteration per time step. The system of equations in Algorithm 6-1 can be solved either by a direct method or a sparse iterative solver depending on the total number of equations. In this work, a ILU(0) preconditioned QMR solver is used. This iterative solver was chosen because of its robustness to deal with systems of equations that possess non-symmetric matrices. The details about the QMR algorithm can be found in FREUND and NACHTIGAL (1991). The solutions obtained by the QMR solver were considered converged when the norm ratio between the current residual (r^i) and the initial residual (r^0) satisfies:

$$\left\|r^i\right\|/\left\|r^0\right\| < 10^{-6} \tag{6.29}$$

where $\|\cdot\|$ stands for the Euclidean norm. The initial solution for all cases was set to zero. This solver can be implemented on distributed memory parallel computers. Details about its implementation are given in the next section.

6.5. Parallel implementation

For parallel computations, the variables were reordered in blocks, depending if the equations correspond to internal, interface, pressure or Lagrange multipliers:

$$UxUyUz - I - P - LM \rightarrow \left\{ \begin{array}{l} u_{\text{int}\,x1}, u_{\text{int}\,y1}, u_{\text{int}\,z1}, \ldots, u_{\text{int}\,xn}, u_{\text{int}\,yn}, u_{\text{int}\,zn}, \\ u_{\text{ifacex}1}, u_{\text{ifacey}1}, u_{\text{ifacez}1}, \ldots, u_{\text{ifacex}m}, u_{\text{ifacey}m}, u_{\text{ifacez}m}, \\ p_1, \ldots, p_n, \\ \lambda_{x1}, \lambda_{y1}, \lambda_{z1}, \ldots, \lambda_{xm}, \lambda_{ym}, \lambda_{zm} \end{array} \right\} \quad (6.30)$$

where subscripts int and iface in (6.30) refer to the internal and interface velocity equations. In this way, linear algebra operations can be performed in parallel for the internal block variables, while the inter-processor communication is only required for the interface velocity and the Lagrange multipliers blocks. To reduce the memory required per processor, a piece of the global matrix of (6.21) is built and stored in each processor.

Load balancing is a key feature in parallel computing. One important issue to consider in the sliding mesh method is that the initial domain decomposition of sliding and moving grids may not be optimal for parallel computing. For example, Figure 6-4a presents the matrix profile where the sliding domain is much larger than the fixed domain. This would cause inefficiencies in the parallel resolution process due to unbalanced load distribution. To alleviate this difficulty, each sub-grid can be further partitioned into smaller partitions (Figure 6-4b) and the Lagrange multiplier method can be applied again over the new subdomain interfaces. The main difference between these new sub-partitions and the original partitions is that they are connected through

interfaces, the nodes which always match, hereafter called matching boundaries, as opposed to the sliding interfaces where the nodes do not match all the time.

Non-zero entries in finite element global matrix

Non-zero entries in finite element global matrix

a)

b)
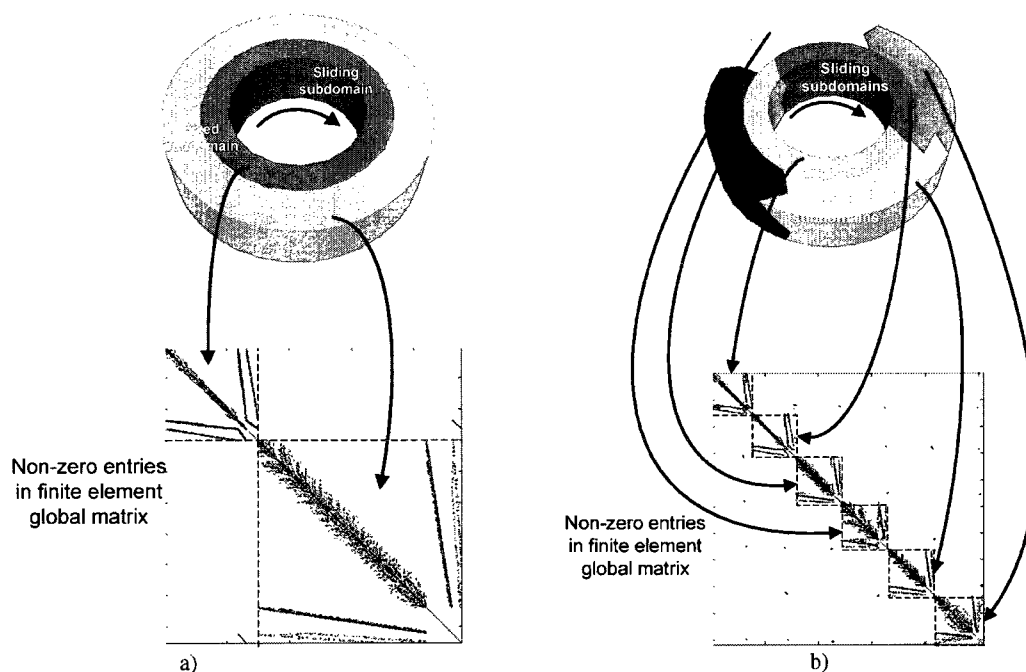
Figure 6-4. Partitioning technique applied to two concentric cylinders: a) one sliding subdomain and one fixed subdomain; b) two sliding subdomains and four fixed subdomains.

Figure 6-5 gives a schematic representation of both types of boundaries. In the case where a single point connects multiples subdomains, only the constraints corresponding to a face (or an edge for two-dimensional problems) connecting subdomains must be imposed, as shown in Figure 6-6. A parallel version of the preconditioned ILU(0)-Quasi-Minimal Residual (QMR) solver (FREUND and NACHTIGAL, 1991) is

employed to solve (6.21), which entails the parallel execution of sparse linear algebra operations (SAAD, 2000).

Figure 6-5. Domain partitioned into four subdomains with boundary□ $\partial\Omega$. The sliding subdomain ($\Omega_1 \cup \Omega_2$) and the fixed subdomain ($\Omega_3 \cup \Omega_4$) are joined by matching boundaries and a sliding interface.
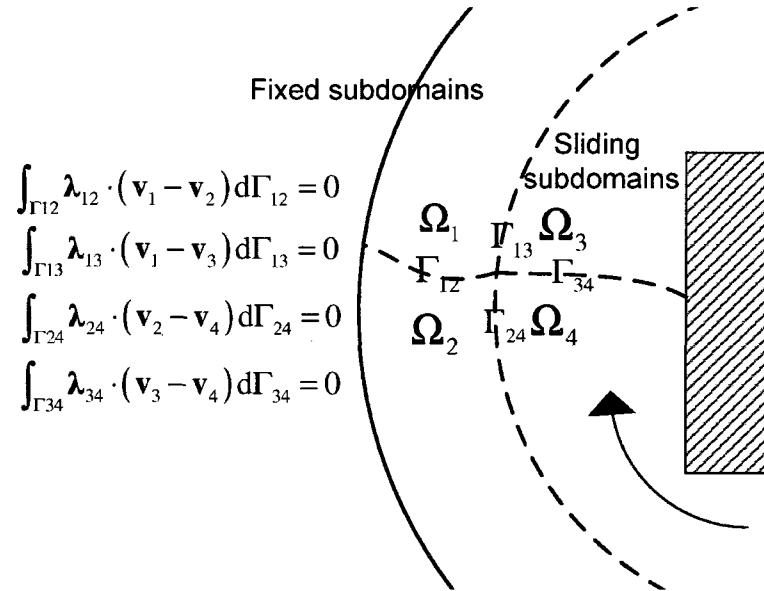
Figure 6-6. Constraints imposed when four partitions share a point in the finite element

sliding mesh technique.

6.6. Numerical examples

In this section, the behaviour and accuracy of the finite element sliding mesh technique

is assessed. Two cases are considered, the two-dimensional flow between two

concentric cylinders and the three-dimensional flow induced by a flat blade turbine in a

baffle-free tank (Figure 6-8a). Simulations of this section were run on a single

processor; the parallel performance is presented in the next section.

6.6.1.   Couette flow

As a first test, the incompressible laminar Couette flow between two concentric cylinders is considered. The inner cylinder has a radius κR and the outer cylinder of radius R rotates at constant speed Ω_0. The analytical solution can be obtained by solving the Stokes equations in cylindrical coordinates:

$$v_\theta = \Omega_0 R\left(\kappa R / r - r / \kappa R\right)/\left(\kappa - 1/\kappa\right) \tag{6.31}$$

The parameters for the simulation were set as $R=0.05$ m, $\kappa =0.5$, $\rho = 1000\ kg\ m^{-3}$, $\mu = 100\ Pa \cdot s$ and $\Omega_0 = 100\,\mathrm{rev\,min^{-1}}$. The problem was discretized with the help of the Crouzeix-Raviart $P2^+\text{-}P1$ element over unstructured three-dimensional grids with different grid sizes as summarized in Table 6-1. For the sliding mesh technique, several time steps were simulated until the solution reached the steady state. At each time step, the outer sub-domain was rotated and the incompressible Navier-Stokes equations in the ALE formulation were solved. For the inner subdomain (fixed), the mesh velocity (v_m) was set to zero and for the outer one, we took $v_m = \Omega_0 \times r$.

Table 6-1: Characteristics of the meshes utilized for the concentric cylinders problem.

Label	Mesh size (mm)	Number of elements	Number of equations
Mesh1	4.96	6,238	9,921
Mesh2	2.39	51,666	85,621
Mesh3	1.73	133,520	223,185
Mesh4	1.22	376,188	634,656

Figure 6-7 shows a plot of the infinity norm of the error on velocity with respect to the grid size. It shows a linear decrease of the error as the mesh is refined. The small deviation from a straight line may be caused by inaccuracies in the evaluation of the mesh size since unstructured meshes were employed, where the mesh size on each element varies.
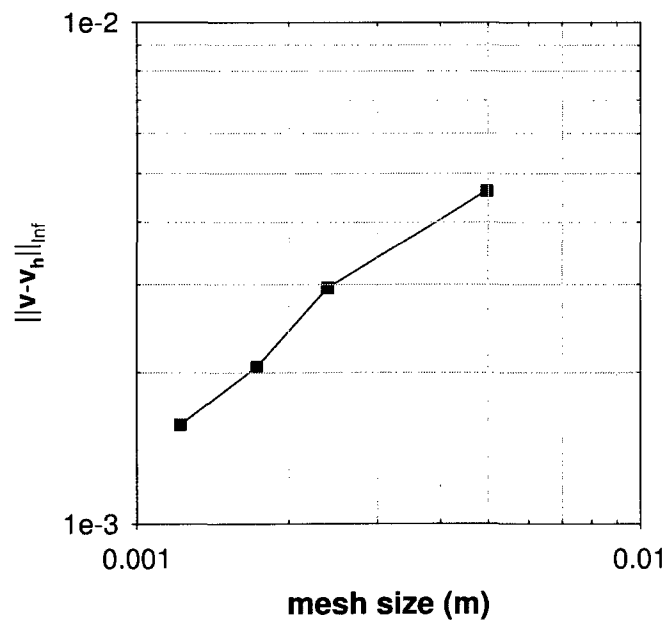
Figure 6-7. Infinity norm of the error on velocity versus mesh size.

6.6.2. Agitated tank

The next step was to simulate the three-dimensional incompressible flow in a stirred tank agitated by a Rushton turbine (Figure 6-8a) by the proposed sliding mesh technique. To validate the sliding mesh method, we resorted to the Lagrangian frame of reference approach that consists in solving the equations of motion from the point of view of an observer that rotates with the impeller. Figure 6-8bc gives a schematic representation of the two approaches.

a)

b)   c)
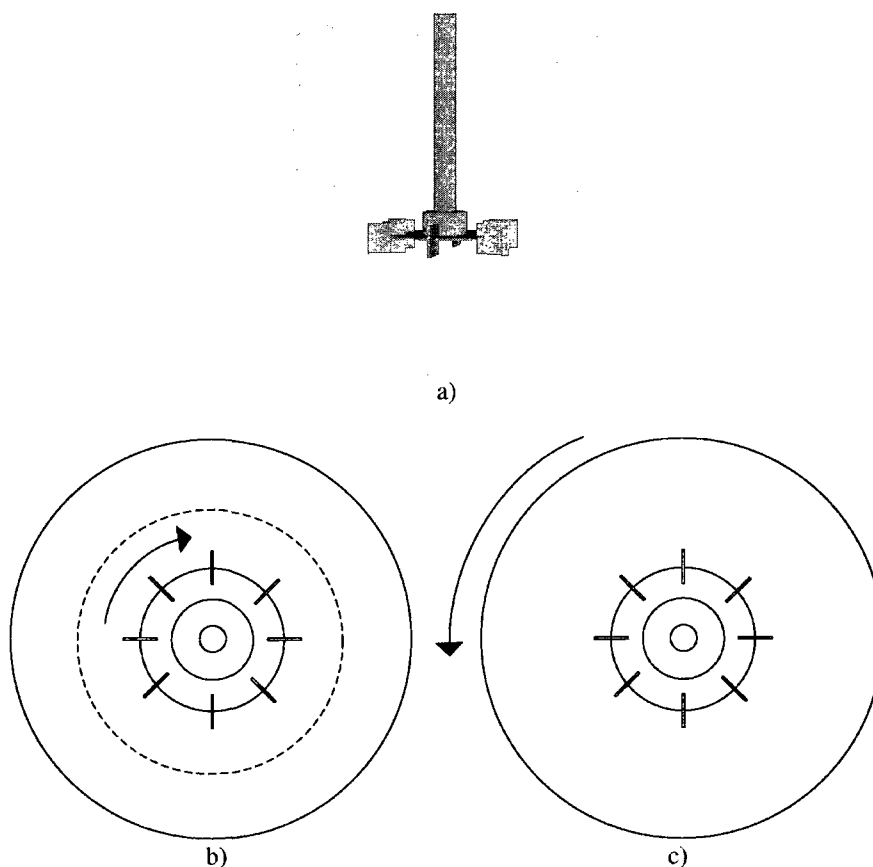
Figure 6-8. a) Stirred tank agitated by a Rushton turbine without baffles; b) sliding

mesh technique; c) Lagrangian frame of reference technique.

The following conditions were considered. The turbine of diameter $D= 0.2$ m was moved at a rotational speed (N) of 100 rev min^{-1}. A Newtonian fluid was considered with a viscosity (μ) of 10 Pa s and a density (ρ) of 1350 kg m^{-3}. In these conditions, the Reynolds number , $\mathrm{Re} = \rho N D^2 / \mu$, is 9, which ensured that the flow was laminar and vortex free at the free surface. For the simulations, the P1^{+}-P0 finite element was used to approximate the velocity and the pressure.

a) Sliding mesh

For the sliding mesh technique, an unstructured three-dimensional mesh comprising 125K tetrahedral elements was used. The computational domain was partitioned into two subdomains. The rotating subdomain included the turbine. The total number of equations was approximately 1M equations. The ALE equations were solved for a mesh velocity defined by $\mathbf{v}_m = \Omega_0 \times \mathbf{r}$ on the rotating subdomain. Boundary conditions were as follows:

- No slip condition at the tank wall
- Rotational speed of 100 rev. min^{-1} on the turbine boundary
- Zero normal velocity at the flat free surface

Several time step sizes were tested to evaluate the effect on the accuracy of the method.

b)   Lagrangian frame of reference

The Lagrangian frame of reference approach simplifies the imposition of the boundary conditions and the problem can be treated at steady state as explained by TANGUY et al. (1992). Consequently, the acceleration term can be omitted. However, as the frame of reference is no longer inertial, the Navier-Stokes equations must be complemented by centrifugal and Coriolis forces.

The solution obtained with the standard finite element method was taken as the reference solution. The same mesh and finite element type that was employed for the sliding mesh was used. The total number of equations was 915K. With this classical approach, the boundary conditions were as follows:

- No slip condition at the turbine boundary

- Rotational speed of 100 rev min^{-1} for the tank walls

- No normal velocity at the free surface

c)   Accuracy and stability of the sliding mesh method

Figure 6-9 shows the axial-radial velocity profiles on a vertical cross-section for the two studied techniques. As can be observed, the sliding mesh technique reproduces the shape of the vortexing rings above and below the impeller.
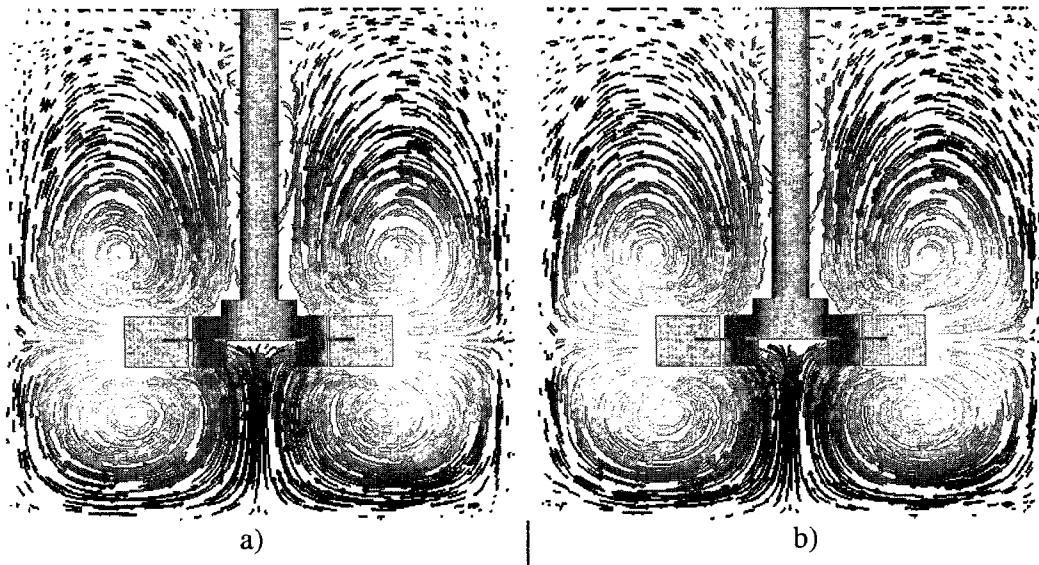
Figure 6-9. Velocity profile on a vertical cross-section at the middle of the tank; a)

Sliding mesh technique; b) Lagrangian frame of reference technique.

Figure 6-10 presents the effect of the time step with respect to the relative error in axial pumping through 100 planes that traverse the vessel height. Both the Newton-Raphson and the semi-implicit schemes were used to deal with the convective term. Axial pumping across these planes is computed as

$$Q_z^+(z) = \int_A v_z^+ dA = -\int_A v_z^- dA \qquad (6.32)$$

The relative error in axial pumping is defined by

$$Error\,Q_z = 100\text{X}\left(Max\|Q_{zi-SM} - Q_{zi-Lag}\|\right)\Big/Max(Q_{zi-Lag}) \qquad (6.33)$$

where Q_{zi-SM} and Q_{zi-Lag} are the axial pumping values obtained for each cross-section

for the sliding mesh and Lagrangian approaches, respectively. The plot shows a

quadratic decrease of the error as the size of time steps is reduced for both Newton-

Raphson and semi-implicit schemes, which is a consequence of the second-order nature

of the Gear scheme. It is noted also in Figure 6-10 that the semi-implicit scheme

slightly reduces the accuracy of the method in comparison with the Newton-Raphson

scheme, mainly when large time step sizes are used, as expected.
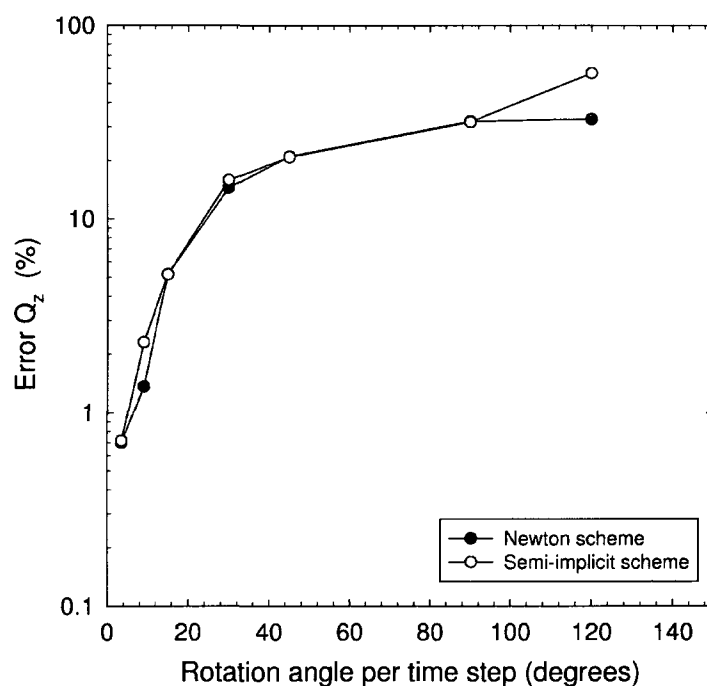
Figure 6-10. Error in axial pumping with respect to the rotation angle per time step for

the stirred tank simulation (Re=9).

Table 6-2 and Table 6-3 present the number of QMR iterations and CPU time for each time step size studied for both the Newton-Raphson and the semi-implicit schemes, respectively. For the Newton-Raphson method, as the time step becomes smaller, the number of QMR iterations and CPU time per time step tend to decrease. On the other hand, the semi-implicit scheme shows an almost constant number of QMR iterations and CPU time per time step for all the time step sizes tested. The semi-implicit scheme shows interesting results. In comparison with the Newton-Raphson scheme, it requires less QMR iterations since it only requires a single fixed-point iteration per time step which saves considerable amount of CPU time. Note that the sliding mesh technique is very stable for both convection schemes, as it is capable to converge regardless of the value of the time step size.

Table 6-2: Number of iterations and CPU time (1 processor) for different rotation angles per time step (Re=9) using the sliding mesh technique in combination with the Newton-Raphson scheme for the convective term.

Rotation angle/time step (degrees)	Newton Raphson iterations/time step	Total number of QMR iterations/time step	CPU time/time step (seconds)	CPU time/ agitator revolution (minutes)
3.6	3	548	1215	2025
9	3	634	1386	924
15	3	735	1630	652
30	3	1014	2350	470
45	3	1105	2416	322
90	4	1024	2232	148
120	4	892	2050	102

Table 6-3: Number of iterations and CPU time (1 processor) for different rotation

angles per time step (Re=9) using the sliding mesh technique in combination with the

semi-implicit scheme for the convective term.

Angle rotation/time step	Total number of QMR iterations	CPU time/time step (seconds)	CPU time/revolution (minutes)
3.6	235	521	869
9	206	457	305
15	205	455	182
30	201	446	89
45	232	515	69
90	265	588	39
120	268	595	30

Figure 6-11 compares the axial pumping produced by the Lagrangian frame of

reference and the sliding mesh techniques with the Newton-Raphson scheme using the

smallest time step employed in this study ($\Delta t = 3.6$ degrees). Sliding mesh gives a

maximum difference (with respect to the Lagrangian solution) of 0.75%. Figure 6-11

presents the average deformation norm through 100 planes that traverse the vessel

height for both Lagrangian and sliding mesh techniques. The deformation norm is

obtained by:

$$\|\dot{\gamma}\| = \sqrt{\frac{1}{2}(|\dot{\gamma}|)\cdot(|\dot{\gamma}|)^{T}} \tag{6.34}$$

where:

$$|\dot{\gamma}| = \frac{1}{2}\left(\nabla\mathbf{v} + (\nabla\mathbf{v})^{T}\right)$$
(6.35)

The error in average deformation norm is smaller than the error obtained for the axial pumping since differences of approximately 0.5 % were found for the sliding mesh method with respect to the Lagrangian velocity field.
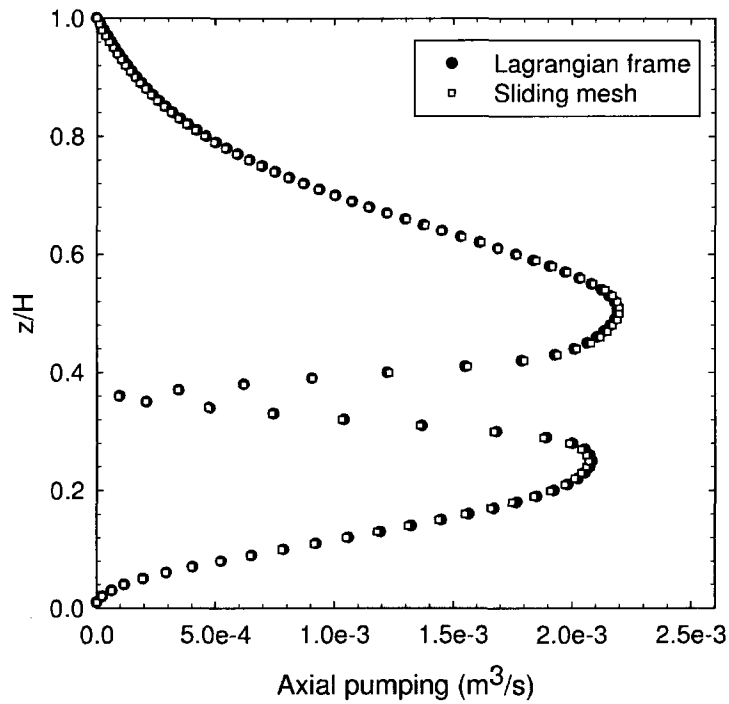
Figure 6-11. Comparison between the Lagrangian and sliding mesh average deformation norms at different tank heights for the flat-blade turbine system.
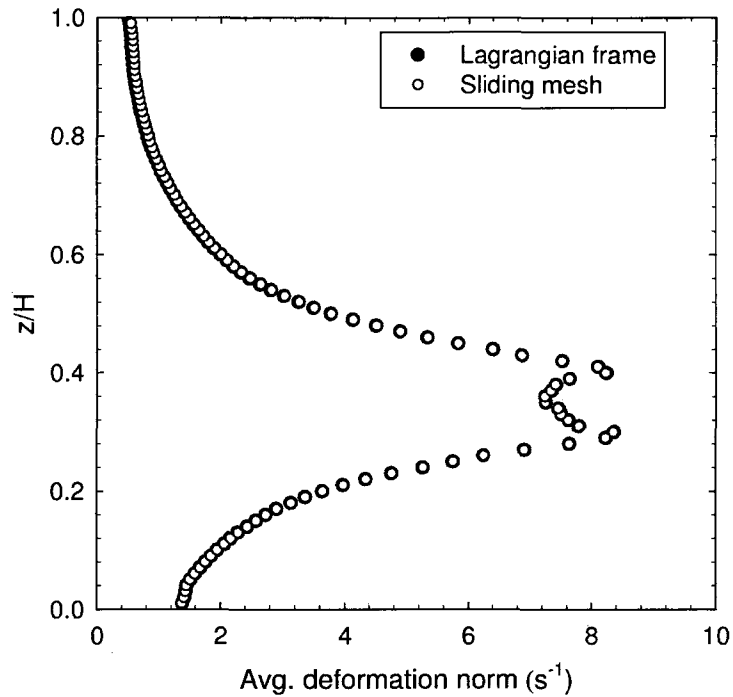
Figure 6-12. Comparison between the Lagrangian and sliding mesh average

deformation norms at different tank heights for the flat-blade turbine system.

6.7. Parallel performance

The parallel performance was evaluated by means of the simulation of the unsteady

flow in a stirred tank with baffles (Figure 6-13). The simulation consisted in solving the

unsteady incompressible Navier-Stokes equations by the sliding mesh technique with

the Newton-Raphson scheme using an IBM-P690 with 64 Gb of shared memory. The

following conditions were considered. The turbine of diameter $D=0.2$ m was moving at

a rotational speed (N) of 200 rev min^{-1}. A Newtonian fluid was considered with a

viscosity (μ) of 5 Pa s and a density (ρ) of 1350 kg m^{-3}. The flow was at the threshold of the transition regime since the Reynolds number is 36. The presence of baffles ensures that the flow was vortex free at the free surface. The time step was set to 0.006 s, which corresponds to a rotation of 7.2 degrees at each time step. The mesh velocity was computed as in the previous section. The boundary conditions were as follows:

- No slip condition at the tank and baffles walls

- Rotational speed of 200 rev min^{-1} on the turbine boundary

- Zero normal velocity at the free surface
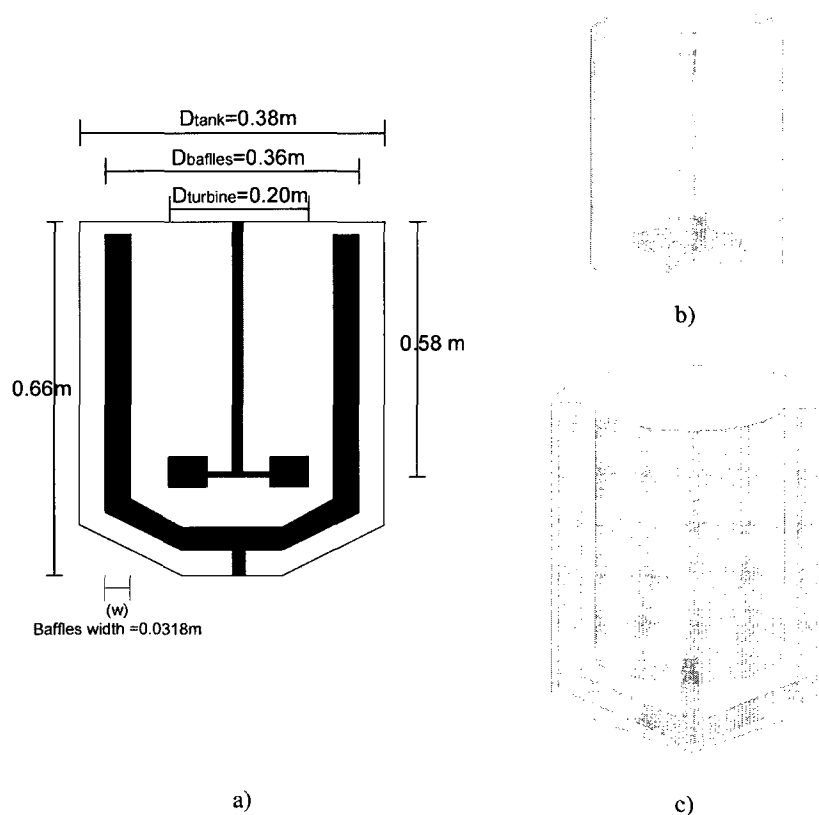
Figure 6-13. a) Geometrical description of the stirred tank agitated by flat-blade turbine with static baffles; b) sliding subdomain (turbine); c) fixed subdomain (baffles).

An unstructured grid comprising 202,083 tetrahedral elements was used for the computation. The mesh was initially partitioned into sliding and fixed subdomains. The fixed partition contained 128,241 elements and the sliding one, 73,842 elements. These partitions were further subdivided to observe the parallel performance of the method as shown in Figure 6-14. The total number of subdomains generated was varied from 2 to 16, distributed in such a way that the total number of elements in each partition was as balance as possible. These partitions were performed with the help of spectral algorithms and the Kerninghan-Lin smoothing techniques included in the Chaco partitioning software (HENDRIKSON and LELAND, 1993).

Figure 6-14. Partitions used to test the parallel performance of an agitated tank with baffles simulation; a) 3 subdomains b) 6 subdomains c) 12 subdomains d) 16 subdomains.

The power consumption (P) for the simulated scenario was computed from the obtained hydrodynamics by

$$P = \int_{\Omega} \tau : \dot{\gamma} d\Omega \qquad (6.36)$$

Table 6-4 compares the numerical power consumption with the experimental results of FARHAT et al. (2007), showing an error of 2.2% that demonstrates the validity of the solutions. Table 6-5 summarizes the parallel performance obtained for the different tests. As the number of partitions increases, the number of equations increases due the generation of additional Lagrange multipliers. Table 6-5 also displays the load distribution defined as:

$$load\ distribution = \min(NNZ)/\max(NNZ) \qquad (6.37)$$

where NNZ stands for a list that contains the number of nonzero entries in each submatrix that assembles the global system of equations in Algorithm 6-1.

Table 6-4: Numerical and experimental power consumption values (W) for the stirred tank with baffles.

Method	Power consumption (W)
Experimental data from FARHAT et al. (2007)	89.60
Sliding mesh method	87.63

Table 6-5: Summary of the speed-ups obtained for the flow in the stirred tank with

baffles case (Re=36).

Number of processors	Number of subdomains per fixed/sliding partitions	Number of equations (x10^6)	Load distribution (fixed partitions)	Load distribution (Sliding partitions)	Overall load distribution (fixed/sliding partitions)	Total QMR iterations	Total CPU time (s) per time step	Overall speed-up
1	1/1	1.546	1	1	0.692	673	2,552	1.0
2	1/1	1.546	1	1	0.692	673	1,698	1.5
3	2/1	1.558	0.987	1	0.725	737	1,057	2.4
6	4/2	1.582	0.952	0.992	0.711	773	624	4.1
12	8/4	1.629	0.910	0.943	0.678	793	383	6.6
16	10/6	1.611	0.917	0.952	0.872	936	342	7.4

As can been seen, the best load distribution values for the sliding partitions and fixed

partitions was around 0.9. However, the overall load distribution for the full simulation

is worse, with values in the range of 0.69-0.82. This anomaly affects the parallel

performance due to the disproportionate amount of work in each processor that leads to

an increase in the overhead time. Figure 6-15 shows a maximum speed-up of 10 for the

QMR iterations when 16 processors are employed. A small deterioration in the QMR

convergence rates can be observed in Table 6-5 as the number of partitions increases,

which can be explained by the larger size of the linear system. An overall speed-up of

7.4 is obtained with the 16 processors. In all cases, increasing the number of processors

always reduced the computational time.
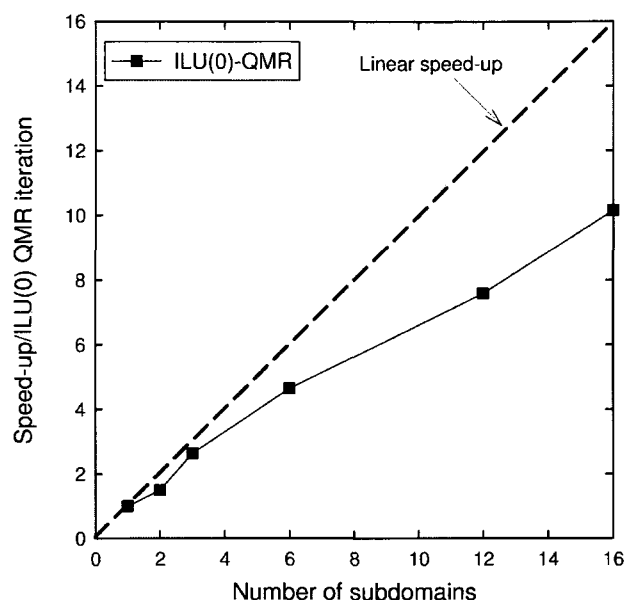
Figure 6-15. Speed-up for the ILU(0)-QMR iterations for the unsteady simulation of

the flow in the stirred tank with baffles.

6.8. Conclusions

The objective of this paper was to present a sliding mesh algorithm based on Lagrange

multipliers for incompressible viscous fluid flows on unstructured tetrahedral grids.

The method consists in the use of discontinuous pressure finite elements and Lagrange

multipliers to enforce continuity at the interfaces between sliding and fixed subdomains.

Then, the obtained global system of equations is solved simultaneously for velocity,

pressure and Lagrange multipliers by a ILU(0)-QMR solver. The method is assessed in

the case of concentric cylinders and stirred tank flows showing excellent accuracy. To

handle the convection, two methods are tested: the fully nonlinear Newton-Raphson

scheme and the semi-implicit linearization proposed by TUREK (1996). It is demonstrated that the sliding mesh technique in combination with the Newton-Raphson scheme provides slightly higher accuracy than with the semi-implicit scheme, mainly when large time step sizes are employed. However, the semi-implicit scheme saves considerable amount of CPU time. It is shown that the sliding mesh technique is very stable, being able to converge using large time steps due the implicit properties of the Gear time discretization scheme. As expected, the technique shows a quadratic reduction in the error as the size of the time steps decreases. The approach is parallelized to simulate the unsteady flows in a stirred tank with baffles. The computed power consumption presented a difference of 2% with respect to experimental data. A speed-up of 7.4 is obtained when running on 16 processors. It is demonstrated that the technique allows to further subdivide both the sliding and fixed partitions into a desired number of partitions, allowing efficient parallelization.

6.9. Acknowledgments

6.10. References

AVALOSSE, T., CROCHET, M. J. (1997). Finite-element simulation of mixing. 1. Two-dimensional flow in periodic geometry. *AIChE Journal, 43*(3), 577-587.

BEHR, M., TEZDUYAR, T. (1999). The Shear-Slip Mesh Update Method. *Computer Methods in Applied Mechanics and Engineering, 174*(3-4), 261-274.

BELYTSCHKO, T., KENNEDY, J. (1975). Finite element approach to pressure wave attenuation by factor fuel subassemblies. *American Society of Mechanical Engineers (Paper), 75*, 172-177.

BERNARDI, C., MADAY, Y., PATERA, A. T. (1994). A new conforming approach to domain decomposition: the mortar element method. In Brezis, H. Lions, J. L. (éds.), *Nonlinear partial differential equations and their applications* (College de france seminar XI, pp. 13-51). Paris, France: Pitman.

BERTRAND, F., TANGUY, P. A., THIBAULT, F. (1997). A three-dimensional fictitious domain method for incompresible fluid flow problems. *International Journal for Numerical Methods in Fluids, 25*(6), 719-736.

BERTRAND, F. H., GADBOIS, M. R., TANGUY, P. A. (1992). Tetrahedral elements for fluid flow. *International Journal for Numerical Methods in Engineering, 33*(6), 1251-1267.

BOHM, M., WECHSLER, K., SCHAFER, M. (1998). A parallel moving grid multigrid method for flow simulation in rotor-stator configurations. *International Journal for Numerical Methods in Engineering, 42*(1), 175-189.

BRAVO, V. L., HRYMAK, A. N., WRIGHT, J. D. (2000). Numerical simulation of pressure and velocity profiles in kneading elements of a co-rotating twin screw extruder. *Polymer Engineering and Science, 40*(2), 525-541.

CONNELLY, R. K., KOKINI, J. L. (2006). Mixing simulation of a viscous newtonian liquid in a twin sigma blade mixer. *AIChE Journal, 52*(10), 3383-3393.

CROUZEIX, M., RAVIART, P. (1973). Conforming and non-conforming finite element methods for solving the stationary Stokes equations. *RAIRO analyse numerique, 7*, 33-76.

DEUFLHARD, P., FOLKMAR, B. (2002). *Scientific computing with ordinary differential equations* (1rst^e éd.). New York: Springer-Verlag.

ESPINOSA-SOLARES, T., BRITO-DE LA FUENTE, E., TECANTE, A., TANGUY, P. A. (1997). Power consumption of a dual turbine-helical ribbon impeller mixer in ungassed conditions. *Chemical Engineering Journal, 67*(3), 215-219.

FARHAT, M., RIVERA, C., FRADETTE, L., HENICHE, M., TANGUY, P. A. (2007). Numerical and experimental study of a dual-shaft coaxial mixer with viscous fluids. *Industrial and Engineering Chemistry Research, 46*(14), 5021-5031.

FOUCAULT, S., ASCANIO, G., TANGUY, P. A. (2006). Mixing times in coaxial mixers with Newtonian and non-Newtonian fluids. *Industrial and Engineering Chemistry Research, 45*(1), 352-359.

FREUND, R. W., NACHTIGAL, N. M. (1991). QMR: a quasi-minimal residual method for non-Hermitian linear systems. *Numerische Mathematik, 60*(3), 315-339.

GARTLING, D. K. (2005). Multipoint constraint methods for moving body and non-contiguous mesh simulations. *International Journal for Numerical Methods in Fluids, 47*(6-7), 471-489.

GEAR, C. (1971). *Numerical initial value problems in ordinary differential equations.* Englewood Cliffs, N.J.: Prentice-Hall.

GLOWINSKI, R., PAN, T.-W., PERIAUX, J. (1994). Fictitious domain method for Dirichlet problem and applications. *Computer Methods in Applied Mechanics and Engineering, 111*(3-4), 283-303.

GLOWINSKI, R., PAN, T. W., KEARSLEY, A. J., PERIAUX, J. (1995). *Fictitious domain methods for viscous flow simulation.* Houston: Rice University.

HENDRIKSON, B., LELAND, R. (1993). *The Chaco user guide, version 1.0.* Alburquerque, NM, USA: Sandia Laboratories.

HOUZEAUX, G., CODINA, R. (2003). A Chimera method based on a Dirichlet/Neumann (Robin) coupling for the Navier-Stokes equations. *Computer Methods in Applied Mechanics and Engineering, 192*(31-32), 3343-3377.

HUERTA, A., LIU, W. K. (1988). Viscous flow with large free surface motion. *Computer Methods in Applied Mechanics and Engineering, 69*(3), 277-324.

JONGEN, T. (2000). Characterization of batch mixers using numerical flow simulations. *AIChE Journal, 46*(11), 2140-2150.

LEVEQUE, R. J., LI, Z. (1994). Immersed interface method for elliptic equations with discontinuous coefficients and singular sources. *SIAM Journal on Numerical Analysis, 31*(4), 1019-1044.

LOHNER, R. (2007). The empty bin: a data structure for spatial search of time-varying data. *Communications in Numerical Methods in Engineering, 23*(12), 1111-1119.

LUO, J. Y., GOSMAN, A. D., ISSA, R. I., MIDDLETON, J. C., FITZGERALD, M. K. (1993). Full flow field computation of mixing in baffled stirred vessels. *Chemical Engineering Research and Design, 71*(A3), 342-344.

PERICLEOUS, K. A., PATEL, M. K. (1987). Modelling of tangential and axial agitators in chemical reactors. *PCH. Physicochemical hydrodynamics, 8*(2), 105-123.

PERNG, C.-Y., MURTHY, J. Y. (1993). Sliding-mesh technique for simulation of flow in mixing tanks. *New Orleans* (pp. 1-9)Publ by ASME.

PESKIN, C. S., MCQUEEN, D. M. (1989). A three-dimensional computational method for blood flow in the heart. I. Immersed elastic fibers in a viscous incompressible fluid. *Journal of Computational Physics, 81*(2), 372-405.

RAI, M. M. (1985). Navier-Stokes simulations of rotor-stator interaction using patched and overlaid grids. *Cincinnati* (pp. 282-298)AIAA (CP854).

RIVERA, C., HENICHE, M., ASCANIO, G., TANGUY, P. (2004). A virtual finite element model for centered and eccentric mixer configurations. *Computers & Chemical Engineering, 28*(12), 2459-2468.

RIVERA, C., FOUCAULT, S., HENICHE, M., ESPINOSA-SOLARES, T., TANGUY, P. A. (2006). Mixing analysis in a coaxial mixer. *Chemical Engineering Science, 61*(9), 2895-2907.

SAAD, Y. (2003). *Iterative methods for sparse linear systems* (2nd ^{e} éd.). Philadelphia: SIAM.

SAKSONO, P. H., DETTMER, W. G., PERIC, D. (2007). An adaptive remeshing strategy for flows with moving boundaries and fluid-structure interaction. *International Journal for Numerical Methods in Engineering, 71*(9), 1009-1050.

SMITH, G. D. (1985). *Numerical Solution of Partial Differential Equations: Finite Difference Methods* (2nd^e éd.). Oxford: Clarendon Press.

SOULAIEMANI, A., FORTIN, M., DHATT, G., OUELLET, Y. (1991). Finite element simulation of two- and three-dimesional free surface flows. *Computer Methods in Applied Mechanics and Engineering, 86*(3), 265-296.

STEGER, J. L., DOUGHERTY, F. C., BENEK, J. A. (1983). Chimera grid scheme. *Houston* (Vol. 5, pp. 59-69)ASME.

STOBIAC, V., HENICHE, M., DEVALS, C., BERTRAND, F., TANGUY, P. (2008). A mapping method based on Gaussian quadrature: Application to viscous mixing. *Chemical Engineering Research and Design, 86*(12), 1410-1422.

TAKEDA, H., NARASAKI, K., KITAJIMA, H., SUDOH, S., ONOFUSA, M., IGUCHI, S. (1993). Numerical simulation of mixing flows in agitated vessels with impellers and baffles. *Computers and Fluids, 22*(2-3), 223-228.

TANGUY, P. A., LACROIX, R., BERTRAND, F., CHOPLIN, L., DE LA FUENTE, E. B. (1992). Finite element analysis of viscous mixing with a helical ribbon-screw impeller. *AIChE Journal, 38*(6), 939-944.

TANGUY, P. A., BERTRAND, F., LABRIE, R., BRITO-DE LA FUENTE, E. (1996). Numerical modelling of the mixing of viscoplastic slurries in a twin-blade planetary mixer. *Chemical Engineering Research and Design, 74*(A4), 499-504.

TEZDUYAR, T. E., SATHE, S., STEIN, K. (2006). Solution techniques for the fully discretized equations in computation of fluid-structure interactions with the space-time formulations. *Computer Methods in Applied Mechanics and Engineering, 195*(41-43), 5743-5753.

TUREK, S. (1996). A comparative study of time-stepping techniques for the incompressible Navier-Stokes equations: from fully implicit non-linear schemes to semi-implicit projection methods. *International Journal for Numerical Methods in Fluids, 22*(10), 987-1011.

VAN LOON, R., ANDERSON, P. D., DE HART, J., BAAIJENS, F. P. T. (2004). A combined fictitious domain/adaptive meshing method for fluid-structure interaction in heart valves. *International Journal for Numerical Methods in Fluids, 46*(5), 533-544.

WECHSLER, K., BREUER, M., DURST, F. (1999). Steady and unsteady computations of turbulent flows induced by a 4/45 pitched-blade impeller. *Journal of Fluids Engineering, Transactions of the ASME, 121*(2), 318-329.

YOTOV, I. (1996). *Mixed finite element method for flow in porous media.* Ph. D. thesis inédit, Rice University, Houston.

ZHANG, L., GERSTENBERGER, A., WANG, X., LIU, W. K. (2004). Immersed finite element method. *Computer Methods in Applied Mechanics and Engineering, 193*(21-22), 2051-2067.

Chapter 7. Finite element modeling of the laminar and transition flow of the Superblend dual shaft coaxial mixer on parallel computers

Authors: Christian A. Rivera[1], Mourad Heniche[1], Katsuhide Takenaka[2] and Philippe A. Tanguy[1]

[1] *Research Unit for Industrial Flows Processes (URPEI)*
Department of Chemical Engineering, École Polytechnique Montreal, Canada

[2] *Sumitomo Heavy Industries Inc., Allentown, USA*

7.1. Presentation of the article

This article was submitted to Chemical Engineering Science. It shows the application of the developed parallel algorithms for the study of a complex mixing tank with two agitators. A characterization based on the obtained hydrodynamics is presented.

7.2. Abstract

The macro-mixing mechanisms of the Superblend coaxial mixer consisting of a Maxblend impeller and a double helical ribbon agitator mounted on two independent coaxial shafts rotating at different speeds are numerically investigated. The simulations are based on the resolution of the Navier-Stokes equations with the help of a parallel three-dimensional finite element solver exploiting the capabilities of high-performance computers. To model the rotation of agitators a hybrid approach based on a novel finite element sliding mesh and a fictitious domain method is used. The simulations allow observing the flow as it evolves from deep laminar (Re=0.1) to transition (Re=520) regime. The power consumption and mixing times obtained from the simulations show good agreement with the ones acquired from a laboratory pilot rig.

7.3. Introduction

The mixing of fluids in stirred tanks is widespread in several industrial processes. Classical examples are polymerization, fermentation, and blending of mineral slurries.

The selection of a mixer for these processes is critical to the success of the mixing operation. It has to be versatile enough to achieve good homogeneity in any region of the flow spectrum, namely; laminar, transition and turbulent regimes. Conventional mixing technologies is unable to provide a satisfactory solution. Standard mixer designs based on turbines, paddles or hydrofoils mounted on a single shaft at the center of the tank are incapable to promote enough mixing for high viscous fluids, on the other hand, close clearance impellers which are very efficient in deep laminar regime perform poorly for medium (10 to 0.5 Pa s) and low viscosity fluids (less than 0.5 Pa s). One alternative is to change the impeller during the process which is rather costly, inefficient, and sometimes unsafe.

A more promising option is the use of multiple impellers. The judicious combination of agitators may deliver a mixing unit capable to adapt to the changing process requirements with minimum modifications. The most common form of multiple impellers system is the case of several turbines stacked on a single shaft. This arrangement is widely found in multiphase system where gas or solids are dispersed. However, as shown numerically in the work of ZALC et al. (2002) when viscosity rises, regions with poor mixing are formed. To handle though mixing processes several unconventional designs have been proposed based on multiple shafts. MARUKO and KUSUMOTO (1992) have presented a dual shaft lattice-type horizontal agitator in a polymerization reactor for handle fluid viscosities of 5 kPa s. TANGUY et al. (1999) employed a planetary mixer where multiple kneading paddles are mounted on carousel

to process polyurethane composites. SCHAFFER et al. (2001) designed a reactor with two co-rotating helical impellers mounted on dual shaft in a tank that was build from two intersecting cylinders for melt-phase polymerization. KHOPKAR et al. (2007) and BARAR POUR et al. (2007) studied the mixing performance of a dual shaft mixers based on a twisted anchor and an off-centered rotor-stator turbine.

An interesting technology due to its wide range of applicability is the dual shaft coaxial mixer as pointed out by RIVERA et al. (2006). It is based on the combination of a high speed agitator and a low-speed close clearance impeller that can be operated either in co- and counter-rotation mode. Recently, a coaxial mixer that combines the wide impeller Maxblend and a double helical ribbon mounted on dual coaxial shafts has been introduced named Superblend. Maxblend is a relative new agitator that consists in a wide paddle that promotes flow circulation and a grid that provides mixing dispersion. Maxblend impeller is characterized by its low energy dissipation, simple geometry making it easy to clean and its capacity of operating over a wide range of Re numbers. Maxblend impeller has been tested for different applications. KOUDA et al. (1997) and HIRUTA et al. (1997) have employed Maxblend in fermentation processes in aerated conditions showing very competitive mass transfer coefficients while keeping the broth culture very well mixed. It has also been employed in TAKAHASHI et al. (2006) in a boiling liquid system with very good results. DOHI et al. (2004) and TAGAWA et al. (2006) found that Maxblend impeller in transition and turbulent regime is more efficient in terms of energy for solid suspension than multiple turbine

systems. In a numerical work, YAO et al. (2001) performed a comparison about the dispersive mixing characteristics of Maxblend and double helical ribbons (DHR). They conclude that while DHR produce good bulk circulation in the tank without strong elongation, Maxblend provides an ideal local dispersive mixing efficiency mainly on the grid part of the impeller, which can induce strong elongation flow. However, Maxblend cannot generate enough circulation in deep laminar regime. These characteristics of the Maxblend have been later confirmed by IRANSHAHI et al. (2007) in an experimental and numerical study. Based on those observations, the combination of Maxblend and a double helical ribbon proposed for Superblend is excellent since double helical ribbons are among the best agitators in deep laminar regime.

Process constraints such as fluid viscosity, heat dissipation, size of the equipment and rheological changes may force the operating conditions to fall in the transition flow regime. Agitated tanks that operate in this regime are typically designed based on extrapolation of information coming from laminar or turbulent regime, whichever is closer to the actual operating conditions. However, the hydrodynamics in transition regime may be considerable different than laminar or turbulent ones. Lack of knowledge of the hydrodynamics in this regime may lead to complications in the control of the process reducing the quality, yield of the final product and sometimes the safety of the process. The accurate numerical modeling of transition flows in agitated tanks is still challenging, the main obstacle being the time and memory required to

accurately predict the effect of the convective term ($v \cdot grad\, v$) in the Navier-Stokes equations which cannot be neglected. As Re increases, the flow structures become more complex so that the computational grid needs to be refined to accurately capture the hydrodynamics. Furthermore, geometries like coaxial mixers require locally refined unstructured grids with high aspect ratios to properly represent the geometrical details such as curved, angled shapes and small gaps. Fortunately, the availability of affordable multi-processor makes possible to simulate the transition regime in coaxial mixers. Nevertheless a particular adaptation of the flow solver must be performed. This issue will be discussed later.

The simulation of multiple shaft impellers rotating at different speeds is not easy to handle. Since the impellers rotate at different speeds, the boundary of the fluid problem moves its position at each time step. In this situation, a change in the frame of reference does not help to simplify the equations. TANGUY et al. (1997) have presented the three-dimensional simulation of the laminar non-Newtonian fluid flow (Re<10) in a coaxial mixer composed of a flat-blade and a helical ribbon by means of the virtual finite element method described in BERTRAND et al. (1997). THIBAULT and TANGUY (2002) and RIVERA et al. (2006) have used the same technique to reproduce the motion of impellers in turbine-anchor coaxial mixers. RUDOLPH et al. (2007) modelled the flow in a coaxial mixer composed of an anchor and a dual set of centered open impellers with help of finite volume sliding mesh technique using three rotating grid zones, one for each impeller.

The objective of this work is to numerically model the flow in the Superblend coaxial to understand the fluid mechanics in the vessel, the interaction between impellers and the macro-mixing mechanism produced when the flow evolves from deep laminar to transition regime. The effect of rotation mode between agitators, co-rotating or counter-rotating, is highlighted herein. A parallel solver based on finite element domain decomposition techniques is used to speed-up the computations. The impellers motion is modeled by the combination of two techniques. The Maxblend agitator motion is taken into account with help of a finite element sliding mesh technique while for the DHR we resort to the virtual finite element method of BERTRAND et al. (1997). The results are validated with experimental data obtained from a pilot rig.

The organization of the paper is as follows: in section 7.4 the Superblend coaxial mixer is presented and the operational conditions studied. In section 3 the numerical model is presented where the motion of the agitators, the parallelization procedure and the discretization of the convective term are described. Section 4 contains the hydrodynamics characterization of the Superblend mixer for co- and counter-rotation modes with special emphasis on the power consumption, flow patterns, pumping rates, shearing and the effect of the Reynolds number in these parameters. In Section 5 a tracer is dispersed by the flow in order to understand the mixing mechanism and determine a numerical mixing time. Finally, in section 6 the efficiency of the mixer is evaluated with help of the mixing energy.

7.4. Superblend coaxial mixer configuration

A Superblend coaxial mixer with capacity of 40 L. is considered in this work. It is composed of a Maxblend and a DHR mounted on independent shafts. The dimensions of the impellers and tank are detailed in Figure 7-1. The rotation velocity of the Maxblend and DHR agitators was set to 100 RPM and 25 RPM, respectively. Newtonian fluids with viscosities in the range from 0.25 to 1400 Pas and densities between 1200 to 1450 kg/m^3 were used as working fluids. Co-rotating and counter-rotating modes were investigated assuming the Maxblend agitator to rotate clockwise while the DHR rotates both clockwise and counter-clockwise.

Figure 7-1: Superblend dual shaft coaxial mixer geometrical dimensions in millimetres (Sumitomo Heavy Industries).

7.5. Numerical model

In this section we present the numerical model based on a parallel fictitious domain and sliding mesh methods. As depicted in Figure 7-2, the sliding partition contains the Maxblend impeller and the fictitious domain method is employed to mimic the helical ribbon.
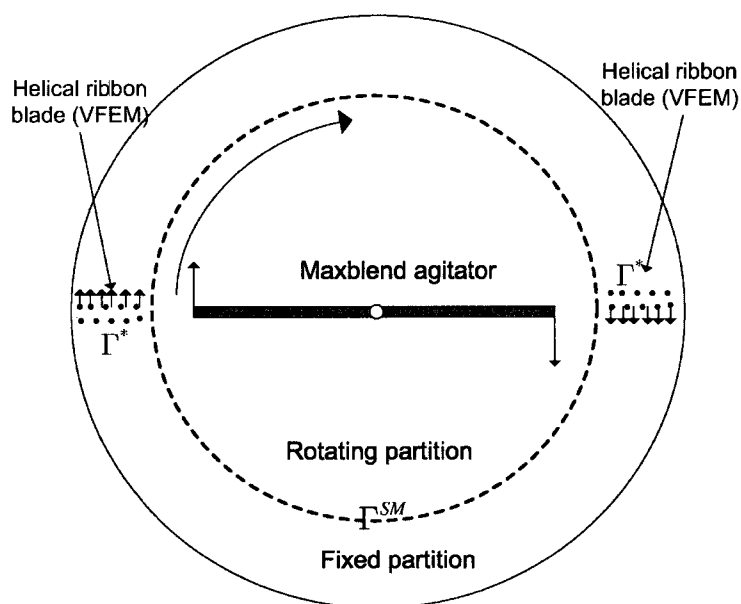
Figure 7-2: Domain partitioning for sliding mesh and control points for VFEM used to reproduce the motion of Maxblend and helical ribbon agitators.

7.5.1. Finite element approximation of the Navier-Stokes equations

Let us consider that the incompressible fluid flow in a stirred tank is governed by the Navier-Stokes equations expressed in the arbitrary Lagrangian-Eulerian (ALE) weighted integral formulation, namely:

$$\int_{\Omega_i} \varphi \cdot \left(\rho \left(\dot{\mathbf{v}} + (\mathbf{v} - \mathbf{v}_m) \cdot \operatorname{grad} \mathbf{v} \right) + \operatorname{div} \boldsymbol{\tau} + \operatorname{grad} p \right) d\Omega_i = 0 \tag{7.1}$$

$$\int_{\Omega_i} \psi \cdot \operatorname{div} \mathbf{v} \, d\Omega_i = 0 \tag{7.2}$$

where for Newtonian fluids:

$$\boldsymbol{\tau} = \mu \dot{\boldsymbol{\gamma}} \tag{7.3}$$

$$\dot{\boldsymbol{\gamma}} = \frac{1}{2} \left(\nabla \mathbf{v} + (\nabla \mathbf{v})^T \right) \tag{7.4}$$

where $\mathbf{v}$ stands for the velocity, $\mathbf{v}_m$ the sliding partition velocity, $\dot{\mathbf{v}}$ the velocity time derivate, p the pressure, μ the Newtonian viscosity, ρ the fluid density, φ and ψ the shape functions for the velocity and pressure, respectively. When the mesh does not move ($\mathbf{v}_m = 0$) the standard formulation is obtained. In this work we have approximated the above equations by means of the finite element method due to its robustness and accuracy to handle complex geometries on unstructured grids.

Unstructured three-dimensional tetrahedral meshes have been utilized. The number of elements and nodes has been varied depending on the flow conditions and summarized in

Table **7-1**. The 9-node tetrahedral finite element P_1^+-P_0 described in BERTRAND et al. (1997) has been chosen to approximate the spatial derivates in (7.1) and (7.2). It belongs to the class of discontinuous pressure elements that satisfies the Babuska-Brezzi-Ladyzhenskaya (BBL) condition that guarantees numerical stability. The grids are generated utilizing elements with a maximum edge size of 0.4 mm near the high speed impeller to avoid high mesh Peclet numbers that could cause solution procedure instabilities as pointed out by ZIENKIEWICZ and TAYLOR (2000).

Table 7-1: Number of elements and nodes utilized for each Re interval.

Name	Re range	Number of elements	Number of nodes	Avg. mesh size (mm)
Mesh 1	0.1-130	492, 727	1,458,057	4.45
Mesh 2	260-520	1,210,508	3,863,664	3.29

Since the flow is unsteady due the impellers rotation, the transient term ($\dot{v}$) in the Navier-Stokes equations is not zero. An implicit method second order accurate is used to discretize the transient term as first proposed by GEAR (1971). The number of time steps per Maxblend revolution for each condition is summarized in Table 7-2.

Table 7-2: Number of time steps per Maxblend revolution and time step size employed

for each Re interval.

Re range	Number of time steps /Maxblend revolution	Time step size (s)
0.1-65	20	0.030
130-260	100	0.006
520	200	0.003

7.5.2. Treatment of convection dominated flows

As the Reynolds number increases, the convective term in the Navier-Stokes equations is no longer negligible and the system of equations becomes nonlinear on the velocity. One way to handle such type of problems is by means of the Newton-Raphson scheme. A different way to deal with the convection term is based on semi-implicit schemes presented by TUREK (1996) where the convection term is linearized by extrapolation in time. Semi-implicit treatment of the convective term permits solving linearized problems at each time step; however, the accuracy depends on the size of the time step. In this work, the fully implicit Newton-Raphson scheme was used for low Reynolds numbers (Re<100) and the semi-implicit scheme for higher Reynolds numbers (Re>100). In the fully implicit Newton-Raphson scheme the convective term is discretized from:

$$\mathbf{v}^{t+1} \cdot \text{grad } \mathbf{v}^{t+1} \qquad\qquad (7.5)$$

In the semi-implicit scheme presented by TUREK (1996) the convection term is linearized by extrapolation in time as:

$$\mathbf{v}^{t} \cdot \text{grad } \mathbf{v}^{t+1} \qquad\qquad (7.6)$$

where the superscript t stands for time step. No turbulence model was used in any of the simulations since for stirred tanks operating in the lower part of the transition regime (Re < 1000) it is much better in terms of accuracy to resort to small grid sizes as evidenced in other works such as ZALC et al. (2001), BARTELS et al. (2002) and KELLY and GIGAS (2003).

7.5.3. Motion of agitators

A finite element sliding mesh (SM) approach was used to reproduce the motion of the Maxblend. Sliding mesh is a very popular technique in the finite volume framework. It consists in dividing the computational grid into two parts: one remains fixed ($\mathbf{v}_m = 0$) and the other one rotates at the speed of the impeller agitator ($\mathbf{v}_m \neq 0$). A critical issue of the methodology is to ensure that both the velocity field and the mass fluxes are unique across the stationary-rotating interface (Γ^{SM}) which guarantees mass conservation. In order to fulfill these conditions in the formulation (7.1) and (7.2),

Lagrange multipliers constraints λ^{SM} are distributed on the interpolation nodes of the interface (Γ^{SM}) of the stationary grid (See Figure 7-2).

The virtual finite element method (VFEM) was first employed to reproduce the motion of the double helical ribbon. Originally it was used to avoid the difficulties in meshing in the small gap between the helical ribbon and the tank wall that a SM technique would require. VFEM is a very flexible approach based on fictitious domain methods that enables to model complex motion of objects immersed in a computational domain. The reader is referred to GLOWINSKI et al. (1994) and BERTRAND et al. (1997) for a complete description of the method. Briefly, it consists in enforcing impeller kinematics through a collocation method. Lagrange multipliers (λ^* for VFEM) are then introduced to impose the velocity field (v^*) over the agitator surface (Γ^*) (See Figure 7-2). At each time step, the position of the agitator surface (Γ^*) is updated and a new fluid flow solution is calculated.

7.5.4. Parallel fictitious domain–sliding mesh solver

A total of 4.4M and 13.5M equations are obtained from the discretization of the equations of change on mesh1 and mesh2, respectively. To speed-up the run, a parallel computing approach based on non-overlapping domain decomposition is used. It consists in partitioning the mesh into several subgrids interconnected through interfaces. A spectral partitioning scheme included in Chaco software of

HENDRIKSON and LELAND (1993) is employed to partition the mesh. To respect the

SM interface, the parallel partitioning strategy is performed in a segregated manner: the

stationary subgrid is partitioned independently of the moving subdomain (Figure 7-3).

Stationary partitions   **Rotating partitions**
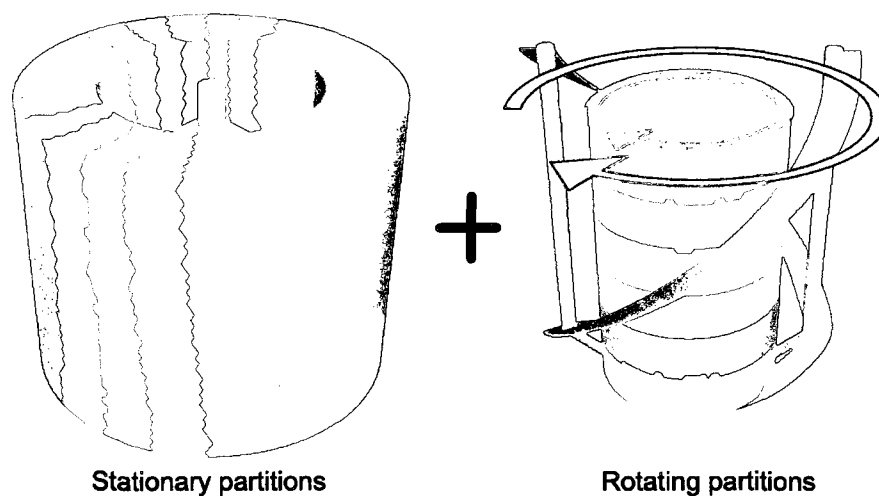
Figure 7-3: Domain decomposition of the Superblend coaxial mixer: 10 partitions for

stationary subdomains and 6 partitions for rotating subdomains.

Lagrange multipliers constraints are applied at these interfaces to ensure the continuity

of the finite element solution. A high performance 16-processor 64 GB shared memory

IBM P690 machine is used to perform the calculations. For each hydrodynamic

scenario run, the number of processors employed and their corresponding CPU time are

summarized in Table 7-3.

Table 7-3: Amount of processors, number of partitions in stationary/rotating

subdomains and CPU time per time step.

Re range	Number of processors	Number partitions stationary subdomain	Number partitions in rotating subdomain	CPU time per time step (min.)
0.1-130	12	8	4	12.28
260-520	16	10	6	18.45

7.6. Hydrodynamics in Superblend coaxial mixer

7.6.1. Power consumption

In order to take into account the motion of both impellers, the Reynolds number is modified according to FARHAT et al. (2008):

$$Re = \frac{\rho N_c D_i^2}{\mu} \qquad (7.7)$$

where N_c is a characteristic speed defined for this type of mixing system as:

$$N_c = \frac{(N_o D_o + N_i D_i)}{D_i} \qquad (7.8)$$

where N_i and D_i are respectively the speed and the diameter of the inner impeller (Maxblend),; and N_o and D_o are respectively the speed and the diameter of the outer

impeller (helical ribbon), respectively. The corresponding power number of the Superblend is expressed as follows:

$$N_p = \frac{P}{\rho(N_i D_i + N_o D_o)^3 D_i^2}$$ (7.9)

From the simulated hydrodynamics scenarios, the power consumption (P) is computed by:

$$P = \int_\Omega \tau : \dot{\gamma} d\Omega$$ (7.10)

Figure 7-4 shows a good agreement between the computed power consumption and the experimental measurements of FARHAT et al. (2008). At low Re (<10) the slope of the log-log plot Np-Re is -1 as expected from laminar mixing theory. From

Figure 7-4, one obtains the following Kp power number values: in co-rotation mode:

$$Kp = Np \times Re = 112.01$$ (7.11)

and in counter-rotation mode:

$$Kp = Np \times Re = 143.11$$ (7.12)
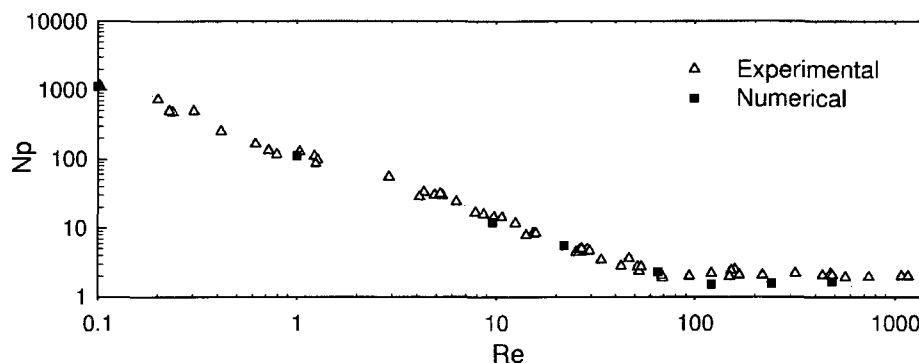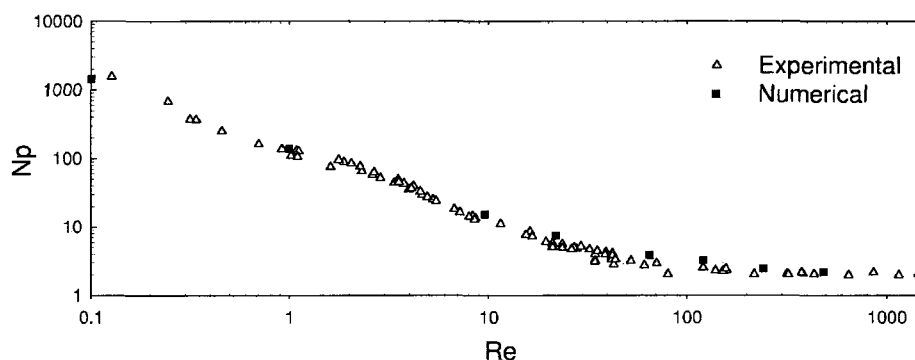
Figure 7-4: Power consumption curves of the Superblend: a) co-rotation mode, b)

counter-rotation mode.

Figure 7-4 reveals that the transition flow regime for the Superblend mixer starts at Re>10. Let us remind that the Re number value at which transition regime starts coincides with the fact that the slope of the power master curve departs from the theoretical value of -1. The values of power consumption obtained from the simulations showed that in the laminar and the transition regimes (Re<500) the power consumption

in counter-rotation mode is systematically higher than the one required in co-rotation mode.

7.6.2. Flow pattern transitions

Figure 7-5 shows the axial pumping over four planes along the height of the tank for both studied rotating modes. Co-rotation mode exhibits an upward flow at the vessel wall that becomes downward near the shaft. The opposite trend is observed for counter-rotation mode where the flow goes downward close to the wall and upward in the vicinity of the shaft.

Velocity[Z]

1.000e-01
5.000e-02
0.000e+00
-5.000e-02
-1.000e-01

a)   b)
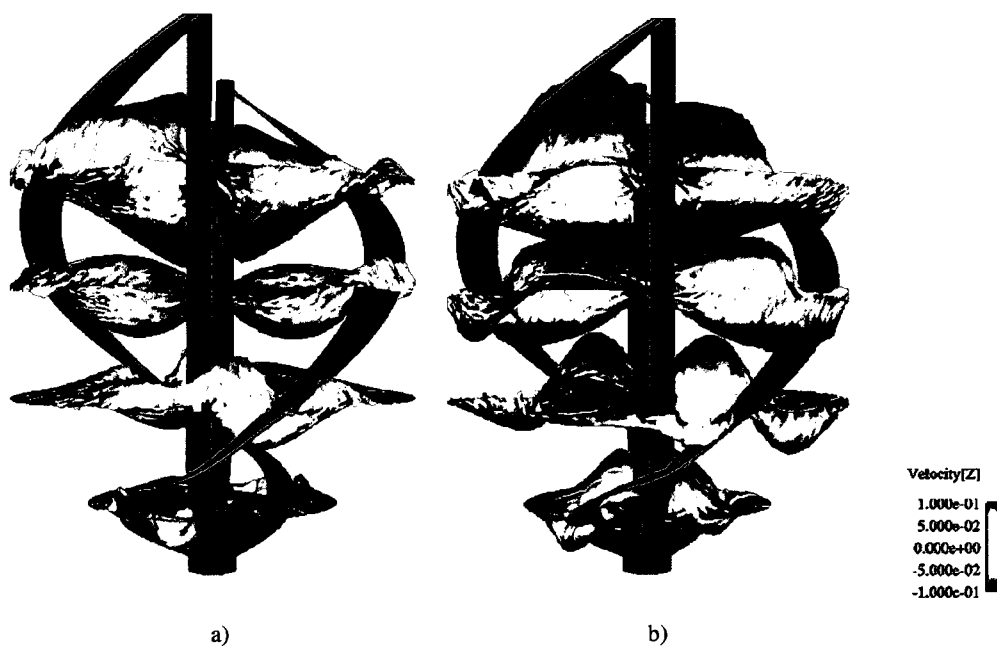
Figure 7-5: Axial flow over four planes at Re=0.1: a) co-rotation mode, b) counter-rotation mode.

Figure 7-6a presents the flow patterns in co-rotation mode projected over a vertical cross-section at the middle of the tank for different Reynolds numbers. In deep laminar regime (Re=0.1-1), the flow pattern remains unchanged and consists of a single main circulation loop. For Re=10, the paddle section of the Maxblend generates a second circulation loop at the lower part of the tank. In the Re range from 10 to 130 the lower circulation zone intensifies and the rotation center of the upper loop moves upward. For Re=260, the upper loop is divided into three smaller loops due the passage of the ribbon. For Re=520, an extra circulation loop rises close to the shaft center.
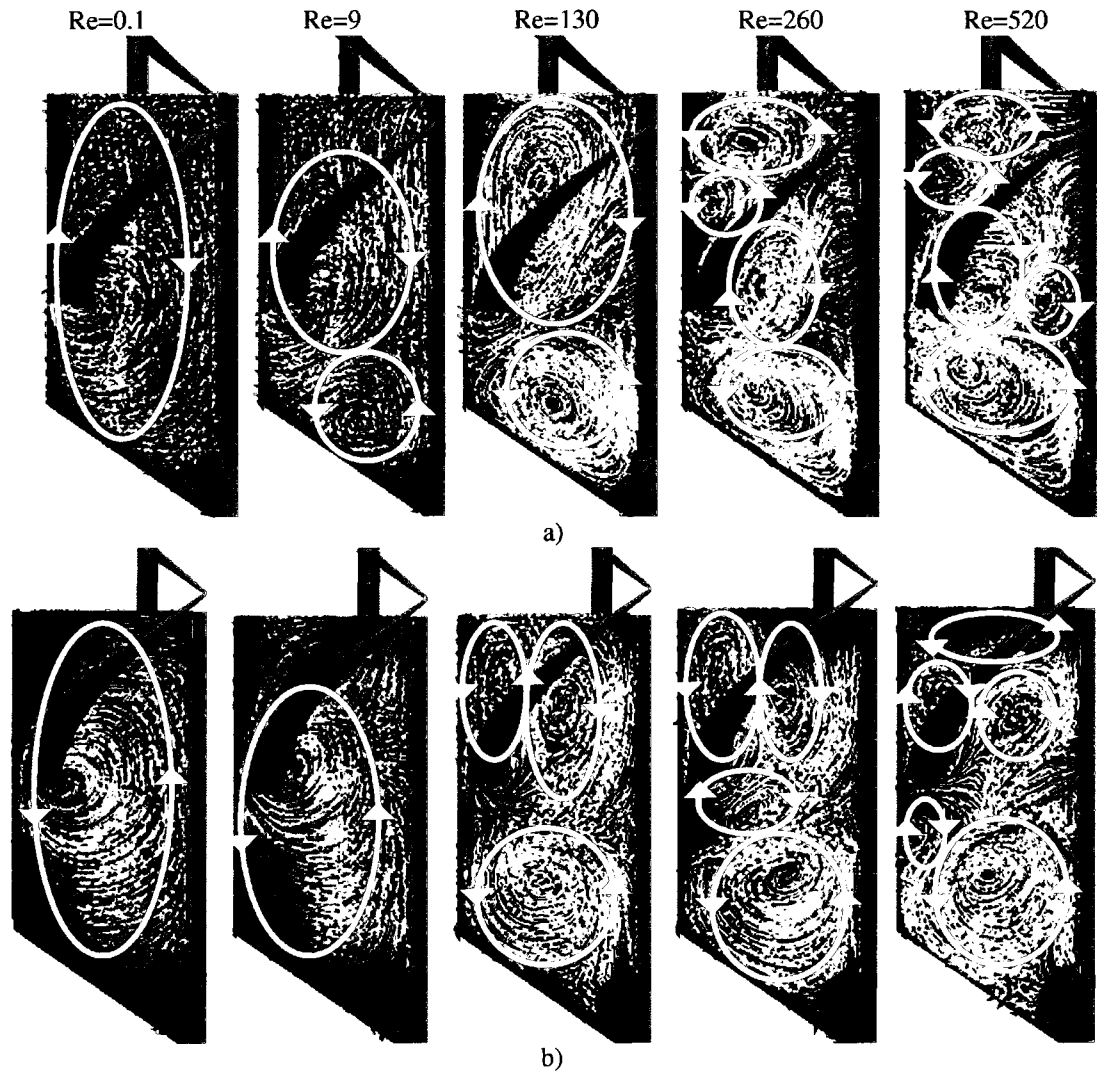
Figure 7-6: The evolution of the instantaneous velocity field projected over a vertical

cross section as Re increases: a) co-rotation mode, b) counter-rotation mode.

Figure 7-6b illustrates the flow patterns for counter-rotation mode. In contrast with the

observations for co-rotation mode, counter-rotation mode does not exhibit a secondary

loop at Re=10. The main effect at this Re with respect to deep laminar regime is a contraction of the primary circulation zone in the upper part of the tank. In the range of Re=10 to 130, the flow patterns changes from a single recirculation loop system to a three-loop one, two above and one below the middle of the vessel. For Re=260, one of the circulation zones positioned at the upper part section of the tank is divided in two circulation zone at the lower part of the ribbon blade. Furthermore, the lower circulation zone is greatly intensified. For Re=520 a small loop is formed at the top the tank.

Figure 7-7 presents the flow streamlines over a cross-section located at 0.25m from the bottom of the tank at four different time steps and Re values operating in counter-rotation mode. The time elapsed between each position in Figure 7-7 is 0.06 s. The presence of many vortices is observed. The number of vortices varies depending of the relative position of the Maxblend with respect to the helical ribbon. In laminar regime, two to six vortices are created in a periodic fashion located in the region between the agitators (Figure 7-7a). As Re increases up to Re = 130, the number of vortices decreases to two, irrespective of the position of the impellers (Figure 7-7b). For Re>130, new vortices are developed close to the wall, at both sides of the ribbon blades as shown in Figure 7-7c due the strong circulation generated by the Maxblend agitator. These high shear vortices explain the larger energy inputs obtained in counter-rotation mode. For all the simulated scenarios, when the agitators co-rotate, no vortices were

observed. The flow is mainly tangential with a radial component that increases according to Re.
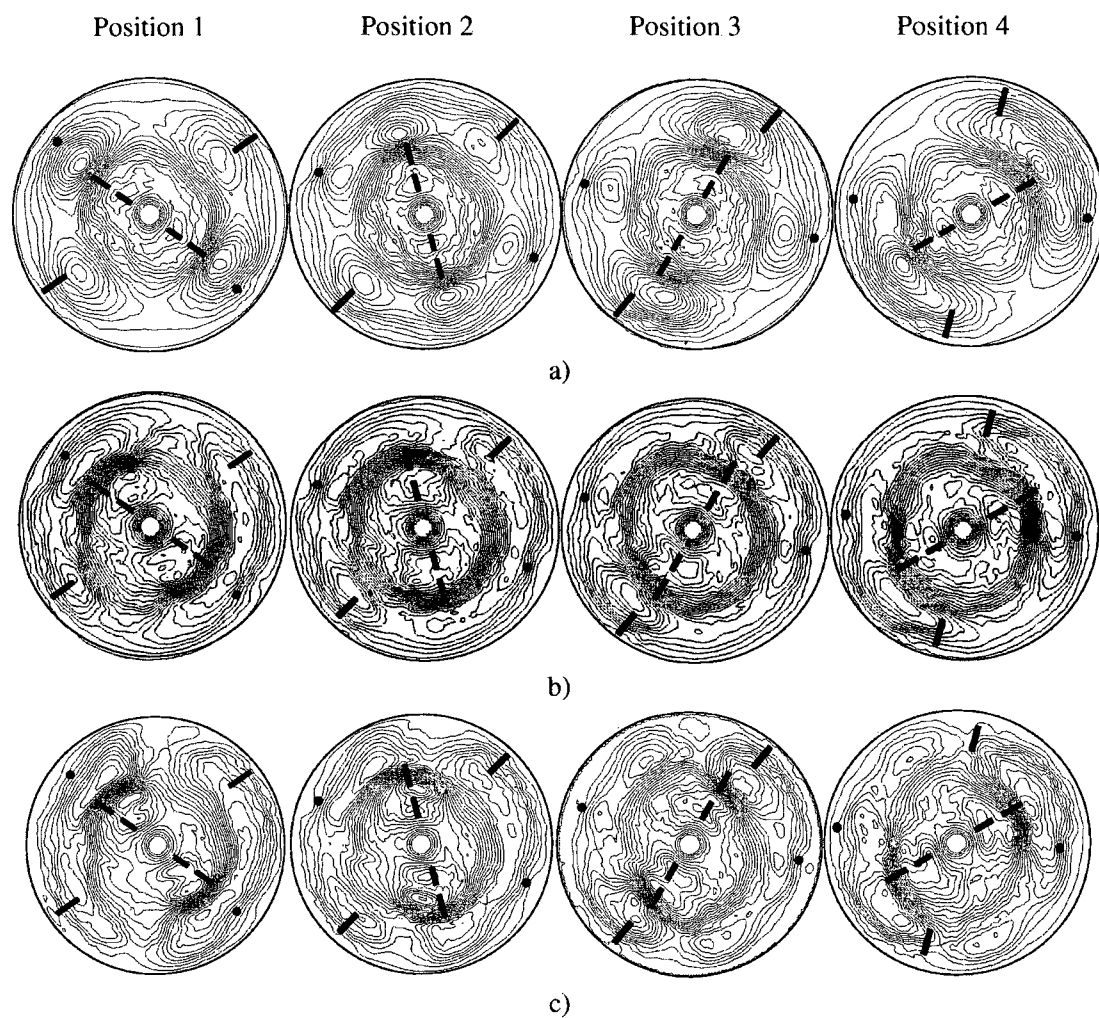
Figure 7-7: Streamlines over a horizontal cross section (time step between position=0.06 s) at the middle of tank for four different time steps: a) Re = 0.1, b) Re = 130, c) Re = 520.

7.6.3.   *Pumping capacity*

Mixing requires suitable amount of pumping in order to achieve a desired degree of homogeneity. For example in bulk polymerization process, a good circulation is required to avoid the formation of hot spots that can damage the quality of the product or degrade the safety of the process. In this work the average radial, tangential and axial pumping capacity has been calculated for both rotation modes with help of 100 cross-sections located at different height of the vessel. We define the pumping number as:

$$Nq_k = \frac{Q_k}{N_c D_i^3} \ , \ k=\theta,r,z \tag{7.13}$$

The total pumping number is obtained from:

$$Nq = \sqrt{Nq_\theta^{\,2} + Nq_r^{\,2} + Nq_z^{\,2}} \tag{7.14}$$

From the calculated values of pumping, averages are computed. Figure 7-8 presents the evolution of total average pumping number ($\overline{Nq}$) for both rotation modes in the Re range 0.1-520. Counter-rotation shows a higher average pumping than co-rotation mode. In laminar regime, $\overline{Nq}$ is constant, being equal to 0.92 in co-rotation mode and 0.93 in counter-rotation mode. In transition flow regime $\overline{Nq}$ increases as Re increases.
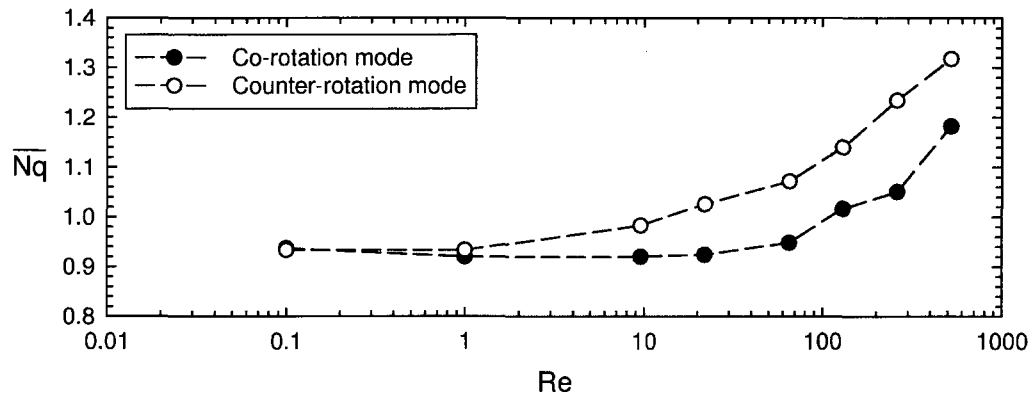
Figure 7-8: Average pumping number ($\overline{Nq}$) with respect to Re for co- and counter-rotation modes.

In the range $0.1 \leq Re \leq 520$ the relation between Re and $\overline{Nq}$ fits in the following correlations:

In co-rotation mode:

$$\overline{Nq} = -2 \times 10^{-7} \, Re^2 + 6 \times 10^{-4} \, Re + 0.9213 \qquad (7.15)$$

and in counter-rotation mode:

$$\overline{Nq} = -2 \times 10^{-6} \, Re^2 + 1.6 \times 10^{-3} \, Re + 0.9578 \qquad (7.16)$$

Figure 7-9 shows the average radial and axial pumping numbers. The average radial pumping exhibits an unusual behaviour in counter-rotation mode; from 0.1 to 1, it is constant with a value of 0.34; in the Re range of 1 to 21, it decreases from 0.34 to 0.23

and between Re=65 to Re=520, it increases again from 0.24 to 0.59. This is a consequence of the growth of the number of vortices in the horizontal cross-section already discussed with respect to Figure 7-7. In the range 0.1 to 260, co-rotation mode shows a slight increase of the radial flow going from 0.15 to 0.20. For Re=520, the radial flow notably increases due the strong jet flow generated by the paddle section of the Maxblend from 0.20 to 0.42.
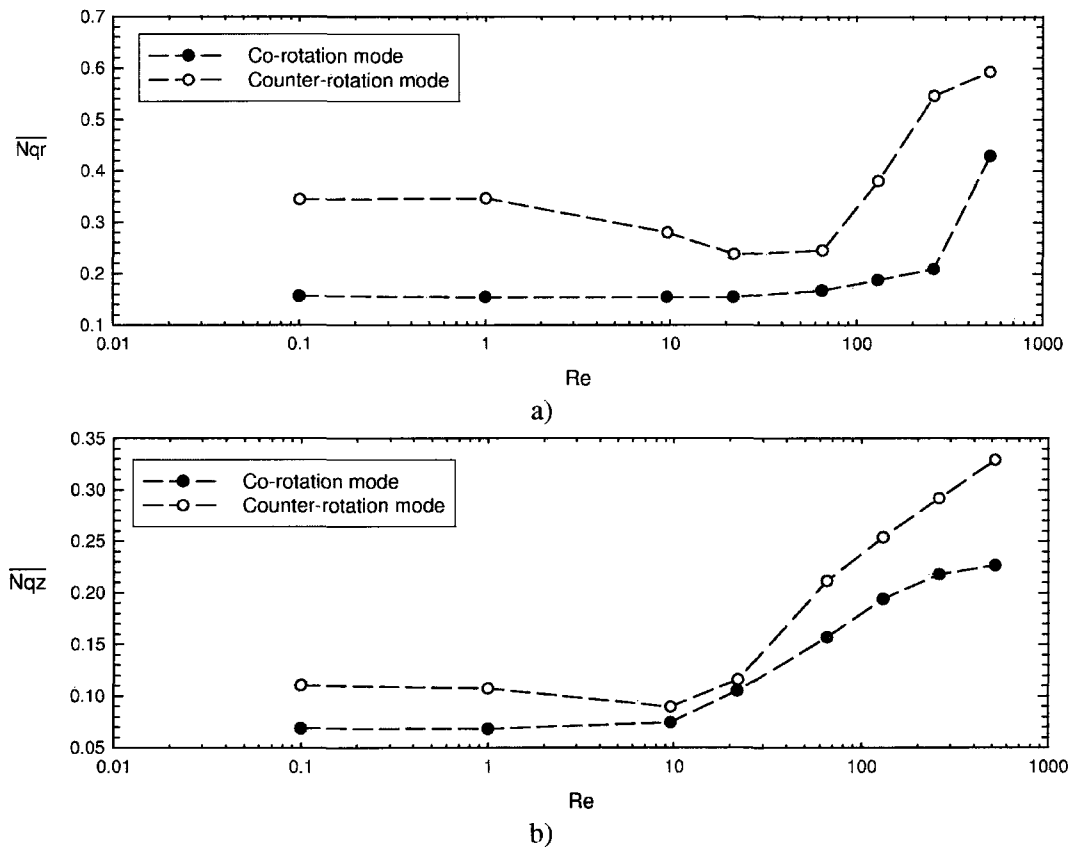
Figure 7-9: Average components of the pumping with respect to Re for co- and counter-rotation modes: a) radial component, b) axial component

With respect to the average axial pumping, the plot shows a constant behaviour in laminar regime for rotating modes, 0.068 for co-rotating mode and 0.11 for counter-rotating mode. In counter-rotating mode there is a slight drop at the beginning of the transition regime (from 0.11 to 0.08) with a constant increase as this regime develops, going from 0.08 to 0.32. It is noted that the average axial circulation for both rotation modes becomes very close at the beginning of transition (Re=10-25). In co-rotation mode the average axial circulation reaches a plateau with a value of 0.21 for Re greater than 260. Figure 7-10a shows the values of axial pumping along the vessel height in co-rotation mode. It is noted that in laminar regime, the most important axial flow region is in the upper section of the vessel, having its maximum at the position z/H=0.8 which corresponds to the grid part of the Maxblend. In the transition flow regime ($Re \geq 10$), two main axial flow regions that expand as Re increases are formed, one above; located between z/H=1 to 0.42, and the other below positioned between z/H=0-0.42. In transition regime the maximum value of axial flow is found at the upper part of the tank at z/H=0.75.
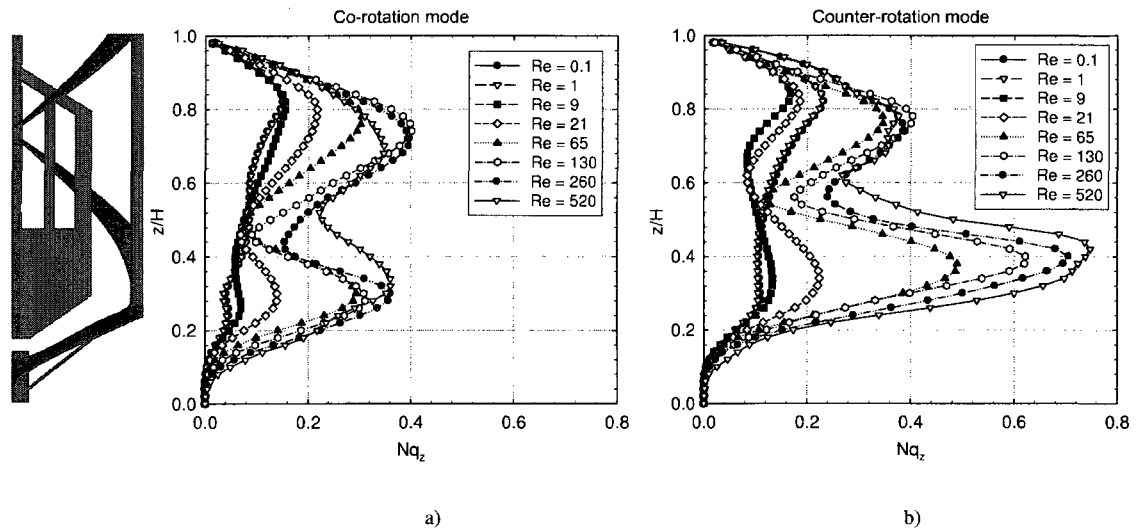
Figure 7-10: Axial pumping along the tank height: a) co-rotation mode, b) counter-rotation mode.

Figure 7-10b presents the axial pumping for counter-rotation mode. In deep laminar regime (Re=0.1 to 1) counter-rotation mode shows a similar trend as co-rotation mode having its maximum at z/H=0.8; however for the transition regime the situation is completely reversed. The main axial flow zone is shifted to the lower part of the tank with a maximum of 0.74 between z/H=0.3 to 0.4, near the paddle zone of the Maxblend. The axial flow on the lower part of the vessel contributes to the larger average axial flow shown for counter-rotation mode in Figure 7-9. Furthermore, the upper axial flow zone is placed between z/H=1 to 0.6 showing a contraction with respect to the situation observed for co-rotation mode. Indeed, careful examination of Figure 7-10 shows that

the zone between z/H=0.1 to 0.6 is where the rotation mode has a significant impact over the axial pumping.

From these results, it is noted that the shape of the Maxblend plays an important role in the flow patterns found in transition regime. The fact that the Maxblend is divided into grid and paddle parts is the main responsible for the creation of the two main axial flow zones observed in Figure 7-6 and Figure 7-10 located at the middle of tank (0.4<z/H<0.6) that coincides with the zone where the impeller changes its shape.

7.6.4.   Deformation rate

For processes as fermentations and emulsions the deformation rate inside a mixer is a key parameter. It affects the quality and the mechanical properties of the end product. In this work we compute an average deformation norm over 100 cross-sections distributed at different height of the vessel for both rotating modes. The deformation norm is obtained by:

$$\|\dot{\gamma}\| = \sqrt{\frac{1}{2}(\dot{\gamma}):(\dot{\gamma})^T}$$

(7.17)

It is possible to define a dimensionless shear number (Ns) as:

$$Ns = \frac{\|\dot{\gamma}\|}{N_c}$$

(7.18)

From the computed Ns values an average $\overline{Ns}$ is calculated. Figure 7-11 presents the variation of $\overline{Ns}$ as Re varies from laminar to transition regime.
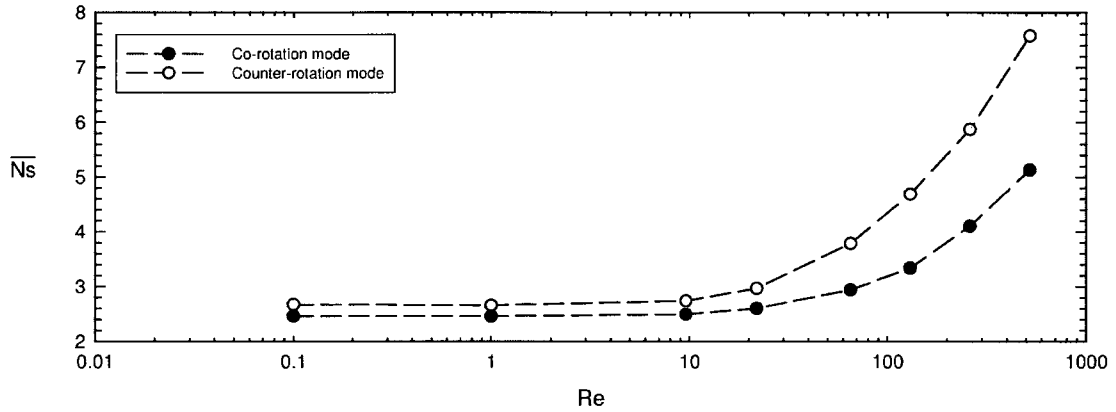
Figure 7-11: Average shear number ($\overline{Ns}$) with respect to Re for co- and counter-rotation modes.

It can be remarked that in any studied scenario the shear is greater in counter-rotation mode than in co-rotation mode, which can be explained by the already discussed vortexing pattern. In the range $0.1 \leq Re \leq 520$ the relation between Ns and Re can be fitted with the following correlations:

In co-rotation mode:

$$\overline{Ns} = -5 \times 10^{-6}\, Re^2 + 8.3 \times 10^{-3}\, Re + 2.437 \qquad (7.19)$$

and in counter-rotation mode:

$$\overline{Ns} = -2 \times 10^{-5}\, Re^2 + 1.78 \times 10^{-2}\, Re + 2.643 \qquad (7.20)$$

Figure 7-12 presents the values of Ns for different locations along the tank height. Co-rotating mode exhibits a homogeneous deformation rate along the tank height. This finding contrasts the localized deformation rates observed in RIVERA et al. (2006) for turbine based coaxial mixers. For counter-rotating mode, the shear rate is almost constant for Re < 10. For Re > 10, Ns remarkably increases and becomes very heterogeneous throughout the vessel. As expected, the shear rate decrease at the bottom of the tank due the low speed of the double helical ribbon.
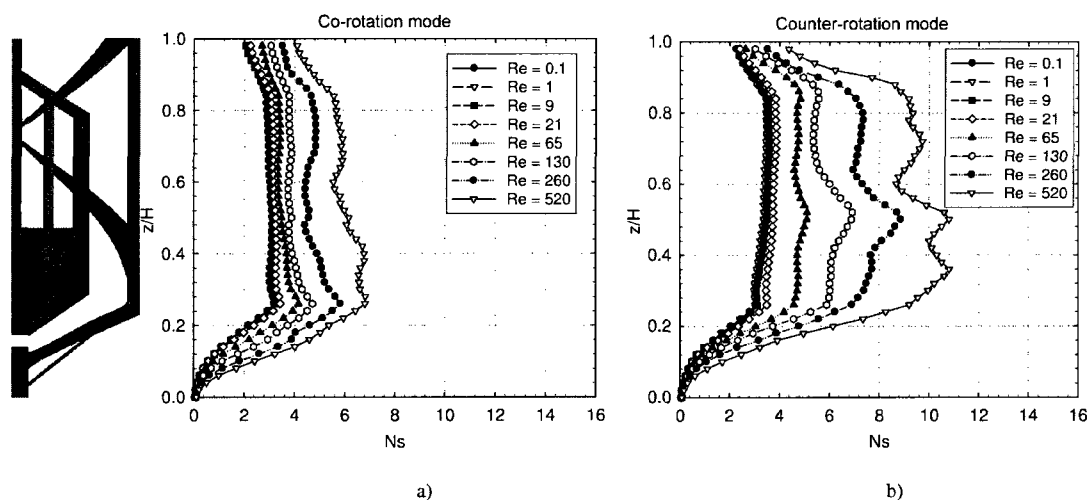
Figure 7-12: Shear number (Ns) along the tank height: a) co-rotation mode, b) counter-rotation mode

The correlations presented in equations (7.19) and (7.20) demonstrate that in the laminar regime the average shear rate is almost constant while in the transition regime, $\overline{Ns}$ strongly depends on Re. This finding has important consequences in the handling of non-Newtonian fluids, where the viscosity is a function of the shear rate distribution

within the tank. It helps to understand why the model proposed by METZNER and OTTO (1957) to estimate the effective shear rate works well in the laminar regime but fails in the transition one. In the transition regime, a model to approximate the shear rate within the tank must consider the three components of the flow (radial, tangential and axial) produced by the agitator and not just the tangential component. Due the flow complexity the development of such model using theoretical or empirical models is not straightforward, showing the utility of high performance CFD modeling for such task.

7.7. Mixing

A passive scalar was dispersed by the flow field into the vessel to determine the mixing time of the simulated scenarios. The simulation is based on the resolution of a pure advection mass transfer equation,

$$\frac{\partial c}{\partial t} + (\mathbf{v} \cdot \nabla c) = 0 \qquad (7.21)$$

where c corresponds to the passive scalar concentration, and $\mathbf{v}$ is the transient velocity field obtained from the simulations. It was assumed that the scalar does not affect the flow hydrodynamics. A Petrov-Galerkin finite element with an implicit second order accurate Gear scheme was used to discretize equation in (7.21). A no flux condition was considered as boundary condition. The injection point was located close to the shaft just below the top of the tank. At each time step, approximately 70K

concentration equations were solved by an iterative solver. The numerical details of the technique can be found in IRANSHAHI et al. (2007). The mixing time was defined as the instant when the coefficient of variation (COV) of the tracer concentration reached an arbitrary value. We recall the COV definition:

$$COV = \frac{s}{\bar{c}} \tag{7.22}$$

where s stands for the standard deviation and $\bar{c}$ the mean concentration of the tracer. The results were validated with help of the mixing times reported in FARHAT et al. (2008) obtained from acid-base decolorization technique. Their experiments show a constant mixing time for Re<5 with a decrease in the Re range 5 to 100. In this interval co-rotation exhibits smaller mixing times than counter-rotation mode. For Re greater than 100 they report that the mixing time is constant and equal for both rotating modes. Figure 7-13 presents a plot of the dimensionless mixing time obtained from our simulations with respect to Re. The numerical results evidence similar trends than the ones observed experimentally. The main discrepancy is attributed to the differences in the determination of the numerical mixing time with respect to colorimetric techniques used in the experimental rig.
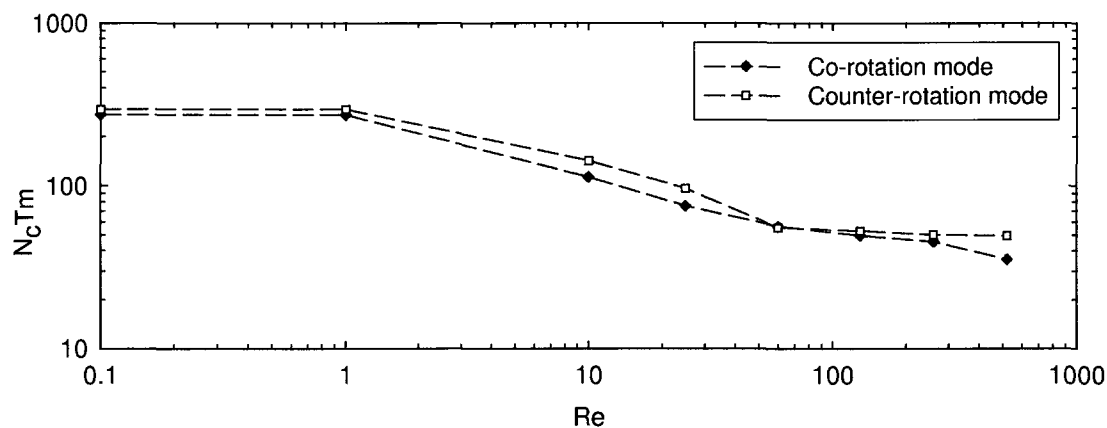
Figure 7-13: Mixing time curves of Superblend for co- and counter-rotation modes.

Figure 7-14 presents the COV evolution for different Re. It is observed that in some cases the COV of counter-rotating mode decreases faster at the beginning of each experiment. As time evolves, co-rotation mode curve intersects the counter-rotating one and finishes earlier.
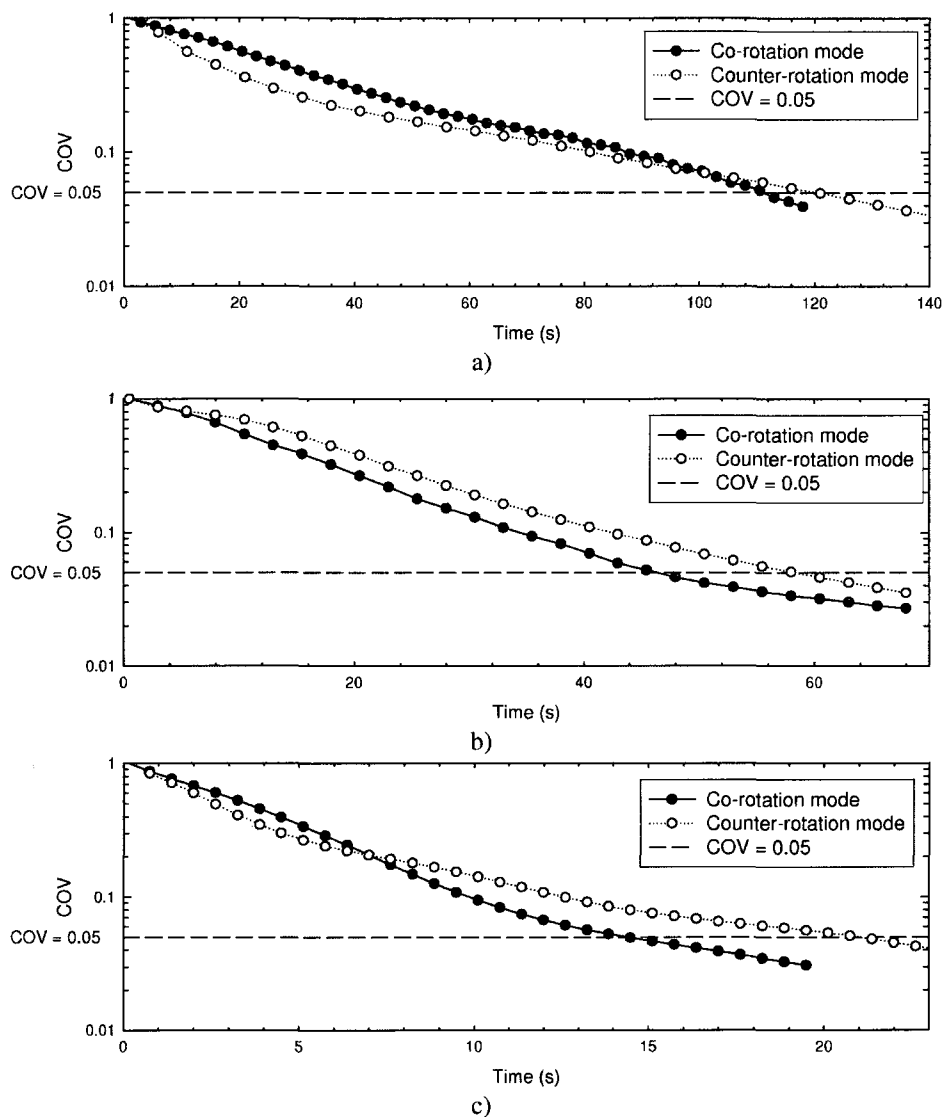
Figure 7-14: Evolution of the coefficient of variation of the tracer concentration (COV)

for co- and counter-rotation mode: a) Re = 0.1, b) Re = 9, c) Re=520.

This phenomenon is explained with help of Figure 7-15 and Figure 7-16 that show

maps of concentration in the vessel at different instants at Re =0.1. For both rotation

modes the mixing mechanism can be divided in two stages. In co-rotation mode the first step consists in the downward pumping of the tracer close to the Maxblend shaft vicinity without much dispersion. In contrast to that, in counter-rotation mode the tracer is pumped in the radial direction towards the wall of the vessel passing by the vortices zone where the radial flow helps to improve dispersion. It is in this stage where the COV of counter-rotation mode is smaller than the one in co-rotation mode. The second part of the mixing begins in co-rotation mode when the tracer reaches the bottom of the tank. There the tracer is pumped upward close to the wall greatly improving its dispersion. On the other hand for counter-rotation mode the process is different. As soon as the tracer reaches the wall, it decays close to the wall in a spiral fashion. Once on the bottom of the tank, the tracer is circulated upward close to the Maxblend shaft. It is during this period that the COV of co-rotation intersects and begins to decrease faster than in counter-rotation mode.
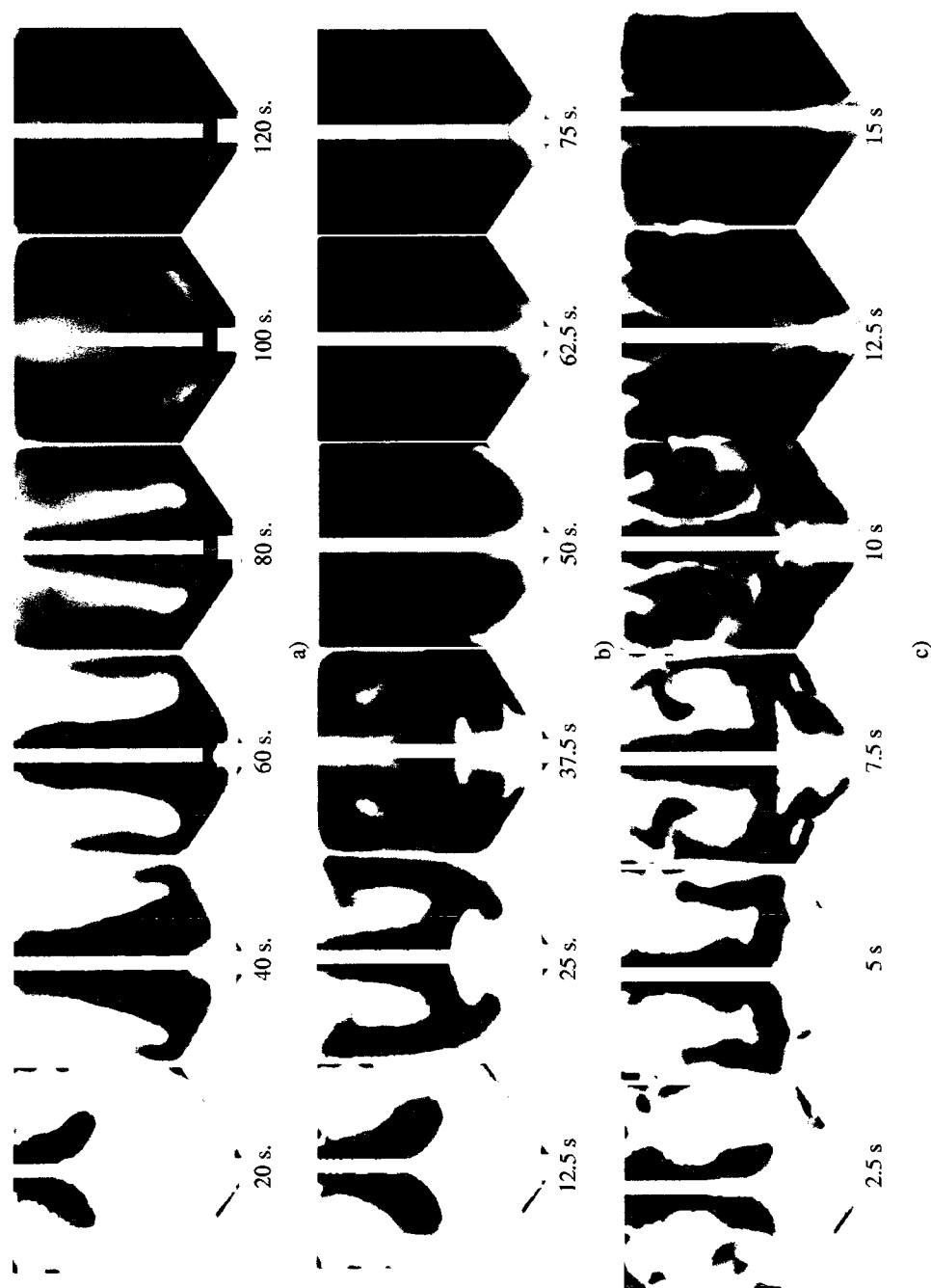
Figure 7-15. Tracer dispersion mechanism in co-rotation mode for different Re

numbers: a) Re = 0.1, b) Re = 9, c) Re = 520.
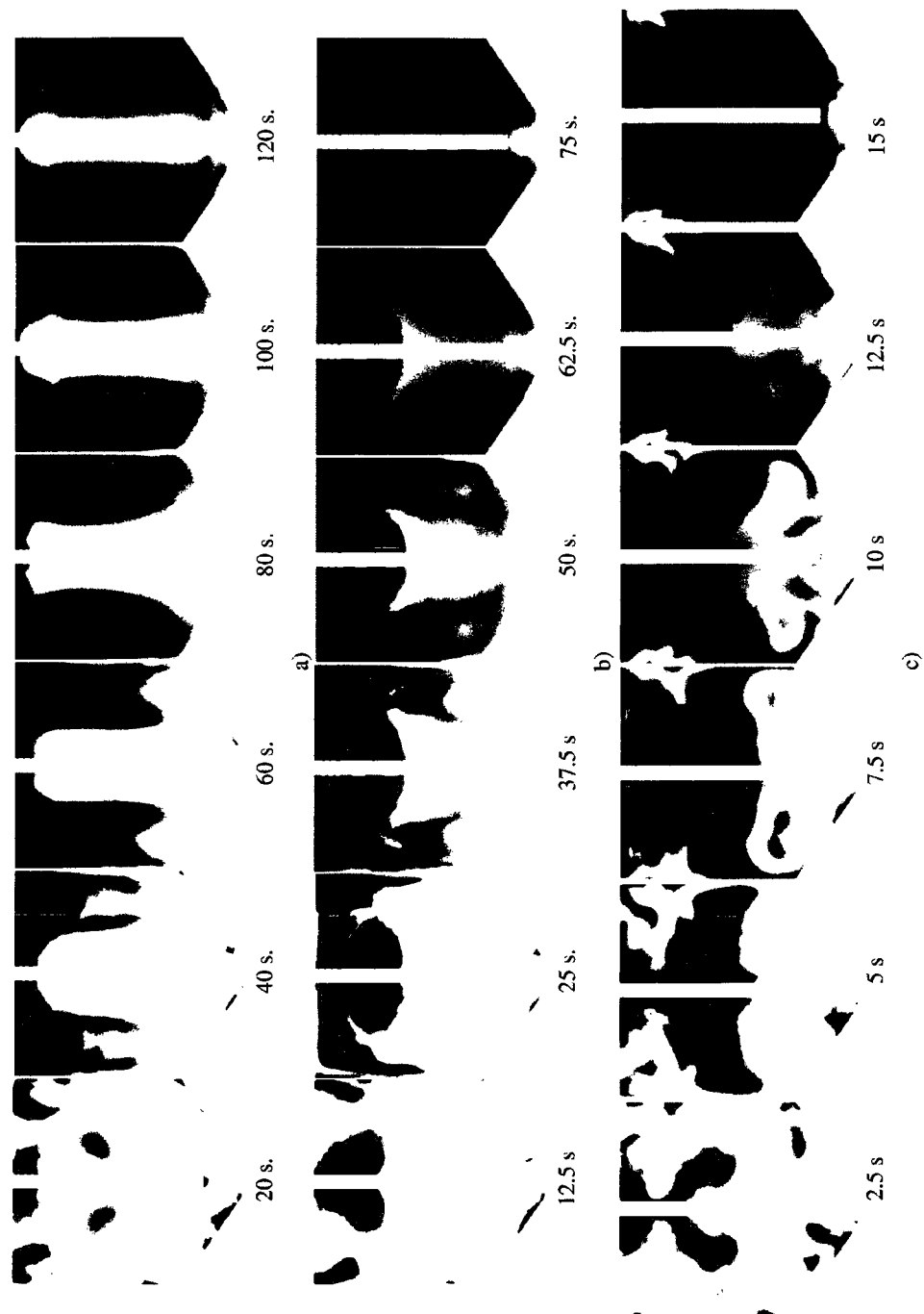
Figure 7-16. Tracer dispersion mechanism in counter-rotation mode for different Re

numbers: a) Re = 0.1, b) Re = 9, c) Re = 520.

It is peculiar that the mixing time for counter-rotation mode is not shorter than co-rotation mode even if counter-rotation creates larger average pumping capacity as already shown in Figure 7-8. Figure 7-15 and Figure 7-16 evidence the dispersion mechanisms. At Re = 9 and 520 it shows that in counter-rotation mode the bottom of the tank region exhibits poor mixing because it remains isolated for the longest period of time. The tracer reaches the button of the tank just at the end of the mixing process, after moving out of the upper zone and going down close the wall. In co-rotation mode such segregation does not exist, the tracer being dispersed with help of recirculation zones, below and above the middle of the tank, which are visualized in the transition regime.

7.8. Mixing efficiency

From the mixing time and power consumption it is possible to compute a mixing energy as:

$$E_{mix} = Np \times Tm \times N_c \tag{7.23}$$

Figure 7-17 presents the obtained mixing energy for both rotation modes in the Re range of 0.1 to 520. As expected co-rotation modes requires less energy than counter-rotation mode in that interval.
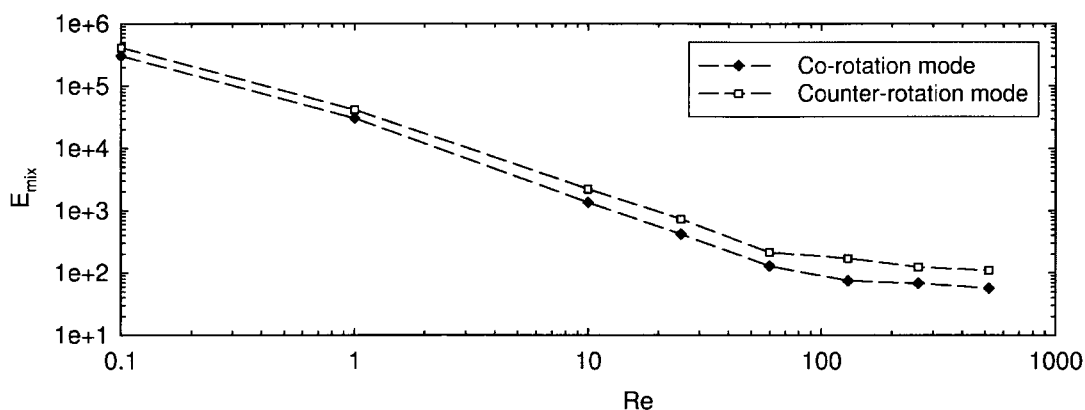
Figure 7-17: Mixing energy curves of the Superblend for co- and counter-rotation modes.

In Figure 7-18 we have plotted the ratio between the average pumping number ($\overline{Nq}$) and the average shear number ($\overline{Ns}$) with respect to the power number Np. The ratio gives an idea of the cost of pumping or shearing, the main parameters to successfully perform the mixing operation. In laminar regime, the ratios are equal in both rotation modes. In transition regime the cost of both variables decreases, co-rotation mode being more energy efficient than counter-rotation mode.
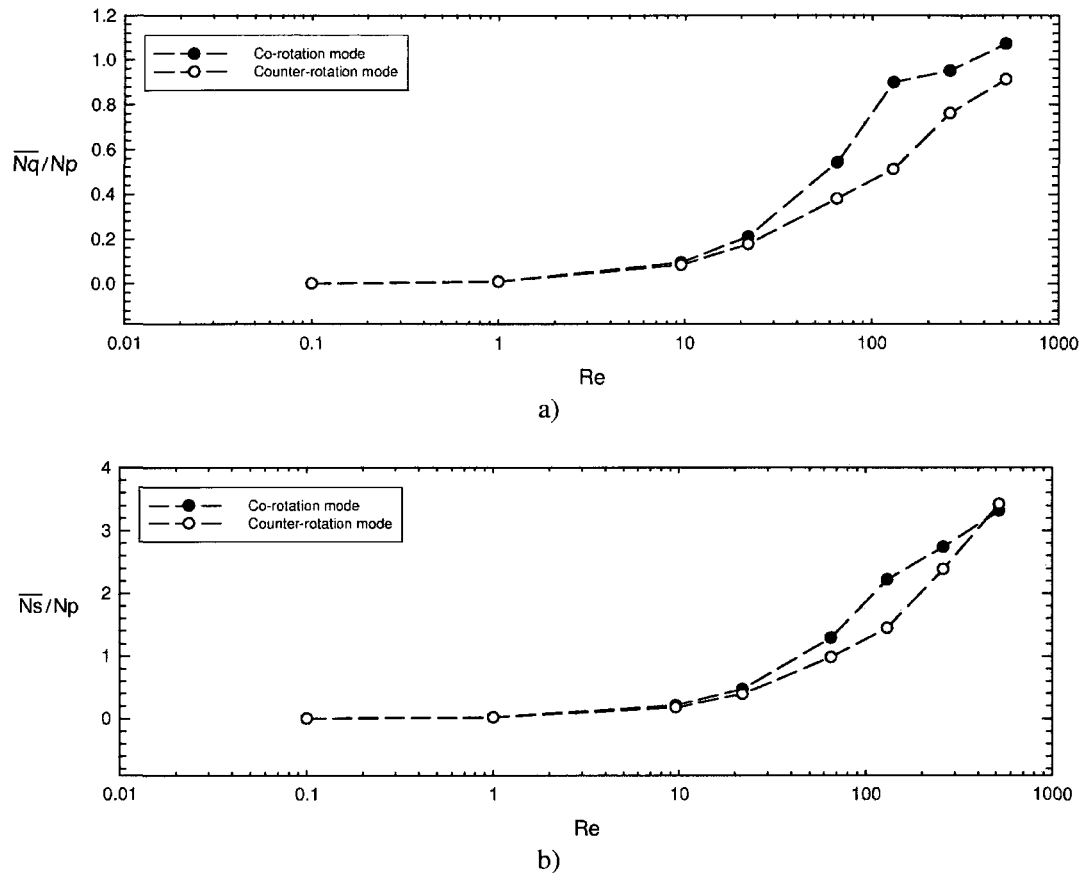
Figure 7-18: Cost of pumping and shearing in co- and counter-rotation modes: a)

$\overline{Nq}/Np$ (pumping cost) b) $\overline{Ns}/Np$ (shearing cost).

7.9. Conclusions

Three-dimensional CFD simulations with unstructured grids comprising 1.4 to 3.8M of nodes of the flow in the Superblend coaxial mixer are presented. A parallel finite element solver is employed to accelerate the computations. To model the rotation of agitators, which rotates at different speeds, a hybrid approach based on the novel finite

element sliding mesh and fictitious domain method is used. The simulations allow observing the flow patterns induced by the Superblend coaxial mixer as the hydrodynamics evolve from deep laminar to transition regime. The flow is characterized by the formation of several recirculation zones above and below the middle of the tank. For counter-rotation mode several vortices that fluctuate in number as agitator move were found over a horizontal cross-section at the middle of tank. This phenomenon is not observed in co-rotation mode. Furthermore, the flow patterns in co-rotation mode show an upward flow at the vessel wall that becomes downward near the shaft. The opposite pattern is observed for counter-rotation mode where the fluid moves downward close to the wall and upward in the proximity of the shaft.

From the values of pumping and shearing along the height of the mixer, it is found that the average pumping and shearing numbers are higher in counter-rotation mode than in co-rotation mode. However, when impeller counter-rotate these variables show a heterogeneous distribution along the height of the tank which contrasts with more homogenous patterns observed in co-rotation mode. Both shearing and pumping numbers show constant values in the laminar regime and an important increase in the transition region. Furthermore it is evidenced that the main effect of rotation mode over the axial pumping is that in co-rotation mode the main axial flow zone is located at the upper part of the vessel, while in counter-rotation mode it is positioned at the lower region of the tank.

In terms of the energy requirements, it is evidenced that co-rotation mode requires less power consumption and exhibits equal or shorter mixing times than counter-rotating mode. The larger power consumption required by counter-rotating mode is caused by the presence of high shear vortices generated between the two coaxial impellers. It is shown that the longer mixing times obtained for the counter-rotation mode are caused by the difficulties of the tracer to reach the most important axial flow zone in the mixer located below the middle of the tank. Finally, based on the mixing energy concept, it is found that the co-rotation mode is more efficient than the counter-rotation mode. The energy cost to pump and shear decreases when impellers co-rotate.

7.10. Acknowledgements

7.11. References

BARAR POUR, S., FRADETTE, L., TANGUY, P. A. (2007). Laminar and slurry blending characteristics of a dual shaft impeller system. *Chemical Engineering Research and Design, 85*(9 A), 1305-1313.

BARTELS, C., BREUER, M., WECHSLER, K., DURST, F. (2002). Computational fluid dynamics applications on parallel-vector computers: computations of stirred vessel flows. *Computers & Fluids, 31*(1), 69-97.

BERTRAND, F., TANGUY, P. A., THIBAULT, F. (1997). A three-dimensional fictitious domain method for incompresible fluid flow problems. *International Journal for Numerical Methods in Fluids, 25*(6), 719-736.

DOHI, N., TAKAHASHI, T., MINEKAWA, K., KAWASE, Y. (2004). Power consumption and solid suspension performance of large-scale impellers in gas-liquid-solid three-phase stirred tank reactors. *Chemical Engineering Journal, 97*(2-3), 103-114.

FARHAT, M., FRADETTE, L., TANGUY, P., HORIGUCHI, H., YATOMI, R. (2008). An investigation of the Superblend mixer. *AIChE annual meeting, Philadelphia.*

GEAR, C. (1971). *Numerical initial value problems in ordinary differential equations.* Englewood Cliffs: Prentice-Hall.

GLOWINSKI, R., PAN, T.-W., PERIAUX, J. (1994). Fictitious domain method for Dirichlet problem and applications. *Computer Methods in Applied Mechanics and Engineering, 111*(3-4), 283-303.

HENDRIKSON, B., LELAND, R. (1993). *The Chaco user guide, version 1.0.* Alburquerque: Sandia Laboratories.

HIRUTA, O., YAMAMURA, K., TAKEBE, H., FUTAMURA, T., IINUMA, K., TANAKA, H. (1997). Application of Maxblend fermentor for microbial processes. *Journal of Fermentation and Bioengineering, 83*(1), 79-86.

IRANSHAHI, A., DEVALS, C., HENICHE, M., FRADETTE, L., TANGUY, P. A., TAKENAKA, K. (2007). Hydrodynamics characterization of the Maxblend impeller. *Chemical Engineering Science, 62*(14), 3641-3653.

KELLY, W., GIGAS, B. (2003). Using CFD to predict the behavior of power law fluids near axial-flow impellers operating in the transitional flow regime. *Chemical Engineering Science, 58*(10), 2141-2152.

KHOPKAR, A. R., FRADETTE, L., TANGUY, P. A. (2007). Hydrodynamics of a dual shaft mixer with Newtonian and non-Newtonian fluids. *Chemical Engineering Research & Design, 85*(A6), 863-871.

KOUDA, T., YANO, H., YOSHINAGA, F. (1997). Effect of agitator configuration on bacterial cellulose productivity in aerated and agitated culture. *Journal of Fermentation and Bioengineering, 83*(4), 371-376.

MARUKO, M., KUSUMOTO, S. (1992). Power consumption characteristics of a lattice-type, twin-shaft, high-viscosity agitator. *International chemical engineering, 32*(4), 759-766.

METZNER, A. B., OTTO, R. E. (1957). Agitation of non-Newtonian fluids. *Chemical Engineering Progress, 3*(1), 3-10.

RIVERA, C., FOUCAULT, S., HENICHE, M., ESPINOSA-SOLARES, T., TANGUY, P. A. (2006). Mixing analysis in a coaxial mixer. *Chemical Engineering Science, 61*(9), 2895-2907.

RIVERA, C. (2009). *Parallel finite element modeling of the hydrodynamics in agitated tanks*. Ph. D. thesis inédit, Ecole Polytechnique de Montreal, Montreal.

RUDOLPH, L., SCHAFER, M., ATIEMO-OBENG, V., KRAUME, M. (2007). Experimental and numerical analysis of power consumption for mixing of high viscosity fluids with a co-axial mixer. *Chemical Engineering Research & Design, 85*(A5), 568-575.

SCHAFFER, M. A., MARCHILDON, E. K., MCAULEY, K. B., CUNNINGHAM, M. F. (2001). Assessment of mixing performance and power consumption of a novel polymerization reactor system. *Chemical Engineering and Technology, 24*(4), 401-408.

TAGAWA, A., DOHI, N., KAWASE, Y. (2006). Dispersion of floating solid particles in aerated stirred tank reactors: Minimum impeller speeds for off-surface and ultimately homogeneous solid suspension and solids concentration profiles. *Industrial and Engineering Chemistry Research, 45*(2), 818-829.

TAKAHASHI, T., TAGAWA, A., ATSUMI, N., DOHI, N., KAWASE, Y. (2006). Liquid-phase mixing time in boiling stirred tank reactors with large cross-section impellers. *Chemical Engineering and Processing, 45*(4), 303-311.

TANGUY, P. A., THIBAULT, F., BRITO-DE LA FUENTE, E., ESPINOSA-SOLARES, T., TECANTE, A. (1997). Mixing performance induced by coaxial flat blade-helical ribbon impellers rotating at different speeds. *Chemical Engineering Science, 52*(11), 1733-1741.

TANGUY, P. A., THIBAULT, F., DUBOIS, C., AIT-KADI, A. (1999). Mixing hydrodynamics in a double planetary mixer. *Chemical Engineering Research and Design, 77*(4), 318-324.

THIBAULT, F., TANGUY, P. A. (2002). Power-draw analysis of a coaxial mixer with Newtonian and non-Newtonian fluids in the laminar regime. *Chemical Engineering Science, 57*(18), 3861-3872.

TUREK, S. (1996). A comparative study of time-stepping techniques for the incompressible Navier-Stokes equations: from fully implicit non-linear schemes to semi-implicit projection methods. *International Journal for Numerical Methods in Fluids, 22*(10), 987-1011.

YAO, W., MISHIMA, M., TAKAHASHI, K. (2001). Numerical investigation on dispersive mixing characteristics of Maxblend and double helical ribbons. *Chemical Engineering Journal, 84*(3), 565-571.

ZALC, J. M., ALVAREZ, M. M., MUZZIO, F. J., ARIK, B. E. (2001). Extensive validation of computed laminar flow in a stirred tank with three Rushton turbines. *AIChE Journal, 47*(10), 2144-2154.

ZALC, J. M., SZALAI, E. S., ALVAREZ, M. M., MUZZIO, F. J. (2002). Using CFD to understand chaotic mixing in laminar stirred tanks. *AIChE Journal, 48*(10), 2124-2134.

Chapter 8.   General discussion and

conclusions

The main objective of this thesis was to develop a finite element algorithm to model the transition flow regime using parallel computers. The work was divided in three parts; the first two steps were devoted to the development of a numerical methodology able to simulate the flow in stirred tanks using parallel computers. The final stage consisted in the application of the proposed strategy for the simulation of an agitated tank in the laminar and the transition flow regime.

8.1.   Parallel finite element solver

In the first stage of the thesis, a parallelization strategy based on domain decomposition was presented. The distinctive characteristics of the proposed numerical methodology are summarized next.

The parallel algorithm was based on a finite element non-overlapping domain decomposition method for the resolution of the Stokes equations. Lagrange multipliers were used to enforce continuity at the boundaries between subdomains. The Lagrange multiplier space was approximated using Dirac functions. This allowed the imposition of the point-wise interface constraint, and therefore eliminating the need to compute the

surface integrals at the parallel boundary. The velocity-pressure-Lagrange multiplier system of equations was solved simultaneously by a distributed memory parallel ILU preconditioned Krylov method which exploits the block structure of the resulting global matrix. A penalty function on the interface constraints equations was introduced to avoid the locking of the ILU factorization algorithm.

The second step was to verify the algorithm in terms of speed-up for two benchmark cases (pipe and cavity flow). These tests were carried out with discontinuous pressure finite element approximations ($P1^+$-P0/$P2^+$-P1) and unstructured tetrahedral grids with different mesh sizes. In this step we found that:

- As the number of partitions increase, the speed-up was not linear due to two factors:

    a. The overhead caused by the lack of an ideal balance load distribution on the processors.

    b. The increment in the number of conjugate gradient iterations required to reach convergence with respect to the number of partitions.

- The speed-up obtained for the pipe flow case was better than the one obtained for the cavity flow case. This was attributed to the fact that in the latter, the number of iterations showed a considerable increase with respect to the number of partitions.

To improve the parallel performance, two factors were studied:

1. the ordering of physical variables (velocity, pressure, Lagrange multipliers)

2. the partitioning strategy

From that study, two important findings were identified:

- There is a specific ordering of the velocity, pressure and Lagrange multiplier variables that consistently gives the lower count of iterations to reach convergence.

- The increase in the number of iterations of this particular algorithm can be controlled by the use of suitable partitioning strategies where the smoothness of the interface and the partition connectivity are key parameters to obtain low iteration counts.

8.2. Parallel sliding mesh technique

The second stage of the project involved the development of a technique capable to take into account the unsteady effects caused by the rotation of the agitators. Sliding mesh technique was chosen due its ability to preserve the exact shape of the moving boundaries. In view of the fact that the parallel solver and the sliding mesh technique are based on domain decomposition methods, it was a good opportunity to re-use the knowledge learned in the first stage of this thesis to formulate a sliding mesh technique based on Lagrange multipliers. Thus, a parallel sliding mesh algorithm for the finite

element simulation of three-dimensional Navier-Stokes equations was developed. As expected, the proposed methodology resembles the one utilized for the parallel solver, i.e., Lagrange multiplier constraints at the subdomain interfaces and parallel Krylov solvers. Nonetheless, extra features needed to be added to the algorithm to deal with the mesh motion (Lagrangian acceleration), and the convective and the unsteady terms in the Navier-Stokes equations. These features are summarized next.

- Due to the fact that in the sliding mesh technique one partition moves with respect to the other, an arbitrary Lagrangian-Eulerian formulation was used.

- To handle the convection, a fully nonlinear Newton-Raphson scheme and the semi-implicit linearization proposed by TUREK (1996) were employed.

- To deal with the unsteady term in the Navier-Stokes equations, a second order accurate implicit Gear scheme was utilized.

The method was validated in the case of concentric cylinders and stirred tank flows, showing excellent accuracy. Based on the results obtained from numerical experiments we found that:

- The sliding mesh technique, in combination with the Newton-Raphson scheme, provides slightly higher accuracy than with the semi-implicit scheme, mainly when large time step sizes are employed. However, the semi-implicit scheme saves considerable amount of CPU time.

- The sliding mesh technique is very stable, converging using large time steps, due to the implicit properties of the Gear time discretization scheme. As

expected, the technique shows a quadratic reduction in the error as the size of the time steps decreases.

- The technique permits to further partition both the sliding and fixed partitions into a desired number of partitions, allowing efficient parallelization.

8.3. Simulation of the hydrodynamics of a stirred tank in the transition regime

Finally, the hydrodynamics and macro-mixing mechanisms of a coaxial mixer composed of a large paddle (Maxblend) impeller and a double helical ribbon agitator mounted on two independent coaxial shafts was numerically investigated. The simulations were based on the resolution of the Navier-Stokes equations using the parallel algorithms. To model the rotation of agitators, which rotates at different speeds, a hybrid approach based on the novel finite element sliding mesh and fictitious domain method was used. The more refined tetrahedral unstructured mesh contained 3.8M nodes yielding 13.5M equations.

The simulations permitted to analyse the flow patterns induced by the Superblend coaxial mixer as the hydrodynamics evolved from deep laminar (Re=0.1) to transition regime (Re=520). The following conclusions were drawn:

- As the Reynolds number increases, several recirculation zones above and below the middle of the tank are formed.

- For counter-rotation mode several vortices that vary in number as the agitators move were found over a horizontal cross-section at the middle of the tank. This phenomenon is not observed in co-rotation mode.

- The flow patterns in co-rotation mode show an upward flow at the vessel wall that becomes downward near the shaft. The opposite pattern is observed in counter-rotation mode where the fluid moves downward close to the wall, and upward in the vicinity of the shaft.

- The average pumping and shearing numbers are higher in counter-rotation mode than in co-rotation mode. However, when the impellers counter-rotate these variables show a heterogeneous distribution along the height of the tank which contrasts with the almost homogenous patterns observed in co-rotation mode.

- Both shearing and pumping numbers show constant values in the laminar regime with an important increase in the transition region. This has important repercussions on the handling on non-Newtonian fluids where the process viscosity depends on the average deformation rate.

- In co-rotation mode, the main axial flow zone is located at the upper part of the vessel, while in counter-rotation mode it is positioned at the lower region of the tank.

- Co-rotation mode requires less power consumption and exhibits equal or shorter mixing times than counter-rotating mode.

- The larger power consumption required by counter-rotating mode is caused by the presence of high shear vortices generated between the two coaxial impellers.

- The longer mixing times obtained for the counter-rotation mode are caused by the difficulties of the tracer to reach the most important axial flow zone in the mixer located below the middle of the tank.

- Co-rotation mode is more efficient than the counter-rotation mode. The energy cost to pump and to shear decreases when the impellers co-rotate.

Chapter 9. Recommendations for future research

9.1. Parallel algorithms

The parallel algorithms developed in this thesis open a window of possibilities for research in fluid mechanics since they allow using higher number of elements or more accurate finite element approximations. CPU time results obtained in this thesis showed encouraging results. Several ideas for future research are given next.

- To verify the parallel solver using massive parallel computing (hundreds or thousands of processors) in order to check the limits of the proposed approach. Furthermore, to explore the effect of the type of machine (shared or distributed memory) on the obtained speed-up.

- To combine the developed parallel solver with multi-grid techniques in view of controlling the increase of iterations with respect to the number of subdomains.

- To extend the domain decomposition method to allow the use of low order continuous pressure finite element approximations such as the MINI element in order to solve problems with larger number of elements.

- To extend the methodology to multi-physics, non-Newtonian and turbulent problems in view of reducing the gap between the presented CFD simulations and industrial conditions.

9.2. Simulation of agitated and the transition flow regime

As shown in the particular example given in this thesis, the hydrodynamics in the transition flow regime are quite different than the laminar ones. Thus, further studies are still required. It is still necessary to characterize the transitional flow of coaxial mixers in the following scenarios:

- Different set of speeds between the inner and outer agitators.

- Include the effect on non-Newtonian rheology.

- Different scales of mixers to assess scale-up rules.

- Different combination of agitators.

References

ACHDOU, Y., KUZNETSOV, Y. A., PIRONNEAU, O. (1995). Substructuring preconditioners for the Q1 mortar element method. *Numerische Mathematik, 71,* 419-449.

ADAMS, L. W., BARIGOU, M. (2007). CFD analysis of caverns and pseudo-caverns developed during mixing of non-Newtonian fluids. *Chemical Engineering Research and Design, 85*(5 A), 598-604.

AGGARWAL, R., KEUNINGS, R., ROUX, F. X. (1994). Simulation of the flow of integral viscoelastic fluids on a distributed memory parallel computer. *Journal of Rheology, 38*(2), 405-419.

AMESTOY, P. R., DUFF, I. S., L'EXCELLENT, J. Y. (2000). Multifrontal parallel distributed symmetric and unsymmetric solvers. *Computer Methods in Applied Mechanics and Engineering, 184*(2), 501-520.

ASCANIO, G., CASTRO, B., GALINDO, E. (2004). Measurement of power consumption in stirred vessels - a review. *Chemical Engineering Research and Design, 82*(A9), 1282-1290.

AVALOSSE, T., CROCHET, M. J. (1997). Finite-element simulation of mixing. 1. Two-dimensional flow in periodic geometry. *AIChE Journal, 43*(3), 577-587.

BAKKER, A., LAROCHE, R. D., WANG, M. H., CALABRESE, R. V. (1997). Sliding mesh simulation of laminar flow in stirred reactors. *Chemical Engineering Research and Design, 75 A1*(A1), 42-44.

BARAR POUR, S., FRADETTE, L., TANGUY, P. A. (2007). Laminar and slurry blending characteristics of a dual shaft impeller system. *Chemical Engineering Research and Design, 85*(9 A), 1305-1313.

BARTELS, C., BREUER, M., WECHSLER, K., DURST, F. (2002). Computational fluid dynamics applications on parallel-vector computers: computations of stirred vessel flows. *Computers & Fluids, 31*(1), 69-97.

BEHR, M., TEZDUYAR, T. (1999). The Shear-Slip Mesh Update Method. *Computer Methods in Applied Mechanics and Engineering, 174*(3-4), 261-274.

BELYTSCHKO, T., KENNEDY, J. (1975). Finite element approach to pressure wave attenuation by factor fuel subassemblies. *American Society of Mechanical Engineers (Paper), 75*, 172-177.

BENZI, M., SZYLD, D. B., VAN DUIN, A. (1999). Orderings for incomplete factorization preconditioning of nonsymmetric problems. *SIAM Journal of Scientific Computing, 20*(5), 1652-1670.

BERNARDI, C., MADAY, Y., PATERA, A. T. (1994). A new conforming approach to domain decomposition: the mortar element method. In Brezis, H. Lions, J. L. (éds.), *Nonlinear partial differential equations and their applications* (College de france seminar XI, pp. 13-51). Paris, France: Pitman.

BERTRAND, F., TANGUY, P. A., THIBAULT, F. (1997). A three-dimensional fictitious domain method for incompresible fluid flow problems. *International Journal for Numerical Methods in Fluids, 25*(6), 719-736.

BERTRAND, F. H., GADBOIS, M. R., TANGUY, P. A. (1992). Tetrahedral elements for fluid flow. *International Journal for Numerical Methods in Engineering, 33*(6), 1251-1267.

BLADES, E. L., MARCUM, D. L. (2007). A sliding interface method for unsteady unstructured flow simulations. *International Journal for Numerical Methods in Fluids, 53*(3), 507-529.

BOHM, M., WECHSLER, K., SCHAFER, M. (1998). A parallel moving grid multigrid method for flow simulation in rotor-stator configurations. *International Journal for Numerical Methods in Engineering, 42*(1), 175-189.

BORELLO, D., CORSINI, A., RISPOLI, F. (2003). A finite element overlapping scheme for turbomachinery flows on parallel platforms. *Computers and Fluids, 32*(7), 1017-1047.

BRAKKEE, E., VUIK, C., WESSELING, P. (1998). Domain decomposition for the incompressible Navier-Stokes equations: solving subdomain problems accurately and inaccurately. *International Journal for Numerical Methods in Fluids, 26*(10), 1217-1237.

BRAVO, V. L., HRYMAK, A. N., WRIGHT, J. D. (2000). Numerical simulation of pressure and velocity profiles in kneading elements of a co-rotating twin screw extruder. *Polymer Engineering and Science, 40*(2), 525-541.

BRUCATO, A., CIOFALO, M., GRISAFI, F., MICALE, G. (1998). Numerical prediction of flow fields in baffled stirred vessels: A comparison of alternative modelling approaches. *Chemical Engineering Science, 53*(21), 3653-3684.

CABARET, F., BONNOT, S., FRADETTE, L., TANGUY, P. A. (2007). Mixing time analysis using colorimetric methods and image processing. *Industrial and Engineering Chemistry Research, 46*(14), 5032-5042.

CAI, X.-C., KEYES, D. E., MARCINKOWSKI, L. (2002). Non-linear additive Schwarz preconditioners and application in computational fluid dynamics. *International Journal Numerical Methods Fluids, 40*, 1463-1470.

CALGARO, C., LAMINIE, J. (2000). On the domain decomposition method for the generalized stokes problem with continuous pressure. *Numerical Methods for Partial Differential Equations, 16*(1), 84-106.

CAOLA, A. E., JOO, Y. L., ARMSTRONG, R. C., BROWN, R. A. (2001). Highly parallel time integration of viscoelastic flows. *Journal of Non-Newtonian Fluid Mechanics, 100*(1-3), 191-216.

CAOLA, A. E., BROWN, R. A. (2002). Robust iterative methods for solution of transport problems with flow: A block two-level preconditioned Schwarz-domain decomposition method for solution of nonlinear viscous flow problems. *Chemical Engineering Science, 57*(21), 4583-4594.

CAREY, G. F., SHEN, Y., MCLAY, R. T. (1998). Parallel conjugate gradient performance for least-squares finite elements and transport problems. *International Journal for Numerical Methods in Fluids, 28*(10), 1421-1440.

CHAU, M., SPITERI, P., BOISSON, H. C. (2007). Parallel numerical simulation for the coupled problem of continuous flow electrophoresis. *International Journal for Numerical Methods in Fluids, 55*(10), 945-963.

CHENG, J., CARREAU, P. J. (1994). Mixing in the transition flow regime with helical ribbon agitators. *Canadian Journal of Chemical Engineering, 72*(3), 418-430.

CHOI, B. S., WAN, B., PHILYAW, S., DHANASEKHARAN, K., RING, T. A. (2004). Residence time distributions in a stirred tank: Comparison of CFD predictions with experiment. *Industrial and Engineering Chemistry Research, 43*(20), 6548-6556.

COESNON, B., HENICHE, M., DEVALS, C., BERTRAND, F., TANGUY, P. A. (2008). A fast and robust fictitious domain method for modelling viscous flows

in complex mixers: The example of propellant make-down. *International Journal for Numerical Methods in Fluids, 58*(4), 427-449.

COHEN, D., LANGHORN, K. (2004). Mix it up. *Chemical Processing magazine, 67*(4), 1-3.

CONNELLY, R. K., KOKINI, J. L. (2006). Mixing simulation of a viscous newtonian liquid in a twin sigma blade mixer. *AIChE Journal, 52*(10), 3383-3393.

CROUZEIX, M., RAVIART, P. (1973). Conforming and non-conforming finite element methods for solving the stationary Stokes equations. *RAIRO analyse numerique, 7*, 33-76.

DARWISH, M., SAAD, T., HAMDAN, Z. (2008). Parallelization of an additive multigrid solver. *Numerical Heat Transfer, Part B: Fundamentals, 54*(2), 157-185.

DEUFLHARD, P., FOLKMAR, B. (2002). *Scientific computing with ordinary differential equations* (1rst^e éd.). New York, USA: Springer-Verlag.

DISTELHOFF, M. F. W., MARQUIS, A. J. (1998). An LIF line scan system for the measurement of scalar concentration in a continuously operated stirred tank. *Experiments in Fluids, 25*(1), 77-88.

DOHI, N., TAKAHASHI, T., MINEKAWA, K., KAWASE, Y. (2004). Power consumption and solid suspension performance of large-scale impellers in gas-liquid-solid three-phase stirred tank reactors. *Chemical Engineering Journal, 97*(2-3), 103-114.

DOLEAN, V., LANTERI, S. (2004). Parallel multigrid methods for the calculation of unsteady flows on unstructured grids: Algorithmic aspects and parallel performances on clusters of PCs. *Parallel Computing, 30*(4), 503-525.

DRYJA, M., WIDLUND, O. B. (1987). *An Additive Variant of the Schwarz Alternating Method for the Case of Many Subregions.* N. Y: Courant institute, University of New York.

DUCCI, A., YIANNESKIS, M. (2005). Direct determination of energy dissipation in stirred vessels with two-point LDA. *AIChE Journal, 51*(8), 2133-2149.

DUDUKOVIC, M. P. (2002). Opaque multiphase flows: Experiments and modeling. *Experimental Thermal and Fluid Science, 26*(6-7), 747-761.

DUFF, I. S., VAN DER VORST, H. A. (1999). Developments and trends in the parallel solution of linear systems. *Parallel Computing, 25*(13), 1931-1970.

DUNLOP, A. E., KERNIGHAN, B. W. (1985). A procedure for placement of standard-cell VLSI circuits. *IEEE Transactions on Computer-Aided Design of Integrated Circuits and Systems, CAD-4*(1), 92-98.

DURST, F., SCHAFER, M. (1996). A parallel block-structured multigrid method for the prediction of incompressible flows. *International Journal for Numerical Methods in Fluids, 22*(6), 549-565.

DUTTO, L. C., HABASHI, W. G. (1999). Parallelization of the ILU(0) preconditioner for CFD problems on shared-memory computers. *International Journal for Numerical Methods in Fluids, 30*(8), 995-1008.

DYSTER, K. N., KOUTSAKOS, E., JAWORSKI, Z., NIENOW, A. W. (1993). LDA study of the radial discharge velocities generated by a rushton turbine: Newtonian fluids, Re > 5. *Chemical Engineering Research and Design, 71*(A1), 11-23.

ESCUDIE, R., LIN, A., KIENER, P. (2002). Experimental analysis of hydrodynamics induced by a Moritz HAS impeller in laminar and turbulent regimes. *Canadian Journal of Chemical Engineering, 80*(4), 566-579.

ESCUDIE, R., LIN, A. (2003). Experimental analysis of hydrodynamics in a radially agitated tank. *AIChE Journal, 49*(3), 585-603.

ESPINOSA-SOLARES, T., BRITO-DE LA FUENTE, E., TECANTE, A., TANGUY, P. A. (1997). Power consumption of a dual turbine-helical ribbon impeller mixer in ungassed conditions. *Chemical Engineering Journal, 67*(3), 215-219.

ESPINOSA-SOLARES, T., BRITO-DE LA FUENTE, E., TECANTE, A., MEDINA-TORRES, L., TANGUY, P. A. (2002). Mixing time in rheologically evolving model fluids by hybrid dual mixing systems. *Chemical Engineering Research & Design, 80*, 817-823.

FARHAT, C., ROUX, F.-X. (1991). Method of finite element tearing and interconnecting and its parallel solution algorithm. *International Journal for Numerical Methods in Engineering, 32*(6), 1205-1227.

FARHAT, C., FEZOUI, L., LANTERI, S. (1993). Two-dimensional viscous flow computations on the Connection Machine: unstructured meshes, upwind

schemes and massively parallel computations. *Computer Methods in Applied Mechanics and Engineering, 102*(1), 61-88.

FARHAT, M., RIVERA, C., FRADETTE, L., HENICHE, M., TANGUY, P. A. (2007). Numerical and experimental study of a dual-shaft coaxial mixer with viscous fluids. *Industrial and Engineering Chemistry Research, 46*(14), 5021-5031.

FARHAT, M., FRADETTE, L., TANGUY, P., HORIGUCHI, H., YATOMI, R. (2008). An investigation of the Superblend mixer. *AIChE annual meeting, Philadelphia.*

FENWICK, C. L., ALLEN, C. B. (2006). Development and validation of sliding and non-matching grid technology for control surface representation. *Proceedings of the Institution of Mechanical Engineers, Part G (Journal of Aerospace Engineering), 220*(G4), 299-315.

FORSCHNER, P., KREBS, R., SCHNEIDER, T., KAPLAN, L., SMITH, G. (1992). Scale-up procedures for power calculation in mixing of non-Newtonian liquids. *AICHE Symposium series* (Vol. 88, pp. 38)AICHE.

FOUCAULT, S., ASCANIO, G., TANGUY, P. A. (2006). Mixing times in coaxial mixers with Newtonian and non-Newtonian fluids. *Industrial and Engineering Chemistry Research, 45*(1), 352-359.

FREUND, R. W., NACHTIGAL, N. M. (1991). QMR: a quasi-minimal residual method for non-Hermitian linear systems. *Numerische Mathematik, 60*(3), 315-339.

GARTLING, D. K. (2005). Multipoint constraint methods for moving body and non-contiguous mesh simulations. *International Journal for Numerical Methods in Fluids, 47*(6-7), 471-489.

GEAR, C. (1971). *Numerical initial value problems in ordinary differential equations.* Englewood Cliffs, N.J.: Prentice-Hall.

GLOWINSKI, R., PAN, T.-W., PERIAUX, J. (1994). Fictitious domain method for Dirichlet problem and applications. *Computer Methods in Applied Mechanics and Engineering, 111*(3-4), 283-303.

GLOWINSKI, R., PAN, T. W., PERIAUX, J. (1994). Fictitious domain method for Dirichlet problem and applications. *Computer Methods in Applied Mechanics and Engineering, 111*(3-4), 283-303.

GLOWINSKI, R., PAN, T. W., KEARSLEY, A. J., PERIAUX, J. (1995). *Fictitious domain methods for viscous flow simulation*. Houston: Rice University.

GLOWINSKI, R., PAN, T. W., PERIAUX, J. (1995). Fictitious domain/domain decomposition methods for partial differential equations. *Domain-based parallelism and problem decomposition method in computational science and engineering, Philadelphia* (pp. 177-192)SIAM.

GOSMAN, A. D., ISSA, R. I., LEKAKOU, R. I., LOONEY, M. K., POLITIS, S. (1992). Multidimensional modeling of turbulent two-phase flow in stirred vessels. *AIChE Journal, 38*, 1946-1956.

GOULD, N. I. M., HU, Y., SCOTT, J. A. (2005). *A numerical evaluation of sparse direct solvers for the solution of large sparse, symmetric linear systems of equations*. Oxfordshire: CCLRC Rutherford Appleton Laboratory.

GROPP, W. D., KAUSHIK, D. K., KEYES, D. E., SMITH, B. F. (2001). High-performance parallel implicit CFD. *Parallel Computing, 27*(4), 337-362.

HARVEY, P. S., GREAVES, M. (1982). Turbulent flow in an agitated vesel - 2. numerical solution and model predictions. *Transactions of the Institution of Chemical Engineers, 60*(4), 201-210.

HENDRIKSON, B., LELAND, R. (1993). *The Chaco user guide, version 1.0*. Alburquerque: Sandia Laboratories.

HENICHE, M., SECRETAN, Y., LECLERC, M. (2001). Efficient ILU preconditioning and inexact-Newton-GMRES to solve the 2D steady shallow equations. *Communications in Numerical Methods Engineering, 17*, 69-75.

HENRIKSEN, P., KEUNINGS, R. (1994). Parallel computation of the flow of integral viscoelastic fluids on a heterogeneous network of workstations. *International Journal for Numerical Methods in Fluids, 18*(12), 1167-1183.

HIRUTA, O., YAMAMURA, K., TAKEBE, H., FUTAMURA, T., IINUMA, K., TANAKA, H. (1997). Application of Maxblend fermentor for microbial processes. *Journal of Fermentation and Bioengineering, 83*(1), 79-86.

HOCKEY, R. M., NOURI, J. M. (1996). Turbulent flow in a baffled vessel stirred by a 60 pitched blade impeller. *Chemical Engineering Science, 51*(19), 4405-4421.

HOLLAND, F. A., CHAPMAN, F. S. (1966). *Liquid mixing and processing*. New York: Reinhold.

HOUZEAUX, G., CODINA, R. (2003). A Chimera method based on a Dirichlet/Neumann (Robin) coupling for the Navier-Stokes equations. *Computer Methods in Applied Mechanics and Engineering, 192*(31-32), 3343-3377.

HU, Q., SHI, Z., YU, D. (2004). Efficient solvers for saddle-point problems arising from domain decompositions with lagrange multipliers. *SIAM Journal on Numerical Analysis, 42*(3), 905-933.

HUERTA, A., LIU, W. K. (1988). Viscous flow with large free surface motion. *Computer Methods in Applied Mechanics and Engineering, 69*(3), 277-324.

HUGHES, T. J. R., LEVIT, I., WINGET, J. (1983). An element-by-element solution algorithm for problem of structural and solid mechanics. *Computer Methods in Applied Mechanics and Engineering, 36,* 241-254.

HWANG, F.-N., CAI, X.-C. (2005). A parallel nonlinear additive Schwarz preconditioned inexact Newton algorithm for incompressible Navier-Stokes equations. *Journal of Computational Physics, 204*(2), 666-691.

IRANSHAHI, A., DEVALS, C., HENICHE, M., FRADETTE, L., TANGUY, P. A., TAKENAKA, K. (2007). Hydrodynamics characterization of the Maxblend impeller. *Chemical Engineering Science, 62*(14), 3641-3653.

JAHANGIRI, M., GOLKAR-NARENJI, M. R., MONTAZERIN, N., SAVARMAND, S. (2001). Investigation of the viscoelastic effect on the Metzner and Otto coefficient through LDA velocity measurements. *Chinese Journal of Chemical Engineering, 9*(1), 77-83.

JAHANGIRI, M. (2006). Fluctuation velocity for non-Newtonian liquids in mixing tank by rushton turbine in the transition region. *Iranian Polymer Journal (English Edition), 15*(4), 285-290.

JAHANGIRI, M. (2007). Velocity distribution of helical ribbon impeller in mixing of polymeric liquids in the transition region. *Iranian Polymer Journal (English Edition), 16*(11), 731-740.

JOHAN, Z., MATHUR, K. K., JOHNSSON, S. L., HUGHES, T. J. R. (1995). A case study in parallel computation: viscous flow around an ONERA M6 wing. *International Journal for Numerical Methods in Fluids, 21,* 877-884.

JOHN, V., TOBISKA, L. (2000). Numerical performance of smoothers in coupled multigrid methods for the parallel solution of the incompressible Navier-Stokes equations. *International Journal for Numerical Methods in Fluids, 33*(4), 453-473.

JONGEN, T. (2000). Characterization of batch mixers using numerical flow simulations. *AIChE Journal, 46*(11), 2140-2150.

KARYPIS, G., KUMAR, V. (1998). *METIS: A software package for partitioning unstructured graphs, partitioning meshes, and computing fill-reducing orderings of sparse matrices.* Minnesota: University of Minnesota.

KASHIYAMA, K., TAMAI, T., INOMATA, W., YAMAGUCHI, S. (2000). Parallel finite element method for incompressible Navier-Stokes flows based on unstructured grids. *Computer Methods in Applied Mechanics and Engineering, 190*(3-4), 333-344.

KELLY, W., GIGAS, B. (2003). Using CFD to predict the behavior of power law fluids near axial-flow impellers operating in the transitional flow regime. *Chemical Engineering Science, 58*(10), 2141-2152.

KERNIGHAN, B. W., LIN, S. (1970). An efficient heuristic procedure for partitioning graphs. *Bell System Technical Journal, 49*(2), 291-308.

KHOPKAR, A. R., FRADETTE, L., TANGUY, P. A. (2007). Hydrodynamics of a dual shaft mixer with Newtonian and non-Newtonian fluids. *Chemical Engineering Research & Design, 85*(A6), 863-871.

KHOPKAR, A. R., FRADETTE, L., TANGUY, P. A. (2007). Hydrodynamics of a dual shaft mixer with Newtonian and non-Newtonian fluids. *Chemical Engineering Research & Design, 85*(A6), 863-871.

KLAWONN, A., WIDLUND, O. B. (2000). A domain decomposition method with Lagrange multipliers and inexact solvers for linear elasticity. *SIAM Journal on Scientific Computing, 22*(4), 1199-1219.

KLAWONN, A., RHEINBACH, O. (2007). Inexact FETI-DP methods. *International Journal for Numerical Methods in Engineering, 69*(2), 284-307.

KOUDA, T., YANO, H., YOSHINAGA, F. (1997). Effect of agitator configuration on bacterial cellulose productivity in aerated and agitated culture. *Journal of Fermentation and Bioengineering, 83*(4), 371-376.

KOUTSAKOS, E., NIENOW, A. W., DYSTER, K. N. (1990). Laser anemometry study of shear thinning fluids agitated by a Rushton turbine. *Institution of Chemical Engineers Symposium Series*(121), 51-73.

KUZNETSOV, Y. A. (1995). Efficient iterative solvers for elliptic finite element problems on non-matching grids. *Russian Journal Numerical Analysis Mathematical Modeling, 10*, 187-211.

LETELLIER, B., XUEREB, C., SWAELS, P., HOBBES, P., BERTRAND, J. (2002). Scale-up in laminar and transient regimes of a multi-stage stirrer, a CFD approach. *Chemical Engineering Science, 57*(21), 4617-4632.

LEVEQUE, R. J., LI, Z. (1994). Immersed interface method for elliptic equations with discontinuous coefficients and singular sources. *SIAM Journal on Numerical Analysis, 31*(4), 1019-1044.

LI, X. S., DEMMEL, J. W. (2003). SuperLU_DIST: a scalable distributed-memory sparse direct solver for unsymmetric linear systems. *ACM Transactions on Mathematical Software, 29*(2), 110-140.

LIN, P. T., SALA, M., SHADID, J. N., TUMINARO, R. S. (2006). Performance of fully coupled algebraic multilevel domain decomposition preconditioners for incompressible flow and transport. *International Journal for Numerical Methods in Engineering, 67*(2), 208-225.

LOHNER, R. (2007). The empty bin: a data structure for spatial search of time-varying data. *Communications in Numerical Methods in Engineering, 23*(12), 1111-1119.

LUO, J. Y., GOSMAN, A. D., ISSA, R. I., MIDDLETON, J. C., FITZGERALD, M. K. (1993). Full flow field computation of mixing in baffled stirred vessels. *Chemical Engineering Research and Design, 71*(A3), 342-344.

MANN, R., WILLIAMS, R. A., DYAKOWSKI, T., DICKIN, F. J., EDWARDS, R. B. (1997). Development of mixing models using electrical resistance tomography. *Chemical Engineering Science, 52*(13), 2073-2085.

MARUKO, M., KUSUMOTO, S. (1992). Power consumption characteristics of a lattice-type, twin-shaft, high-viscosity agitator. *International chemical engineering, 32*(4), 759-766.

MAVROS, P., XUEREB, C., BERTRAND, J. (1996). Determination of 3-D flow fields in agitated vessels by laser-Doppler velocimetry: effect of impeller type and

liquid viscosity on liquid flow patterns. *Chemical Engineering Research and Design, 74*(A6), 658-668.

METZNER, A. B., OTTO, R. E. (1957). Agitation of non-Newtonian fluids. *Chemical Engineering Progress, 3*(1), 3-10.

METZNER, A. B., FEEHS, R. H., RAMOS, H. L., OTTO, R. E., TUTHILL, J. D. (1961). Agitation of viscous Newtonian and non-Newtonian fluids. *AIChE Journal, 7*(1), 3-9.

MIDDLETON, J. C., PIERCE, F., LYNCH, P. M. (1986). Computations of flow flelds and complex reaction yield in turbulent stirred reactors, and comparison with experimental data. *Chemical Engineering Research and Design, 64*(1), 18-22.

MONTES, J. L., BOISSON, H. C., FORT, I., JAHODA, M. (1997). Velocity field macro-instabilities in an axially agitated mixing vessel. *Chemical Engineering Journal, 67*(2), 139-145.

MURTHY, J. Y., MATHUR, S. R., CHOUDHURY, D. (1994). CFD simulation of flows in stirred tank reactors using a sliding mesh technique. *IChemE Symposium series* (Vol. 136)IChemE.

MURTHY, S., JAYANTI, S. (2002). CFD study of power and mixing time for paddle mixing in unbaffled vessels. *Chemical Engineering Research and Design, 80*(5), 482-498.

NIENOW, A. W., EDWARD, M. F., HARNBY, N. (1997). *Mixing in the process industries* (2nd^e éd.): Butterworth-Heinemann.

NOURI, J. M., WHITELAW, J. H. (1990). Flow characteristics of stirred reactors with Newtonian and non-Newtonian fluids. *AIChE Journal, 36*(4), 627-629.

NOVAK, V., RIEGER, F. (1969). Homogenization with helical screw agitators. *47*(10), t335-t340.

OLIKER, L., XIAOYE, L., HUSBANDS, P., BISWAS, R. (2002). Effects of ordering strategies and programming paradigms on sparse matrix computations. *SIAM Review, 44*(3), 373-393.

PAUL, E. L., ATIEMO-OBENG, V. A., KRESTA, S. M. (2003). *Handbook of industrial mixing: science and practice*: John Wiley and Sons, Inc.

PERICLEOUS, K. A., PATEL, M. K. (1987). Modelling of tangential and axial agitators in chemical reactors. *PCH. Physicochemical hydrodynamics, 8*(2), 105-123.

PERNG, C.-Y., MURTHY, J. Y. (1993). Sliding-mesh technique for simulation of flow in mixing tanks. *New Orleans, LA, USA* (pp. 1-9)Publ by ASME.

PESKIN, C. S., MCQUEEN, D. M. (1989). A three-dimensional computational method for blood flow in the heart. I. Immersed elastic fibers in a viscous incompressible fluid. *Journal of Computational Physics, 81*(2), 372-405.

POLLARD, J., KANTYKA, T. A. (1969). Heat Transfer to Agitated Non-Newtonian Fluids. *Transactions of the Institution of Chemical Engineers, 47*(1), t21-t27.

RAI, M. M. (1985). Navier-Stokes simulations of rotor-stator interaction using patched and overlaid grids. *Cincinnati, OH, USA* (pp. 282-298)AIAA (CP854).

RAMMOHAN, A. R., KEMOUN, A., AL-DAHHAN, M. H., DUDUKOVIC, M. P. (2001). Characterization of single phase flows in stirred tanks via computer automated radioactive particle tracking (CARPT). *Chemical Engineering Research and Design, 79*(8), 831-844.

RANADE, V. V., JOSHI, J. B. (1990). Flow generated by a disc turbine. Part II. Mathematical modelling and comparison with experimental data. *Chemical Engineering Research and Design, 68*(1), 34-50.

RANADE, V. V., DOMMETI, S. M. S. (1996). Computational snapshot of flow generated by axial impellers in baffled stirred vessels. *Chemical Engineering Research and Design, 74*(A4), 476-484.

RANADE, V. V., TAYALIA, Y., KRISHNAN, H. (2002). CFD predictions of flow near impeller blades in baffled stirred vessels: Assessment of computational snapshot approach. *Chemical Engineering Communications, 189*(7), 895-922.

REVSTEDT, J., FUCHS, L. (2001). Handling complex boundaries on a Cartesian grid using surface singularities. *International Journal for Numerical Methods in Fluids, 35*(2), 125-150.

RICCI, E., KELLY, W. J. (2004). The effects of power law fluid rheology on coil heat transfer for agitated vessel in the transitional flow regime. *Canadian Journal of Chemical Engineering, 82*(6), 1275-1283.

RIVERA, C., HENICHE, M., ASCANIO, G., TANGUY, P. (2004). A virtual finite element model for centered and eccentric mixer configurations. *Computers & Chemical Engineering, 28*(12), 2459-2468.

RIVERA, C., FOUCAULT, S., HENICHE, M., ESPINOSA-SOLARES, T., TANGUY, P. A. (2006). Mixing analysis in a coaxial mixer. *Chemical Engineering Science, 61*(9), 2895-2907.

RUDOLPH, L., SCHAFER, M., ATIEMO-OBENG, V., KRAUME, M. (2007). Experimental and numerical analysis of power consumption for mixing of high viscosity fluids with a co-axial mixer. *Chemical Engineering Research & Design, 85*(A5), 568-575.

SAAD, Y. (2003). *Iterative methods for sparse linear systems* (2nd ^{e} éd.). Philadelphia: SIAM.

SAHIN, M., WILSON, H. J. (2008). A parallel adaptive unstructured finite volume method for linear stability (normal mode) analysis of viscoelastic fluid flows. *Journal of Non-Newtonian Fluid Mechanics, 155*(1-2), 1-14.

SAKSONO, P. H., DETTMER, W. G., PERIC, D. (2007). An adaptive remeshing strategy for flows with moving boundaries and fluid-structure interaction. *International Journal for Numerical Methods in Engineering, 71*(9), 1009-1050.

SCHAFER, M., YIANNESKIS, M., WACHTER, P., DURST, F. (1998). Trailing vortices around a 45 pitched-blade impeller. *AIChE Journal, 44*(6), 1233-1246.

SCHAFFER, M. A., MARCHILDON, E. K., MCAULEY, K. B., CUNNINGHAM, M. F. (2001). Assessment of mixing performance and power consumption of a novel polymerization reactor system. *Chemical Engineering and Technology, 24*(4), 401-408.

SCOTT, J. A. (2003). Parallel frontal solvers for large sparse linear systems. *ACM Transactions on Mathematical Software, 29*(4), 395-417.

SHADID, J. N., TUMINARO, R. S., DEVINE, K. D., HENNIGAN, G. L., LIN, P. T. (2005). Performance of fully coupled domain decomposition preconditioners for finite element transport/reaction simulations. *Journal of Computational Physics, 205*(1), 24-47.

SHEU, T. W. H., WANG, M. M. T., TSAI, S. F. (1999). Element-by-element parallel computation of incompressible Navier-Stokes equations in three dimensions. *SIAM Journal of Scientific Computing, 21*(4), 1387-1400.

SMITH, B. F., BJORSTAD, P., GROPP, W. D. (1996). *Domain decomposition: parallel multilevel methods for elliptic partial differential equations* (1rst^e éd.). Cambridge, UK: Cambridge university press.

SMITH, G. D. (1985). *Numerical Solution of Partial Differential Equations: Finite Difference Methods* (2nd^e éd.). Oxford, UK: Clarendon Press.

SOULAIEMANI, A., FORTIN, M., DHATT, G., OUELLET, Y. (1991). Finite element simulation of two- and three-dimesional free surface flows. *Computer Methods in Applied Mechanics and Engineering, 86*(3), 265-296.

STAFF, O., WILLE, S. (2005). Parallel ILU preconditioning and parallel mesh adaptation with load balancing for general domain decompositions for the Navier-Stokes equations. *International Journal for Numerical Methods in Fluids, 47*(10-11), 1301-1306.

STEGER, J. L., DOUGHERTY, F. C., BENEK, J. A. (1983). Chimera grid scheme. *Houston, TX, USA* (Vol. 5, pp. 59-69)ASME.

STEIJL, R., BARAKOS, G. (2008). Sliding mesh algorithm for CFD analysis of helicopter rotor-fuselage aerodynamics. *San Francisco, CA, United states* (Vol. 1, pp. 34-47)Curran Associates Inc.

STOBIAC, V., HENICHE, M., DEVALS, C., BERTRAND, F., TANGUY, P. (2008). A mapping method based on Gaussian quadrature: Application to viscous mixing. *Chemical Engineering Research and Design, 86*(12), 1410-1422.

TAGAWA, A., DOHI, N., KAWASE, Y. (2006). Dispersion of floating solid particles in aerated stirred tank reactors: Minimum impeller speeds for off-surface and ultimately homogeneous solid suspension and solids concentration profiles. *Industrial and Engineering Chemistry Research, 45*(2), 818-829.

TAKAHASHI, T., TAGAWA, A., ATSUMI, N., DOHI, N., KAWASE, Y. (2006). Liquid-phase mixing time in boiling stirred tank reactors with large cross-section impellers. *Chemical Engineering and Processing, 45*(4), 303-311.

TAKEDA, H., NARASAKI, K., KITAJIMA, H., SUDOH, S., ONOFUSA, M., IGUCHI, S. (1993). Numerical simulation of mixing flows in agitated vessels with impellers and baffles. *Computers and Fluids, 22*(2-3), 223-228.

TANGUY, P. A., LACROIX, R., BERTRAND, F., CHOPLIN, L., DE LA FUENTE, E. B. (1992). Finite element analysis of viscous mixing with a helical ribbon-screw impeller. *AIChE Journal, 38*(6), 939-944.

TANGUY, P. A., BERTRAND, F., LABRIE, R., BRITO-DE LA FUENTE, E. (1996). Numerical modelling of the mixing of viscoplastic slurries in a twin-blade planetary mixer. *Chemical Engineering Research and Design, 74*(A4), 499-504.

TANGUY, P. A., THIBAULT, F., BRITO-DE LA FUENTE, E., ESPINOSA-SOLARES, T., TECANTE, A. (1997). Mixing performance induced by coaxial flat blade-helical ribbon impellers rotating at different speeds. *Chemical Engineering Science, 52*(11), 1733-1741.

TANGUY, P. A., THIBAULT, F., DUBOIS, C., AIT-KADI, A. (1999). Mixing hydrodynamics in a double planetary mixer. *Chemical Engineering Research and Design, 77*(4), 318-324.

TATTERSON, G. (1991). *Fluid mixing and gas dispersion in agitated tanks.* New York, USA: McGraw-Hill.

TEZDUYAR, T. E., LIOU, J. (1989). Grouped element-by-element iteration schemes for incompressible flow computations. *Computer Physics Communications, 53*(1-3), 441-453.

TEZDUYAR, T. E., BEHR, M., ALIABADI, S. K., MITTAL, S., RAY, S. E. (1992). New mixed preconditioning method for finite element computations. *Computer Methods in Applied Mechanics and Engineering, 99*(1), 27-42.

TEZDUYAR, T. E., SATHE, S., STEIN, K. (2006). Solution techniques for the fully discretized equations in computation of fluid-structure interactions with the space-time formulations. *Computer Methods in Applied Mechanics and Engineering, 195*(41-43), 5743-5753.

THIBAULT, F., TANGUY, P. A. (2002). Power-draw analysis of a coaxial mixer with Newtonian and non-Newtonian fluids in the laminar regime. *Chemical Engineering Science, 57*(18), 3861-3872.

TOSELLI, A., WIDLUND, O. B. (2005). *Domain decomposition methods algorithms and theory* (1rst^e éd.). Berlin: Springer-Verlag.

TUREK, S. (1996). A comparative study of time-stepping techniques for the incompressible Navier-Stokes equations: from fully implicit non-linear schemes

to semi-implicit projection methods. *International Journal for Numerical Methods in Fluids, 22*(10), 987-1011.

VAINIKKO, E., GRAHAM, I. G. (2004). A parallel solver for PDE systems and application to the incompressible Navier-Stokes equations. *Applied Numerical Mathematics, 49*(1), 97-116.

VAN LOON, R., ANDERSON, P. D., DE HART, J., BAAIJENS, F. P. T. (2004). A combined fictitious domain/adaptive meshing method for fluid-structure interaction in heart valves. *International Journal for Numerical Methods in Fluids, 46*(5), 533-544.

VANDERSTRAETEN, D., KEUNINGS, R. (1998). A parallel solver based on the dual Schur decomposition of general finite element matrices. *International Journal for Numerical Methods in Fluids, 28*(1), 23-46.

VASCONCELOS, J. M. T., BARATA, J. M., ALVES, S. S. (1996). Transitional mixing in multiple-turbine agitated tanks. *Chemical Engineering Journal, 63*(1), 53-58.

VEREECKE, B., BAVESTRELLO, H., DUREISSEIX, D. (2003). An extension of the FETI domain decomposition method for incompressible and nearly incompressible problems. *Computer Methods in Applied Mechanics and Engineering, 192*(31-32), 3409-3429.

VERZICCO, R., FATICA, M., IACCARINO, G., ORLANDI, P. (2004). Flow in an impeller-stirred tank using an immersed-boundary method. *AIChE Journal, 50*(6), 1109-1118.

WASSMER, K.-H., HUNGENBERG, K.-D. (2005). A unified model for the mixing of Non-Newtonian fluids in the laminar, transition, and turbulent region. *Macromolecular Materials and Engineering, 290*(4), 294-301.

WAYMEL, F., MONNOYER, F., WILLIAM-LOUIS, M. J. P. (2006). Numerical simulation of the unsteady three-dimensional flow in confined domains crossed by moving bodies. *Computers and Fluids, 35*(5), 525-543.

WECHSLER, K., BREUER, M., DURST, F. (1999). Steady and unsteady computations of turbulent flows induced by a 4/45 pitched-blade impeller. *Journal of Fluids Engineering, Transactions of the ASME, 121*(2), 318-329.

WILLE, S. O., STAFF, O., LOULA, A. F. D. (2003). Parallel ILU preconditioning, a priori pivoting and segregation of variables for iterative solution of the mixed

finite element formulation of the Navier-Stokes equations. *International Journal for Numerical Methods in Fluids, 41*(9), 977-996.

WITCHERLE, K., KADLEC, M., ZAK, L., MITSCHKA, P. (1984). Shear rates on turbine impeller blades. *Chemical Engineering Communications, 26*(1-3), 25-32.

WU, H., PATTERSON, G. K. (1989). Laser-doppler measurements of turbulent-flow parameters in a stirred mixer. *Chemical Engineering Science, 44*(10), 2207-2221.

YAO, W., MISHIMA, M., TAKAHASHI, K. (2001). Numerical investigation on dispersive mixing characteristics of Maxblend and double helical ribbons. *Chemical Engineering Journal, 84*(3), 565-571.

YOTOV, I. (1996). *Mixed finite element method for flow in porous media*. Ph. D. thesis inédit, Rice University, Houston.

ZALC, J. M., ALVAREZ, M. M., MUZZIO, F. J., ARIK, B. E. (2001). Extensive validation of computed laminar flow in a stirred tank with three Rushton turbines. *AIChE Journal, 47*(10), 2144-2154.

ZALC, J. M., SZALAI, E. S., ALVAREZ, M. M., MUZZIO, F. J. (2002). Using CFD to understand chaotic mixing in laminar stirred tanks. *AIChE Journal, 48*(10), 2124-2134.

ZEPPENFELD, R., MERSMANN, A. B. (1988). New fluid dynamic model for mixing of Newtonian and power-law liquids in the transient regime. *Chemical Engineering and Technology, 11*(3), 162-170.

ZHANG, L., GERSTENBERGER, A., WANG, X., LIU, W. K. (2004). Immersed finite element method. *Computer Methods in Applied Mechanics and Engineering, 193*(21-22), 2051-2067.

ZIENKIEWICZ, O. C., TAYLOR, R. L. (2000). *The finite element method: fluid dynamics* (Vol. 3). Oxford: Butterworth and Heinemann.

ZLOKARNIK, M. (2001). *Stirring: theory and practice* (1rst^e éd.). Weinheim, Germany: Wiley-VCH.

ZSAKI, A., RIXEN, D., PARASCHIVOIU, M. (2003). A substructure-based iterative inner solver coupled with Uzawa's algorithm for the Stokes problem. *International Journal for Numerical Methods in Fluids, 43*(2), 215-230.